Adaptive Control and Dynamic Demand Response for the Stabilization of Grid Frequency

Mazin T. Muhssin

School of Engineering

Institute of Energy

Cardiff University

A thesis submitted for the degree of
Doctor of Philosophy

2018

Abstract

Over the past few years, there has been a marked increase in the output from wind and solar generation in many countries. High levels of distributed generation provide variable energy and the increasing share of converter-connected plant results in a reduction in system inertia. Consequently, the rate of change of frequency, especially during and after severe faults, becomes more rapid. This thesis describes the use of heat pumps and fridges to provide ancillary services of frequency response so that to continuously balance the supply with demand.

A decentralized digital controller namely: Adaptive DeadBeat (ADB) is designed to improve the frequency behaviour in an interconnected power system during and after faults. Simulation results show that the ADB controller can be considered as a contribution of digital control application to improve the frequency behaviour in an interconnected power system with reduced system inertia.

The thermal performance of domestic buildings using heat pumps, and of fridges using thermostat temperature control is modelled.

A dynamic frequency control (DFC) algorithm is developed to control the power consumption of the load in response to the grid frequency without affecting the overall performance of the load. Then, the dynamic frequency control algorithm is applied to a population of over 10 million aggregated units that represent the availability of load to provide frequency response. A dynamic relationship between the temperature and pre-defined trigger frequencies is given to ensure smooth and gradual load switching.

A simulation is undertaken by connecting the controllable heat pumps to the reduced dynamic model of the Great Britain power system. Following a loss of 1,800 MW of generation, it is shown that the DFC reduces 1,000 MW of heat pumps demand and hence the frequency deviation is maintained within acceptable limits. In addition, a population of heat pumps and fridges are connected to the electrodynamic master model of the GB power system that is at present used by the

GB transmission system operator, National Grid plc. Results show that the aggregated domestic heat pumps and fridges controlled by the DFC algorithm can participate in the Firm Frequency Response (FFR) service and provide rapid frequency response to the GB power system, mimicking the behaviour of the frequency-sensitive generators.

Declaration

This work has not been submitted in substance for any other degree or award at this or any other university or place of learning, nor is being submitted concurrently in candidature for any degree or other award.

Signed ………………………………. (candidate)   Date …………………………

STATEMENT 1

This thesis is being submitted in partial fulfilment of the requirements for the degree of PhD.

Signed ………………………………. (candidate)   Date …………………………

STATEMENT 2

This thesis is the result of my own independent work/investigation, except where otherwise stated.
Other sources are acknowledged by explicit references. The views expressed are my own.

Signed ………………………………. (candidate)   Date …………………………

STATEMENT 3

I hereby give consent for my thesis, if accepted, to be available for photocopying and for inter-library loan, and for the title and summary to be made available to outside organisations.

Signed ………………………………. (candidate)   Date …………………………

STATEMENT 4: PREVIOUSLY APPROVED BAR ON ACCESS

I hereby give consent for my thesis, if accepted, to be available for photocopying and for inter-library loans **after expiry of a bar on access previously approved by the Academic Standards & Quality Committee.**

Signed ………………………………. (candidate) Date …………………………

Acknowledgement

Table of Contents

List of Figures

xi

List of Tables

Nomenclature

ACE	Area Control Error
ADB	Adaptive DeadBeat
AGC	Automatic Generation Control
BM	Balancing Market
BS	Balancing Service
BT	Bitumen Tank
CDLC	Central direct load control
DDC	Dynamic Demand Control
DFC	Dynamic Frequency Control
DFR	Dynamic Frequency Reserve
DG	Distributed Generation
DLL	Dynamic Link Library
DNO	Distribution Network Operator
DSO	Distribution System Operator
DSR	Demand Side Response
EFR	Enhanced Frequency Response
ETP	Equivalent Thermal Parameter
ETYS	Electricity Ten Year Statement
EV	Electric Vehicle
EWH	Electric Water Heater
FCDM	Frequency Control by Demand Management
FFR	Firm Frequency Response
FIS	Fuzzy Inference System
FLC	Fuzzy Logic Control
FMS	Frequency Sensitive Mode
GA	Genetic Algorithm
GB	Great Britain

HVAC	Heating Ventilation and Air-Conditioning
HVDC	High Voltage Direct Current
ICT	Information and Communications Technology
LFC	Load Frequency Control
LFSM	Limited Frequency Sensitive Mode
MF	Membership Function
MFR	Mandatory Frequency Response
MP	Melting Pot
NFR	Number of heat pumps
NHP	Number of Fridges
ODE	Ordinary Differential Equation
PCC	Point of Common Coupling
PI	Proportional Integral
PID	Proportional Integral Derivative
PSO	Particle Swarm Optimisation
PV	Photovoltaic
RC	Resistance Capacitance
RoCoF	Rate of Change of Frequency
SOF	System Operability Framework
SWH	Space and Water Heating
TCLs	Thermostatically Controlled Loads
TSO	Transmission System Operator
UK	United Kingdom
ZOH	Zero Order Hold

Chapter 1

Introduction

1.1 Diversity of electricity generation sources

Until recently the United Kingdom (UK) electricity was mainly produced by centralised large-scale generating units driven by nuclear and fossil fuel sources. The majority of these generators were connected to the high-voltage network. Continuing to rely on fossil fuels to produce the energy has two main problems. A potential shortage of fossil fuels at reasonable prices and harmful emissions that come from burning fuels. The available options to generate electricity without emitting CO_2 are limited to the use of renewable energy sources, nuclear energy sources, and fossil fuel generators equipped with carbon capture and storage.

The UK government has set two main environmental targets to control the level of renewable energy and reduce greenhouse gases emissions. These targets aim to deliver at least 15% of energy consumption from renewable sources by 2020, and to reduce overall carbon emissions by at least 80% from 1990 levels by 2050 [1]. While a substantial increase in the use of renewable electricity sources has been achieved over the past years, rapid progress is still needed to decarbonise heating and transportation demand. National Grid, the system operator of the Great Britain (GB)[1] transmission system, considered four plausible scenarios to reflect the possible directions of the future generation and demand [1]:

- **Gone Green scenario:** aims to achieve the 2020 renewable energy and 2050 carbon reduction targets from various forms of low carbon energy. The scenario considers an ambitious intervention by the government for investment and innovation, and more money for consumers to spend on low carbon technology.

---

[1] Note that in this thesis GB is used to describe the UK (excluding Northern Ireland).

- **Consumer Power scenario:** this is a market-driven world with limited intervention by government. The consumers drive the innovation by spending money on the latest technology but have little focus on the environment.
- **Slow Progression scenario:** this is a low growth economy with a focus on a cost but on the longer-term intervention policies. Long-term effective policy intervention results in a mixture of renewable and low carbon technologies and high levels of distributed generation.
- **No progression scenario:** this is the least optimistic scenario. There is less will to invest and innovate in low carbon technologies. The focus is more on maintaining system security at low cost.
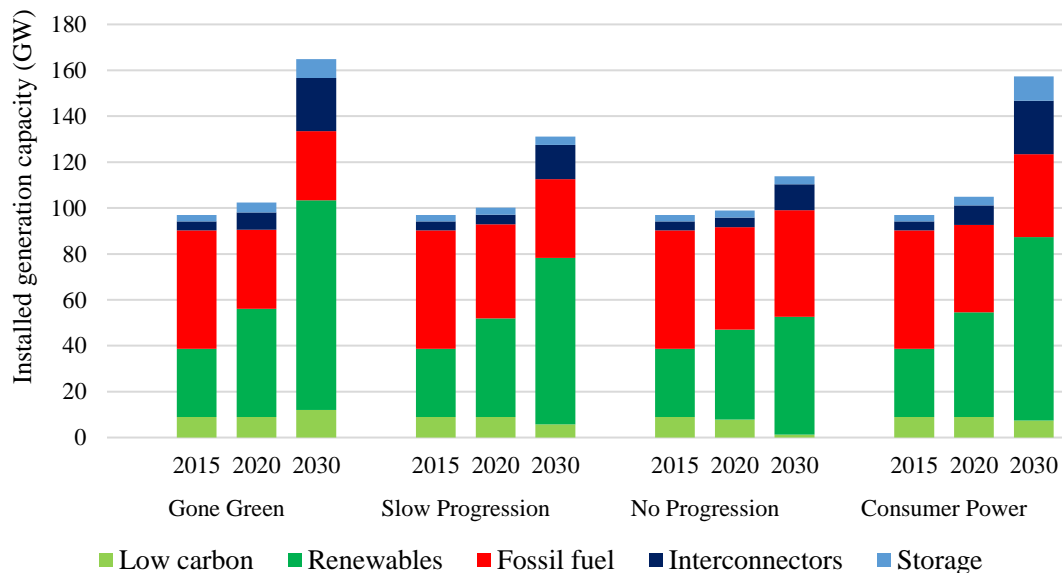
Fig. 1.1 Generation capacity by fuel type (2015-2030) [1]

Fig. 1.1 shows how the installed capacity of different generation types may change between 2015 and 2030. The level of renewables is substantially increasing across all the scenarios, except for ''No Progression''. According to the ''Gone Green'' scenario[2], more than 50% of GB's electricity will be supplied by renewable energy

---

[2] Some of the National Grid's scenarios are renamed in the FES-2017 document. All forms of low carbon energy are presented instead of solely renewables. The installed generation capacity is slightly increased.

sources by 2050, including the hydro and biomass sources. The generation capacity of fossil fuels will be replaced by wind and solar generation capacity, which will be connected not only to the high-voltage networks but also to the distribution networks and to commercial, industrial and domestic buildings [1]. Therefore, the GB power system is going through a period of significant changes to decarbonise the electricity generation sector.

However, increasing the penetration of renewables causes two essential challenges:

i.   Increasing intermittent sources provide a large proportion of variable and less flexible generation. Hence, an instantaneous balance between supply and demand is becoming a real challenge facing GB power system [2].

ii. System inertia is reduced as more and more converter connected generators displace conventional generation.

1.2   Electrification of demand

By 2030, five million additional people and two million new homes will be added in GB, and this number is expected to double by 2050 [1]. Domestic energy demand currently accounts for approximately 40% of gas and about 35% of electricity demand [2]. However, the use of electricity is expected to increase over gas demand in the future due to carbon reduction policies which focus on replacing gas with electricity. Electrification of the heat demand, by heat pumps, and the transport demand, by electric vehicles (EVs) are the main reasons to change the demand uptake from gas to electricity [3]. Fig. 1.2 shows the projected numbers of domestic heat pumps and EVs in two scenarios, i.e. ''Gone Green'' and ''Element Energy'' Scenarios. According to the ''Gone Green'' scenario, about 6 million domestic heat pumps and 3.2 million EVs will be connected to GB network in 2030. Another plausible scenario[3] has been suggested by Element Energy, an energy consultancy

_____

[3] This scenario is considered in this thesis for the provision of frequency response, and is hereafter called ''Element Energy Scenario''

3

in GB, to anticipate the numbers of heat pumps and EVs in GB [3]. The ''Element Energy'' scenario predicted that approximately 5 million EVs and 3.8 million domestic heat pumps will be connected to the GB power system in 2030.
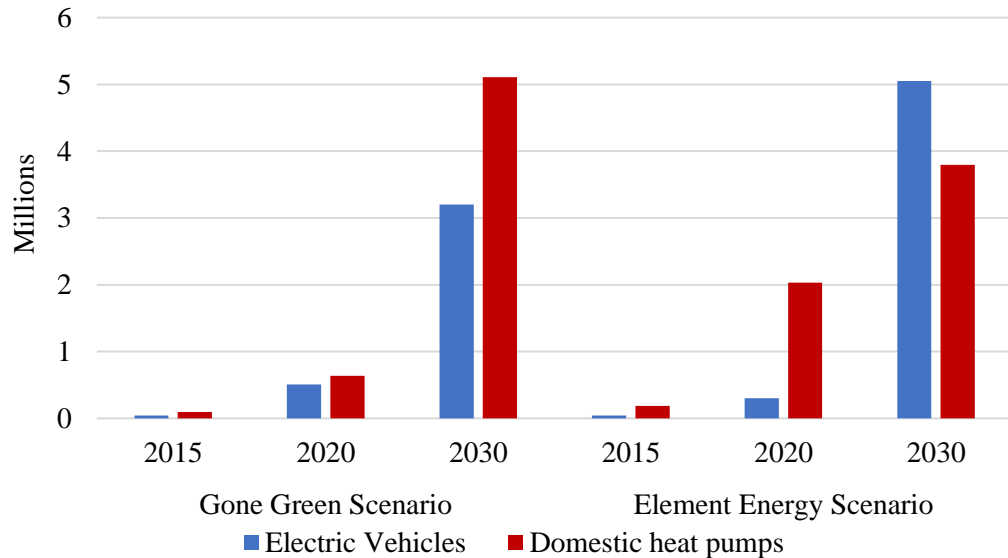
Fig. 1.2 Number of electric vehicles and domestic heat pumps (modified based on [3])

1.3 Anticipated contribution of demand to the power system

The demand profile in GB is changing. The current GB's electricity peak demand is around 60GW and could be as much as 83GW by 2050 [2]. The electrification of heat and transport, as well as the rapid growth of domestic and industrial load will increase peak demand significantly if no action will be taken. The power system will need to manage the growth of demand in such a way as to reduce network peaks. The methods that can be used to manage the growth of load include:

- **Distributed generation (DG)**, where low carbon electricity can be generated locally at home or at commercial premises.
- **Energy storage**, where batteries or other forms of storage systems can be installed to store the electricity when the solar generation exceeds the demand or

when the electricity is cheap. This stored electricity can be then used at a time when it is needed.

- **Demand side response (DSR)**, where a process to deliberately change the users' natural pattern in response to a signal from other parties is used. Businesses and consumers can turn up, turn down, or shift their flexible demand in real-time during peak time to save their electricity cost after receiving a price signal or to provide frequency response service after receiving a frequency signal. Smart meters will make this process achievable in real time. DSR providers will use smart meters to accurately monitor the users real-time use of electricity and decide to take action when necessary [4].

In a future GB power system, the domestic sector, especially with the high uptake of heat pumps, will make an important contribution to DSR. The provision of frequency control is achieved by temporarily interrupting consumption of the appliances that are presented in the form of thermal storage, e.g. heat pumps, fridges, while maintaining the temperatures within pre-defined settings.

1.4 Problems statements

Changes in electricity generation sources will create significant problems in balancing generation with demand, as stated by National Grid [2]:

1. High levels of embedded electricity generation (e.g. wind, solar generation) provide variable generation dispatch. Balancing supply with demand is becoming more difficult with the increase in such intermittent generation sources.

2. The rapid increase of electric power of demand due to electrification of heat and transport will increase peak demand.

3. The frequent infeed loss risk limit (the maximum volume of the generation which can be disconnected from the transmission system [5]) has increased from 1,320 MW to 1,800 MW in 2014. As a result, more part loaded fossil

fuel generators are needed to meet demand when there is severe loss of generation.

4. The replacement of conventional generation by converter connected wind and solar generation will reduce the natural system inertia [6], and cause the rate of change of system frequency to become more rapid.

1.5   Aims and objectives of the thesis

This thesis aims to investigate the potential of a new control system to improve grid frequency in an interconnected power system and to examine the capability of using demand to provide ancillary services, such as frequency response service to the GB power system. The aims of this thesis will be met by the following objectives:

Objective of chapter 2

Review of the state of art technologies that are used to control the frequency of the power system.

Methodology: To provide a detailed review of the topic of frequency response. To review the current findings in the field of frequency control and ongoing research activities in balancing services provided by demand side response.

Objective of chapter 3

1. **Study the frequency control in an interconnected low inertia power system.**

   Methodology: Develop a simplified system model derived from physical data, for interconnected zones north and south of Scotland. This model is designed to conform to the National Grid's 2020 and 2030 future Gone Green energy scenario for the GB power system, where regional frequency control is likely to be a significant issue [7].

2. **Improve the stability and performance of the interconnected power system.**

   Methodology: Develop a new control approach, called Adaptive Deadbeat Controller (ADB), to efficiently control the frequency response in each region

and help continuously maintain the power interchanges over the tie- lines at scheduled levels.

Objective of chapter 4

Modelling of heat pumps and fridges in the form of thermal storage flexible demand.

Methodology: Build a thermodynamic model for a population of domestic buildings equipped with heat pumps, and a thermodynamic model for a population of domestic fridges. More specifically, to identify the suitable number of heat pump and fridge models that accurately represent the entire number of load connected to the GB power system for frequency control studies. Include a thermostat temperature control to keep the temperature at comfortable levels.

Objective of chapter 5

Investigate the use of domestic heat pumps for grid frequency support.

Methodology: To design a new decentralised dynamic frequency control (DFC) algorithm for the provision of dynamic demand response. This will enable the heat pumps to alter their power consumption in response to a grid frequency without undermining the occupant's comfort. Design a decentralised temperature control algorithm to control the building temperature and the heat pump's ON and OFF cycles. To avoid high payback by ensuring smooth switching events during the frequency deviation. In addition, to collaborate with National Grid in order to examine the potential of DFC models geographically by connecting the heat pump models to the National Grid's dynamic model of GB power system.

Objective of chapter 6

Examine the potential of demand side response aggregation.

Methodology:

1. Investigates the availability of domestic heat pumps and fridges load over the time of day for the provision of frequency response service to the GB power system.

2. Identifies the combination of heat pumps and fridges to deliver sufficient amount of power to participate in the Firm Frequency Response (FFR) service.

3. To collaborate with National Grid in order to validate the aggregated model by using their master GB electrodynamic system model. This is to be accomplished by connecting the aggregated model to the GB's Distribution network operators (DNOs) for the provision of dynamic frequency response.

1.6   Research structure

Table 1.1 summarises the research structure. This research is structured into seven chapters. A summary is provided for each chapter, and the related research objectives are listed.

Table 1.1 Summary of thesis chapters and related research objectives

Chapter No.	Chapter summary of contents
1	Conducts the background, the problems statements, the aims, the questions, objectives, and the contribution of the thesis.
2	Discusses the frequency response services of the GB power system. Provide an overview of the interconnected power system. Summarises the state of art strategies to control the power output of generators. Provides an overview of the research activities in balancing services that are provided by the demand side response.
3	Develops a simplified interconnected system model for the north and south Scotland zones. Designs a novel ADB controller that controls the frequency in each zone, as well as rescheduling the power flow between the interconnected zones. Conducts case studies to investigate the robustness and performance of ADB controller in comparison with other standard methods.
4	Presents a thermal model to represent a population of domestic buildings equipped with heat pumps. Identifies the suitable number of heat pump models that accurately represent the entire number of heat pumps. Presents the thermal model of the fridges that was used in literature. Evaluates the operation of both loads model.
5	Develops a new dynamic frequency control algorithm that controls the heat pumps operation in response to the grid frequency. Integrates the developed control system with the GB transmission/ generation reduced model which was developed by National Grid.
6	Presents the availability of domestic heat pumps and fridges to provide frequency response services to the GB power system at different times during the day. Finds a relationship between the number of heat pumps and the No. of fridges for the provision of FFR. Verifies the potential of aggregated loads to provide frequency response services by integrating the whole model to the GB master dynamic model which is used at presents by National Grid.
7	Concludes and summarises the thesis, and suggests future work

Chapter 2

Overview of the Frequency Control Strategies and Demand Side Response

This chapter highlights the provision of frequency response to an electric power system and frequency response services in the GB power system. In particular, the question of frequency control in an interconnected power system is addressed. This chapter also reviews the state-of-art research activities in balancing services provided by the demand side response.

2.1   Frequency response services in the GB power system

System frequency is a variable that refers to a second-by-second balance between power demand and generation. The nominal value of the frequency in the GB power system is 50 Hz, with the upper/lower operating limit being set to $\pm$ 1% Hz of the nominal value [8]. The grid frequency rises when there is more generated power than the demand. Conversely, the grid frequency drops when the power consumed by the demand surpasses the production.

The provision of frequency response services in GB is dynamic and non-dynamic [8]. The dynamic frequency response is a service that is used to continuously manage the second-by-second changes in the system frequency. Meanwhile, the non-dynamic frequency response is usually a discrete service that is triggered at a pre-defined change in the frequency. The frequency response of the GB power system is obtained through services that are described in the following subsections.

2.1.1 Mandatory frequency response service

National Grid procures frequency response services from the generators through a Mandatory Frequency Response (MFR) service [9]. All large generators (based on their connection agreement)[4] can provide an automatic change in their power output in response to a frequency change. The MFR service is provided through three types of frequency response services. Primary, secondary and high-frequency response services. The primary low-frequency response service is the provision of an additional active power (or a decrease in demand) within 10 seconds of sensing a large drop in frequency, which continues for a further 20 seconds. The secondary response service is the provision of a low-frequency response within 30 seconds after a large frequency drop, which lasts for another 30 minutes. In the high-frequency response service, the generators' active power is reduced within 10 seconds of detecting a large frequency rise, which continues until the frequency is restored to 50Hz.

2.1.2 Firm frequency response service

The Firm Frequency Response (FFR) is an alternative service that counters the same incidents as MFR [10]. It is often open to any consuming or generating plant that can meet the service requirements. National Grid procures an FFR service by competition tender, which allows a provider to bid a service by either reducing demand or increasing the generation when instructed by National Grid. The FFR service can be provided by either:

- *Dynamic Service* where electricity demand changes continuously to maintain the normal operation of grid frequency.
- *Non-dynamic Service* where electricity demand changes occur at a defined frequency deviation value and remains at a set level.

---

[4] Generators with capacity equal or larger than 100 MW in England and Wales and equal or larger than 10 MW in Scotland.

In this service, National Grid instructs the FFR providers to set their units into frequency sensitive mode for dynamic response or they use an automatic relay for a non-dynamic response. This will then automatically change the unit's output in response to changes in system frequency. The frequency response providers must deliver at least 10MW of frequency response to participate in the FFR service.[5]

2.1.3 Frequency control by demand management service

The Frequency Control by Demand Management (FCDM) provides frequency response through the interruption of customers demand [12]. In the existing GB power system, some of the electricity demand is automatically interrupted when the system frequency transgresses the low-frequency relay setting on-site (typically 49.7Hz). The demand usually requires a manual reconnection when the frequency is restored to the nominal value.

2.1.4 Enhanced frequency response service

The Enhanced Frequency Response (EFR) is a dynamic frequency response service that is used to stabilise the grid frequency at closer to 50Hz [8]. To participate in this service, the EFR providers must automatically deliver a minimum of 1MW of frequency response within one second in response to frequency change. The frequency response can be obtained from a single load (or generator) unit or it may be aggregated from several units.

---

[5] The threshold for participating in Firm Frequency Response service might be reduced in the future to increase the accessibility for smaller market participants [11]

2.2 Frequency control of the power system

The system frequency should be maintained nearly constant to ensure the stable operation of the power system. The frequency is highly dependent on the active power change because most generators are directly coupled to the grid. The frequency deviation is a direct result of an imbalance between the active power of the electrical load and the power supplied by the connected generators. A large frequency deviation can damage equipment, degrade load performance, cause the transmission lines to be overloaded and it may interfer with the system protection schemes that lead to an unstable condition for the power system as a whole. [13]

In real power systems, there are three typical control actions to maintain the stability of the grid frequency [14] (as shown in Fig. 2.1), as follows:

- The primary control service is an automatic frequency control action that is provided by generators (i.e. droop control loop in Fig. 2.1) and the load responds within a few seconds to the change in grid frequency. The primary service aims to manage a small frequency deviation.

- The secondary control service is used to manage a larger frequency deviation. The secondary control loop (see Fig. 2.1) initialises a centralised and an automatic control task, which drives the generator to provide an additional real power change within 5–10 minutes after the event and can be continued until the frequency is restored to the nominal value. This service can be also provided by demand.

- The tertiary control service is used for a severe power mismatch between supply and demand and is associated with a fast rate of change in grid frequency. The tertiary control action, often known as a manual frequency control, is typically provided by stand-alone generators that respond in the timescale of tens of minutes up to hours after a frequency event.
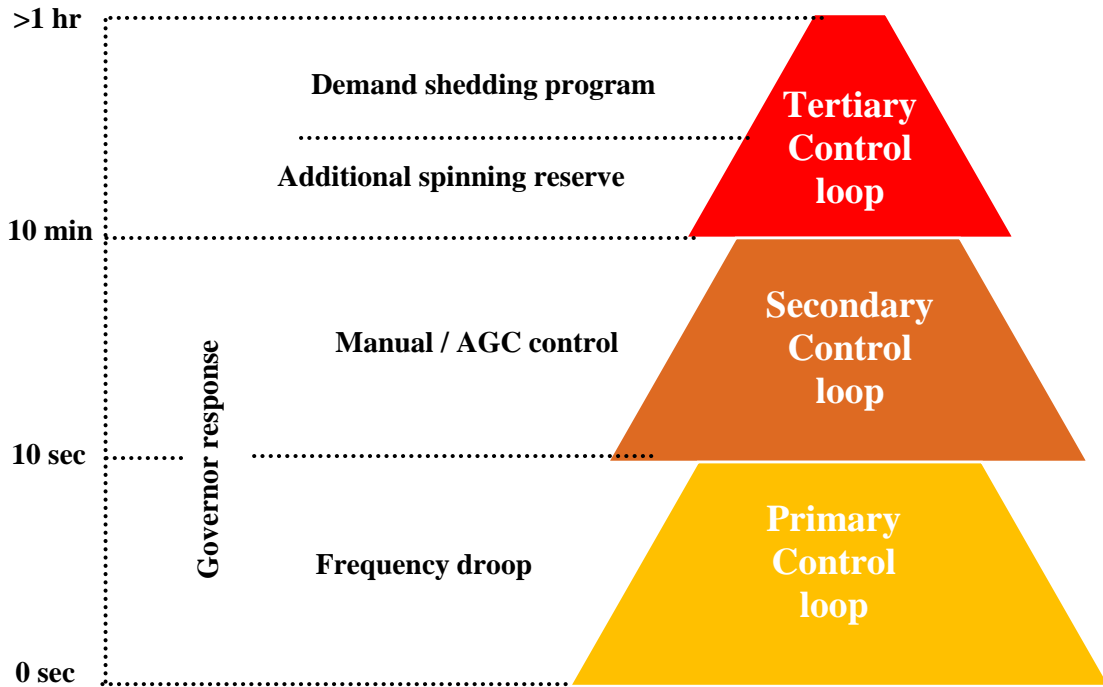
Fig. 2.1 Frequency control loops in a power system [13]

In the GB power system, the uncertainty in demand forecasting is met by ensuring a sufficient amount of spinning reserve from large-scale generating units driven by nuclear and fossil fuel sources. These generators alter their active power output in response to the frequency change. Fig. 2.2 shows the frequency control and stability of the GB power system [15]. Under the normal operating condition, frequency deviation needs to be maintained within ± 0.2Hz of the nominal grid frequency. For a sudden loss of generation or demand changes up to 300MW, the maximum frequency deviation is limited to ± 0.2 Hz. For a sudden loss of generation or demand changes to 300MW but less than 1,320MW, the maximum frequency change is limited to ± 0.5Hz of the nominal grid frequency. For a sudden loss of generation or demand changes to 1,320MW but less than 1,800MW, the maximum frequency change is limited to - 0.8Hz with frequency restored to 49.5Hz within 1min.
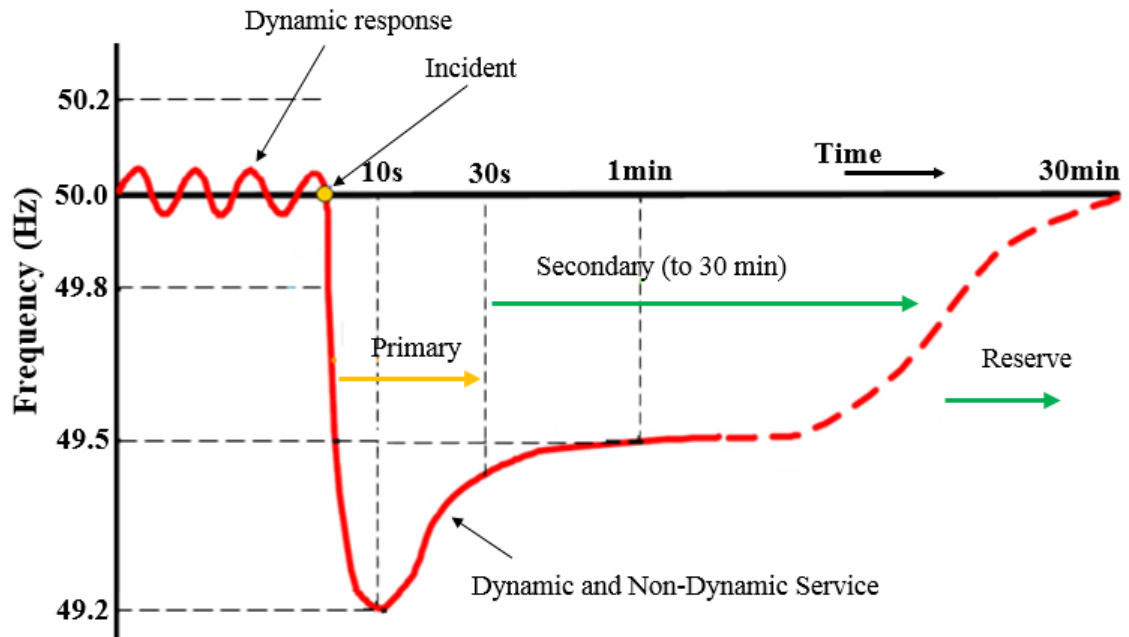
Fig. 2.2 Frequency control and stability of the GB power system [15]

2.2.1 Frequency control from the generation side

In a large power system, synchronous generators are directly coupled and, hence have the same frequency value (i.e. 50 Hz in the GB power system) [16]. Consequently, the frequency control of a power system can be illustrated as the frequency control of one lumped generator unit. The schematic block diagram of one synchronous generator is described in Fig. 2.3 [17]. The change in load is expressed as an instantaneous change in the electrical torque output T_e of the generator. The imbalance between the mechanical torque T_m and electrical torque T_e refers to the frequency variations in the system according to the equation of motion. The governor (speed changer) has two inputs:

1. The change in the reference power (ΔP_{ref}), which is either adjusted manually by the system operator or automatically using AGC control system.
2. The change in the speed of shaft (w_m), which results from the imbalance between T_m and T_e.

Controlling the frequency is accomplished by controlling the mechanical output torque (T_m). The governor adjusts the position of the steam valve to control the

15

mechanical torque output (T_m). When the level of the reference power P_{ref} is increased, the governor moves the steam valve to a more opened state to increase T_m. When P_{ref} is decreased, the governor moves the steam valve to a more closed state to decrease T_m. The governor also monitors the shaft speed w_m, which is used as a feedback signal to maintain the balance between T_m and T_e. If T_m is higher than T_e, then w_m increases and the governor reduces the valve inlet to reduce T_m. Similarly, if T_m is less than T_e, then the governor extends the valve inlet to increase T_m.
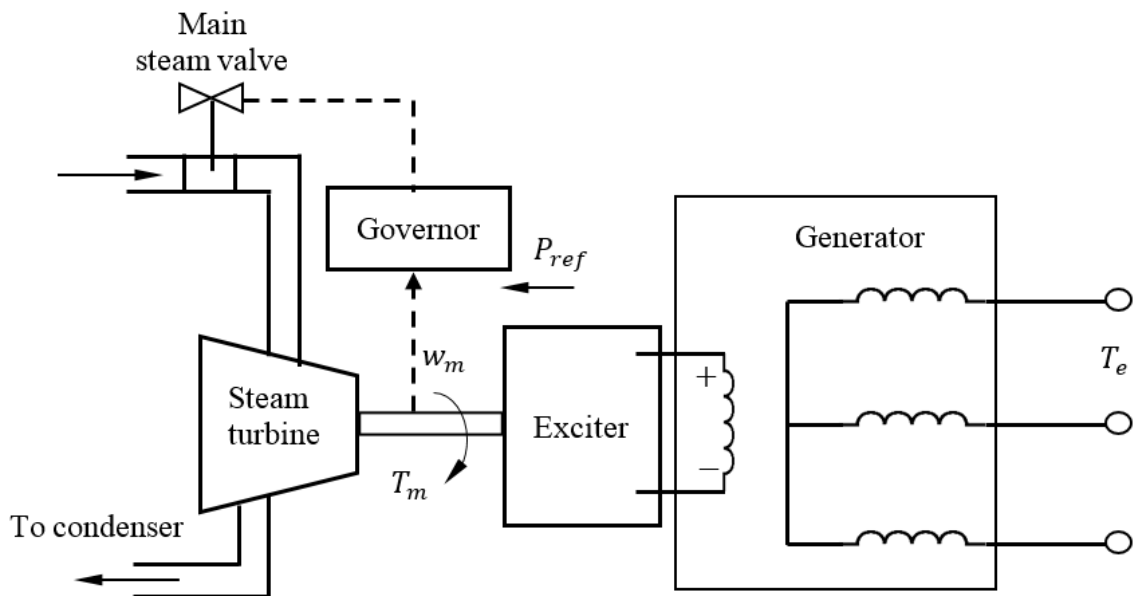
Fig. 2.3 Schematic block diagram of a synchronous generator [17]
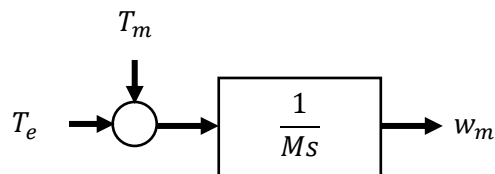
Fig. 2.4 The transfer function relating the speed and torque of synchronous generator [17]

Fig. 2.4 shows the relationship between shaft speed as a function of T_m and T_e. However, for load frequency studies, it is more likely to express this relationship in terms of mechanical and electrical power instead of torque. The relationship between power P(W) and torque T(N.m) is given by Equation (2.1), where w_m (rad/sec) is the angular velocity of the shaft [13].

$$P = w_m.T \tag{2.1}$$

The power can be written as the sum of the steady-state value and a derivative term,

$$P = P_0 + \Delta P \tag{2.2}$$

Similarly, the speed of torque and shaft are written as follows

$$T = T_0 + \Delta T \tag{2.3}$$

$$w = w_{m0} + \Delta w_m \tag{2.4}$$

Deriving Equation (2.1) at the equilibrium value and with respect to time yields the following Equation

$$\Delta P = w_{w0}\, \Delta T + T_0\, \Delta w_m \tag{2.5}$$

Therefore,

$$\Delta P_m - \Delta P_e = (w_{m0}\, \Delta T_m + T_0\, \Delta w_m) - (w_{m0}\, \Delta T_e + T_{e0}\, w_m) \tag{2.6}$$

For a steady-state value; that is $T_{m0} = T_{e0}$,

$$\Delta P_m - \Delta P_e = w_{m0}\, (\Delta T_m + \Delta T_e) \tag{2.7}$$

The net torque (T_{net}) is related to the speed change as follows

$$T_{net} = \Delta T_m + \Delta T_e = I \, d/dt(\Delta w_m) \tag{2.8}$$

From Equations (2.7) and (2.8), Equation (2.9) can be rewritten as

$$\Delta P_m + \Delta P_e = w_{m0} \, I \, d/dt(\Delta w_m)) \tag{2.9}$$

where I (kg.m^2) is the moment of inertia of the generator and turbine. The quantity $w_{m0}I$ is called angular inertia constant and can be denoted by $2H$ [18]. Therefore, Equation (2.9) is rewritten as

$$\Delta P_m + \Delta P_e = 2H \, d/dt(\Delta w_m) \tag{2.10}$$

In general, loads in power systems are a mixture of miscellaneous electrical devices. For instance, lights as resistive loads are independent of frequency. In the case of motors, their consumption changes with frequency due to changes in the motor's speed. Therefore, the change of electrical power ΔP_e due to changes in frequency is expressed as [13]:

$$\Delta P_e = \Delta P_L + D \, \Delta w_m \tag{2.11}$$

where ΔP_L is a non-frequency sensitive load change, $D \, \Delta w_m$ is a frequency sensitive load change, and D is the load damping coefficient. The damping coefficient D is often equal to 1.5% change in load for one percent change in frequency [19]. For instance, a typical value of 1.5 of D means a 1% change in the frequency would trigger a 1.5% change in frequency sensitive load. By combining Equations (2.10) and (2.11), and taking Laplace Transform to the outcome, Equation (2.12) is obtained, which is represented in Fig. 2.5.

18

$$\Delta P_m + \Delta P_L = \Delta w_r (2Hs + D) \tag{2.12}$$
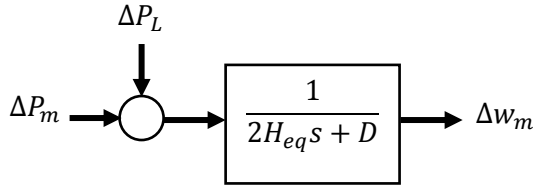
Fig. 2.5 The transfer function of a synchronous generator including the effect of the load damping [17]

2.2.2 Frequency control in the GB power system

A simplified governor-generator model of the GB power system was developed in [20] and is shown in Fig. 2.6. This model is used for power system frequency analysis and control design. First order transfer functions are used to model the governor-turbine.
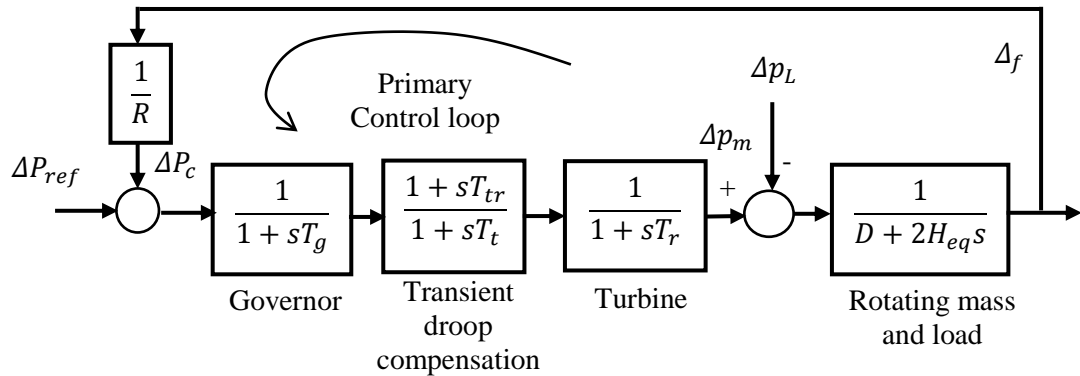
Fig. 2.6 GB power system primary frequency control model [20]

The governor and turbine time constants (T_g, T_t, T_{tr}, and T_r) are tabulated in Table 2.1 [19]. For the provision of a primary response, all generators should have a governor droop setting (R) between 3%−5%, according to the GB Grid Code [21]. The droop gain (R) is defined by the ratio of frequency change Δf to the change of generator power output ΔP, as shown in Fig. 2.7. The purpose of the turbine-

governor control is to maintain the desired system frequency by adjusting the mechanical output power of the turbine ΔP_m.

Table 2.1 Parameters of the Simplified Power System

1/R (MW/Hz)	T_g(sec)	T_{tr}(sec)	T_t(sec)	T_r(sec)	K_i
20	0.2	2	20	0.3	0.05
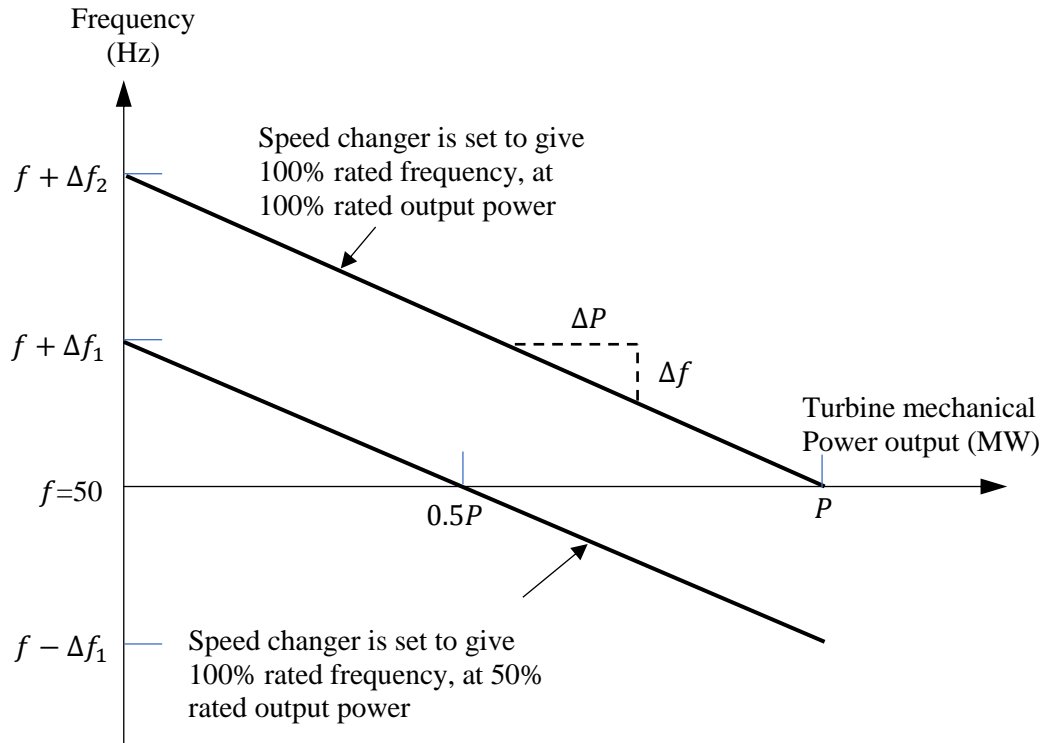
Fig. 2.7 Steady-state frequency-power relationship of a turbine-governor control [17]

The frequency-power relationship of turbine-governor control is shown in Equation (2.13):

$$\Delta P_c = \Delta P_{ref} - \frac{1}{R} \times \Delta f \tag{2.13}$$

The term $\Delta P_c - \Delta P_{ref}$ is denoted by ΔP, and the droop gain is defined as

$$-R = Slope = \frac{\Delta f}{\Delta P} \tag{2.14}$$

The governors use droop control to regulate the power output of the generators in response to frequency deviations. This is referred to the primary frequency control, which is provided automatically by governors. For example, if the demand power is increased (or the generation power is decreased) and this causes a drop in frequency, then the low-frequency response is provided automatically by the governors. Similarly, for a loss in demand (causing a frequency rise), a high-frequency response service is provided by the governors.

There are two modes of frequency control operation [22]; frequency sensitive mode (FMS) and limited frequency sensitive mode (LFSM). As shown in Fig. 2.8(a), FSM is used to maintain the frequency within the range (49.5–50.5 Hz) by using droop control. The limited frequency sensitive mode is only used to provide a high-frequency response; that is, when the frequency rises more than 50.4 Hz. In this mode, the generators must reduce their output power by a minimum of 2% for every 0.1 Hz increase above 50.4 Hz, as seen in Fig. 2.8(b).

Active Power (MW)

to 47Hz

Deadband<0.03 Hz

49.5   50.5   52 $f(Hz)$

Droop 3-5%

Power reduction =2%
output for each 0.1 Hz
above 50.5 Hz

(a) Power/frequency characteristic for FSM

Power (MW)

Power reduction =2%
output for each 0.1 Hz
above 50.4 Hz

$f(Hz)$

47Hz   49.5Hz   50Hz   50.4Hz
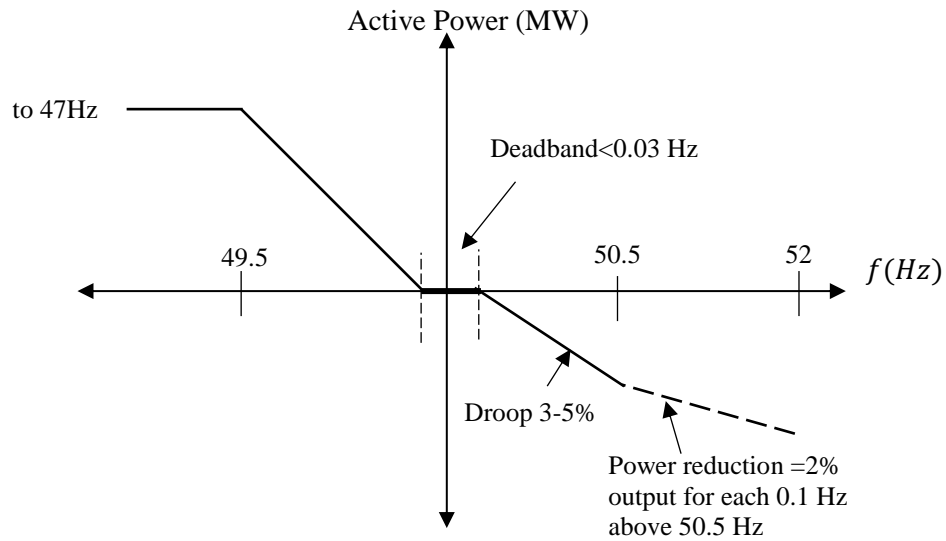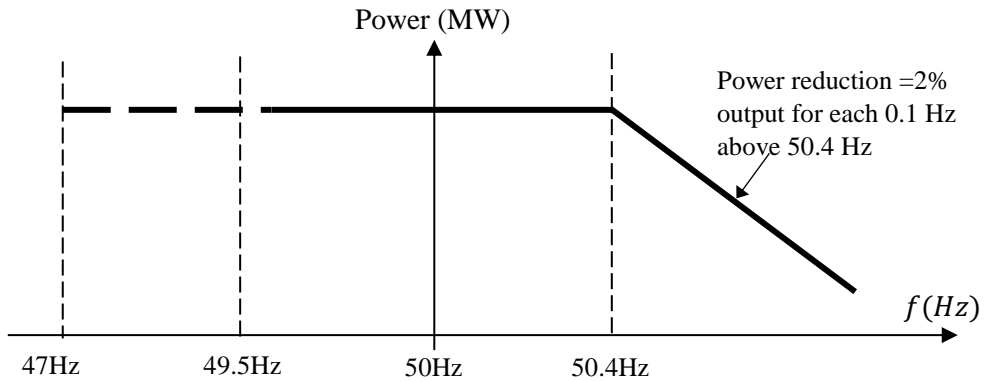
(b) Power/frequency characteristic for LFSM

Fig. 2.8 Modes of Frequency control operation of generators [22]

2.3 Impact of renewable generation on system inertia and the rate of frequency change

System inertia is the sum of kinetic energy that is stored in the rotating mass of the generators that are directly coupled to the system. It is a key measure of how resilient the system is in response to changes in grid frequency [23]. In the simplified model that was presented in Section 2.2.2, system inertia is represented by the inertia constant (as shown in Fig. 2.6). The inertia constant of each generating unit (H_{gen}) is set according to the generator type. Table 2.2 illustrates the inertia constant of different types of generators in the GB power system [24]. The equivalent system

22

inertia (H_{eq}) is defined based on Equation (2.15), where S_{gen} (in MVA) is the power rating of each power plant, S_{sys} (in MVA) is the total power rating of the system, and N is the number of power plants [24-26].

Table 2.2 Inertia constant of different generators [24]

H_{gen}	H_{coal}	H_{gas}	$H_{nuclear}$	H_{CCGT}	$H_{interconnetor}$	H_{wind}
Value (sec)	4.5	6	3	9	0	0-4

$$H_{eq} = \Sigma_i^N H_{gen} \times \frac{S_{gen}}{S_{sys}} \tag{2.15}$$

The large synchronous generators naturally provide the majority of the system inertia in the GB power system. Meanwhile, the non-synchronous generators are connected to the network via different technologies of power electronics and, hence, have a lower and different contribution to system inertia compared to synchronous generators. However, the volume of non-synchronous generation (e.g. wind and solar power plants) connected to the system and the received power through interconnectors are expected to increase rapidly and significantly over the coming decades. The changing landscape of the power system and the increasing prevalence of converter-connected generation will decrease the system inertia and cause the Rate of Change of Frequency (RoCoF, as measured in Hz/sec) to become more rapid [23, 25, 27]. The RoCoF is an important measure of how strong the power system is, especially at an early stage following the frequency incident (as shown in Fig. 2.9) [28]. The response rate action required from generators connected to the system after a large frequency deviation to hold the RoCoF is expected to increase in the future. Table 2.3 shows the future response rate needed to achieve fast action following a frequency event with the reduction of system inertia according to the National Grid's ''slow progression'' and ''Gone Green'' scenarios [27].

23

Frequency (Hz)

50 Hz

RoCoF based protection
operators ~500ms

Demand disconnection

49.2 Hz

48.8 Hz

Time

Instantaneous infeed
loss

Primary frequency
response fully delivered
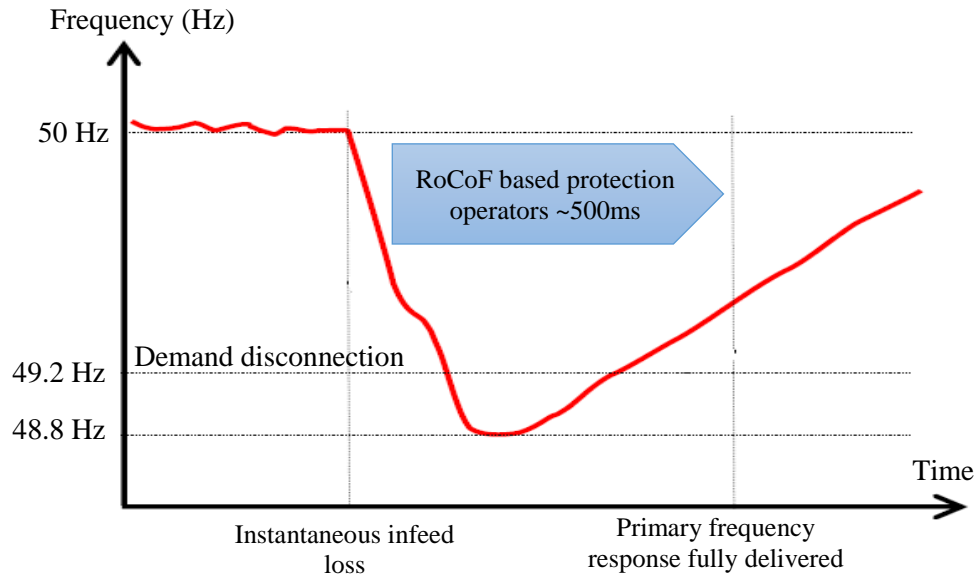
Fig. 2.9 Grid frequency during a frequency event [28]

Table 2.3 Future ramp rate requirements with decreasing system inertia [27]

RoCoF (Hz/s)	Slow Progression	Gone Green	Inertia (GW.sec)	Action Time (to reach 49.2Hz)	Response Rate (MW/s)
0.125	2013/14	2013/14	360	9	185
0.2	2019/20	2018/19	225	4	400
0.22	2022/23	2019/20	205	3.4	489
0.25	2023/24	2020/21	180	2.4	679
0.3	2024/25	2021/22	150	1.2	1148

Two approaches are assumed to maintain the stability of the system frequency and restrict the RoCoF under the conditions of an expected reduction in system inertia. The first approach, as outlined in Fig. 2.10(a), is a more traditional approach because it is based on the existing arrangements (which requires more numbers of large and costly power plants). The arrangements based on this approach are expected to

24

increase CO_2 levels and cost the UK £250 million per annum by 2020 [27]. The second approach, as outlined in Fig. 2.10(b), is a smart method that is based on possible arrangements that use smart solutions obtained from a range of resources. These solutions can be implemented at a reasonable cost to the system and they produce less CO_2 emissions. This approach can be implemented through the following services:

- Demand Side Response (DSR) service, which can provide a rapid deloading to the network in response to signals corresponding to high RoCoF.

- Frequency control-based energy storage services.

- Synthetic inertia service, which can be achieved by reprogramming the power converters coupled to the wind turbines and photovoltaic (PV) so that they imitate the behaviour of synchronous generators.

- Aggregated diesel generators, which can add real rotating inertia to the system.

- Another smart service can be obtained by controlling the power output of some other renewable energy resources, such as solar PV systems, in response to changes in the system frequency.

(a) Traditional Approach

(b) Smart Approach
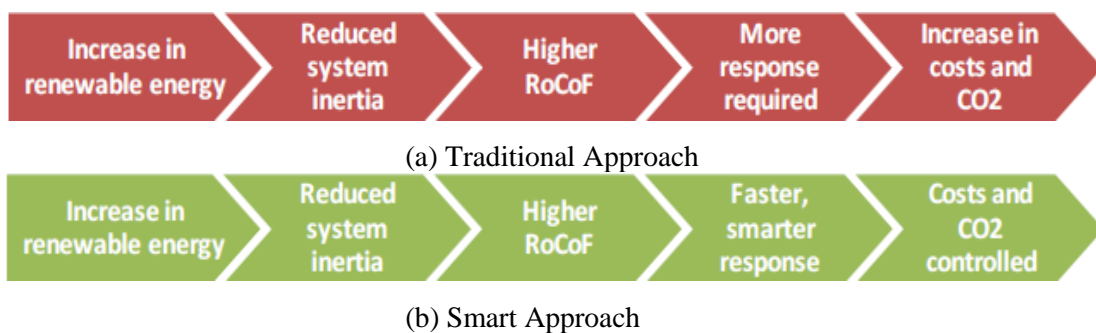
Fig. 2.10 Consequences of renewable energy [27]

2.4 Frequency control in an interconnected power system

In an isolated power system, one generating unit is designed as a regulating unit and would be manually adjusted to maintain system frequency at the desired value. The remaining units are controlled with speed droop to share the load in proportion to their rating. However, in the interconnected power system, many units in the system can participate in regulation, reducing wear on a single unit's control and improving overall system frequency efficiency, stability, and economy [13]. The interconnected power system consists of multi-areas that are connected to each other by high voltage AC (and sometimes DC) transmission tie-lines. Each control area is considered as a coherent system consisting of a group of generators and loads, where all generators respond to the changes in load or speed changer settings [13, 19]. The change of frequency measured in each area is an indicator of the change of the power mismatch between generation and demand in the same area and other interconnected areas. In the interconnected power system, a supplementary (i.e. secondary) frequency control (which often refers to an Automatic Generation Control (AGC) controller) should control the frequency of the area and also the power interchange with other control areas. The model presented in Fig. 2.6 must be modified by including the tie-lines model to describe the generalised model of the interconnected power system. Fig. 2.11 illustrates the schematic diagram of N-controlled areas connected through transmission tie-lines with reactance X_{ij}. Each controlled area can be represented by an equivalent generating unit exhibiting its overall performance. The composite model is used to simplify the analysis of the interconnected system model because the inter-machine oscillations at each area are not the main concern. The power flow through the tie-line from area (A_1) to area (A_2) is represented in Equation (2.16).
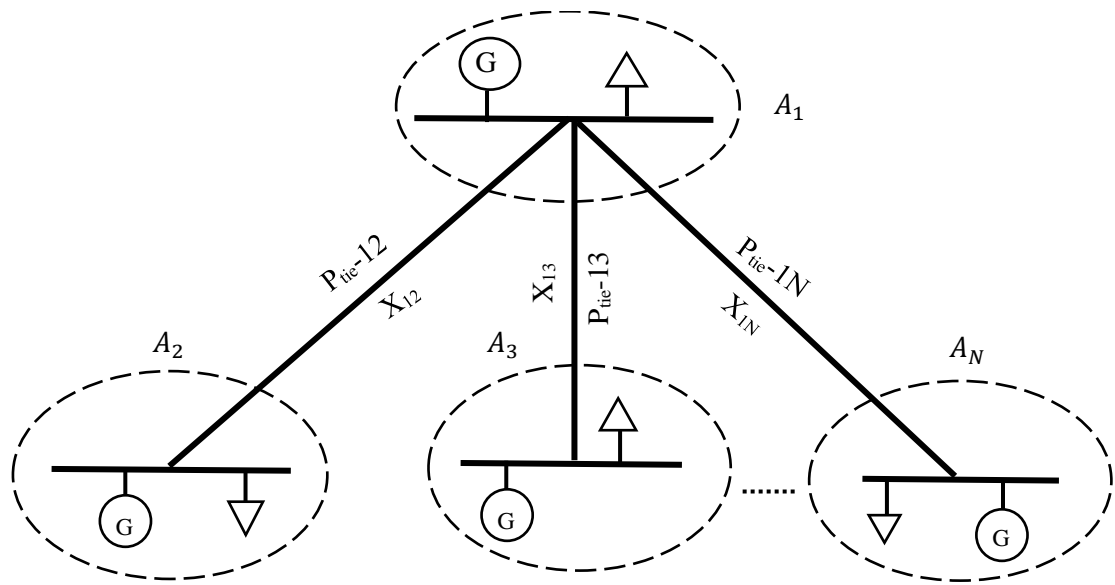
Fig. 2.11 A schematic diagram of an N-control areas power system [13]

$$P_{tie,12} = \frac{E_1 E_2}{X_{12}} Sin(\delta_1 - \delta_2) \qquad (2.16)$$

where E_1, E_2 are the voltages (in p.u.) at equivalent machines of A1 and A2; and δ_1, δ_2 are the angles (in p.u.) of equivalent machines of A1 and A2. By deriving Equation (2.16) at the initial operating point, represented by $\delta_1 = \delta_1^0$ and $\delta_2 = \delta_2^0$, Equation (2.16) can be rewritten as follows

$$\Delta P_{tie,12} = T_{12}(\Delta \delta_1 - \Delta \delta_2) \qquad (2.17)$$

where T_{12} represents the synchronizing torque coefficient given by

$$T_{12} = \frac{E_1 E_2}{X_{12}} Cos(\delta_1^0 - \delta_2^0) \qquad (2.18)$$

By considering the relationship between the power angle and frequency and taking Laplace Transform to the outcome, Equation (2.17) is rewritten as follows

$$\Delta P_{tie,12}(s) = \frac{2\pi}{s} T_{12}(\Delta f_1(s) - \Delta f_2(s)) \qquad (2.19)$$

27

Similarly, the net power interchange between A₁ and A₃ is given in Equation (2.20):

$$\Delta P_{tie,12}(s) = \frac{2\pi}{s} T_{13}(\Delta f_1(s) - \Delta f_3(s)) \qquad (2.20)$$

The result of the total tie-line power change through N-control areas is represented in Equation (2.21).

$$\Delta P_{tie,i} = \frac{2\pi}{s}\left[\sum_{\substack{j=1\\j\neq i}}^{N} T_{ij}\,\Delta f_i - \sum_{\substack{j=1\\j\neq i}}^{N} T_{ij}\,\Delta f_j\right] \qquad (2.21)$$

Equation (2.21) can be represented by a block diagram, which can be added to the mechanical power mismatch ($\Delta P_m - \Delta P_L$) that was described in Fig. 2.6. Hence, the simplified block diagram of the interconnected power system is shown in Fig. 2.12.
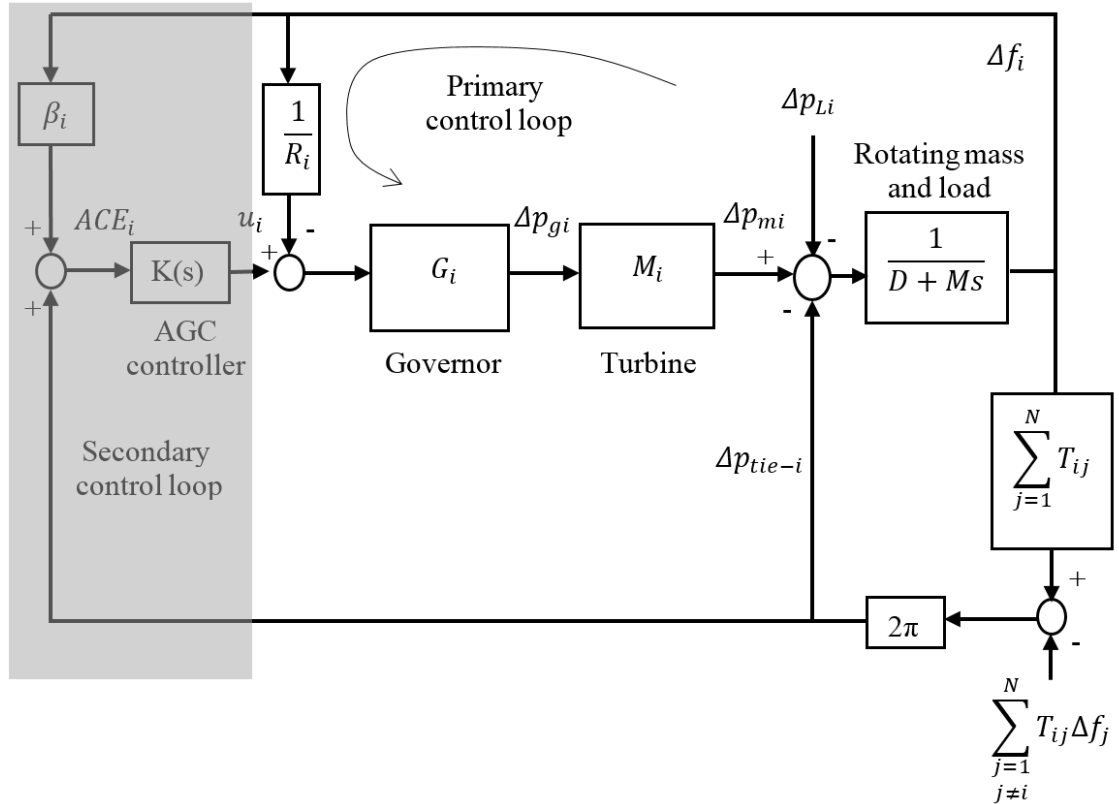
Fig. 2.12 A simplified interconnected power system with AGC controller [13]

The turbine-governor block diagrams (G_i and M_i) have three representations: non-reheat steam unit, reheat steam unit, and hydraulic unit [13]. The shaded block in Fig. 2.12 represents the secondary control loop in a presence of a tie-line. The secondary controller is not only responsible for regulating the area's frequency, but it also maintains the net interchange power with neighbouring area(s) at scheduled values. The tie-line power flow change (Δp_{tie-i}) is added to the frequency change (Δf_i) through a secondary feedback loop. The area control error (ACE_i) signal is then computed as shown in Equation (2.22) and applied to the controller K(s):

$$ACE_i = \Delta P_{tie,i} + \beta_i\,\Delta f_i \tag{2.22}$$

where β_i is a bias factor, which can be obtained according to Equation (2.23) [13]:

$$\beta_i = \frac{1}{R_i} + D_i \tag{2.23}$$

In the case of area frequency drop occurrence, the AGC controller $K(s)$ will correct the value of ACE_i (drive it back to zero) and send the control signal to the governor. That is, to regulate the area frequency and maintain the net-interchange power at scheduled level.

2.5 Automatic generation control-value and strategies

Interconnected power systems consist of control areas representing a group of generators with similar frequency. These generators are not only responsible for controlling the power mismatch of the current area, but they also regulate the frequency of all the interconnected areas through a contractual tie-line power exchange. As explained in Section 2.2.2, every generator must have a primary droop controller for the provision of primary frequency response under normal operation. However, the primary frequency control action is sometimes insufficient to cope

with the frequency, especially in an interconnected power system. In addition, the primary controller does not control the interchange power between the control areas. Therefore, a secondary frequency controller (i.e. AGC) is required to adjust the power output of some generators, maintain the net interchange power between the interconnected areas at scheduled value, and correct the value of ACE_i in response to any frequency change. The value of the AGC controller is summarised in the following:

- AGC is a significant control process that continuously balances the generation and demand at minimum cost, especially in a modern complex power system with a large number of constraints [29].
- AGC provides an automatic action that helps to maintain the power interchanges over the tie-lines at scheduled levels.
- For a control system-based computer, AGC can be the most economical unit to adjust.
- The uncertainties issues involved in the operation and control of power systems have become increasingly challenging. An example of these uncertainties is the lack of complete knowledge of the perfect value of system inertia and other system parameters. These uncertainties can be represented using appropriate modelling of a robust AGC controller [13].

The existing implemented AGC system is based on steady state assumptions. However, with fast and persistent fluctuations caused by wind and solar generation, the frequency regulation in systems can no longer be viewed as steady-state problem. Thus, the structure of AGC can be changed and further utilize the new structure to systematically provide fast frequency response. Over the past few decades, many control strategies for AGC control system and optimisation techniques have been studied [30-33]. This section places emphasises on the AGC control configurations with the latest achievements. It appears that the most significant improvements that were achieved in the AGC design appeared to cope with system uncertainties, changing of a controller's structure and system

nonlinearities. The main design of the AGC controller is based on classical, adaptive, intelligent, and robust concepts.

The classical AGC controller consists of a proportional integral (PI) [34, 35] and proportional integral derivative (PID) [36-38]. The integral controller is used to bring the frequency deviation back to zero after the frequency event, while the derivative term is applied to improve the transient response after the event. The problem with the classical controllers is that their parameters are fixed during the time, which causes the system to be less robust against the operating constraints. Recently, several approaches have been used to improve the behaviour of the classical controllers. For example, adaptive and self-tuning methods were used to find the optimal parameters of the controller, which make the behaviour of PI/PID more efficient during the time [39-41]. The idea of these approaches is to tune the controllers' parameters around a certain limit using several fitness functions to increase the robustness of the system in response to the operating adversities (e.g. changing the system parameters over time). In recent years, modern intelligent approaches have been widely considered in the literature, such as Fuzzy Logic Control (FLC), Multiagent Systems, Genetic Algorithms (GAs), Particle Swarm Optimisation (PSO), Ant-Colony Optimisation, and some other new methods for AGC. Artificial intelligent methods can cover a wider range of operating constraints than the traditional controller because they mimic the human's natural ability to control nonlinear and complex systems. The following two FLC approaches have been recognised in the AGC system:

i.   Dynamic Fuzzy Controller [42-45]. A general scheme for a fuzzy logic based AGC system is shown in Fig. 2.13. The fuzzy controller has three main parts:

   a. **Input**: This is the fuzzifier part where the crisp input is fuzzified into a truth input by using inputs membership functions (MF). In a FLC-based AGC system, the input signal is usually the area control error (ACE). The ACE is considered to be a disturbance to the system and it must be reduced to zero as soon as possible.

b. **Fuzzy Inference System (FIS)**: This is the central part of the fuzzy rules base, which identifies the necessary fuzzy logic rules to control the input signal. The rule base emulates the skills and abilities of a human operator who decides how to manage the behaviours with minimum error and fast response.

c. **Output**: This part represents the controller action (u) where the fuzzy output is converted into crisp output using output MF.

ii. The other FLC-based AGC category is the PI and PID in the form of FLC [46-49]. FLC is used as an elementary source to tune the controller parameters. The PI gains are driven by a set of control rules chosen based on experience. An FLC-like PI control has achieved better response and wider capability to cover a large range of system parameters uncertainties [49]. Other methods consider the combination of optimisation methods, such as PSO and GA as with FLC [49]. Optimisation techniques are used to tune the MF of the FLC-based AGC controller. The online optimisation increases the robustness and performance of the system because the controllers' gains are updated throughout time. References [49, 50] have presented an intelligent online approach by using a combination of FLC and the PSO method to optimally tune the PI controller and they concluded that the proposed method is superior to the pure fuzzy PI controller.
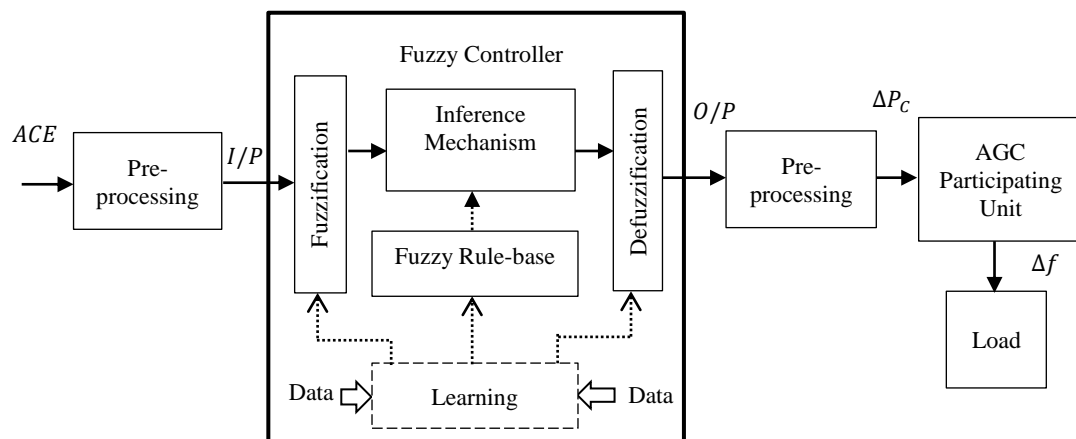
Fig. 2.13 Basic scheme for a fuzzy logic based AGC [14]

Another approach for the AGC scheme is the design of H_∞ and multi-objective H_2/H_∞ based AGC control [13, 51, 52]. In these methods, the designer can model the system uncertainties, such as time delay and parameters uncertainties. The controller is then used to control all of these uncertainties. The H_∞ unit is used to increase the robustness of the close-loop system against system uncertainties, while H_2 is used to minimise the effect of the ACE and achieve fast frequency response with small overshoot.

The AGC controllers based H_∞ and combined H_2/H_∞ algorithms require a high order dynamic control system, which is impractical for industry purposes. There are, however, alternative approaches which require less computational calculations, such as those from the pole placement family[6]. Unlike those methods that rely on gain optimisation, the main synthesis of pole placement is to shift the system roots from an unstable (or undesired) region and positions them into a stable region [53-55]. With these controllers, the designer can decide where to assign the system close-loop poles to change the system behaviour in a more favourable way. Frequency decline-based pole placement and adaptive pole placement approaches in an interconnected power system were introduced by [56, 57] in the presence of high penetration of wind generation.

The deadbeat controller has also come under the pole placement control family, and it has been studied analytically and numerically by many researchers [58-60]. However, the deadbeat controller adds improving roots to the system, which eliminate the effect of the undesired roots and, hence, increase the stability and performance of the system. The main merits of the deadbeat controller are its ability to achieve a precise behaviour and it satisfies the requirement for a very fast transient response. So far, and to the author's best knowledge, no deadbeat control synthesis has yet been carried out on an AGC control system. Chapter Three of this thesis will consider the modelling of a novel adaptive deadbeat (ADB) controller, which represents the AGC controller in an interconnected power system.

---

[6] Pole placement is a method employed in feedback control system to place the closed-loop poles of a system in pre-determined location in the s-plane.

2.6   Demand side response

The volatility of renewable generation sources poses significant challenges to the operation of the power system. In this section, the contribution of demand to the power system is addressed.

2.6.1   Demand side response: concepts and benefits

The electrification of heating and transport energy loads by heat pumps and electric vehicles and the increase in the UK population will change the characteristics of underlying electrical demand. Demand side response (DSR) can make an important contribution to the GB power system if it is used correctly. DSR can be described as the end-users changing their usage pattern of power in response to a signal, as described in [61-63]. From the perspective of market operators, controllable loads are another source that can help to balance the power supply with the demand. As shown in Fig. 2.14, loads can be engaged in the balancing services and can offer many services to the system, such as load shifting, peak clipping, valley filling and load shedding services [64]. In the load shifting service, as shown in Fig. 2.14(a), a DSR can redistribute the end-users' electricity demand to other times of the day without undermining the overall energy consumption of the loads. The peak clipping service shown in Fig. 2.14(b) aims to reduce the system demand during the peak demand period [65]. In valley filling service, as shown in Fig. 2.14(c), the off-peak periods are filled by demand. In an emergency frequency occurrence, load shedding service can be used as a control action to manage the demand during a frequency incident, as shown in Fig. 2.14(d).
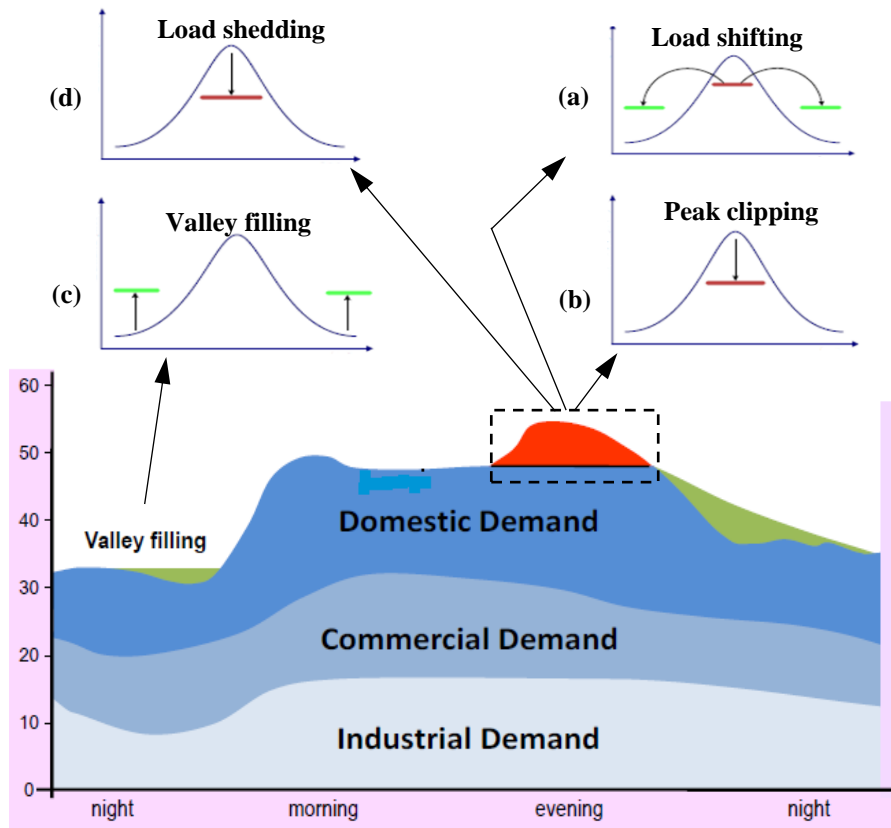
Fig. 2.14 Effect of DSR on the typical GB demand profile (Modified figure based on [62])

The DSR works with three modes [62]. The first two are turn down and turn up modes, in which users temporarily decrease or increase their power consumption. The third mode is to reduce the utility demand by using on-site generation or energy storage. According to [62], there is a potential to use 1–20 GW of unused on-site generation power in the GB's commercial and industrial sector for DSR.

DSR can bring a broad range of potential benefits to the system in terms of system operation, reliability and cost. Previous studies have outlined the benefits of DSR, as follows:

- DSR reduces the generation margin and improves the transmission and distribution network efficiency. DSR also decreases the congestion of demand by converting the passive demand into smart and active demand [15, 66].

- DSR can be applied to the system to provide a primary and secondary frequency response in proportional to a sudden power plant outage. This can be achieved

by reducing or increasing the power consumption of some units, e.g. electric vehicles, heat pumps, air-conditioning, water tanks and other types of flexible units in response to the system frequency [67, 68].

- The benefits of DSR have been demonstrated from economic and environmental perspectives [69-71]. The increase of intermittent renewable power generation requires further frequency response services. To meet the frequency response requirements based on the traditional arrangements not only requires a construction of new costly conventional plants but also will limit the ability of system to accommodate renewable generation. DSR is a cost saving mechanism that can provide a frequency response service in a pattern similar to that provided by frequency sensitive generators. DSR can also be used to reduce the overall generation power during the peak demand period, which is currently supplied by an expensive power plants such as the open gas turbine units [72]. Furthermore, DSR has the potential to deliver financial benefits by deferring a planned reinforcement scheme in GB [73].

- DSR is an environmentally-friendly mechanism because it can displace the peaking generation units and, hence, the CO_2 emissions will be reduced [66, 69].

2.6.2 Potential role of demand side response from the GB domestic electricity sector

In 2015, there were 27,468 million households in GB, which account for 30% of the GB final energy consumption [74, 75]. At the same time, the amount of domestic electricity consumption was approximately 109,706 GWh [74]. This was distributed between space heating (24%), water heating (5%), and lighting and other appliances (71%), as shown in Fig. 2.15 [76]. Hence, the majority of the GB domestic energy relies on the lighting and other appliances category. The diversity according to different lighting and appliances categories is shown in Fig. 2.16. The load characteristics vary between different types of appliances because they are related

to the consumer's use of electricity. For instance, lighting, and TV appliances have an immediate relationship to the consumer; that is, they are required to be turned ON as long as the consumers engage with these appliances. Other appliances, such as heat spacing, washing/drying and cold appliances can operate with a degree of independence from the consumer and, therefore, it is possible to control these units in response to an external signal without harming the comfort of the consumers.
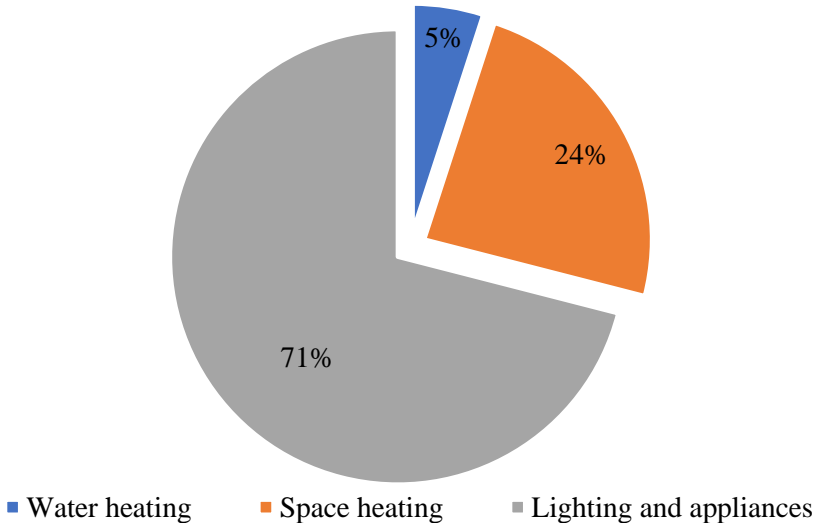
Fig. 2.15 Annual domestic electricity consumption in GB, 2015 [76]
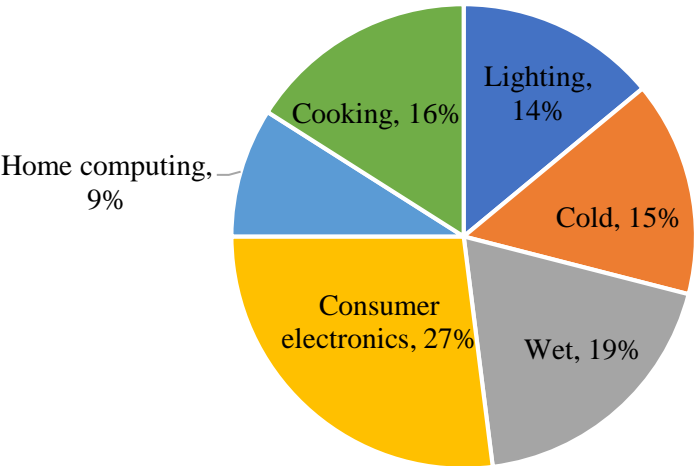
Fig. 2.16 Lighting and appliances annual domestic electricity consumption, 2015 [76]

Flexible demand is useful in the future balancing markets. Future markets can expect long-term energy security, capacity markets and services supporting distribution networks [77]. According to [78], the GB domestic electricity demand will experience a significant increase from the previous years by 2030. Interestingly, the main increase is found in space and water heating (SWH) and wet categories. Fig. 2.17 shows the annual use trends of different domestic load categories between years 2012 and 2030. The use of electricity according to load category is summarised below:

- By 2030, the GB annual electricity demand of SWH is expected to rise from 31,114GWh in 2012 to 34,684 GWh, with less reliance on gas. Reference [78] forecasts that 28% of space heating will be delivered from heat pumps by 2030. The same study assumes that heat pumps will supply 28% of water heating.

- Cold appliances in GB include chest freezers, fridge freezers, refrigerators, and upright freezers. Electricity demand for cold appliances is expected to drop from 13,595 GWh in 2012 to 10,585 GWh in 2030.

- Wet appliances include washing machines, washer dryers, dishwashers and tumble dryers. Wet appliance electricity demand is projected to increase from 15,073 GWh in 2012 to 22,938 GW in 2030.

- Lighting appliances in GB include standard light bulbs, halogens, fluorescent strip lights, and LEDs. Electricity consumption for domestic lighting appliances in GB is predicted to decline from 13,747GWh in 2012 to 12,949GWh in 2030. Standard light bulbs will be replaced by smart energy saving bulbs which will cause a major reduction in light demand.

- The total annual electricity demand for appliances such as TVs, DVD/VCRs, set-top boxes, game consoles and power supplies is predicted to increase from 21,725GWh in 2012 to 26,656GWh in 2030.

- Home computing demand includes desktops, laptops, monitors, printers and multi-function devices. The total annual electricity consumption of home computing appliances is predicted to decline from 6827 GWh in 2012 to 4909 GWh in 2030.

- Cooking appliances include electric hobs, electric ovens, kettles and microwaves. The total electricity demand is predicted to rise from 13,270 GWh in 2012 to 14,337 GWh in 2030.
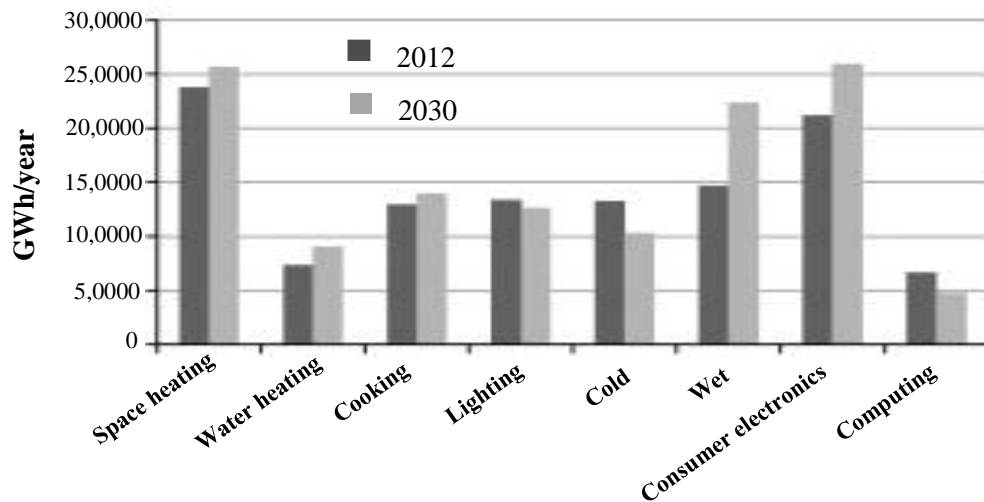
Fig. 2.17 GB domestic electricity demand 2012 and 2030 [78]

The flexibility of demand is measured by the extent of loads to be interrupted as a function of time without undermining the natural control of the load [79]. The key point is to maintain the standard level of comfort to the load owners during the time of load interruption. Appliances that can operate independently from consumers, such as washing machines and fridges, can be more flexible to provide demand response without undermining their primary function [68, 80]. Electric space heating and cold appliances have thermal storage characteristics that allow the load to be curtailed, reduced or postponed in a non-disruptive way. Electric vehicles can be charged and discharged at different times of the day offering load shifting service to the system [77]. However, other devices, such as televisions and lighting, are less flexible because the consumers are usually engaged with their function.

Table 2.4 presents the suitability of different domestic loads that could contribute to the primary and secondary frequency response services, FCDM service and fast reserve service. The primary frequency response service requires loads that can respond to the frequency event with less than 10 seconds and last to a further 20

seconds. For a secondary frequency response service, the load should respond within 30 seconds and continue to a further 30 minutes. In the FCDM service, the domestic load should be curtailed within 2 seconds and it should last for longer than 30 minutes. Fast reserve service requires load response within 2 minutes and it should last to an extra 15 minutes.

Table 2.4 Domestic load suitability to participate in the GB balancing market (modified table based on [77, 78])

	Primary frequency response	Primary frequency response	FCDM	Fast reserve
SWH	Partly seasonal	Partly seasonal	Partly seasonal	Partly seasonal
Cold	Yes	Yes	Yes	Yes
Cooking	No	No	No	No
Wet	No	Partly	Partly	Yes
Consumer Electronics	No	No	No	No
Lighting	No	No	No	No
Home Computing	No	No	No	No
Electric Vehicle	Partly	Partly	Partly	Partly

2.7 Use of demand for frequency control

This section aims to describe the latest strategies that exploit the demand to provide ancillary services of frequency response to continuously balance the supply with demand. Recent studies have demonstrated the concepts and benefits of DSR, although they have not directly referred to a specific load technology. For example, references [71, 81, 82] summarise the technical features and economic benefits of using demand control algorithms. These studies used a stochastic control algorithm and have applied it to the load to stabilize the system frequency. The responsive load in these studies has the potential to provide a considerable operating cost saving and reduce the carbon emissions by replacing the spinning reserve service of the generators with the frequency response service of demand. In [83, 84], large battery

applications for frequency response provision were studied. Battery storage systems can be installed to store the electricity when the solar generation exceeds the demand or when the electricity is cheap. This stored electricity can be then used at a time when it is needed. However, the use of large batteries for frequency response provision implies a large investment cost. However, EVs may be used for the same purpose with less investment cost. In [85-89], a population of EVs were used as a source of demand response to regulate the grid frequency and provide rapid frequency response with the presence of large scale of intermittent wind generation. A dynamic EV frequency control algorithm that considered the travelling behaviour of EV users was developed to drive the EVs charging/discharging in response to changes in the grid frequency [88]. The authors in [89] developed an estimation tool to estimate the 24- hour EV charging load for frequency control study based on statistical analysis and according to the EV type.

Thermostatically controlled loads (TCLs), such as fridges, heat pumps, water heaters, industrial bitumen tanks (BTs) are also flexible candidates for DSR [90-93]. The normal operation of these appliances can be temporarily interrupted without a noticeable effect on the temperature. Because of large number of thermal loads connected to the grid and their thermal storage characteristics, the TCLs could potentially involve a significant economic value throughout the provision of various forms of ancillary services. Two main TCL frequency control algorithms have been used for the provision of frequency response service, namely centralised and decentralised control.

2.7.1 Central control of demand strategies overview

Central control of demand aggregation is a direct load control that requires the support of high-performance communication between the load and the upper layer representors (i.e. the demand aggregators, and system operators). This communication is often referring to as Information and Communications Technology (ICT). The central control of demand has different modelling strategies.

In [94], a central direct load control (CDLC) algorithm is proposed. A comprehensive DSR strategy has been developed to balance the power mismatch between generation and demand. Demand response suppliers that own the central controller use a calculation centre to determine the amount of DSR that is required to regulate the frequency as shown in Fig. 2.18. The frequency, measured at the point of common coupling (PCC) of the microgrid, was assumed as a variable input signal to the central controller. Three operational modes are defined based on the magnitude of the frequency deviation:1) the normal ''mode'' represents the state in which no control action is required, 2) the ''event mode'' represents the duration of the frequency being out the desired range, and 3) the ''third mode'' is proposed when the frequency is recovered to the normal operation.
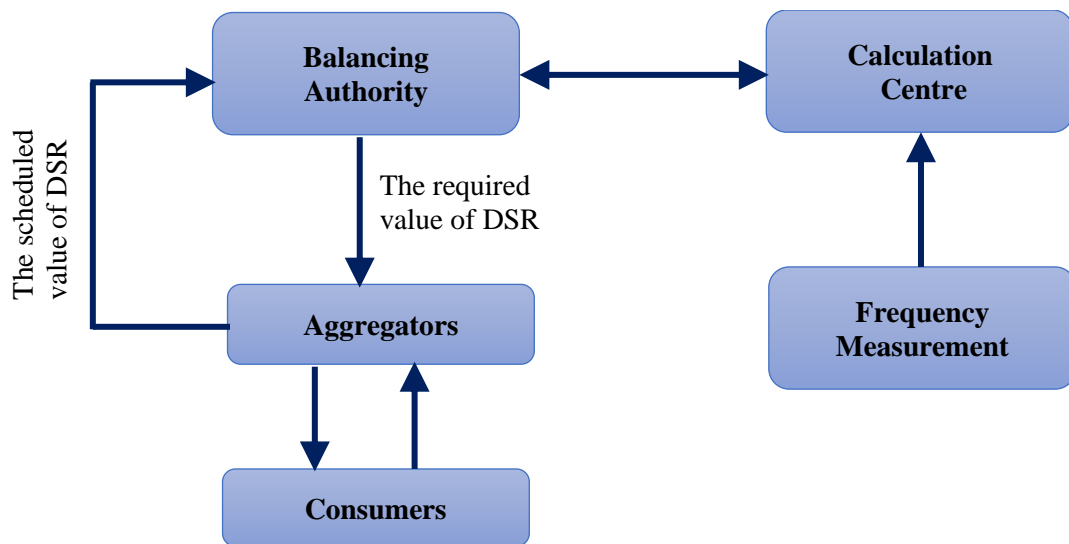
Fig. 2.18 The scheduling process of the central DR strategy [94]

Another direct control scheme was proposed in [95]. This scheme requires two-way communication between the controllable loads and the system operator. At each sample time, the centralised controller calculates the appliances' states based on the previous state and send the states to the upper layer which is called a distribution system operator (DSO) [95]. The DSO collects the states of the appliances and creates a histogram of the total appliances power consumption to be sent to the transmission system operator (TSO). The TSO then analyses the histogram from all

DSOs and generates the ON/OFF states, which will be then sent back to the appliances through the DSO. The final ON/OFF operational states of each appliance are controlled by comparing the states received from the DSO with a desired state signal.

In [96], a direct control algorithm was presented to regulate the system frequency by controlling the aggregation of small loads such as electric water heating (EWH). The power system operator operates the central controller, which monitors the ON/OFF state conditions of each load and decides to turn them ON or OFF in response to the grid frequency.

Direct control load based thermal load is widely addressed in the literature [97-99]. Thermal loads are time-flexible loads that can provide frequency regulation without harming the consumers' comfort. For instance, reference [97] examined a direct control load algorithm of a population of heating ventilation and air-conditioning (HVAC) units. A temperature forecaster was equipped with the central controller to estimate the temperature of the building for the next step and the HVACs were triggered ON or OFF in response to an external signal only at specific temperature levels.

Another type of central control algorithm for thermal loads, as a source of energy storage is used in [98, 99]. For example, a group of heating and cooling units were controlled thermostatically. The centralised controller allowed a group of these units to track a setpoint trajectory with their aggregated power consumption, acting as a distributed virtual energy storage [98]. Furthermore, reference [99] assumed that an aggregator could manage a portfolio of collective small ON and OFF devices, acting as energy storage to provide a primary frequency response service. A centralised coordinating algorithm was developed to control the energy storage devices in conjunction with domestic heat pumps to provide power smoothing [100]. The centralised controller was assumed to be allocated in the microgrid management centre and it worked in two-way communication with the heat pump and storage devices.

Another type of direct load control was proposed in [101] to provide a supplementary frequency control in an interconnected power system via the aggregation of air-conditioning loads. In particular, two levels were assumed in [101], the ''macro'' level and ''micro'' level. In the ''macro'' level, the load dispatching centre controls the power consumption limit of the domestic loads and detects the frequency and tie-line power fluctuations. In the ''micro'' level, change-time priority list method was employed to control the ON and OFF states of the loads in response to frequency deviation signal.

2.7.2   Decentralised control of demand

The cost and complexity associated with the two-way communications between substantial number of loads and the control centre seemed to be a considerable obstacle. Decentralised control algorithms have also been used for frequency regulation and are installed locally. Hence, two-way communication with the system operator is not needed. There are two types of decentralised control algorithm, namely: static and dynamic.

2.7.2.1 *Static decentralised frequency control algorithm concepts*

The basic concept of a static control algorithm is summarised as turning the load ON or OFF when the frequency deviation goes above or below constant pre-defined threshold values [102-104]. The DSR developed in [102] introduced a triggering control algorithm at different regions (i.e. different constant set-points), as shown in Fig. 2.19. The frequency controller triggers the load ON or OFF only when the frequency deviation exceeds these regions. Each region has finite intervals so that the units can be triggered step by step after the frequency event. Similarly, in [103] a logic control algorithm was implemented to control the power consumption of a group of water heaters. Static (i.e. constant) tripping frequency (typically 0.1Hz) and constant temperature set-points for the heater water were considered. For instance,

if the grid frequency becomes lower than 49.9Hz, all the heaters (i.e. within the temperature set-points) will be switched OFF together.

Another detailed decentralised control algorithm was developed in [104] to provide rapid frequency response to the grid from thermostatically controlled refrigerators without real-time communication and in a non-disruptive way. In [104], a linear control method was developed to determine the reference power profile for the TCLs. The total power consumption of TCLs was controlled as a linear function of the locally measured frequency and the RoCoF. Another method was proposed in the same reference to make the aggregated consumption of TCLs follow a pre-set power profile depending on the estimated infeed loss.
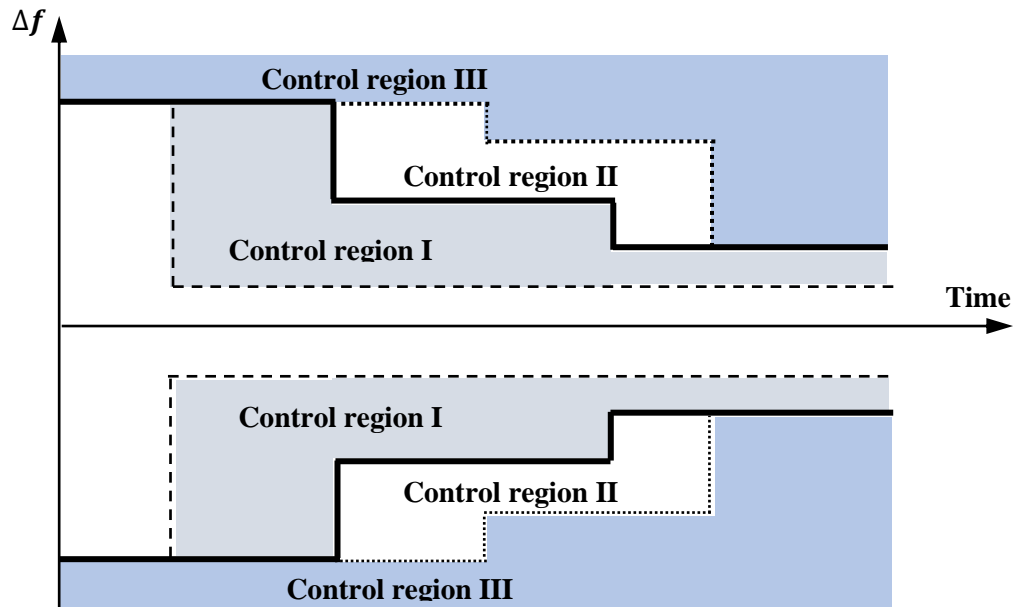
Fig. 2.19 Triggering regions of load controller [102]

2.7.2.2 *Dynamic decentralised frequency control algorithm concepts*

A dynamic demand control is another class of the decentralised control algorithm, which usually aims to control the thermal load (i.e. TCLs). The main concept of this kind of control algorithm is to dynamically control the power consumption of TCLs

with the temperature set-points without any interaction from the system operator [68, 103, 105-107].

Reference [68, 106] developed a dynamic demand control (DDC) algorithm that controls the power consumption of refrigerators linearly. Each refrigerator was assigned with variable temperature set-points. The temperature of each refrigerator is controlled through a thermostat temperature control to maintain the temperature within lower and upper temperature setpoints. Each refrigerator was randomly assigned with different defined trigger frequencies over range of 49.5–50.5Hz. Then, a linear relationship is given to the trigger frequencies to vary dynamically with the temperature, as shown in Fig. 2.20. The DDC algorithm compares the grid frequency continuously with the trigger frequency and turns the refrigerators OFF in ascending order when the frequency is declined. If the frequency is increased, then the DDC algorithm turns the refrigerators ON in descending order to ensure smooth and gradual load switching.
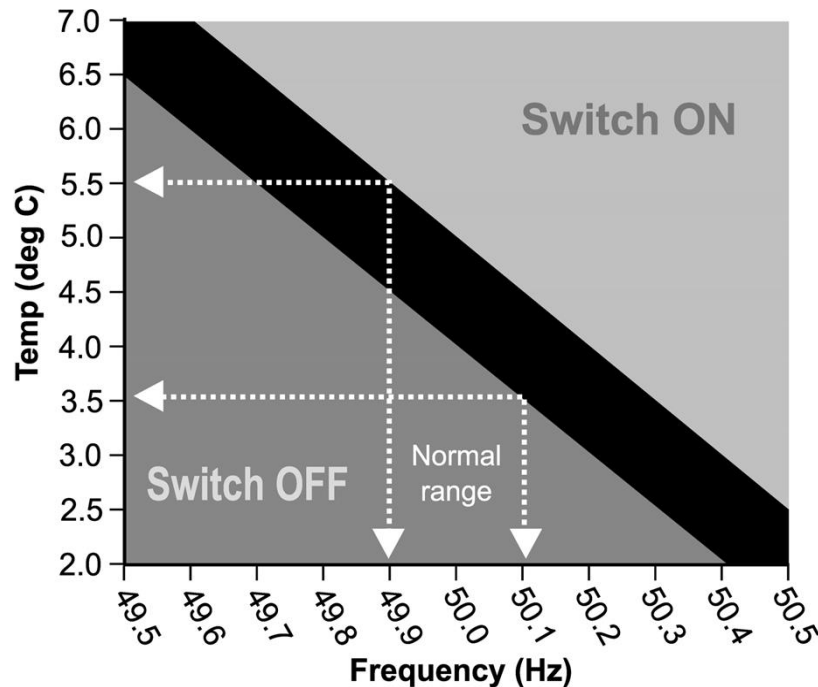
Fig. 2.20 Operation process of a dynamically controlled refrigerator [68]

Reference [103] also presented a collective behaviour of 100 heaters with dynamic control of their temperature set-points. The heaters' temperature is initialised based on random uniform distribution between upper and lower temperature set-points.

A demand frequency reserve (DFR) algorithm was developed in [105] to control the power consumption of electric heating. This algorithm assumes three scenarios, as shown in Fig. 2.21. The first scenario represents the normal operation of load (i.e. no frequency event). The second scenario is assumed for load disconnection (i.e. when the frequency is declined). The system frequency is compared with a target frequency F_{off}. The F_{off} of each appliance was randomized in a range of 49.8–49.9Hz. When the system frequency drops lower than F_{off}, the loads are tripped OFF in descending order starting from the load with high F_{off}. The third scenario is assumed for load reconnection, which is employed by comparing the system frequency with the target frequency F_{on}. The F_{on} is randomized in a range of 49.9–50.1Hz. When the system frequency is recovered to above F_{on}, then each appliance is reconnected according to their own defined F_{on}. In this algorithm, the number of appliances that are reconnected at the same time after they were switched OFF is minimised.
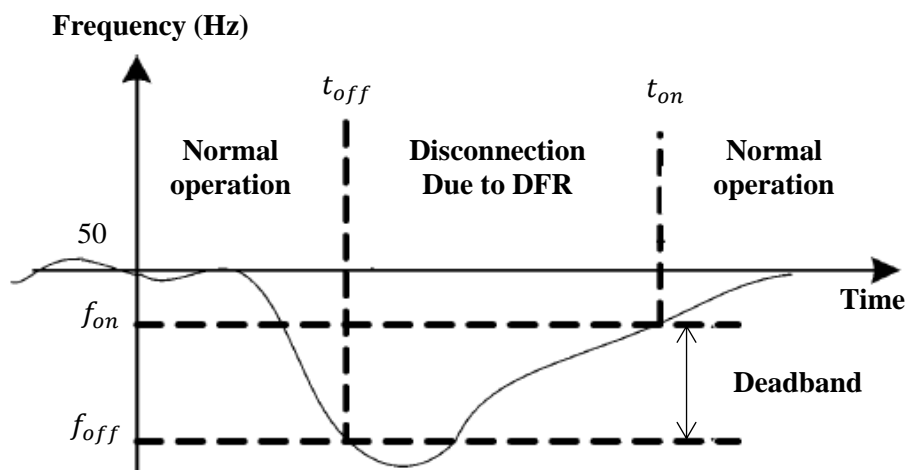
Fig. 2.21 DFR control operation and critical parameters [105]

47

In [107], distributed control algorithm was applied to industrial Melting Pot (MP) which dynamically alters the aggregated power consumption of MPs in proportion to deviation in grid frequency while maintaining the primary heating function of each MP.

An aggregation model of industrial BTs was introduced in [92]. Each BT was controlled individually through a small frequency controller. The frequency control algorithm used in [92] was designed to work independently from the temperature controller. Hence, the trigger frequencies F_{on} and F_{off} were only updated in relation to system frequency.

The decentralised control algorithms presented in [68, 92, 106, 107] were connected to the GB power system. It has been shown that the DDC is feasible and can provide a frequency response in a manner similar to, or faster than the response obtained by traditional peaking large power generation

2.7.3 Potential of heat pumps and fridges as a source of flexible demand

Element Energy published a report that assessed the potential of heat pumps and EVs to contribute to the frequency response [67]. This report projected the total number of residential heat pumps from 2015 to the next decade based on three uptake scenarios (i.e., Slow Progression, Element Energy, and Gone Green). According to the 2030 Element Energy scenario [67], there are expected to be 3.8 million heat pumps in GB dwellings by 2030. Furthermore, the same report claimed that these heat pumps could provide 2.5 GW of average low-frequency response to the grid, which accounts for 170% of the projected response requirement in 2030. If the uptake is high (i.e. Gone Green scenario), then the response of the heat pumps will rise to 3.3 GW, accounting for 227% of the response requirement. The response will decrease to 375 MW, accounting for 27 % of the required response in the Slow Progression scenario. Table 2.5 illustrates the annual revenue per heat pump for frequency response provision compared with two payment costs (£10/MW/hr and £20/MW/hr). The net benefit per residential heat pump is estimated to be £51/year,

as shown in Fig. 2.22. Element Energy claimed that this could save approximately 9% of a typical annual electric heating bill[7]. Element Energy found that domestic heat pumps can provide a dynamic frequency response, that is, they are able to respond constantly to the frequency deviation. The dynamic frequency response from the heat pumps has the potential to avoid approximately 1.8 tons of Carbon Dioxide CO_2/year.

Table 2.5 Revenues per heat pump for frequency response provision [67]

	Revenue/year £10/MW/hr payment	Revenue/year £20/MW/hr payment
Residential heat pump	£72	£144

£/yr 71
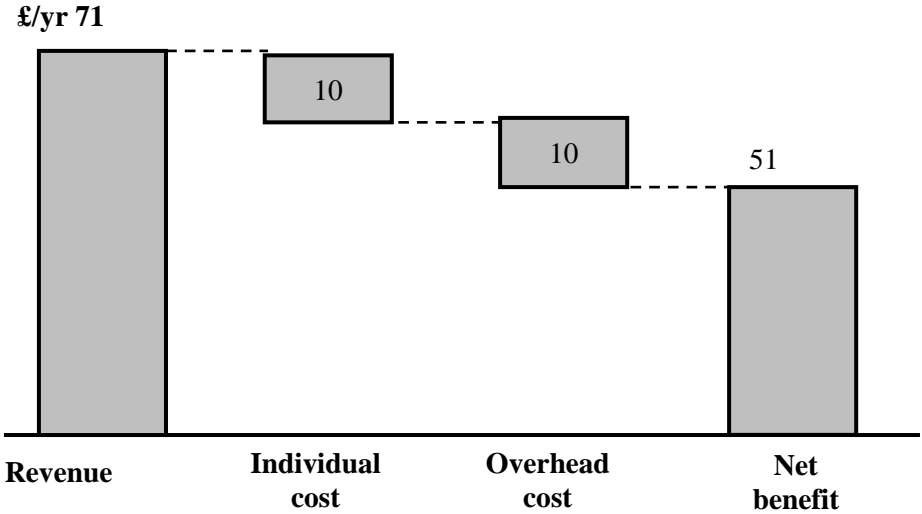
Fig. 2.22 Annual cost benefit in the provision of frequency response from the residential heat pump, all in £/year [67]

Fridge appliances, which include upper and lower freezers, also have heat storage properties. Hence, the power consumption of fridges can be curtailed or interrupted without affecting the overall performance of the load. Fridges are engaged in consumer use in all seasons, and throughout the day and night. Therefore, they are

---

[7] Assumes heat pumps electricity bill of £550/year (15kWh consumption per day, with electricity price of 10p/kWh)

available to participate in frequency control service at all times. In addition, fridges are increasing in number due to the consistent growth in the number of homes and population. By 2030, there will be approximately 48 million fridges according to the all scenarios of the National Grid. Reference [78] shows that in 2030 the value that fridges can offer for the frequency response service will be £1.97/household/year.

2.8   Summary

Three frequency control services are used to control the frequency of the traditional power system (i.e. primary, secondary and tertiary). In the current Great Britain power system, National Grid procures frequency response through three main services (i.e. FFR, MFR, and FCDM). The simplified GB power system and the multi-area power system have been modelled in the literature of frequency control. The literature review indicates that the system inertia of the future GB power system will decline thanks to the growth of converter-connected renewable generation.

A comprehensive review of the latest strategies to design the AGC in interconnected power systems was provided. It was shown that an The AGC controller is necessary to control the frequency of the area, and also the power interchange with other control areas.

Demand Side Response is an important element that can control the grid frequency instead of further frequency response from the frequency sensitive generators. An extensive literature review of centralised and decentralised demand control algorithms has shown that they can be used without affecting the overall performance of the load for the consumer. Centralised control algorithms require complex and expensive communication infrastructure between thousands of loads and the system operator. A decentralised DDC algorithm was presented without the need for communication between the load and system operator. It has been shown that the DDC is feasible and can provide rapid frequency response to the power system.

Chapter 3

Interconnected power system based Adaptive Controllers

An Adaptive DeadBeat (ADB) controller was devel(oped to investigate its capability in providing a frequency response to an electrical power system. This controller was developed to improve the behaviour of the frequency in an interconnected power system. The ADB controller was then integrated with the multiarea model of the north and south zones of Scotland. This model was developed in order to conform to the future energy requirements scenario stated by National Grid whereby regional control can be provided in both the north and south of Scotland. The performance of ADB controller is compared with two standard controllers (i.e. PI and Fuzzy-PI).

3.1   Introduction

System frequency is a variable that refers to a continuous balance between system demand and generation. In the GB power system, the standard operating frequency is 50 Hz with the upper/lower statutory limit being ± 1% Hz of nominal system frequency, i.e. ±0.5 Hz [8]. Wind generators are a rapidly evolving technology and the latest generation of some turbine vendors has already demonstrated the capability for inertia and governor response. However, present wind generators are mostly mechanically decoupled from the grid, have rotating shafts that differ from those of the conventional generator, and provide less inertia to the system [24], [108]. In Scotland, it is anticipated that the operating capacity of onshore and offshore wind generators will surpass 50% of the total generation capacity by 2030 [109]. Therefore, increasing renewable energy in Scotland will reduce the regional and overall system inertia of the GB's power system and make

it variable and non-uniform across the grid. Because of low inertia, the absolute value of the rate of change of frequency (RoCoF) could be increased significantly and in the worst case could even degrade system stability. Thus, fast frequency response technology is required to avoid the possible drawbacks of low inertia.

National Grid divided the GB power system into zones and boundaries in ''2015 Electricity Ten Year Statement (ETYS)" annual report for future energy scenarios. The purpose of these boundaries is to introduce control frameworks that quickly and effectively control the frequency deviation at each zone before propagating to the system [27, 110]. On the other hand, National Grid has also been trying to study new innovative control technologies to operate at a regional level, and to provide a rapid response and reduce the CO_2 emissions at a reasonable cost. One of these technologies is to design an intelligent controller to provide fast ramp rate action. This can be accomplished by a supplementary feedback loop control system designed to manage the power flow between interconnected zones during a high volume and speed of frequency change [27].

The deadbeat control approach comes under the pole placement family where system control is based on the shifting of the undesired roots or adding improving roots to the system that eliminate the effect of the undesired roots. Thus, a deadbeat controller is a suitable approach that shows a precise behaviour and satisfies the requirement for a very fast transient response [59, 111]. Although an ADB controller can compensate for the fast frequency change, thus far and to the author's best knowledge, no research has been yet carried out on this issue. Therefore, the main contributions of this chapter are:

1. Introducing a new approach for load frequency control system: the chapter highlights how the novel ADB controller can improve the frequency behaviour during and after a frequency event.

2. Development of a system model, derived from physical data, for interconnected zones north and south of Scotland. This model was developed to conform to the future Gone Green energy scenario for the Scottish power system, where regional frequency control is likely to be a major issue [110].

3. Evaluate the operation of the ADB controller by comparing its behaviour with other two important controllers such as the standard PI controller and intelligent Fuzzy- PI controller.

3.2 Scottish power system

Scotland is currently experiencing massive development in renewable generation resources, which reduces system inertia and causes faster frequency change. To clarify the way the model is designed, several assumptions were considered:

- The north and south Scotland zones are made up of boundaries (B_0–B_5) and B_6 respectively as shown in Fig. 3.1 (a) and (b) [110]. The installed generation data in each boundary is shown in Appendix I. These data were given by National Grid [110].

- For simplicity, all generators located within these boundaries that are of a similar type are replaced with one generator considering their total aggregated power generation.

- It was assumed that thermal plants and onshore/offshore wind generators produce 80% and 40% of their total capacity respectively [24].

- A Load Frequency Control (LFC) model is used to study the power system frequency. Thus, transmission lines are not described in the model.

- System inertia is reduced, as some synchronous thermal plants are being replaced by asynchronous wind generators [27].

- To ensure the controller's robustness and performance, the ADB controller was designed based on the lowest (worst) system inertia scenario, i.e., the 2029/2030 scenario.

- The Scotland zones model was considered as a test system to investigate the potential of ADB controller to provide frequency response in a low inertia zone. Therefore, the rest of the GB zones were not considered in this chapter.
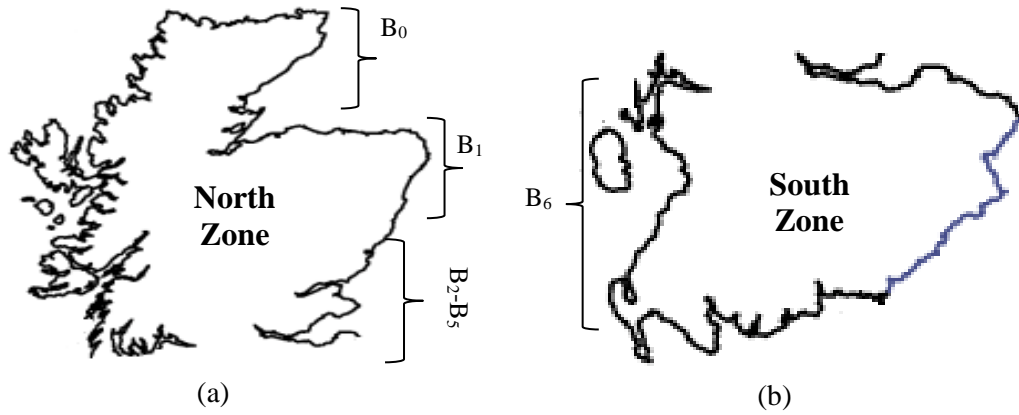
Fig. 3.1 Boundaries (a) North zone (b) South zone of Scotland [110]

3.2.1 North Scotland zone

Table 3.1 shows the operating generation capacity of north Scotland zone for the years 2014/2015, 2019/2020 and 2029/2030 according to the National Grid's Gone Green scenarios. System inertia H_{eq} was normalized to the total generation capacity. The generation and demand data are available in [110]. This zone is expected to have experienced massive growth of renewables by 2030, especially after the offshore wind farms at the Moray Firth and the Firth of Forth enter into service. The Moray Firth wind farm will add 780 MW whereas the wind farm at the Firth of Forth will give 1,075 MW by 2019/2020.

By 2030, the energy capacity of wind turbines in this zone will have reached 44% of the total operating generation capacity. This will cause the system inertia in proportion to the total power capacity of this zone to decrease from 3.067 sec.pu in 2015 to 1.764 sec.pu in 2030 according to the generation data described in Table 3.1. The system inertia of this zone is calculated according to Equation (3.1) [24, 27]. The values of system inertia are shown in Table 3.1.

$$H_{eq} = \sum_i^N H_i \times \frac{S_i}{S_{zone}} \qquad (3.1)$$

54

Where H_i is the equivalent inertia constant for each power plant according to the fuel type, S_i is the power rating for each power plant, S_{zone} is the total power rating for the current zone, and N is the number of power plants.

Table 3.1 Generators data and system inertia of north of Scotland

North of Scotland		2014/2015			2019/2020			2029/2030	
Generator Type	Operating Capacity MW	Hi sec	Heq sec.pu	Operating Capacity MW	Hi sec	Heq sec.pu	Operating Capacity MW	Hi sec	Heq sec.pu
Coal	1827.2	4.5	1.776	1827	4.5	1.2566	1827	4.5	0.996
Gas	342.4	6	0.444	342.4	6	0.314	342.4	6	0.248
Hydro	871.2	4.5	0.847	871.2	4.5	0.5992	951.2	4.5	0.518
Onshore	986.92	0	0	2117.48	0	0	2228.68	0	0
Offshore	0	0	0	430	0	0	1430	0	0
Other	600	0	0	954.4	0	0	1472	0	0
Total	4627.72		3.067	6542.48		2.1698	8251.28		1.764

3.2.2 South Scotland zone

The generation data of the south Scotland zone according to a fuel type was taken from [110] and is shown in Table 3.2. This zone has a lower installed generation capacity than has the north zone. However, the onshore/offshore wind turbine generation are projected to exceed 50% of the total operating capacity of this zone in 2030 [109]. As a consequence, system inertia in this zone will undoubtedly vary significantly, i.e., it will decline from 2.08 sec.pu in 2015 to 1.274 sec.pu in 2030 according to the generation data described in Table 3.2. System inertia in this area was calculated according to Equation (3.1) and tabulated in Table 3.2.

Table 3.2 Generators data and system inertia of south of Scotland

South of Scotland	2014/2015			2019/2020			2029/2030		
Generator Type	Operating Capacity MW	Hi Sec	Heq sec. pu	Operating Capacity MW	Hi sec	Heq sec. pu	Operating Capacity MW	Hi sec	Heq sec. pu
Nuclear	2163	3	1.859	2163	3	1.416	2163	3	1.131
Gas	112	6	0.1926	112	6	0.1466	112	6	0.117
Hydro	26.4	4.5	0.034	26.4	4.5	0.026	33	4.5	0.026
Onshore	1152.24	0	0	1644.68	0	0	1747.68	0	0
Offshore	0	0	0	600	0	0	1646	0	0
Other	36	0	0	36	0	0	36	0	0
Total	3489.64		2.0856	4582.08		1.588	5737.68		1.274

3.3 Interconnected model of Scotland zones

A simplified interconnected power system model for the north and south zones of Scotland was developed to study the power system frequency response as shown in Fig. 3.2. The secondary controller block shown in Fig. 3.2 hereafter refers to the Automatic Generation Control (AGC).

To simplify the model simulation, all generators that are of a similar type are replaced with one generator taking into consideration their total aggregated power generation. For instance, in the north zone of Scotland, G1 block represents the coal plants, G2 block includes the gas plants, whereas the hydro plants are integrated into block G3. Similarly, in the south zone of Scotland, G4 block represents the nuclear plant, G5 represents the gas plants, and G6 represents the hydro plants. The power generation drawn by wind turbines and other resources are added into the total installed capacity. The load frequency dependence in both zones were lumped into a damping constant D, which was set to 1 p.u. For the provision of a primary response, all generators should have a governor droop setting between 3%−5% according to the GB grid code [112]. The speed governor deadband of models G1−G6 should be no greater than 0.03Hz; however, to increase certainty, it was selected

here to be ±0.015Hz [112]. The governor droop was represented by the gain $1/R$ and was set to 20 p.u. in all scenarios. The parameters used in Fig. 3.2 are given in Table 3.3, where $T_g, T_t, T_r, T_{tr}, T_R, T_1$ and T_w are generator-turbine time constants [19]. The B is a frequency bias constant and was set to 21 p.u. according to Equation (3.2) [13].

$$B = \frac{1}{R} + D \tag{3.2}$$

Table 3.3 Generators and system model parameters

$R(pu)$	$B(pu)$	T_g	T_t	T_r	T_{tr}	T_1	T_R	T_w	K_{12}	K_{21}
0.05	21	0.2s	0.3s	7s	2.1s	38s	5s	1s	0.2 p.u	-0.2 p.u

The principles of power flow using a tie-line from one area to another were detailed in [13]. A multi-area power system refers to the areas interconnected by high voltage transmission tie-lines. In addition to controlling the frequency in each zone, the AGC controller installed at each control area must control the tie-line power transfer, minimizing the area control error with the neighbouring area (i.e. ACE_1 and ACE_2 in Fig. 3.2). The proposed net interchange power between north and south Scotland is given in Equations (3.3) and (3.4).

$$\Delta P_{tie,12} = \frac{2\pi}{s} K_{12}(\Delta f_1(s) - \Delta f_2(s)) \tag{3.3}$$

$$\Delta P_{tie,21} = \frac{2\pi}{s} K_{21}(\Delta f_2(s) - \Delta f_1(s)) \tag{3.4}$$
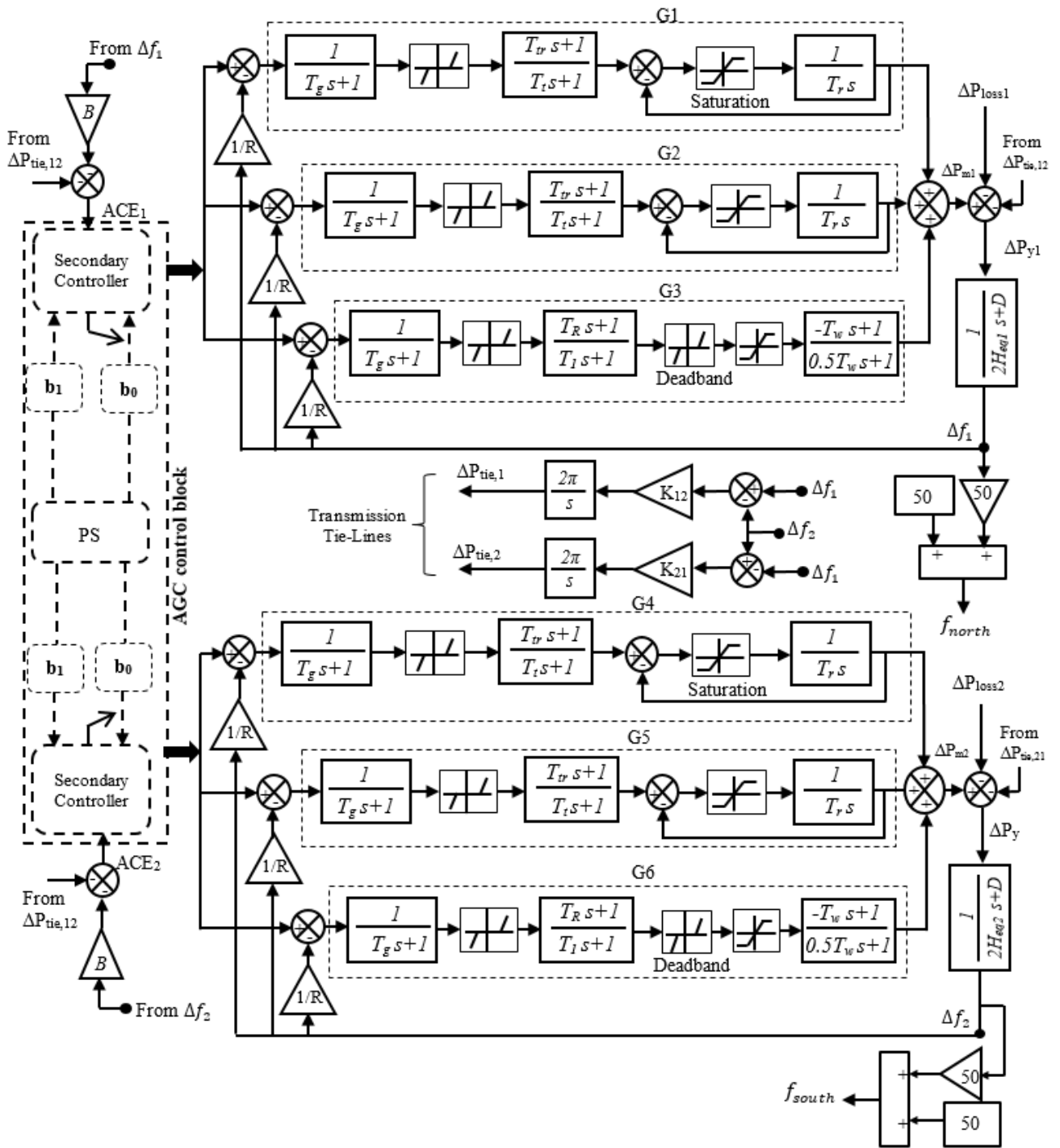
Fig. 3.2 Simplified interconnected Scottish power system model

K_{12} and K_{21} represent the synchronizing torque coefficients. Δf_1 and Δf_2 are the frequency deviations in the north and south zones. The frequencies f_{north} and f_{south} shown in Fig. 3.2 are defined as the north and south frequency zones. They can be obtained by multiplying the frequency change of both zones (in per unit) by the base frequency constant in GB (50 Hz), then add 50 Hz to the outcome. At any generation loss or sudden change in demand in one zone, the AGC controller will drive the generators at each area to increase their generation and re-scheduling the tie-lines power flow so that one zone exports and the other absorbs the power. To ensure nominal frequency at each zone, the linear combination error between zonal frequency and connected tie-line should be reduced to zero. This error is often called Area Control Error (ACE), as shown in Fig. 3.2 and is given in Equations (3.5) and (3.6).

$$ACE_1(t) = \Delta P_{tie,12}(t) + B \times \Delta f_1(t) \tag{3.5}$$

$$ACE_2(t) = \Delta P_{tie,21}(t) + B \times \Delta f_2(t) \tag{3.6}$$

3.4 Integrated secondary controller structure design

3.4.1 Integrated fuzzy logic controller

The structure of this control system is shown in Fig. 3.3. The design of Fuzzy Logic Control (FLC) based PI controller is divided into four main parts as presented in Fig. 3.4.

- **Input Part:** this is a fuzzifier part where a crisp input is fuzzified into truth input by using input membership functions (MF). In this study, two inputs were considered at each zone: the control error inputs (ACE_1 and ACE_2), and the rate of change of area control error inputs (d/dt ACE_1 and d/dt ACE_2).
- **Rule-Base part** holds the knowledge, in a form of a set of rules, describing the best way to control the system.

- **Fuzzy Inference System (FIS)** evaluates which control rules are relevant in each step time and then decides what input of the plant should be enabled. The standard fuzzy PI controller using Mamdani inference system has three linguistic variables (Negative, Zero, Positive), based on the signs of each input [113]. Therefore, the control output (u) has nine possible fuzzy control rules as shown in Table 3.4. The ranges of both input and output triangular membership functions are normalized to [-10, 10]. The degree of membership range is [0, 1]. The output range is [-20, 20]. The fuzzy rules are defined as the following:

1. If error input is Negative and change in error input is Negative, then control output (u) is -20.

2. If error input is Negative and change in error input is Zero, then control output (u) is -10.

3. If error input is Negative and error change is Positive, then control output (u) is 0.

4. If error input is Zero and change in error input is Negative, then control output (u) is -10.

5. If error input is Zero and change in error input is Zero, then control output (u) is 0.

6. If error input is Zero and change in error input is Positive, then control output (u) is 10.

7. If error input is Positive and change in error input is Negative, then control output (u) is 0.

8. If error input is Positive and change in error input is Zero, then control output (u) is 10.

9. If error input is Positive and change in error input is Positive, then control output (u) is 20.

- **Output Part:** this part represents the controller action (u) where fuzzy output is de-fuzzified into a crisp output using output membership function.
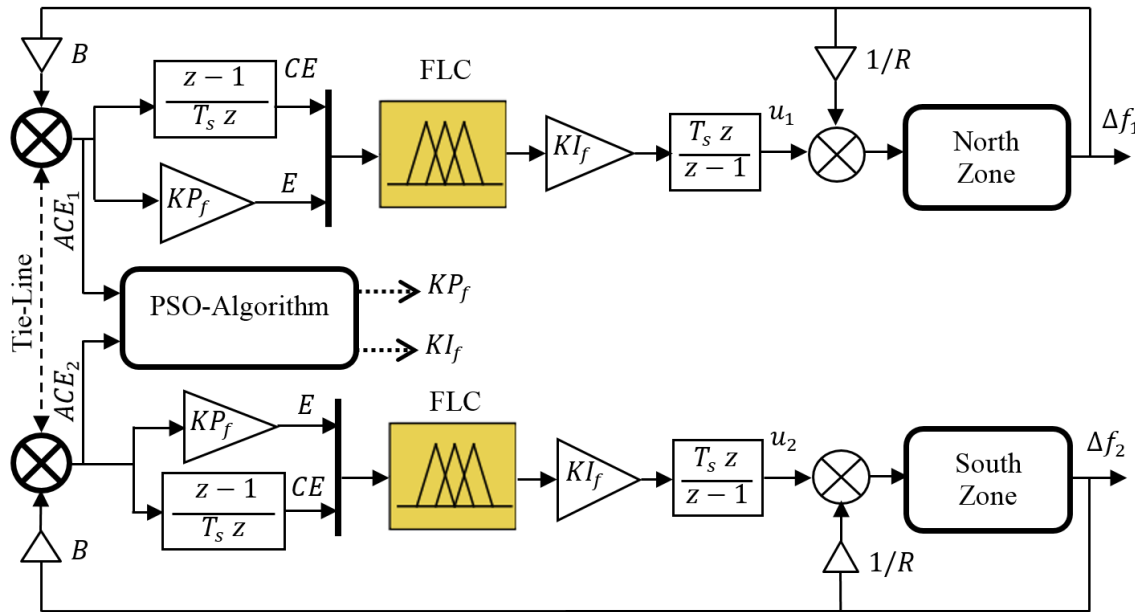
Fig. 3.3 Structure of AGC based Fuzzy-PI Controller
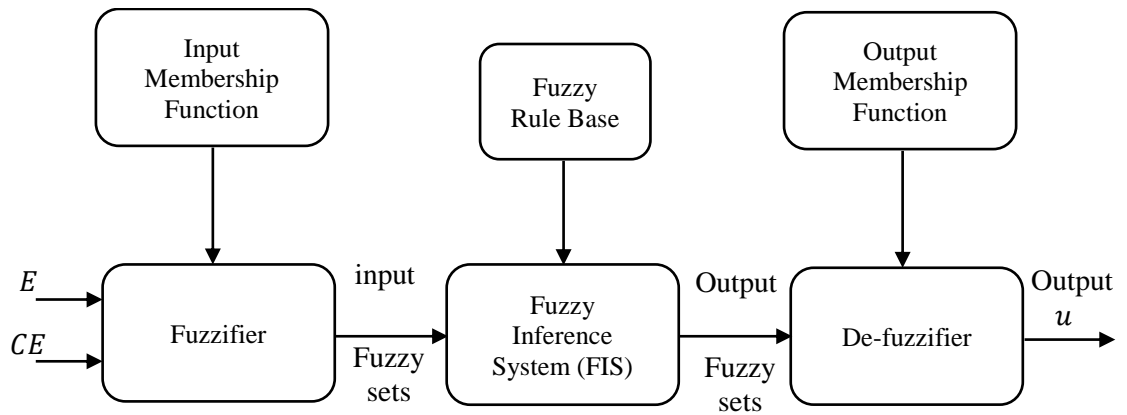
Fig. 3.4 Block diagram of Fuzzy Logic Control (FLC)

61

Table 3.4 Fuzzy control rules

Positive	Zero	Negative	CE ╲ E
0	-10	-20	Negative
10	0	-10	Zero
20	10	0	Positive

3.4.2 Integrated ADB controller

The structure of this control scheme is shown in Fig. 3.5. The deadbeat characteristics for linear control systems are stated as follows [114]:

1. zero steady-state error
2. minimum rise time and settling time
3. small overshoot and undershoot
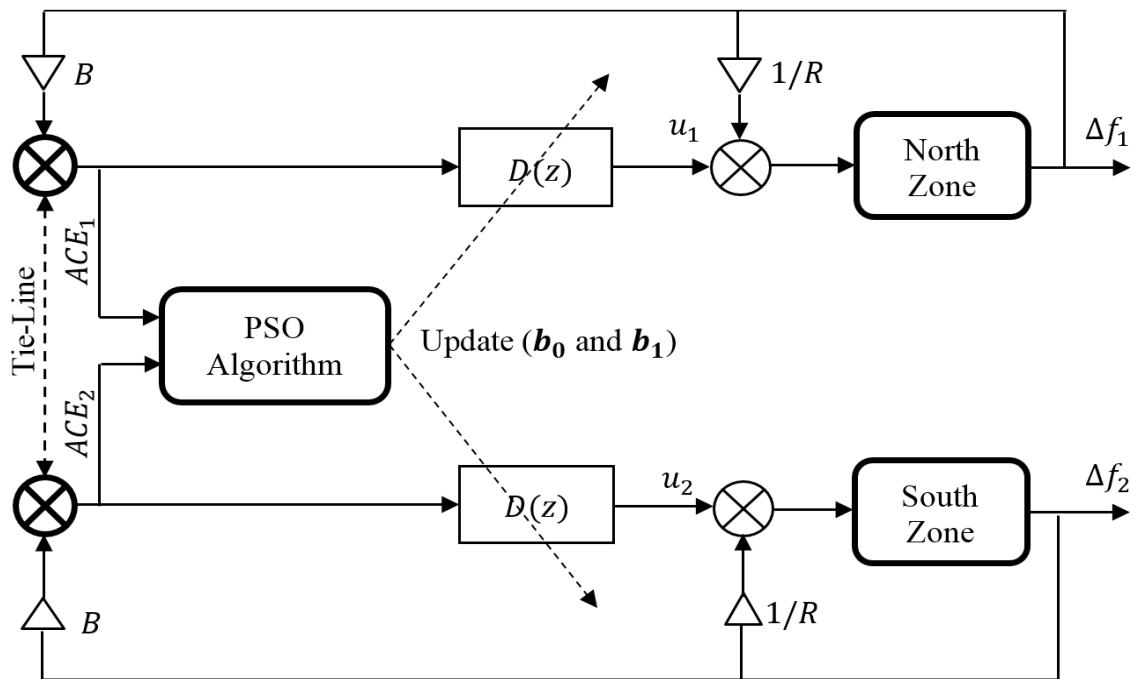
Fig. 3.5 Structure of AGC based ADB controller

In LFC-based on ADB controller, the frequency response performance of the power system is predictable because the designer can select the controller's parameters to compensate for the effect of undesirable roots (poles and zeros) for the system. That is, the transfer functions of the open loop system of the model of both zones in Scotland are addressed first to identify the critical and undesired roots. Typically, the open loop transfer function parameters in each zone are changing with the time since they depend on the generation units committed at every point of time. For example, the system inertia drawn by the generation units, with the presence of high wind and low wind generation, are different. Therefore, the designation of the ADB based AGC controller in this research is employed for the worst (lowest) system inertia, that is, the 2029/2030 scenario in the south Scotland zone, to cope with the expected variations in system inertia. Based on the zones open loop transfer functions, the close loop control system using an ADB controller was designed. The primary form of the digital deadbeat controller is given in Equation (3.7) [114], where $Q(z)$, and $1 - Q(z)$ are the controller roots, and $GH(z)$ is the open loop transfer function of the system.

$$D(z) = \frac{1}{GH(z)} \times \frac{Q(z)}{1-Q(z)} \tag{3.7}$$

In Equation (3.8), $GH(z^{-1})$ was obtained by taking the z-transform to the open loop transfer function of the south zone shown in Fig. 3.5. The Zero Order Hold (ZOH) method was used to achieve an exact conversion from continuous to discrete system. The sampling time T_s was set to 0.2 sec [T_s= (0.1….0.5) ×τ_s], where τ_s= 0.4 sec is the system time constant.

$$GH(z^{-1}) = \frac{Kz^{-1}(1+0.5753z^{-1})\times(1-1.2578z^{-1})}{(1-0.9948z^{-1})\times(1-0.9718z^{-1})\times(1-0.939z^{-1})} \times$$

$$\frac{(1-0.9784z^{-1})(1-0.9525z^{-1})\times(1-0.519z^{-1})}{(1-0.6703z^{-1})\times(1-0.5134z^{-1})\times(1-0.3679z^{-1})} \tag{3.8}$$

To analyse the undesired roots in Equation (3.8), all roots are surrounded by the stability unit circle margin $|Z| = 1$, as shown in Fig. 3.6, where $|Z|$ is the absolute value of the complex number (Z) and is given in Equation (3.9).

$$|Z| = \sqrt{R_e^2 + I_m^2} \tag{3.9}$$

For a stable system, all the roots should be located inside the stable circle. The weaknesses of the internal roots increase the closer they come to the circle boundary.
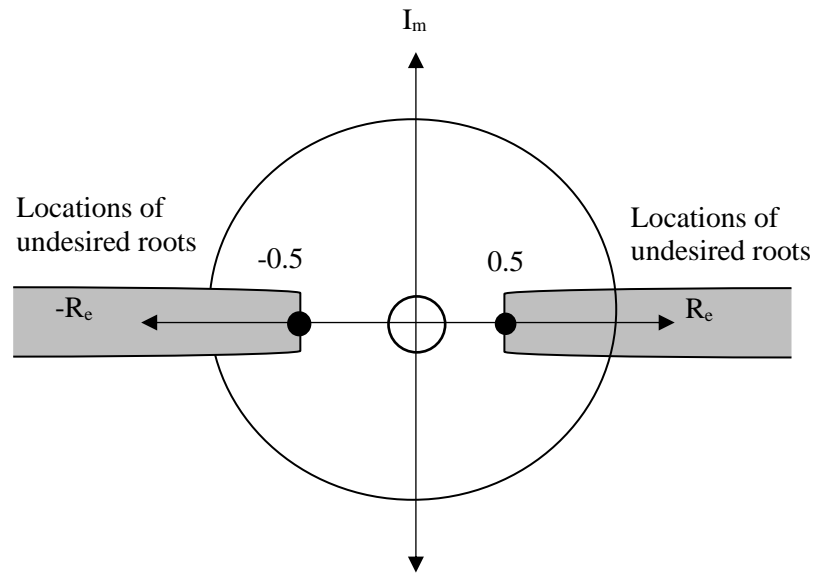
Fig. 3.6 Stability margin of system roots

For a proper design in this research, all roots that are located in the intervals [-∞, -0.5] and [0.5, ∞] are called undesired roots. It was found that there were four undesired zeros $R_z(z^{-1})$ and four undesired poles $R_p(z^{-1})$ as illustrated in Equations (3.10) and (3.11), respectively.

$$R_z(z^{-1}) = (1 + 0.5753z^{-1}) \times (1 - 1.2578z^{-1}) \times (1 - 0.9784z^{-1}) \times$$
$$(1 - 1.9525z^{-1}) \qquad\qquad R_z \in [0.5, \infty] \tag{3.10}$$

$$R_p(z^{-1}) = (1 - 0.9948z^{-1}) \times (1 - 0.9718z^{-1}) \times$$
$$(1 - 0.939z^{-1}) \times (1 - 0.6703z^{-1}) \qquad R_p \in [0.5, \infty] \qquad (3.11)$$

Although the zero root $(1\text{-}0.519z^{-1})$ and the pole root $(1\text{-}0.5134z^{-1})$ are located in the interval $[0.5, \infty]$, they have close value to each other, i.e. one cancels the effect of each other. Hence, they were not considered as undesired roots. The undesired roots can have an adverse impact on system performance, especially in response to a sudden disturbance in power generation or demand ΔP_{loss}. The aim of the deadbeat controller is to add improving roots to the system, which eliminate the effect of the undesired roots in Equations (3.10) and (3.11). The controller's numerator $Q(z)$ in Equation (3.12) includes a part of the roots that eliminates the effect of the undesired zeros of $GH(z)$ as well as the part of the new roots $F_1(z^{-1})$ that improves the system stability and performance.

$$Q(z^{-1}) = R_z(z^{-1}) \times F_1(z^{-1}) \qquad (3.12)$$

Equation (3.13) represents the denominator of the controller. It has two parts: the first part is used to cancel the effect of the undesired poles of $GH(z)$, whereas the second part, $F_2(z^{-1})$, carries the improving roots.

$$1 - Q(z^{-1}) = (1 - z^{-1}) \times R_p(z^{-1}) \times F_2(z^{-1}) \qquad (3.13)$$

The number of samples of $Q(z)$ that are required to solve Equations (3.12) and (3.13) must be equal to or greater than the system order in Equation (3.8). To achieve a proper designation, seven samples are considered in the highlighted case studies in this chapter. The improving roots $F_1(z^{-1})$ and $F_2(z^{-1})$ were selected to match the required number of samples. Then, Equations (3.14) and (3.15) are obtained.

$$\sum_{n=1}^{n} a_{n-1} \times z^{-n} = R_z(z^{-1}) \times \sum_{m=1}^{n-3} \hat{a}_{m-1} \times z^{-m} \qquad (3.14)$$

$$1 - \sum_{n=1}^{n} a_{n-1} \times z^{-n} = (1 - z^{-1})R_p(z^{-1}) \times \sum_{m=1}^{n-5} b_{m-1} \times z^{-m} \qquad (3.15)$$

The number of controller's coefficients was reduced into two (b_0 and b_1) by substituting Equation (3.15) into Equation (3.14). The combination results are:

$$\hat{a}_0 = b_0 - 4.576 \qquad (3.16)$$

$$\hat{a}_1 = -1.963b_0 + b_1 - 3.62 \qquad (3.17)$$

$$\hat{a}_2 = 1.68168b_0 - 1.963b_1 - 10.0311 \qquad (3.18)$$

The final deadbeat controller $D(z)$ in Equation (3.19) was obtained by substituting the last four equations together with Equations (3.14) and (3.15) into Equation (3.7).

$$D(z) = \frac{K(z - 0.3679) \times (\hat{a}_0 z^{-2} + \hat{a}_1 z + \hat{a}_2)}{(z - 1) \times (z^2 + b_0 z + b_1)} \qquad (3.19)$$

The designed controller described in Equation (3.19) was used in both zones as an AGC controller. The value of K was calculated by using the trial and error method [115]. After several simulations runs and under different generation-loss conditions, K was set to 0.001, which gave the most satisfactory result. The steady state error that was achieved using the designed ADB controller in Equation (3.19) was proved theoretically. The error signal $\Delta y_2(z)$ of the south zone, shown in Fig. 3.5, is written as in Equation (3.20)

$$\Delta P_{y2}(z) = \sum \{f(R(z), \Delta P_{tie,21}(z), \Delta P_{m2}(z)\} \qquad (3.20)$$

The $R(z)$ is the disturbance signal (i.e. ΔP_{loss}) and is represented by a step input

given in Equation (3.21).

$$R(z) = \frac{1}{(1-z^{-1})} \tag{3.21}$$

To achieve a zero-steady state error, final value theorem in Equation (3.22) was applied.

$$f.s.s.r(t) = \lim_{k \to \infty} e(kT) = \lim_{z \to 1}(1 - z^{-1}) \times \frac{\Delta P_{y2}(z)}{1+G(z) \times D(z) \times H(z)} \tag{3.22}$$

By substituting Equations (3.19) and (3.20) into Equation (3.22) and by considering the ADB coefficients, given in Table 3.5, the final steady state error $f.s.s.r(t)$ in Equation (3.22) is always converge to zero because the ADB controlled added a root at the origin.

It is important to notice that Equation (3.19) has multiple solutions based on the values of parameters b_0 and b_1. Those parameters should be accurately selected to ensure a robust response, as they represent the coefficients of the new roots that were added to improve the performance of the system. To avoid the complex analytical techniques and for the reasons mentioned in section 3.5, particle swarm optimization (PSO) was used to tune parameters b_0 and b_1. The next section addresses the usages of the PSO algorithm to find the optimal values of PI, Fuzzy PI and ADB parameters.

3.5   Particle swarm optimization (PSO) algorithm for controller

The structure of the integrated ADB controller is shown in Fig. 3.5. So far, several search algorithms have been suggested to identify the optimization problems, including Genetic Algorithm (GA), Bee Colony, and Ant Colony. In this work, based on the LFC system features and previous experience with various intelligent approaches [45, 50] for the tuning of parameters employed in the robust PI and Fuzzy-PI controllers, the PSO is used as a flexible and powerful intelligent

algorithm. Other outstanding features of the PSO algorithm were highlighted in [116, 117].

PSO was used to optimize the FLC-based PI parameters (KP_f and KI_f) and the ADB parameters (b_0 and b_1) so that optimal values of these parameters can be obtained by reducing the fitness function given in Equation (3.23). The fitness function is defined as the integration of the summation of the square area control error for the north Scotland zone (ACE₁) and the south Scottish zone (ACE₂) multiplied by the time (t).

$$J = \int_0^\infty t * (ACE_1^2 + ACE_2^2)dt \tag{3.23}$$

In this algorithm, the groups of particles denoted (swarm) are randomly searching for their target in the space of the problem. The position and speed of the particles were updated according to Equations (3.24) and (3.25).

$$V_{ij}(t+1) = W.V_{ij}(t) + c_1.\text{rand}\left(\text{pbest(t)} - X_{ij}(t)\right) + c_2.\text{rand(gbest(t)} - $$
$$X_{ij}(\text{t})) \tag{3.24}$$

$$X_{ij}(t+1) = X_{ij}(t) + V_{ij}(t+1) \tag{3.25}$$

where $V_{ij}(t)$ is the particle velocity, $X_{ij}(t)$ is the current particle position, W is the inertia weight, pbest(t) is the best position of the current particle, and gbest(t) is the best position obtained by all particles, while c_1 and c_2 are learning factors.

The PSO steps for finding the optimal values of fuzzy PI parameters (KP_f and KI_f) and ADB parameters (b_0 and b_1) are summarized as follows:

- Define the multi-area model shown in Fig. 3.3 and Fig. 3.5 and PSO parameters.
- Create an initial swarm of particles with random position and velocity.
- Calculate the fitness function in Equation (3.23) for each initial parameter that

is required to be optimized (b_0 and b_1) and (KP_f and KI_f).

- Evaluate pbest(t) of each particle and gbest(t) of the population.

- Update the velocity of each particle according to Equation (3.24).

- Upgrade the position of each particle according to Equation (3.25).

- If the number of iterations reaches the maximum, then go to the next step; otherwise, proceed to step 3.

- Save the latest optimal parameters of the controllers pbest(t).

3.6 Case studies on the proposed controller model

Four case studies were undertaken for the proposed model presented in Fig. 3.2 considering the scenarios of the years 2014/2015, 2019/2020, and 2029/2030 in proportion to the generation loss incident. The 2029/2030 scenario, the robustness and performance of the ADB controller were investigated with a set of step and continuous imbalance contingencies. Matlab was used for the modelling study. All model parameters are given in Table 3.3. The controllers' parameters that were optimized using PSO method are presented in Table 3.5.

Table 3.5 Controller parameters

Type of Controller	2014/2015	2019/2020	2029/2030
PI	$K_p = 0.197$	$K_p = 0.1262$	$K_p = 0.1947$
	$K_i = 0.1398$	$K_i = 0.166$	$K_i = 0.2921$
ADB	$b_0 = 0.29$	$b_0 = 0.4142$	$b_0 = 0.1632$
	$b_1 = 0.1368$	$b_1 = 0.2471$	$b_1 = 0.2808$
Fuzzy PI	$K_{pf} = 0.4786$	$K_{pf} = 0.1057$	$K_{pf} = 0.4071$
	$K_{if} = 0.3486$	$K_{if} = 0.3237$	$K_{if} = 0.202$

3.6.1 Case study 1

The first case study was carried out for the year 2014/2015 scenario in which the system base load was assumed to be 4627.72 MW in the north Scotland zone and 3489.64 MW in the south Scotland zone. The system inertia calculated for north and south areas was 3.067 sec.pu and 2.0856 sec.pu respectively, as presented in Table 3.1 and Table 3.2.

The loss of 120 MW ($\Delta P_{loss2} = 0.026$ pu), which occurred between 29 May 2000 and 10 June 2000 at BP Grangemouth power station in the south of Scotland, was injected to the model at the time 10 sec. The simulation results are shown in (Fig. 3.7-Fig. 3.9).

Fig. 3.7 reveals the comparison results of the frequency after the loss of generation at the south zone with ADB, PI, and Fuzzy-PI controllers. Fig. 3.8 shows the absolute RoCoF at the south zone (the area of disturbance). Fig. 3.7 shows the changes of aggregated power output of the generators (ΔP_{m2}) placed in the south zone (see the left axis) and the tie line power absorbed from the north zone ($\Delta P_{tie,21}$) (see the right axis).

It can be observed that with the use of the ADB controller, the maximum frequency deviation Δf_2 was reduced to 13% of the value when PI and Fuzzy-PI controllers were used (from $|\Delta f_2| \approx 0.31$ Hz to $|\Delta f_2| \approx 0.27$ Hz). At the earliest sub-seconds following the incident, Fig. 3.8 shows that the ADB controller has slightly reduced the RoCoF more than the PI and Fuzzy-PI controllers.

Fig. 3.9 shows that at time 11 sec (the time when the frequency dipped to its maximum value), the change of aggregated output power from the south zone generators (ΔP_{m2}) increased from 70 MW when PI and PI-controllers were used to 100 MW when the ADB controller was used. However, the net interchange power at this time increased by 10.5 MW in each approach.
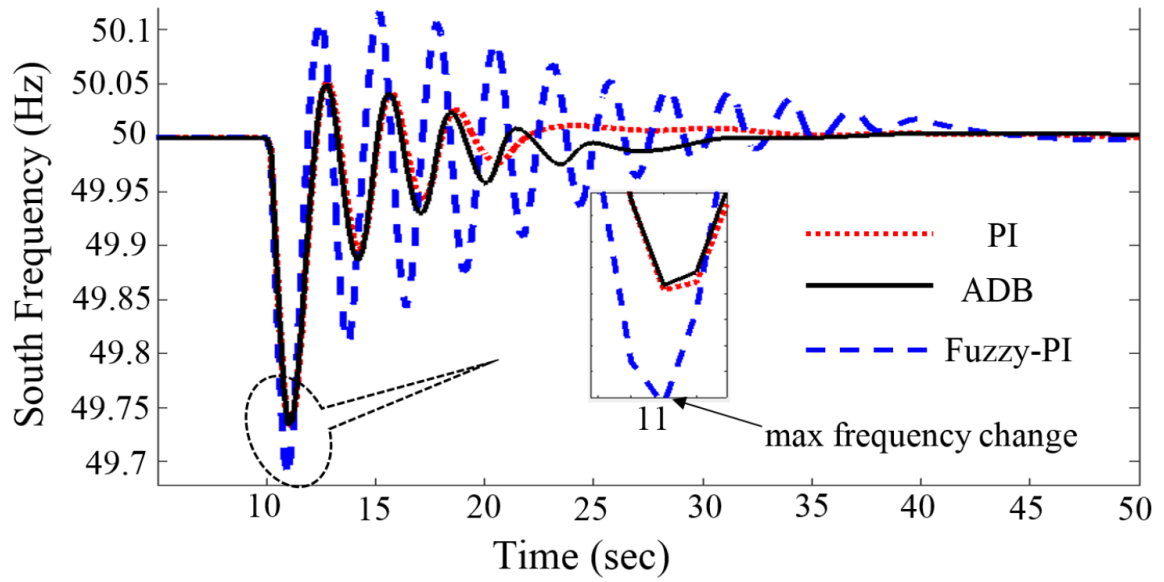
Fig. 3.7 Variation of the grid frequency. South zone with $H_{eq} = 2.0856$ sec.pu (Case1: 2014/2015)
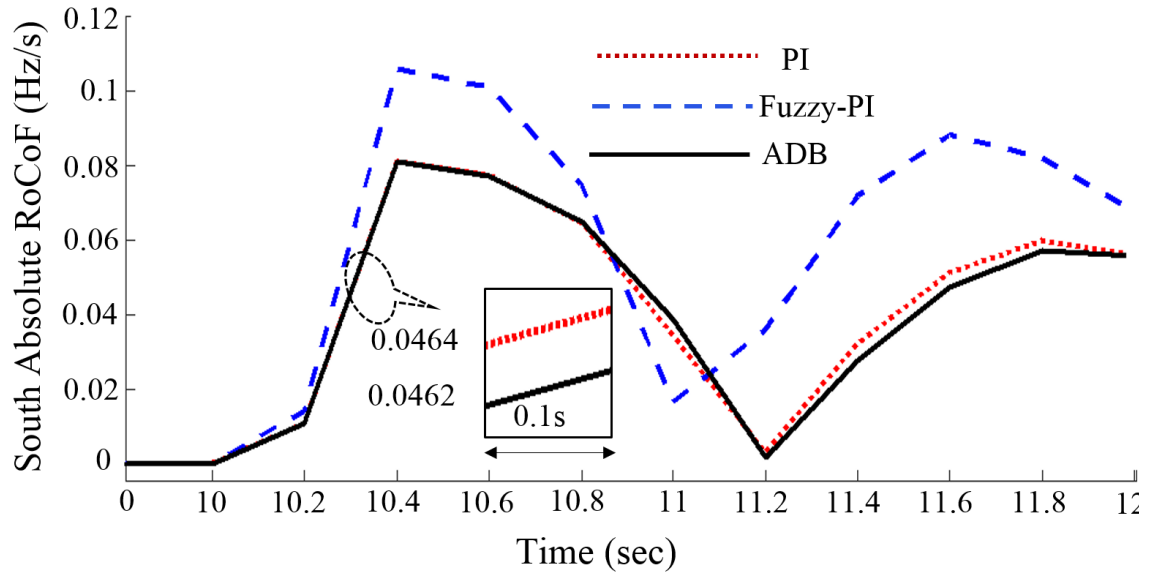
Fig. 3.8 South Absolute rate of change of frequency with $H_{eq} = 2.0856$ sec.pu (Case1: 2014/2015)
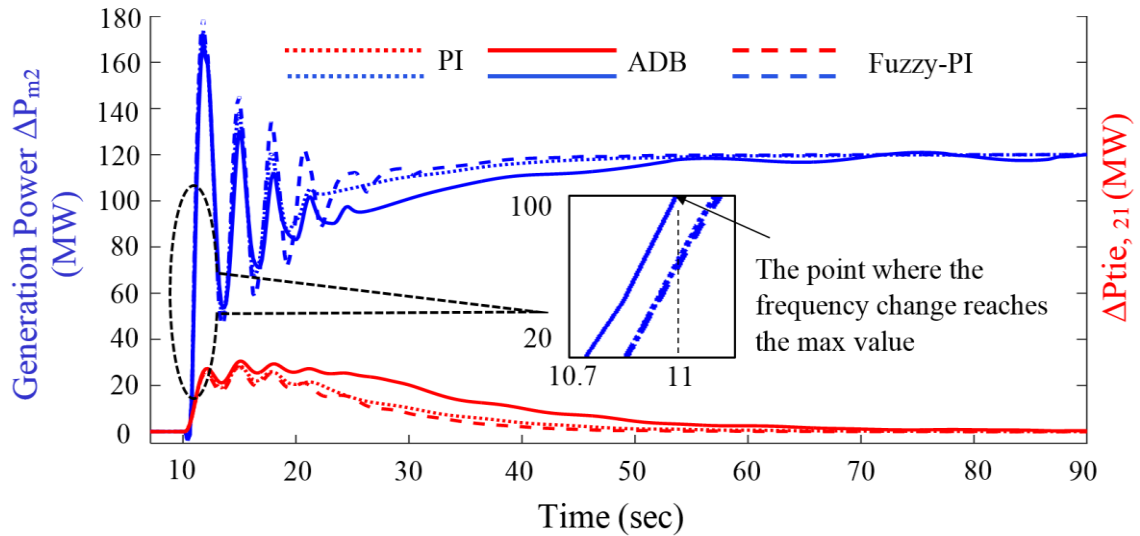
Fig. 3.9 Change of Tie line power ($\Delta P_{tie,21}$) and generator output power (ΔP_{m2}) at the south zone (Case1: 2014/2015)

3.6.2 Case study 2

The second case study was carried out for the year 2019/2020 scenario, which represents the future power system in which an enormous reduction in system inertia might take place. The loss of the BP Grangemouth power station leads to a loss of 120 MW (ΔP_{loss2} =0.026 p.u.) in generation in the south of Scotland zone. The system inertia in the north zone will be decreased from 3.067 sec.pu to 2.1698 sec.pu and in the south zone from 2.0856 sec.pu to 1.5886 sec.pu due to the massive growth of renewables in Scotland. For fair observation of the RoCoF between the first and second case studies, the same system base load as in the first case study was considered.

The simulation results for this scenario are shown in (Fig. 3.10-Fig. 3.12). Fig. 3.10 reveals the frequency response in the south zone (area of disturbance) after the generation loss with the use of PI, Fuzzy-PI, and ADB controllers. The frequency in the south zone at the time of the disturbance exceeded the acceptable limit (<49.5 Hz) when the PI and Fuzzy PI controllers were used while the ADB controller maintained the frequency within the acceptable limit (<49.5 Hz).

Regarding the RoCoF, Fig. 3.11 shows that RoCoF was lower when the ADB

approach was used, especially at the crucial sub-seconds after the incident. According to Fig. 3.12, in comparison with PI and Fuzzy-PI controllers at time 11 sec (where the frequency deviates to the maximum value), the ADB controller achieved the maximum aggregated output power change from the south zone generators. That is, ΔP_{m2} =180 MW with the ADB controller, and 150 MW with PI and fuzzy-PI controllers. The power transfer through the tie line from the north to the south zone has similar values in the three approches.
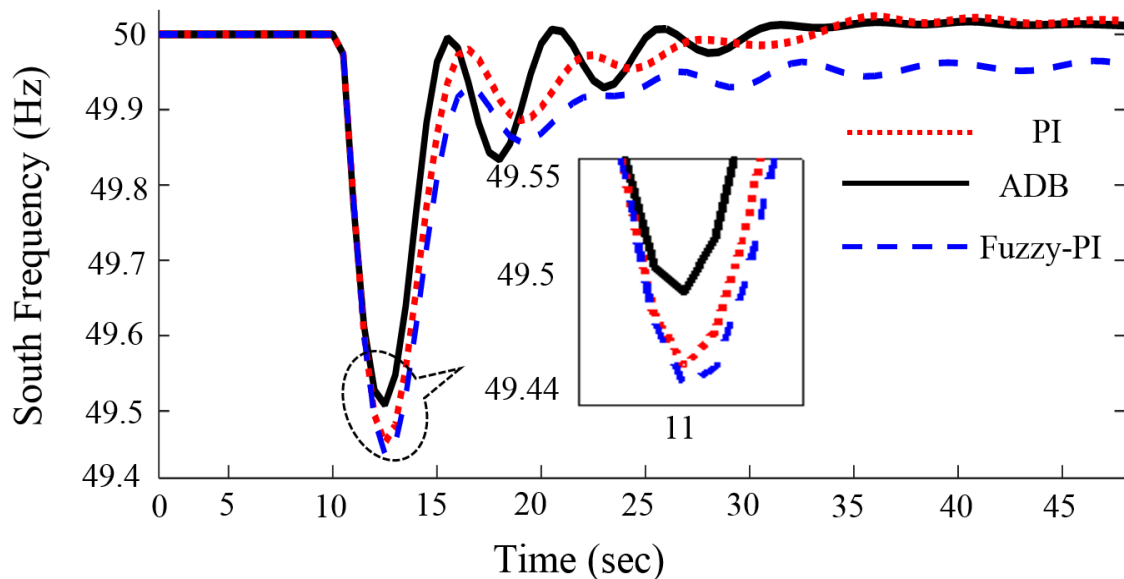
Fig. 3.10 Variation of the grid frequency. South zone with $H_{eq} = 1.5886$ sec.pu (Case2: 2019/2020)
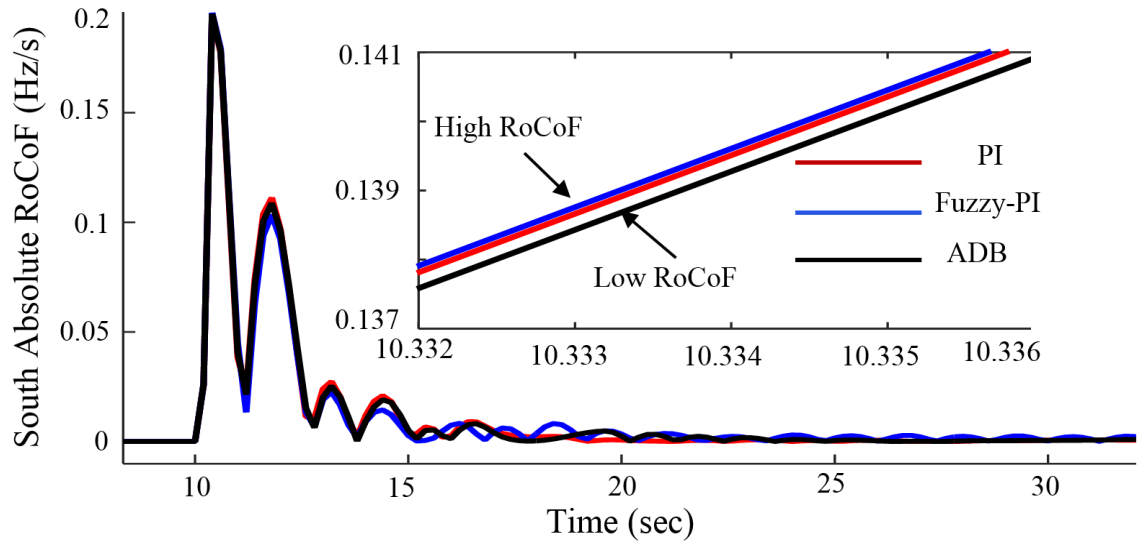
Fig. 3.11 South Absolute rate of change of frequency with $H_{eq} = 1.5886$ sec.pu (Case2: 2019/2020)
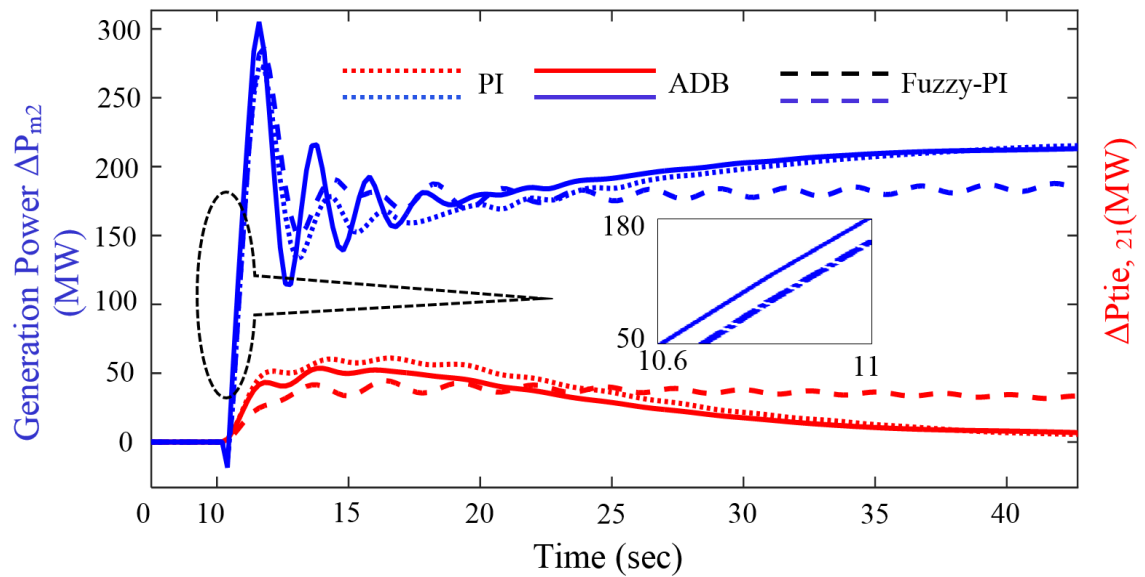
Fig. 3.12 Change of Tie line power ($\Delta P_{tie,21}$) and generator output power (ΔP_{m2}) at the south zone (Case2: 2019/2020)

3.6.3 Case study 3

This case study was considered for the most intense scenario (2029/2030) in which the system inertia in Scotland experiences a significant decline.

Fig. 3.13 and Fig. 3.14 quantify the robustness and performance of the ADB

controller by showing the average absolute RoCoF and average frequency deviation Δf_2 that would result from imbalance contingencies ranging from 0.028 to 0.286 p.u.; that is, the size and speed of the power change were very different. In each contingency incident, the simulation was run and the average RoCoF and average frequency deviation were recorded.

In this range of large contingencies shown in Fig. 3.13, it is clearly observed that the ADB controller provided a robust and stable RoCoF. The ADB halted the RoCoF faster than the PI and Fuzzy-PI controllers. Similarly, in Fig. 3.14, the average frequency deviation in the south zone Δf_2 as a function of the size of the imbalance contingency remained more robust when the ADB controller was used.
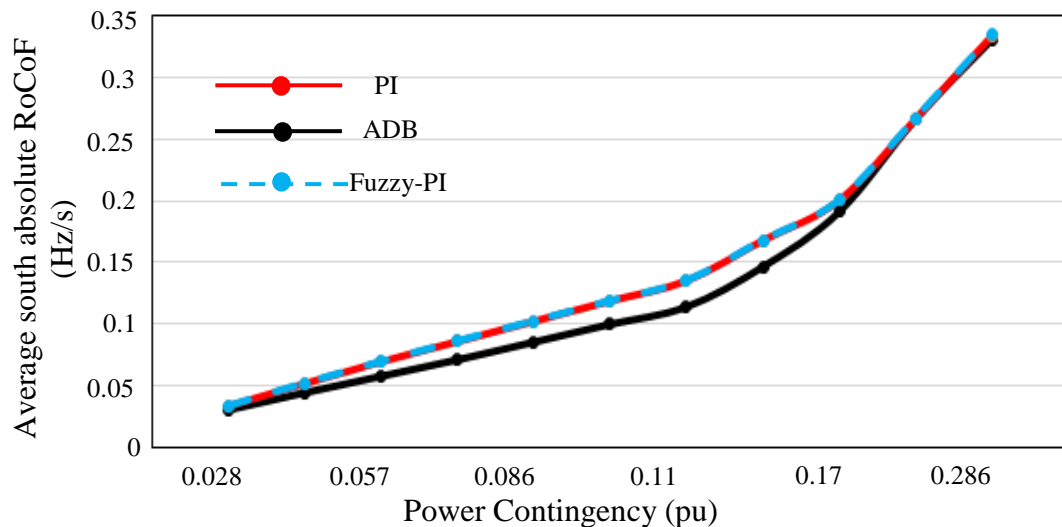
Fig. 3.13 Average absolute RoCoF of south zone against different contingencies (Case3: 2029-2030)
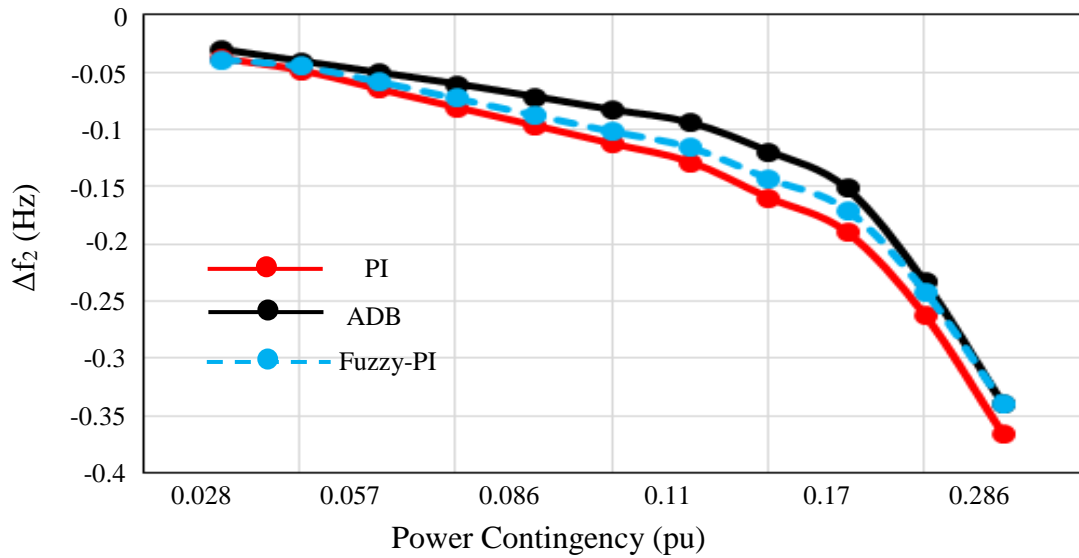
Fig. 3.14 Average frequency deviation of the south zone against severe contingencies (Case3: 2029-2030)

3.6.4 Case study 4

In reality, the power mismatch between generation and demand has a smoother shape and continues deviation rather than just a sudden step deviation. Therefore, the ramp change of power due to a loss of generation and demand within (-0.3 to 0.3 p.u.) was considered, as shown in Fig. 3.15. This case study was undertaken for the year 2029/2030 scenario.

It is clearly shown from Fig. 3.16 that the designed ADB controller has the ability to slow down the RoCoF over large continuous contingencies.

Similarly, Fig. 3.17 shows that the ADB controller provided a robust high and low frequency response in proportion to large continuous disturbances. In addition, ADB controller reduced the volume of frequency deviation more than the PI and Fuzzy- PI controllers.

In summary, in comparison with PI and Fuzzy-PI controllers, the ADB controller has the strongest response, which can conform to the future energy scenario in which there is a reduction in the system inertia. That is, to decrease the regional frequency deviation, to halt the regional RoCoF subsequent to normal, large, and continuous

76

frequency incidents.
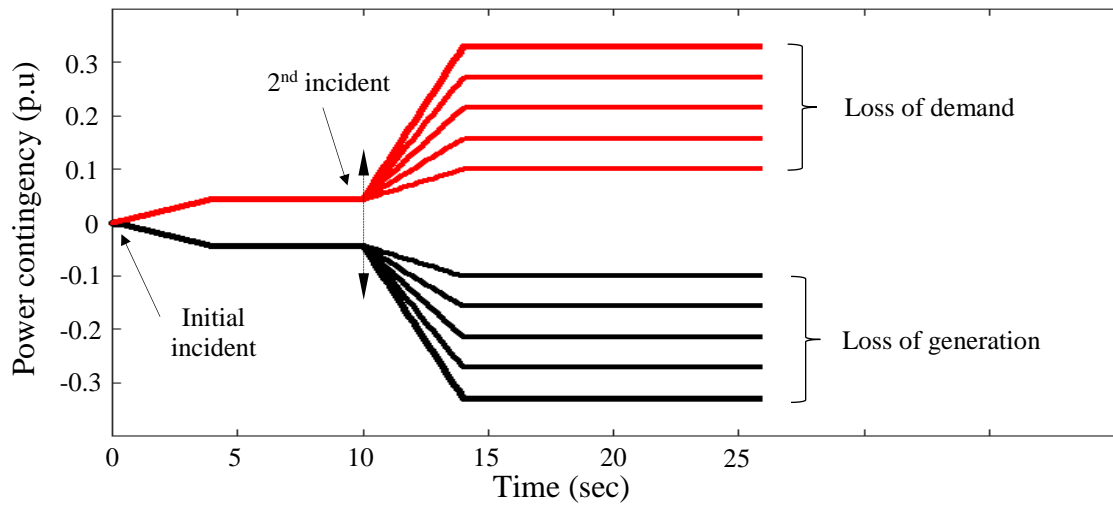
Fig. 3.15 High and low continuous power contingencies (p.u) (Case 4)
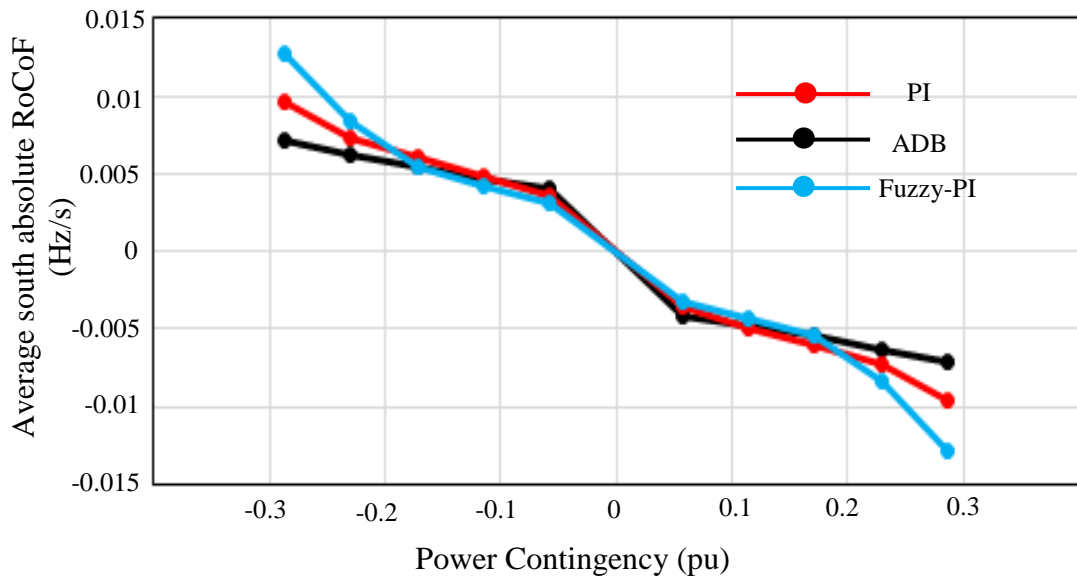
Fig. 3.16 Average absolute RoCoF of the south zone as a function of different continues disturbances (Case 4)
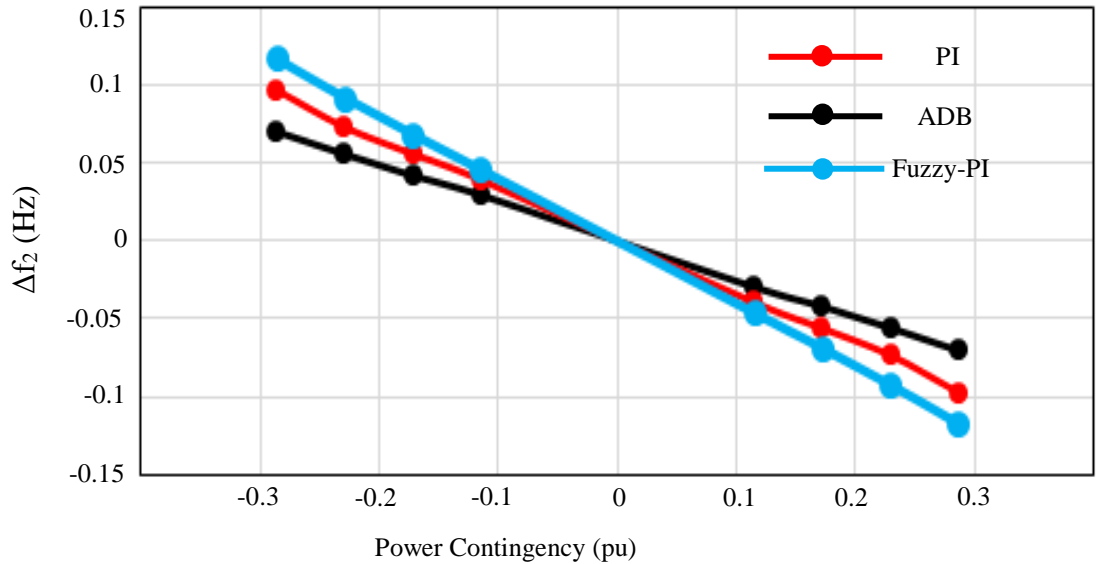
Fig. 3.17 Average frequency deviation of south zone as a function of different continues disturbances (Case 4)

3.7 Conclusion

In this research, an adaptive deadbeat (ADB) controller was developed to improve the frequency behaviour in the interconnected power system. A simplified interconnected model for north and south zones of Scotland was developed for the future frequency response study and was used as a test system.

In comparison with PI and Fuzzy-PI controllers, the ADB controller achieved the most satisfactory response in terms of reducing the frequency deviation and slowing down the RoCoF during and after the frequency incidents. In addition, the ADB controller showed a robust behaviour against a wide range of disturbance conditions when there is a reduction in system inertia.

Chapter 4

Thermodynamic models of domestic heat pumps and Fridges

4.1 Introduction

Domestic demand currently accounts for about 40% of gas and about 35% of electricity demand in GB [118]. However, the use of electricity is expected to increase over gas demand in the future due to carbon reduction policies which focus on replacing gas with electricity. Electrification of the heat demand (i.e. heat pumps) is one of the main reasons to change the demand uptake from gas to electricity. The GB annual electricity demand for space and water heating is expected to rise to 34,684 GWh in 2030 with less reliance on gas fuel. Over 28% of the total space heating will be delivered from heat pumps by 2030 [78]. This will pose challenges to the System Operator who is responsible for balancing the power system. For this reason, new Balancing Services (BS) should be developed to maintain the balance between demand and supply second by second and in real time. One of the options highlighted in the System Operability Framework report [118], prepared by National Grid, is to provide frequency response by demand side response using a large number of small loads that have the potential to provide in aggregation a frequency response similar to the response of large generation plants. Different small load units could provide frequency response. The loads with natural thermal storage or inertia are particularly suited, for example, heat pumps and fridges.

This Chapter investigated the model of aggregated heat pumps as a source of flexible load in GB. A simplified thermal model was developed to represent a population of domestic buildings equipped with heat pumps. Five case studies were conducted to identify the suitable number of individual heat pump models that can be aggregated to represent the predicted number of heat pumps accurately and could

be used for a frequency control study in the GB power system. In addition, a simplified thermal model of a population of fridges was developed and will be used in chapter 6 together with the heat pumps model to offer a load aggregation scheme over a time of day that could provide dynamic frequency response to the grid.

4.2 Modelling of the thermal performance of buildings using heat pumps

A diagram of a domestic heat pump unit installed in a building is shown in Fig. 4.1 [119]. The building has a thermal contact to the cold outdoor environment. Therefore, heat is transferred from the buildings indoor to the environment through the thermal contact between them. This heat transfer causes the temperature inside the buildings to drop. The actual heat gain from the environment takes place in the heat pump's evaporator. The temperature of the building controls the ON and OFF state of the heat pump compressor. If the temperature drops lower than its low set-point T_{min}, the compressor is switched ON and starts warming the building. If the temperature is higher than its high set-point T_{max}, the compressor is switched OFF.

The liquid refrigerant inside the evaporator is boiled and evaporated even in sub-zero degrees. The resulting gaseous is then compressed through the compressor causing its pressure and temperature to rise. The heated refrigerant passes through the condenser, and the heat is then released to the building. After that, the gaseous is converted into a hot liquid which goes through an expansion valve causing its temperature to drop. It can once again absorb the heat from the outside air, and the heat pump cycle starts again.
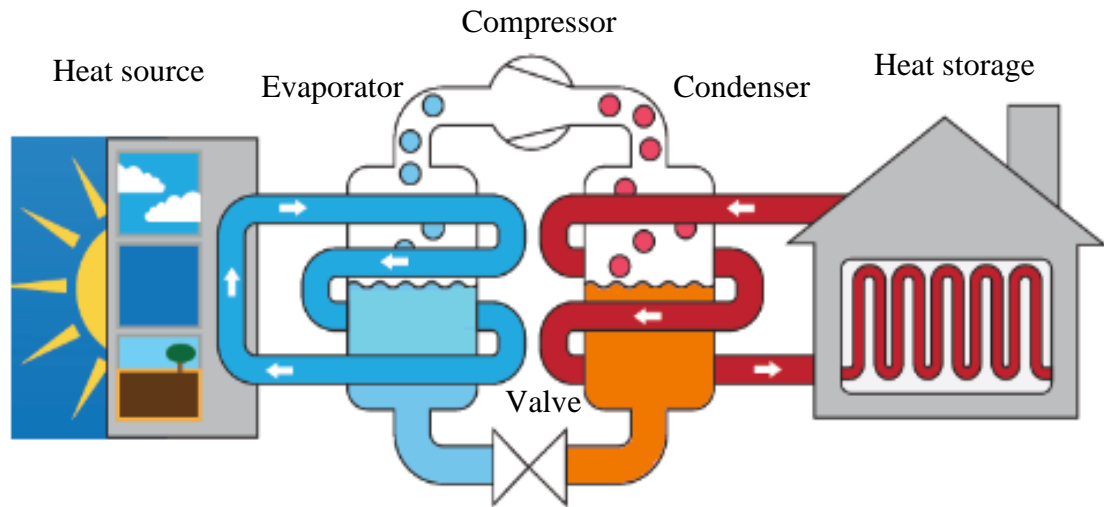
Fig. 4.1 Diagram of a heat pump operation (modified based on [119])

4.2.1 Thermodynamic model of a single domestic building coupled with a heat pump unit

A detailed equivalent thermal parameter (ETP) model is used to represent the domestic buildings. This model is suitable to represent the heat exchange behaviour of the residential and small commercial buildings [120]. The ETP model is represented by analogy to an electrical circuit with lumped thermal parameters based on resistance-capacitance (RC) as shown in Fig. 4.2. The electrical resistors in this circuit represent the thermal resistance of a building. The capacitors represent the building heat capacitance which is able to store potential heat. The heat flow is represented by current, and the temperature is represented by voltage. The electric current source represents the heat rate flow into the building which is provided through a thermostatically controlled heat pump unit coupled to the building. The elements of building are assumed to be lumped into one point (node) with a uniform system temperature [121]. As shown in Fig. 4.2, the ETP model consists of three nodes, one node for the outside air temperature T_o, and two nodes representing the building envelope (one for the indoor air temperature T_{in}, and other for the building mass temperature T_m).

There are two heat transfer processes presented in this model. One heat transfer process is due to the work done by the heat pump's compressor which transfers the heat directly to the room, and due to the thermal contact between the room and outside ambient (T_{in} to T_o via R_1). The second heat transfer process occurs due to the thermal contact between the room and the building mass (T_{in} to T_m via R_2). These heat transfer processes cause a varation in both the temperature of building T_{in} and temperature of mass T_m. The ETP model are mathematically modelled by using the Ordinary Differential Equations (ODE) method. The differential equations descriptions of the ETP model are formulated by calculating the balancing equations of the room and mass temperatures. The varation of T_{in} is represented as a first order differential equation as shown in Equation (4.1).
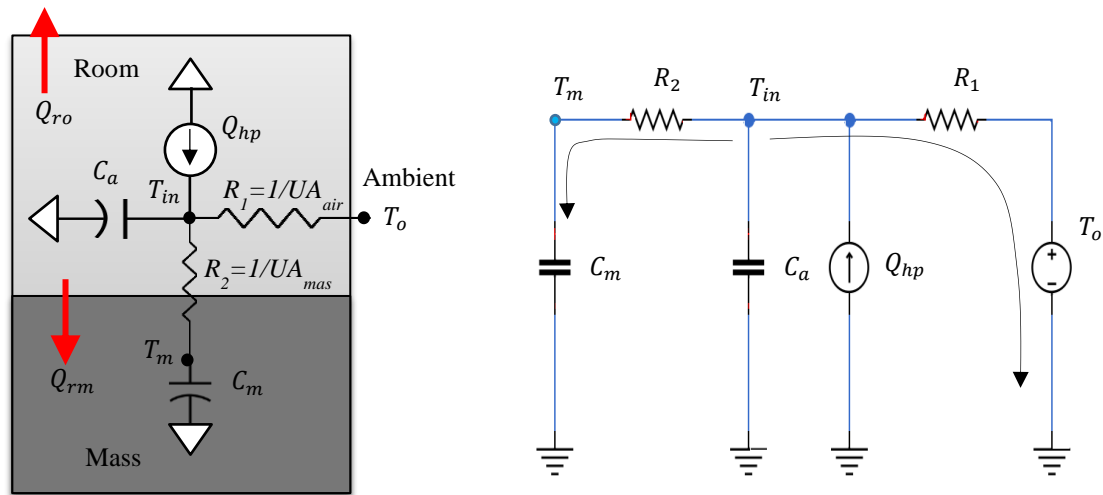
Fig. 4.2 Equivalent thermal model of a domestic building coupled with a heat pump unit

$$C_a \frac{dT_{in}}{dt} = -Q_{rm} - Q_{ro} + Q_{hp} \tag{4.1}$$

In this model, C_a(J/^{0}C) is the building indoor air heat capacity. The Q_{hp}(W) is the heat rate of heat pump unit. The Q_{rm} is the heat transfer between the room and mass, and is represented by Equation (4.2).

$$Q_{rm} = UA_{mass}(T_{in} - T_m) \qquad (4.2)$$

The T_m (^{0}C) is the building mass temperature and UA_{mass} (W/^{0}C) is the heat loss coefficient between the room air and mass. The Q_{ro} is the heat transfer from the room to the ambient, and is represented by Equation (4.3).

$$Q_{ro} = UA_{air}(T_{in} - T_o) \qquad (4.3)$$

The T_o (^{0}C) is the ambient temperature and UA_{air} (W/^{0}C) is the heat loss coefficient from the air to the outdoor ambient.

In this thesis, $1/UA_{air}$ is denoted R_1 and $1/UA_{mass}$ is denoted R_2. By combining Equations (4.1) - (4.3), a first order differential equation of T_{in} is obtained:

$$\frac{dT_{in}}{dt} = -\left(\frac{1}{R_1\,C_a} + \frac{1}{R_2\,C_a}\right)T_{in} + \frac{1}{R_2\,C_a}T_m + \frac{1}{R_1 C_a}T_o + \frac{Q_{hp}}{C_a} \qquad (4.4)$$

For the building mass, a similar analysis was carried out. Due to the thermal contact between the building mass and the building indoor, the mass temperature T_m becomes variable and can be presented in Equation(4.5).

$$\frac{dT_m}{dt} = \frac{1}{R_2\,C_m}T_{in} - \frac{1}{R_2\,C_m}T_m \qquad (4.5)$$

The C_m (J/^{0}C) is the building mass heat capacity. Equations (4.4) and (4.5) together represent the detailed ETP model. Based on Equations (4.4) and (4.5), the state space equations of the detailed ETP model are obtained in Equations (4.6) - (4.10).

$$\dot{x} = Ax + Bu \qquad (4.6)$$

$$y = Cx + Du \qquad (4.7)$$

83

$$\dot{x}^T = [\frac{dT_{in}}{dt} \quad \frac{dT_m}{dt}], \qquad\qquad x^T = [T_{in} \quad T_m] \qquad\qquad (4.8)$$

$$A = \begin{bmatrix} -\left(\frac{1}{R_2 \, C_a} + \frac{1}{R_1 \, C_a}\right) & \frac{1}{R_2 \, C_a} \\ \frac{1}{R_2 \, C_m} & -\frac{1}{R_2 \, C_m} \end{bmatrix} \quad B = \begin{bmatrix} \frac{T_o}{R_1 \, C_a} + \frac{Q_{hp}}{C_a} \\ 0 \end{bmatrix} \qquad (4.9)$$

$$C = \begin{bmatrix} 1 & 0 \\ 0 & 1 \end{bmatrix} \qquad\qquad D = \begin{bmatrix} 0 \\ 0 \end{bmatrix} \qquad\qquad (4.10)$$

4.2.2 Simplified equivalent thermal model of a building

Typically, the building mass thermal storage C_m is large and hence, the temperature variation of the building mass dT_m/dt is small. For this reason, it is assumed that $T_{in} = T_m$ according to Equation (4.5). Therefore, the equivalent ETP model presented in Equations (4.4) and (4.5) is further simplified to Equation (4.11):

$$\frac{dT_{in}}{dt} + \frac{1}{R_1 C_a} T_{in} = \frac{1}{C_a}\left(\frac{1}{R_1} T_o + Q_{hp} \times s_{hp}(t)\right) \qquad (4.11)$$

The differential Equation in Equation (4.11) has two exponential forms depending on the state of the heat pump (s_{hp}). If a heat pump is switched ON ($s_{hp} = 1$), the first exponential form can be written as:

$$T_{in}^{t+1} = T_o + R_1 Q_{hp} - (T_o + R_1 Q_{hp} - T_{initial}^t).e^{-\frac{\tau_{on} t_{on}}{R_1 C_a}} \qquad s_{hp} = 1 \qquad (4.12)$$

When a heat pump is switched OFF ($s_{hp} = 0$), the second exponential form can be written as:

$$T_{in}^{t+1} = T_o - (T_o - T_{initial}^t).e^{-\frac{\tau_{off} t_{off}}{R_1 C_a}} \qquad\qquad s_{hp} = 0 \qquad (4.13)$$

where τ_{on} and τ_{off} are the time constants of the heat pump's ON and OFF cycles. During the heat pump ON- mode, the lower temperature set-point T_{min} represents the $T_{initial}^t$, and the T_{max} represents T_{in}^{t+1}. Therefore, the time constant τ_{on} is calculated as in Equation (4.14). Conversely, during the heat pumps OFF- mode, the upper temperature set-point T_{max} represents the $T_{initial}^t$ and T_{min} represents T_{in}^{t+1}. Then, the time constant τ_{off} is calculated as in Equation (4.15).

$$\tau_{on} = \frac{R_1 C_a}{t_{on}} \ln\left(\frac{T_{min} - T_0 - Q_{hp}R_1}{T_{max} - T_0 - Q_{hp}R_1}\right) \qquad\qquad S_{hp} = 1 \qquad\qquad (4.14)$$

$$\tau_{off} = \frac{R_1 C_a}{t_{off}} \ln\left(\frac{T_{min} - T_0}{T_{max} - T_0}\right) \qquad\qquad S_{hp} = 0 \qquad\qquad (4.15)$$
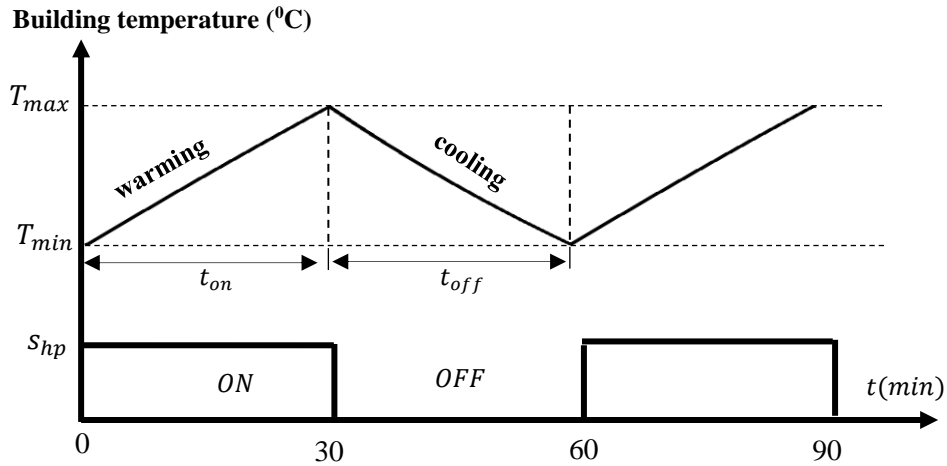
Fig. 4.3 Temperature control of one heat pump unit

The typical ON and OFF periods (t_{on} and t_{off}) of a heat pump and temperature variation of a building are shown in Fig. 4.3. For a typical building the typical t_{on} of a heat pump is around 30min, whilst the typical t_{off} is ≥30min [122]. However, in this thesis, the t_{on} and t_{off} periods of the heat pumps were chosen to be similar.

To simulate the simplified model presented in Equations (4.12) and (4.13), they both require further adjustments to meet the lower and upper-temperature set-points and the ON/OFF heat pump cycles. As can be seen in Fig. 4.3, if the heat pump is

in ON state, the temperature T_{in} starts from $T_{min=}T_{initial}^t$ at $t_{on} = 0$min, and ends to $T_{max=}T_{in}^{t+1}$ at $t_{on} = 30$min. Therefore, Equation (4.12) is re-written as (4.16):

$$T_{in}(t) = \frac{T_{min}e^{-\frac{46.62}{R_1 C_a}}-T_{max}}{e^{-\frac{46.62}{R_1 C_a}}-1} + \frac{T_{max}-T_{min}}{e^{-\frac{46.62}{R_1 C_a}}-1}.e^{-\frac{\tau_{on}t_{on}}{R_1 C_a}} \qquad 0min \leq t_{on} \leq 30min \quad (4.16)$$

Similarly, if the heat pump is in OFF state, the temperature T_{in} starts from $T_{max=}T_{initial}^t$ at $t_{off} = 30$min, and ends to $T_{min=}T_{in}^{t+1}$ at $t_{off} = t - t_{on}$. Hence, Equation (4.13) is rewritten as (4.17):

$$T_{in}(t) = \frac{T_{max}e^{-\frac{159.885}{R_1 C_a}}-T_{min}}{e^{-\frac{159.885}{R_1 C_a}}-1} + \frac{T_{min}-T_{max}}{e^{-\frac{159.885}{R_1 C_a}}-1}.e^{-\frac{\tau_{off}t_{off}}{R_1 C_a}} \qquad 30min \leq t_{off} \leq t - t_{on}$$

$$(4.17)$$

Equations (4.16) and (4.17) were used to simulate the temperature of a single domestic building equipped with a heat pump unit. The temperature set-points T_{min} and T_{max} were set to 19^{0}C and 23^{0}C to represent a building insulated to typical UK levels [123]. With such temperature levels, the heat pump's cycle time $(t_{on} + t_{off})$ is almost one hour. According to the Element Energy study [67], it was assumed that each heat pump unit has a power consumption of 3kW. This power was chosen to be the lower value of the typical range for domestic heat pumps in the UK. The mean values of parameters R_1 and C_a are shown in Table 4.1. These parameters were calibrated based on temperature measurement of typical domestic buildings [122]. A study published in [124] uses a measured operational data and showed that some UK domestic buildings have a near values to the R_1 and C_a presented in Table 4.1. The building temperature and the heat pump state were simulated based on Equations (4.16) and (4.17) as shown in Fig. 4.4. Note that the trajectory of the modelled building temperature matches the building temperature curve which was tuned through measurement [122].

Table 4.1 Model parameters

C_a (J/^{0}C)	R_1 (^{0}C/W)	Q_{hp} (W)	T_0 (^{0}C)	T_{high} (^{0}C)	T_{low} (^{0}C)
3599.3	0.1208	3000	10	23	19
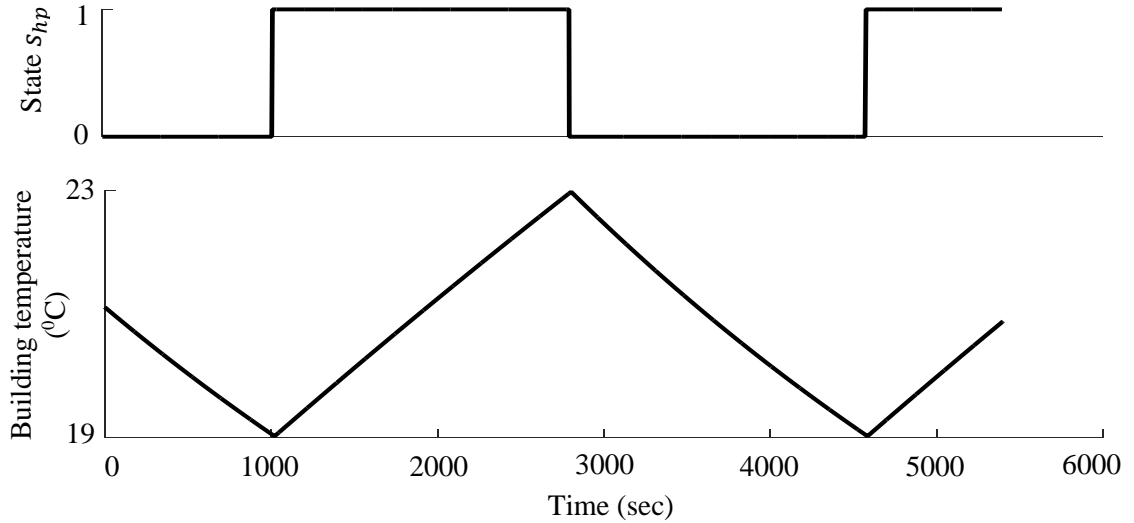
Fig. 4.4 Temperature of a room and heat pump state

4.2.3 Aggregated model of a population buildings and heat pumps

A single ETP model with different thermal parameters can be used to represent a large number of domestic buildings [120]. The thermal parameters (R_1 and C_a) that are required to compute the load vary between buildings. The expected thermal parameters' values for diverse types of UK houses were modelled in [124], using parameter estimation techniques. In this thesis, the population of domestic buildings was modelled by giving ranges to the thermal parameters, where every building was assigned randomly with different values of R_1 and C_a in the ranges established in Table 4.2. To reflect the diversity among a population of heat pumps, the starting time in Equations (4.16) and (4.17) was randomised, using a uniform distribution, and hence each building was randomly assigned with different initial temperature in the range $[T_{min}, T_{max}]$. A simulation was then carried out on a population of heat pumps with different initial ON and OFF state and different temperature state. The

power rating of each heat pump unit is 3 kW. Fig. 4.5 shows the temperature curves of ten buildings. Fig. 4.6 shows the ON/OFF states of ten heat pumps coupled to these buildings. Fig. 4.7 shows the total aggregated power consumption of different numbers of heat pumps. This model should produce satisfactory results and significantly simplifies the forecasting process required to create the temperature priority list for a large number of heat pump units. However, the identification of the numbers of heat pump models in GB is presented in Section 4.4.

Table 4.2 Thermal parameters used in the simulation

Parameters	Values
R_1	(0.005-1.177) ^{0}C/W
C_1	(3,263-15,000) J/^{0}C
T_{in}	(19-23) ^{0}C
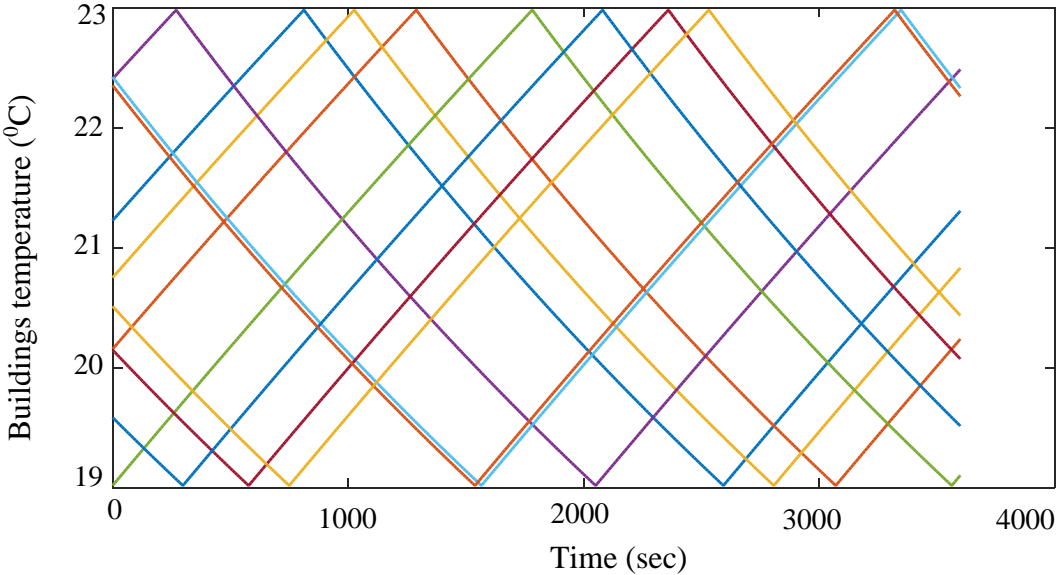
Fig. 4.5 Temperature curves of ten buildings

88
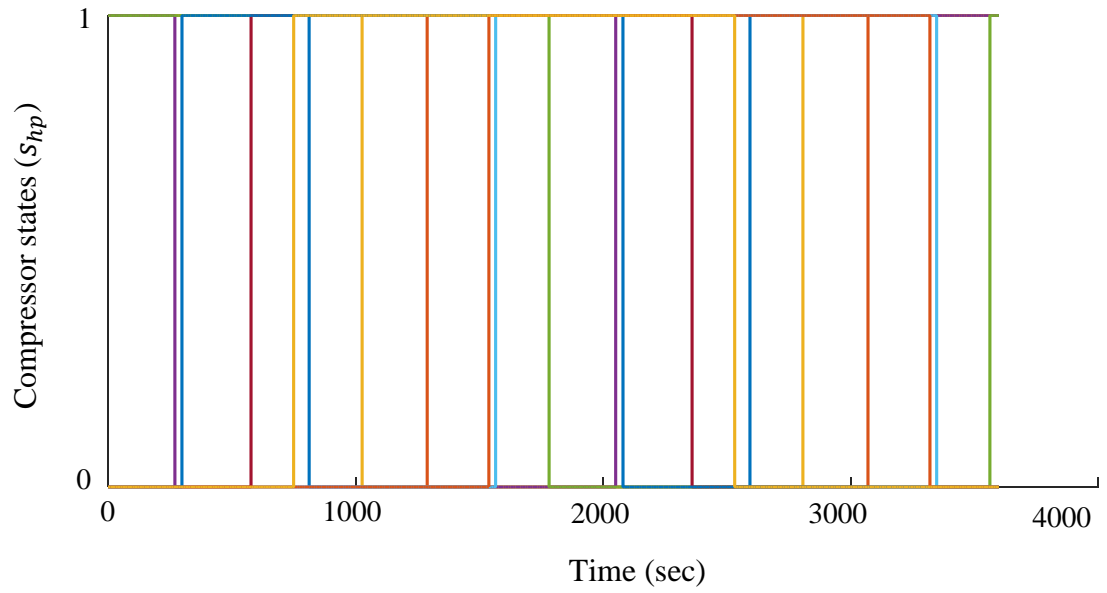
Fig. 4.6 Compressor ON/OFF state of ten heat pumps
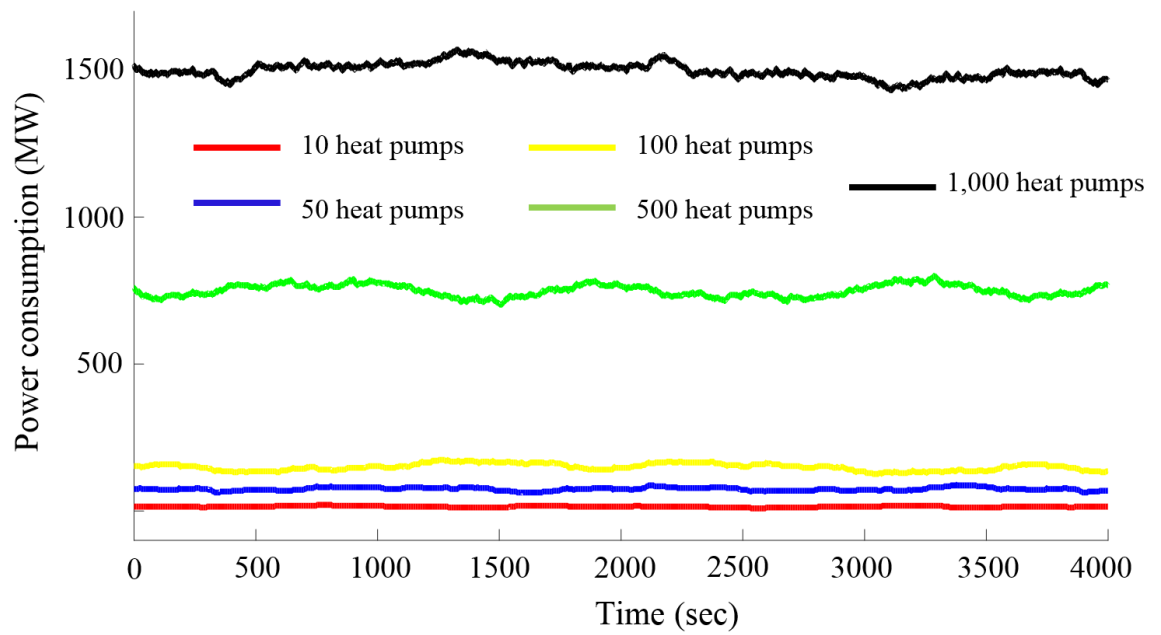
Fig. 4.7 Total power consumption of heat pumps

4.3 Aggregated model of a population of fridges

In this section, a simplified thermal model of the domestic fridges was presented based on reference [125]. This fridges model will be used together with the heat pumps model in Chapter 6 to give a load aggregation scheme over a time of day in the GB power system.

Fig. 4.8 shows the diagram of a fridge including a cooler and Freezer compartments. The cooler compartment is usually large and is used to store the food at a cool temperature. The freezer compartment is generally smaller and is used to make ice and store food below a freezing point. Fridges have a reverse operation to the heat pumps. When the compressor is switched ON, the refrigerant material flows through the pipes. When the refrigerant goes through the evaporator, the hot temperature is released to the room ambient causing the temperature inside the fridge to drop.

Fridges are in service in all seasons. Thus, they can take part in the balancing services all the year round. Because of the thermal storage capacity of the fridges, the power consumption of fridges can be shifted in response to the system frequency with a little disruption to its temperature control performance. By 2030, there will be approximately 48 million fridges connected to the GB power system [126]. According to reference [78], the average load of the cold appliances as estimated for the year 2030 will be approximately 1,000 MW in winter and 1,300 MW in summer.

Temperature in the cooler compartment (T_{Co}) is measured by a temperature control. The temperature control is used to keep the fridge temperature within a lower and upper set-points T_{low} and T_{high}. If the temperature is below the T_{low}, the compressor is switched OFF; and if the temperature is above the T_{high}, the compressor is switched ON. A simplified thermal model of a cooler and Freezer compartments is derived from the heat transfer principles. The heat transfer from the compressor to the cooler compartment causes a temperature variation (dT_{Fr}/dt) inside the freezer, as presented in Equation (4.18). U ($Wm^{-2}K^{-1}$) is the heat transfer coefficient of the thermal contact. A (m^2) is the area of thermal contact. C_{Fr} (J/K) is the freezer heat capacity. T_{Co} (^0C), and T_{Fr} (^0C) are the cooler and freezer temperature. P_{fr}(W) is the power consumption of fridge's compressor, s_{fr} is 1 if compressor is ON and 0 if it is OFF. Note that the term $CoFr$ refers to the thermal contact between the cooler and freezer.

$$\frac{dT_{Fr}}{dt} = \frac{U^{CoFr} A^{CoFr}}{C_{Fr}} \left(T_{Co}(t) - T_{Fr}(t)\right) - \frac{P_{fr} s_{fr}(t)}{C_{Fr}} \tag{4.18}$$

Similarly, the heat transfer from cooler compartment to the room ambient results in variation in the cooler temperature (dT_{Co}/dt) as shown in Equation (4.19). C_{Co} (J/K) is the cooler heat capacity. $T_{Amb}(^0C)$ is the ambient room temperature. Note that the term $CoAmb$ refers to the thermal contact between the cooler compartment and room ambient.

$$\frac{dT_{Co}}{dt} = \frac{U^{CoAmb} A^{CoAmb}}{C_{Co}} \left(T_{Amb}(t) - T_{Co}(t)\right) - \frac{U^{CoFr} A^{CoFr}}{C_{Co}} \left(T_{Co}(t) - T_{Fr}(t)\right) \tag{4.19}$$
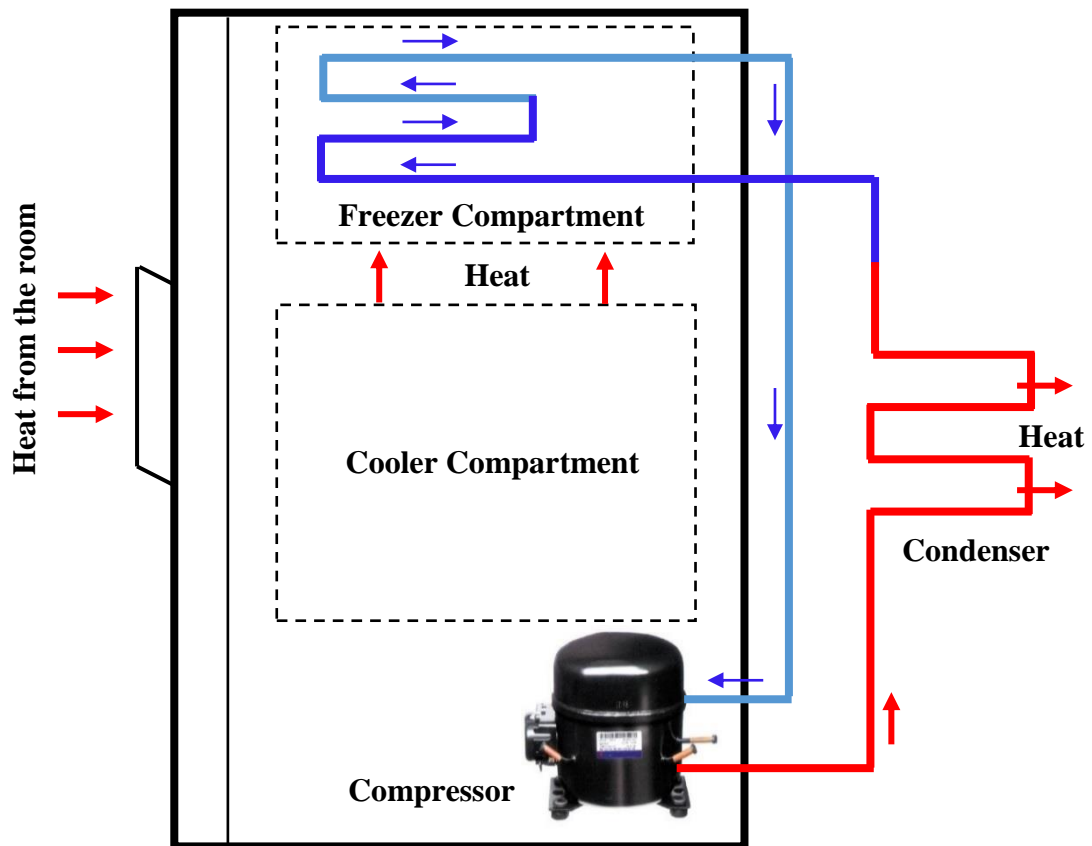
Fig. 4.8 Heat flow in a fridge (modified based on [127])
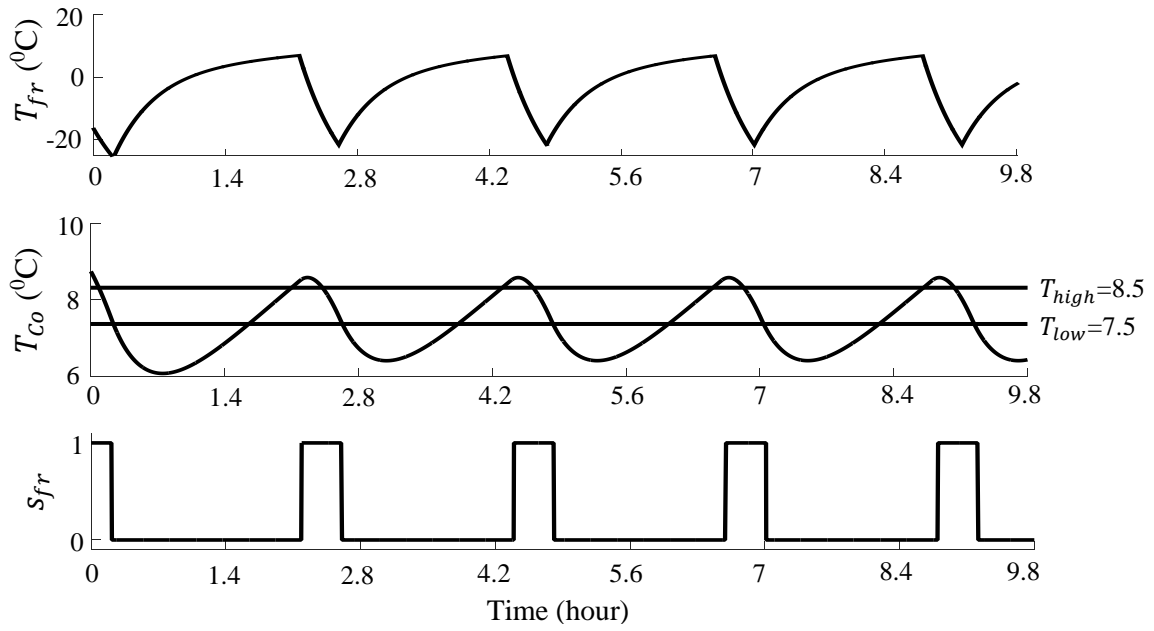
Fig. 4.9 Freezer and cooler temperature based on modelling ($T_{Amb}=22^0C$)

A thermodynamic model of a cooler and freezer is developed in *MATLAB* by simulating the differential Equations (4.18) and (4.19). The physical parameters U^{CoFr}, A^{CoFr}, U^{CoAmb}, A^{CoAmb}, C_{Fr}, and C_{Co} were provided by Open Energi at an ambient room temperature of around 22^0C [125]. The temperature and compressor state of a single fridge is shown in Fig. 4.9. The curves in Fig. 4.9 have a similar behaviour of the fridge curves obtained by field measurement [125]. It can be seen that there is a time delay before the temperature drops lower than T_{max} or rises higher than T_{min}, this is due to the thermal contact between the cooler and the freezer.

There is a range of diversity in the thermal parameters among the fridges (U, A, C_{Fr}, C_{Co}). A single thermal model presented in Equations (4.18) and (4.19) with different thermal parameters can be used to represent a population of fridges. In this research, diversity of 20% of thermal parameters were used [125]. This is carried out by multiplying each of the thermal parameter by a random number in a range of [0.8, 1.2]. To initialize the simulation, the starting temperature T_{Co} and T_{Fr} of each fridge unit was randomised. For ON fridges, the temperature T_{Co} is randomised in the range of [6^0C, 8.5^0C] and T_{Fr} is randomised in the range of [-15^0C, 5^0C]. For the OFF fridges, T_{Co} is randomised in the range of [5.5^0C, 9^0C] and T_{Fr} is randomised in the range of [-10^0C, 10^0C]. The power rating

of each fridge unit is 0.1kW [125]. Fig. 4.10 shows the cooler temperature curves of ten fridges. Fig. 4.11 shows the fridge compressor states of ten fridges. Fig. 4.12 shows the total aggregated power consumption of different numbers of fridges. It can be seen that the power consumption of a population of fridges is lower than the power consumption of heat pumps. This is because the average power rate of each heat pump unit is 30 times higher than the fridge unit.
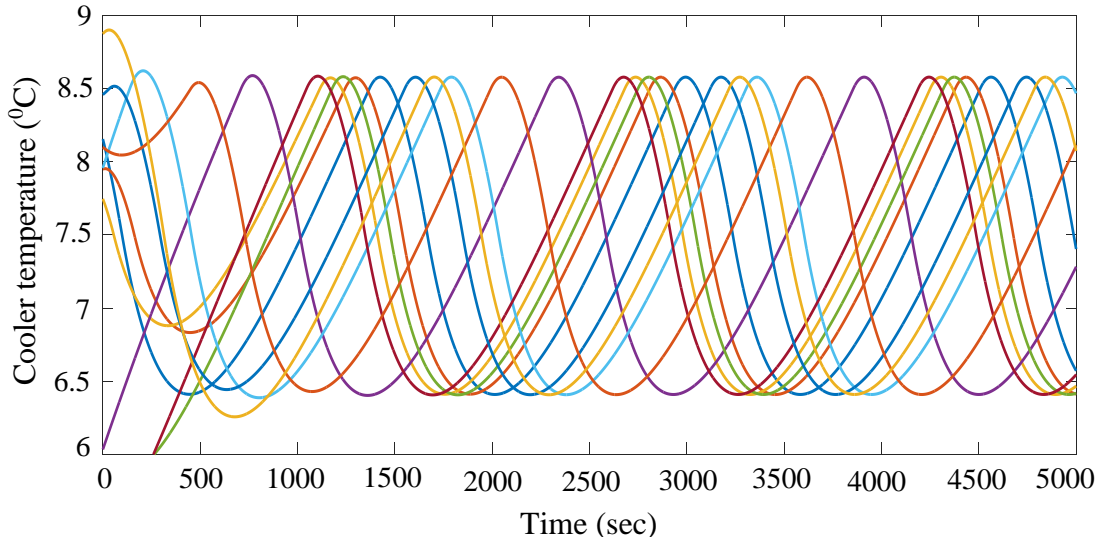
Fig. 4.10 Cooler temperature of ten fridges
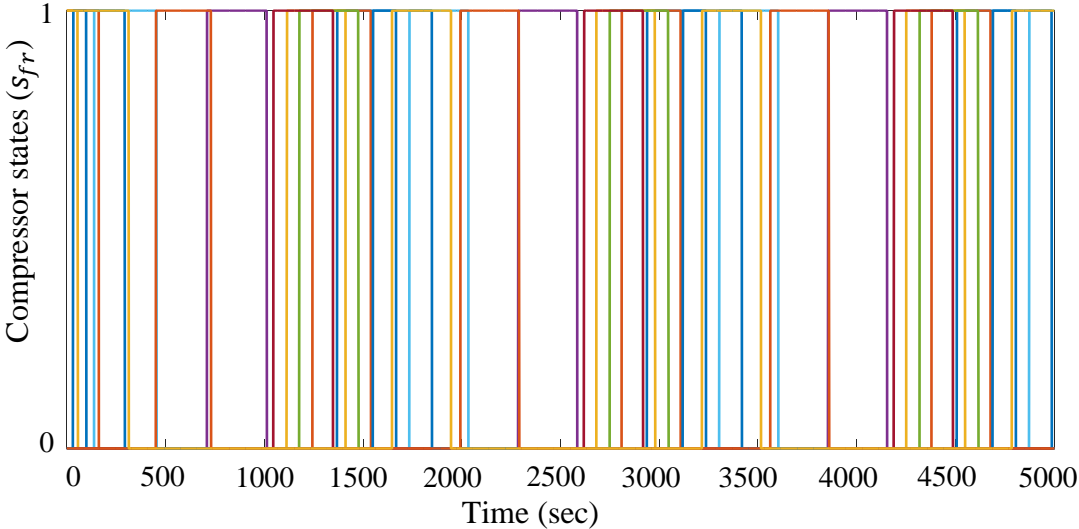
Fig. 4.11 Compressor ON/OFF state of ten fridges
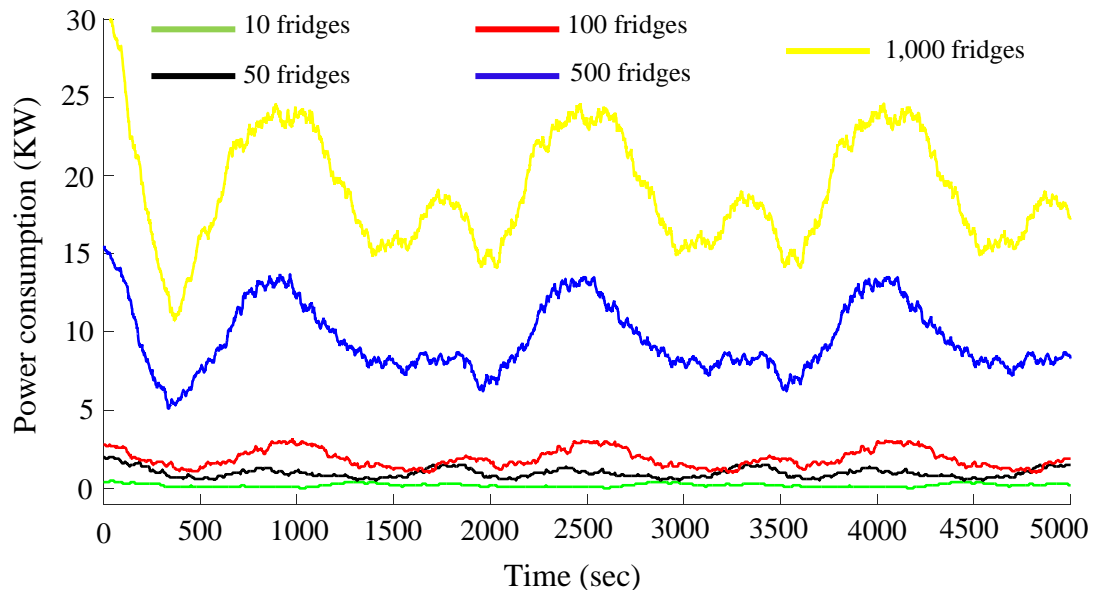
Fig. 4.12 Total power consumption of different number of fridges

4.4 Identification of a suitable number of load models

The diversity in the usage of appliances is the key feature of domestic demand. Reference [66] shows that the demand coincidence factor remains constant when the number of consumers converges to 10,000 as shown in Fig. 4.13. This means that the ratio between the total number of appliances (greater than 10,000) and the number of appliances that would operate (consume electricity) is approximately constant. However, the coincidence factor might be slightly different from one type of load to another. In the next sections, the numbers of the heat pump and fridge models that are suitable to represent the total load are identified.
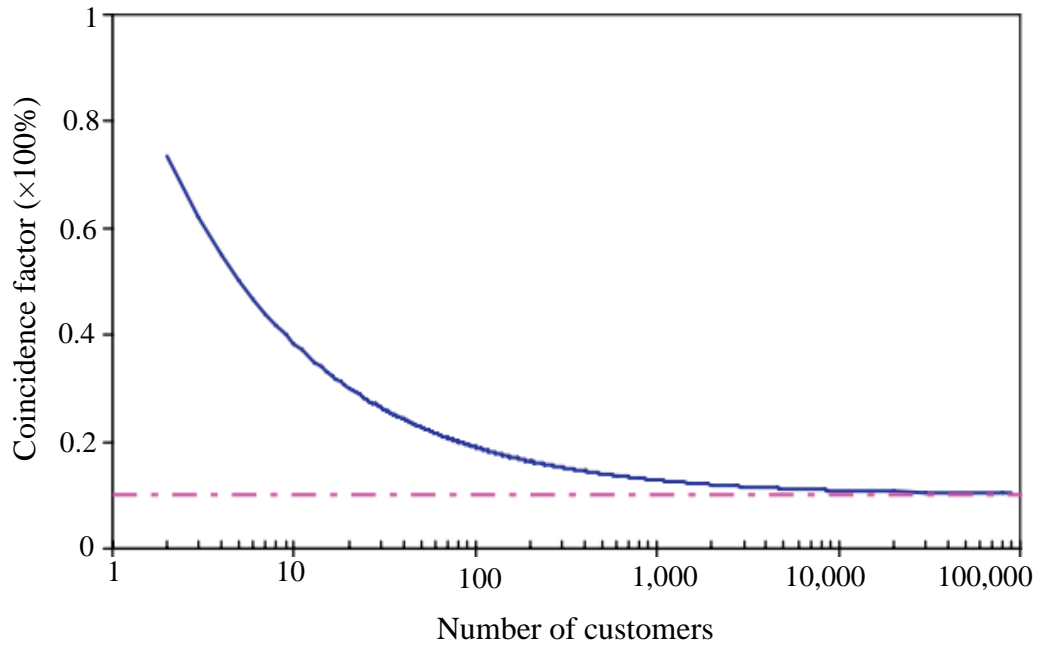
Fig. 4.13 Relationship between the demand coincidence factor and the number of customers [66]

4.4.1 Identification of a suitable number of heat pump models

According to the 2030 medium uptake scenario of Element Energy [67], there are expected to be 3.8 million heat pumps in UK buildings by 2030.

It is unnecessary to have 3.8 million independent heat pump models to represent all connected heat pumps to the GB power system. Therefore, an integrated model with a smaller number of individual heat pumps was developed and then scaled up by multiplying the number of individual heat pumps by a number in order represent the 3.8 million. The number of individual heat pump models, considering five aggregated case studies which are then scaled up to represent the total 3.8 million heat pumps, are shown in Table 4.3. This modelling work was conducted to find the most suitable case to model the behaviour of all 3.8 million heat pumps.

The first case study aggregated model considers the aggregation of 100 individual heat pump models with different states at temperature T_{in} and heat pump's ON/OFF state. By multiplying these aggregated models with 38,000 results in a representation of the entire

heat pump population in the GB power system; this means that 38,000 heat pumps were in the same states. The case study five used an integration of 100,000 individual heat pump models with different states. By multiplying these aggregated models with 38 to represent the entire heat pump population in the GB, this assumed that only 38 heat pumps had similar states.

Following a drop of power at time 100sec, the power consumption behaviour of five case studies of different numbers of heat pumps in each aggregation was compared. The drop of power was represented by a step change in heat pumps compressor states, i.e., all heat pumps were switched OFF at time 100sec, and they started to recover gradually when the temperature reached the minimum set-point T_{min}.

Fig. 4.14 compares the total power consumption of 3.8 million heat pumps in all five case studies following the step change in power for 30 minutes. It can be observed that the power consumption in the aggregated models with 5,000, 10,000, and 100,000 individual heat pump models showed a gradual and similar power change. However, for the aggregated models with 100 and 1,000 individual heat pump models (case studies 1 and 2), the power consumption of the heat pumps was more sensitive and less gradual than the other aggregated models.

The simulation time of each aggregated model was presented in Table 4.3. Considering accuracy and simulation time, the aggregated model in case study three, with 5,000 heat pumps multiplied by scaling number 760, was chosen as the most reasonable model to represent the entire population of heat pumps, for frequency control study in the GB power system.

Table 4.3 Number of aggregated heat pump models

Case Study	Number of individual Heat Pump models	Multiplied Number	Simulation time
1	100	38,000	1 sec
2	1,000	3,800	7 sec
3	5,000	760	45 sec
4	10,000	380	84 sec
5	100,000	38	649 sec
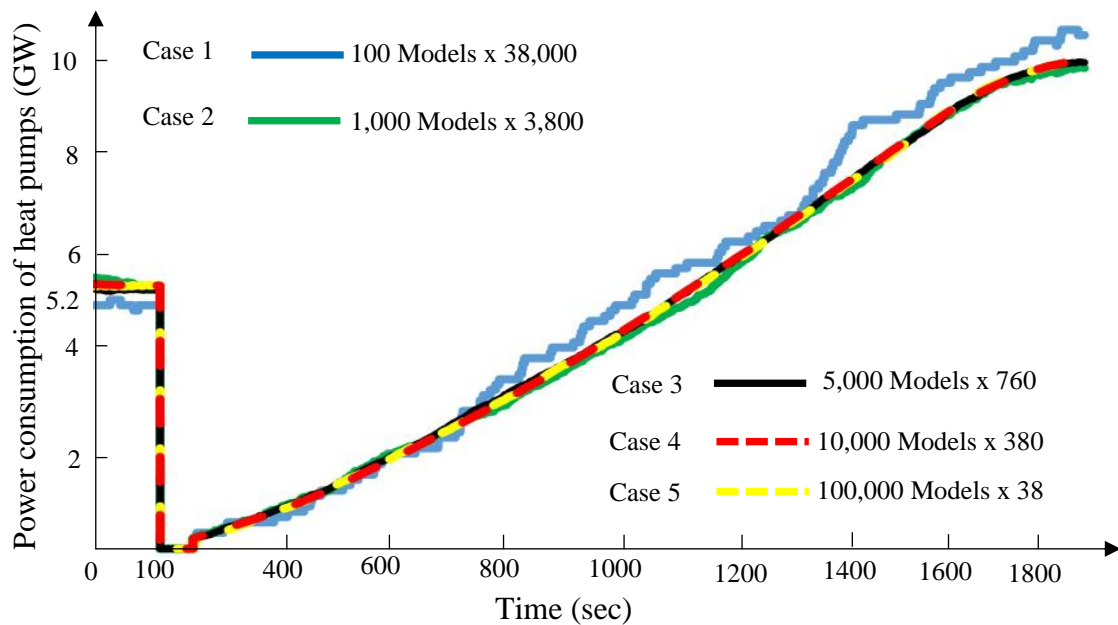
Fig. 4.14 Total Power Consumption of 3.8 million heat pumps obtained from the thermodynamic model

4.4.2 Identification of a suitable number of fridge models

The suitable number of fridge models that represents the entire 48 million fridge population connected to the 2030 GB's power system was found applying the heat pumps methodology as was described previously.

Following a drop of power at time 100sec, the power consumption behaviour of five case studies considering different aggregated number of fridges was compared. The decrease of power was represented by a step change in fridges compressor states, i.e., all fridges were switched OFF at time 100sec, and they started to recover gradually when the temperature reached the minimum set-point T_{min}. As can be seen in Fig. 4.15, the power consumption behavior remained the same when the number of fridge models was equal or greater than 10,000. Therefore, the aggregated model with 10,000 different fridge states multiplied by a scalar number was used in this study to represent the total number of fridges connected to the GB power system.
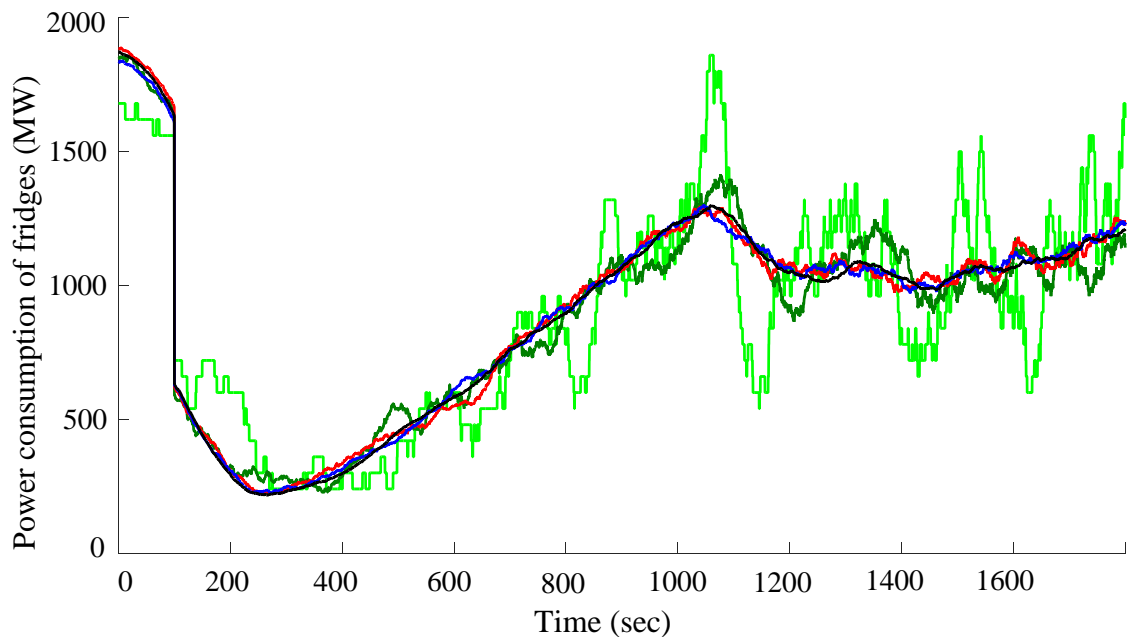
Fig. 4.15 Total Power Consumption of 48 million fridges obtained from the thermodynamic model

4.5 Conclusion

This chapter investigated the model of aggregated heat pumps and aggregated fridges as a source of flexible load in the Great Britain power system. A thermodynamic model of a population of domestic heat pumps and fridges was developed. Seven case studies were used to identify the suitable aggregated number of heat pumps and fridges to accurately represent the 2030 projected number of heat pumps and fridges in Great Britain. An aggregated model representing 5,000 heat pumps was identified as a suitable model to represent the entire population of heat pumps, connected to the 2030 GB power system. Also, an aggregated model representing 10,000 fridges was used as an appropriate model to represent the total population of fridges, connected to the 2030 GB power system.

Chapter 5

Dynamic Frequency Response from Controlled Domestic Heat Pumps

The capability of domestic heat pumps to provide dynamic frequency response to the GB power system was investigated. A decentralised temperature control algorithm was proposed to control the building temperature and the heat pump's ON and OFF cycles. A decentralised dynamic frequency control algorithm was developed, enabling the heat pumps to alter their power consumption in response to system frequency signal. The control algorithm ensures a dynamic relationship between the temperature of building and grid frequency. The availability of heat pumps to provide low-frequency response, was obtained based on data supplied by Element Energy [67]. Case studies were carried out by connecting a representative model of the aggregated heat pumps to the regional Great Britain transmission system model, which was developed by National Grid.

5.1 Introduction

National Grid procures frequency response services from the generators through the Mandatory Frequency Response (MFR) service [128]. All large generators that are covered by the GB Grid Code must be capable of providing three types of frequency service. The primary low-frequency response service provides an additional active power (or decrease in power of demand) within 10 seconds, continuing for a further 20 seconds. The secondary response service provides low-frequency response within 30 seconds, after an incident, and lasts for another 30 minutes. For a loss in power demand incident, the high-frequency response service reduces the active generation power within 10 seconds and can be continued until the frequency is restored to the normal operation. Maintaining an instantaneous

balance between generation and demand is becoming increasingly difficult, due to the increase in the use of renewable energy resources [1]. Integration of wind turbine generators that are mechanically decoupled from the grid, reduces the inertia of the power system and causes the rate of change of frequency (RoCoF) to become more rapid [6]. Thus, a faster frequency response is required to overcome such challenges. The cost of additional frequency response under existing arrangements is expected to increase to £250 million per annum, by 2020, if no alternative technologies will be developed [6].

In its 2015 ''System Operability Framework'' report, National Grid, discusses new innovative control mechanisms, on the demand side, in order to provide rapid frequency response services and reduce the CO_2 emissions at a reasonable cost [118]. Demand Side Response (DSR) is one of these mechanisms that can be used to increase or decrease the power demand of some devices, in order to regulate the system frequency when either unpredicted fluctuations of power occur or during outages of one or several generation units [129]. In the present GB power system, some industrial loads participate in frequency control service through the Frequency Control by Demand Side Management (FCDM) service. Such controlled electricity demand is interrupted when system frequency transgresses a large low-frequency relay setting (typically 49.7Hz) and usually requires manual reconnection [130].

Heat pumps have become increasingly common in the UK [118]. By 2030, domestic heat pumps could provide an average low-frequency response of 2GW in the winter medium uptake scenario of the Element Energy report [67].

This research examines the potential of the aggregation of domestic heat pumps to provide a dynamic frequency response to the GB power system. The control of heat pumps is hereafter referred to as Dynamic Frequency Control (DFC). There are still challenges to the use of DFC in large power systems as shown in papers [68] and [92]. Each type of appliance requires a different thermal model, a suitable model to represent a population of appliances connected to the system, and a different load control characteristic. A new DFC method that controls the power consumption of heat pumps in response to the system frequency is developed without undermining

the inherent operation of heat pumps. The proposed DFC algorithm was validated through the integration of the whole model, into the GB transmission reduced system model. This chapter addresses the following questions.

- How to improve the dynamic operation of the load's triggering frequencies (F_{ON}) and (F_{OFF})?
- Does DFC interfere with the normal operation of heat pumps temperature control?
- What impact will the population of DFC-based heat pumps have on grid frequency?
- Do DFC-based heat pumps reduce the dependency on frequency services that are obtained by expensive peaking generators?
- Does regional DFC affect the system frequency?
- What impact might the DFC have on the rate of change of frequency (RoCoF), when there is a reduction in system inertia?

5.2 Control of heat pumps

5.2.1 Temperature control of heat pumps

A diagram of the Temperature Controller of a heat pump unit is shown in Fig. 5.1. The temperature control is used to maintain the building temperature within set-points T_{min} and T_{max}. The temperature control measures the building temperature T_{in} and generates temperature state signal S_T. If T_{in} reaches T_{max}, the temperature controller sets S_T to '0' and heat pump is turned OFF. If T_{in} reaches T_{min}, the temperature controller sets S_T to '1' and heat pump is turned ON.
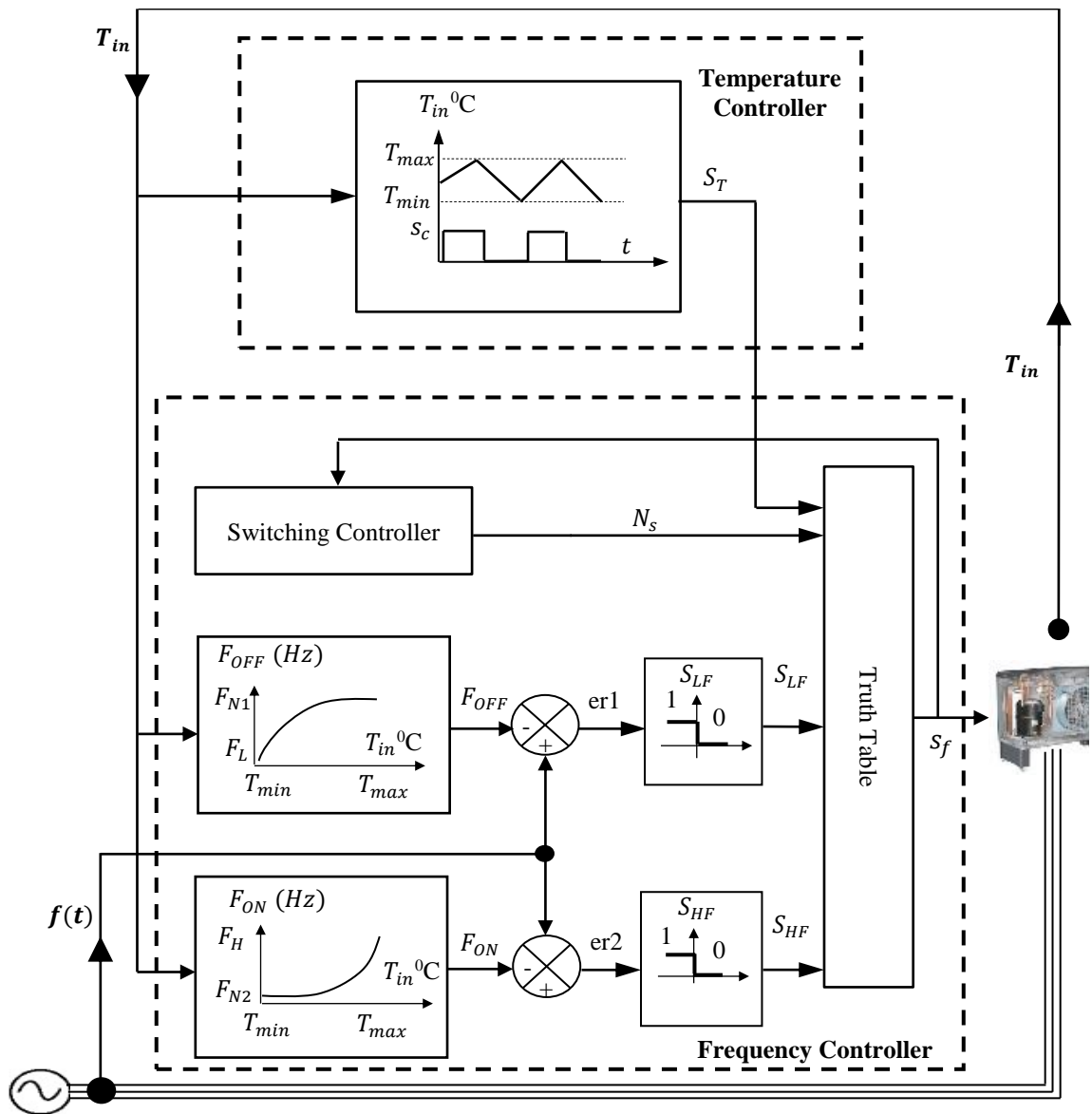
Fig. 5.1 Diagram of a DFC scheme of a heat pump

5.2.2 Integrated frequency control of heat pumps

The Frequency Controller was added to the temperature control in Fig. 5.1. The frequency control is responsible for generating the lower and higher frequency state signals S_{LF} and S_{HF}, by continuously comparing the grid frequency $f(t)$ with the trigger frequencies F_{ON} and F_{OFF}. National Grid assumes a frequency dead-band of around ± 0.1Hz[8], in which no frequency response is needed from an electric load [8,

---

[8] The dead-band value in dynamic FFR service might be narrowed to ± 0.015Hz [11]

131]. Therefore, in this study, F_{ON} has a range of 50.1-50.5Hz and F_{OFF} has a range of 49.5-49.9Hz. The final switching signal S_f is determined at each sampling time $\Delta t = 0.2$sec from the state signals S_{LF}, S_{HF}, S_T as shown in Table 5.1. When the system frequency drops lower than F_{OFF}, the S_{LF} and S_{HF} are both switched to 0 and the heat pump is switched OFF ($S_f = 0$) as presented in rows 1-2.

Similarly, if $f(t)$ rises higher than F_{ON}, the two state signals S_{LF} and S_{HF} turn into 1, and the heat pump is switched ON ($S_f = 1$) as shown in rows 3-4.

Rows 5-6 are the cases in which there is no frequency event ($F_{OFF} < f(t) < F_{ON}$). The heat pump follows the temperature control signal S_T because $S_{LF} = 0$ and $S_{HF} = 1$.

Reference [132] indicates that the maximum number of switching events should not exceed 3 every half hour, otherwise the heat pump's lifetime might be degraded. Therefore, a Switching Controller was added to the control system in Fig. 5.1 to control the maximum number of switching events. The final switching signal S_f is an input to a Switching Controller as shown in Fig. 5.1. The Switching Controller is responsible for generating a switching state signal N_s to limit the maximum number of heat pump switching events to three every 30 minutes. As shown in Table 5.1, if $N_s = 0$, S_f is determined by the frequency state signals S_{LF}, S_{HF}. If $N_s = 1$, this indicates that the number of switching events has exceeded three within 30 minutes and therefore, the heat pump reverts to temperature control and follows S_T.

The temperature T_{in} is another input to the frequency controller. If T_{in} is outside the set-points T_{min} or T_{max}, the temperature state signal S_T is prioritized and the frequency controller will not be triggered.

Table 5.1 Logic operation truth table

Row	S_T	S_{LF}	S_{HF}	if $N_s=0$	if $N_s==1$	if $T_{in} \leq T_{min}$ or $T_{in} \geq T_{max}$
1	0	0	0	$S_f=0$	$S_f=S_T$	$S_f=S_T$
2	1	0	0	$S_f=0$	$S_f=S_T$	$S_f=S_T$
3	0	1	1	$S_f=1$	$S_f=S_T$	$S_f=S_T$
4	1	1	1	$S_f=1$	$S_f=S_T$	$S_f=S_T$
5	0	0	1	$S_f=S_T$	$S_f=S_T$	$S_f=S_T$
6	1	0	1	$S_f=S_T$	$S_f=S_T$	$S_f=S_T$

5.2.3 Dynamic trigger frequencies (F_{OFF} and F_{ON})

The trigger frequencies are variable in proportional to the building indoor temperature. F_{OFF} is defined as the lower trigger frequency setpoint that has a range of 49.5-49.9Hz. F_{ON} is defined as the upper trigger frequency setpoint that has a range of 50.1-50.5Hz[9]. For a frequency drop, heat pumps are switched OFF in descending order starting from the warmest building. For a frequency rise, heat pumps are switched ON in ascending order starting from the coldest building. The relationship between the trigger frequencies and the indoor temperature could be any of the following scenarios, depending on the response the heat pumps provide and the comfort of the customers:

5.2.3.1 DFC based linear method

It is often assumed that F_{OFF} and F_{ON} are linearly proportional to indoor temperature T_{in} as shown in Fig. 5.2.

F_{OFF} is updated based on Equation (5.1). The F_L(49.5Hz) is the lower frequency set point, and F_{N1}(49.9Hz) is the normal frequency low setpoints. For a frequency drop,

---

[9] Note that the dead-band of the trigger frequencies might be narrowed down based on the requirements of the system operator [11]

heat pumps are switched OFF in descending order starting from the one that holds F_{OFF} closest to F_{N1} (which represents the warmest building). For instance, a heat pump at point X_1 (see Fig. 5.2(a)) is switched OFF before the heat pump at X_2, because it has F_{OFF} closer to 49.9 Hz. However, the more the frequency drops, the more heat pumps are triggered.

F_{ON} is updated based on Equation (5.2). The F_H(50.5Hz) is the upper frequency set point, and F_{N2}(50.1Hz) is the normal frequency high set points. For a frequency rise, heat pumps are switched ON in ascending order starting from the one that holds F_{ON} closest to F_{N2} (which represents the coldest building). For example, a heat pump at point X_2 is switched ON before the heat pump at X_1 (see Fig. 5.2(b)), because it has F_{ON} closer to 50.1 Hz. The more the frequency rises, the more heat pumps are switched ON.
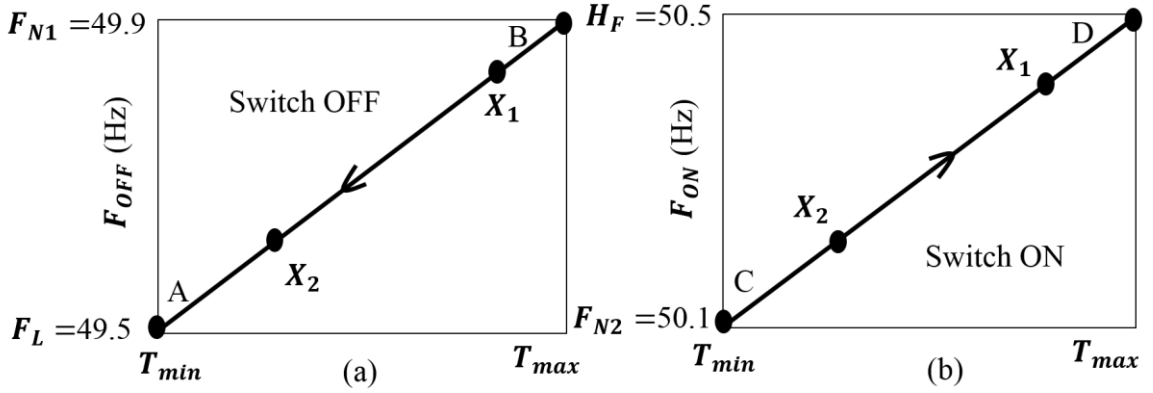
Fig. 5.2 DFC based linear method (a) F_{OFF} varies with T_{in} (b) F_{ON} varies with T_{in}

$$F_{OFF} = \frac{F_{N1}-F_L}{(T_{max}-T_{min})}(T_{in}-T_{min}) + F_L \qquad : T_{in} \in [T_{min}, T_{max}] \qquad (5.1)$$

$$F_{ON} = \frac{F_H-F_{N2}}{(T_{max}-T_{min})}(T_{in}-T_{min}) + F_{N2} \qquad : T_{in} \in [T_{min}, T_{max}] \qquad (5.2)$$

5.2.3.2 DFC based parabolic and linear method

The heat pumps could provide faster frequency response service if a parabolic shape is used. The parabolic shape provides smooth response and the frequency change can be controlled at an early stage following the frequency incident. For a low frequency response, the heat pumps act starting from the building with the higher temperature. Therefore, the trigger frequency F_{OFF} in the buildings with a temperature $T_{mid} \le T_{in} < T_{max}$ is given a parabolic shape as depicted in curve BC in Fig. 5.3. Thus, F_{OFF} is chosen to vary with the building temperature according to Equation (5.3). The T_{m1} is defined as $(T_{min} + T_{max})/2$, and F_{m1} is $(F_L + F_{N1})/2$.

$$F_{OFF} = \frac{F_{m1}-F_{N1}}{(T_{mid}-T_{max})^2}(T_{in} - T_{max})^2 + F_{N1} \qquad T_{in} \in [T_{mid}, T_{max}] \qquad (5.3)$$
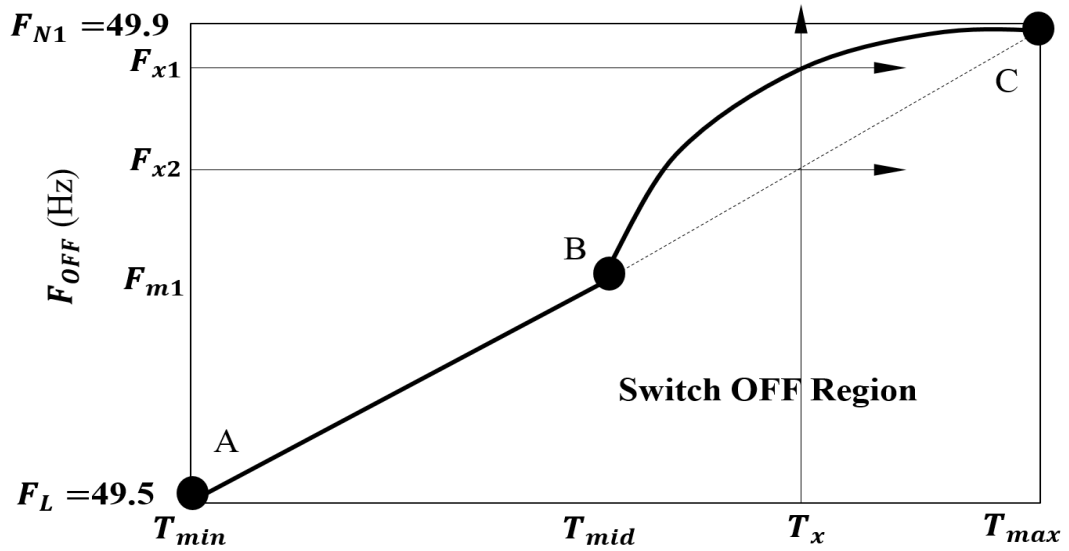
Fig. 5.3 Dynamic F_{OFF} based curve BC and slope AB method

The parabolic curve BC assigns F_{OFF} closer to F_{N1} than the linear slope BC does. This will switch OFF more heat pumps, especially at the earliest stage following the event and the frequency drop will be halted earlier. For instance, for a building with temperature T_x, then the heat pump in this building must have F_{OFF} equal to F_{x1} when a parabolic curve BC is used or equal to F_{x2} when a slope BC is used.

107

Therefore, if the grid frequency drops to the value $F_{x2} < f(t) < F_{x1}$, then the heat pump in this building will be switched OFF only if parabolic shape is used because the grid frequency $f(t)$ becomes lower that the trigger frequency F_{x1}. If the slope shape is used, the heat pump will not be switched OFF because $f(t) > F_{x2}$

However, if the low frequency response is wanted to be less reliant on the buildings with low temperature, then the relationship between F_{OFF} and T_{in} could be maintained linear when $T_{min} \leq T_{in} < T_{mid}$ as shown in slope AB in Fig. 5.3. The relationship between F_{OFF} and T_{in} is described in Equation (5.4).

$$F_{OFF} = \frac{F_{m1}-F_L}{(T_{mid}-T_{min})}(T_{in} - T_{min}) + F_L \qquad\qquad T_{in} \in [T_{min}, T_{mid}] \qquad\qquad (5.4)$$

For a high frequency response, the heat pumps operation is starting from the building with lower temperature. Therefore, the trigger frequency F_{ON} in the buildings with a temperature $T_{min} < T_{in} < T_{mid}$ is given a parabolic shape as depicted in curve DE in Fig. 5.4. Therefore, F_{ON} is chosen to vary with the building temperature according to Equation (5.5). The F_{m2} is defined as $(F_{N2} + F_H)/2$.
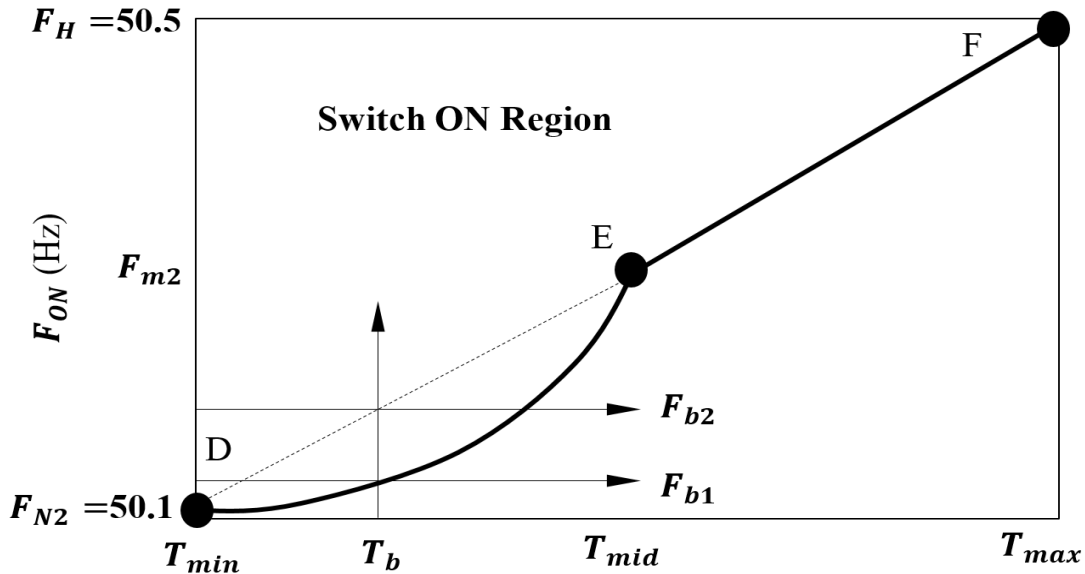
Fig. 5.4 Dynamic F_{ON} based curve BC and slope AB method

$$F_{ON} = \frac{F_{m2}-F_{N2}}{(T_{mid}-T_{min})^2}(T_{in} - T_{mid})^2 + F_{N2} \qquad\qquad T_{in} \in [T_{min}, T_{mid}] \qquad\qquad (5.5)$$

The parabolic curve DE assigns F_{ON} closer to F_{N2} than the linear slope DE does. This will switch ON more heat pumps, especially at the earliest stage following the frequency rise and the frequency change will be halted earlier. For example, if a building has a temperature T_b, then the heat pump in this building must have F_{ON} equal to F_{b1} when a parabolic curve DE is used or equal to F_{b2} when a slope DE is used. Therefore, if the grid frequency rises to the value $F_{b1} < f(t) < F_{b2}$, then the heat pump in this building will be switched ON only if parabolic shape is uthe sed, because the grid frequency $f(t)$ becomes greater than the trigger frequency F_{b1}. If the slope method is used, the heat pump will not be switched ON because $f(t) < F_{x1}$

However, if the high frequency response is required to be less reliant on the buildings with high temperature, then the relationship between F_{ON} and T_{in} could be kept linear when $T_{mid} \leq T_{in} < T_{max}$ as shown in slope EF in Fig. 5.4. The relationship between F_{ON} and T_{in} is described in Equation (5.6).

$$F_{ON} = \frac{F_H-F_{m2}}{(T_{max}-T_{mid})}(T_{in} - T_{mid}) + F_{m2} \qquad\qquad :T_{in} \in [T_{mid}, T_{max}] \qquad\qquad (5.6)$$

The trigger frequencies in this form were designed to offer more reliability to the costumers. That is, the DFC is less reliant on buildings with low temperature when there is a low- frequency event. Similarly, the DFC is less reliant on the buildings that have high temperature in case there is a high- frequency event.

5.2.3.3 DFC based full parabolic method

In this research, the trigger frequencies F_{ON} and F_{OFF} were chosen to vary dynamically with the building temperature T_{in} according to the full parabolic curves AB and CD shown in Fig. 5.5 and Fig. 5.6. These are described by Equations (5.7)

and (5.8). The full parabolic curve causes more heat pumps to respond to the frequency change at any temperature within $T_{min} < T_{in} < T_{max}$ and hence provide faster response.

$$F_{OFF} = \frac{F_L - F_{N1}}{(T_{min} - T_{max})^2} (T_{in} - T_{max})^2 + F_{N1} \qquad : T_{in} \in [T_{min}, T_{max}] \qquad (5.7)$$

$$F_{ON} = \frac{F_H - F_{N2}}{(T_{max} - T_{min})^2} (T_{in} - T_{max})^2 + F_{N2} \qquad : T_{in} \in [T_{min}, T_{max}] \qquad (5.8)$$

For a frequency drop, the parabolic curve AB shown in Fig. 5.5, will assign F_{OFF} closer to F_{N1} than the linear slope AB. This will switch OFF more heat pumps, especially at the earliest stage following the event and the frequency drop will be halted earlier.

Similarly, for a frequency rise, the parabolic curve CD shown in Fig. 5.6, will assign F_{ON} closer to F_{N2} than the linear slope CD. This will switch ON more heat pumps at the earliest stage following the frequency event and the frequency rise will be controlled earlier.

As the grid frequency recovers, heat pumps will be switched ON smoothly, starting from the coldest building or switched OFF smoothly starting from the warmest building. The fact that a population of buildings will be at different temperatures means that heat pumps switching events will be smooth, avoiding simultaneous switching which could result in system problems.
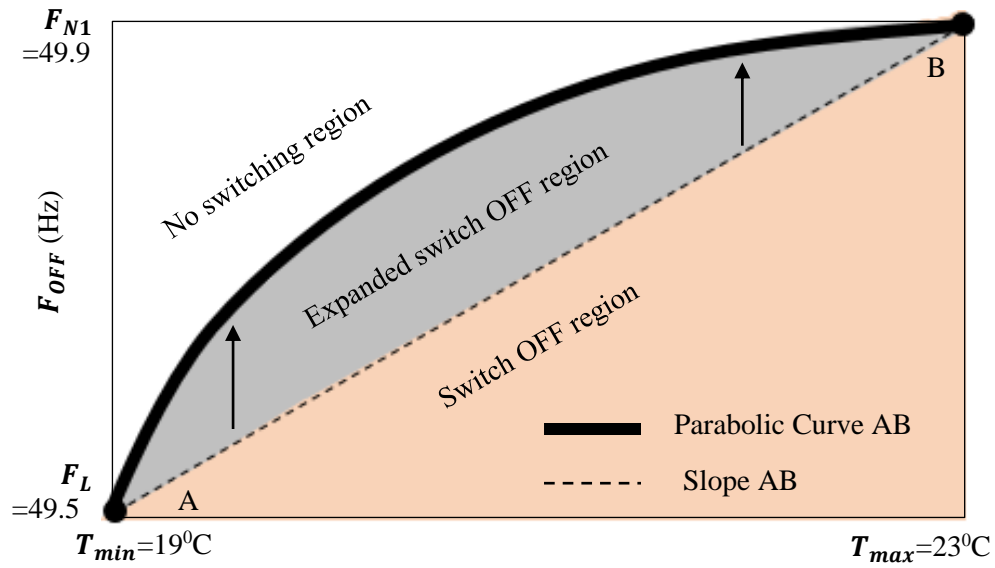
Fig. 5.5 Dynamic F$_{OFF}$ based on parabolic method
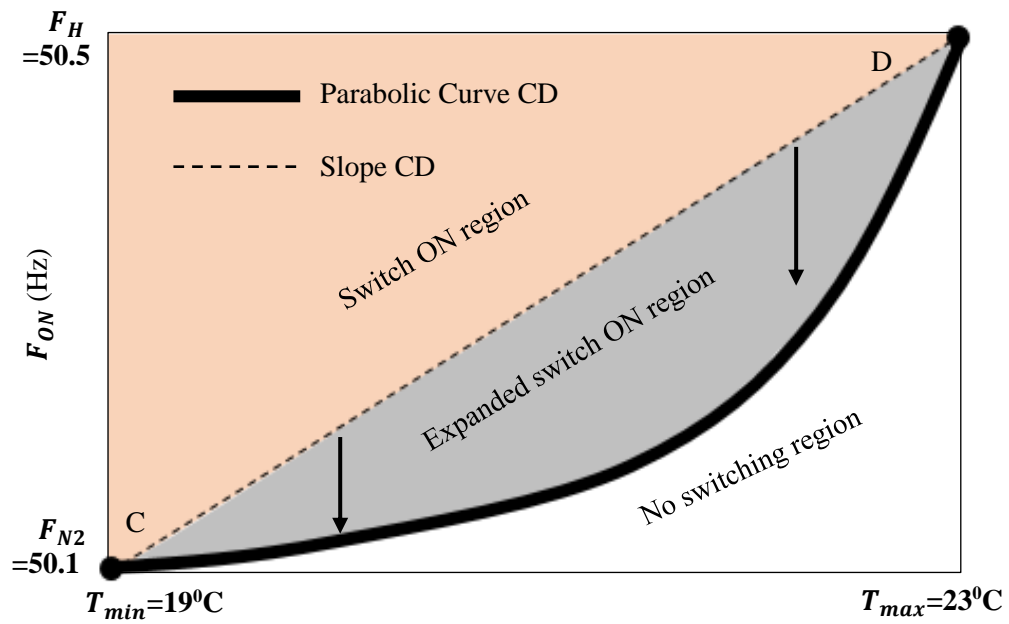
Fig. 5.6 Dynamic F$_{ON}$ based on parabolic method

5.3 Simulation and discussion of the DFC based on full slope and full parabolic methods

This section discusses the operation of the DFC based on the trigger frequencies shown Fig. 5.5 and Fig. 5.6. The impact of the Switching Controller is shown in Fig. 5.7 . Fig. 5.7 shows that the N_s signal is turned to '1' when there are more than three switching events per half hour, and then the heat pump operates normally, only in response to the temperature. The N_s signal is turned to '0' as long as the number of switching events is still within the acceptable limit.

Fig. 5.8 and Fig. 5.9 show the performance of the dynamic trigger frequencies. In Fig. 5.8, F_{OFF1-P} and F_{OFF2-P} represent the lower trigger frequencies of two heat pumps varied with T_{in} based on the Parabolic curve AB, and F_{OFF1-S} and F_{OFF2-S} were varied based on the linear Slope AB. Following a frequency drop, Fig. 5.8 shows that with the use of parabolic curve AB, both heat pumps were switched OFF in response to the frequency drop. With the use of slope AB, only one heat pump was switched OFF.

In Fig. 5.9, F_{ON1-P} and F_{ON2-P} show that the higher trigger frequencies of the two heat pumps were varied based on the Parabolic curve CD, and F_{ON1-S} and F_{ON2-S} were varied based on the linear Slope CD. Following a frequency rise, Fig. 5.9 shows that two heat pumps were switched ON in response to the frequency rise when curve CD was used. However, only one heat pump is switched ON when the linear slope CD was used.

In summary, the trigger frequencies were improved using the parabolic shape, so that more heat pumps have the ability to respond to the frequency change, especially at an early stage following the event.
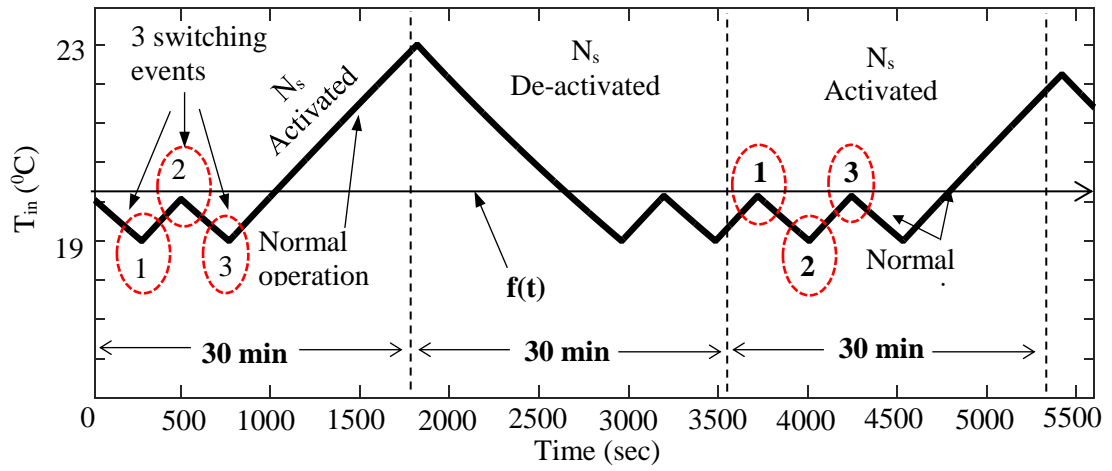
Fig. 5.7 Effect of the logic control N_s on the operation of a heat pump
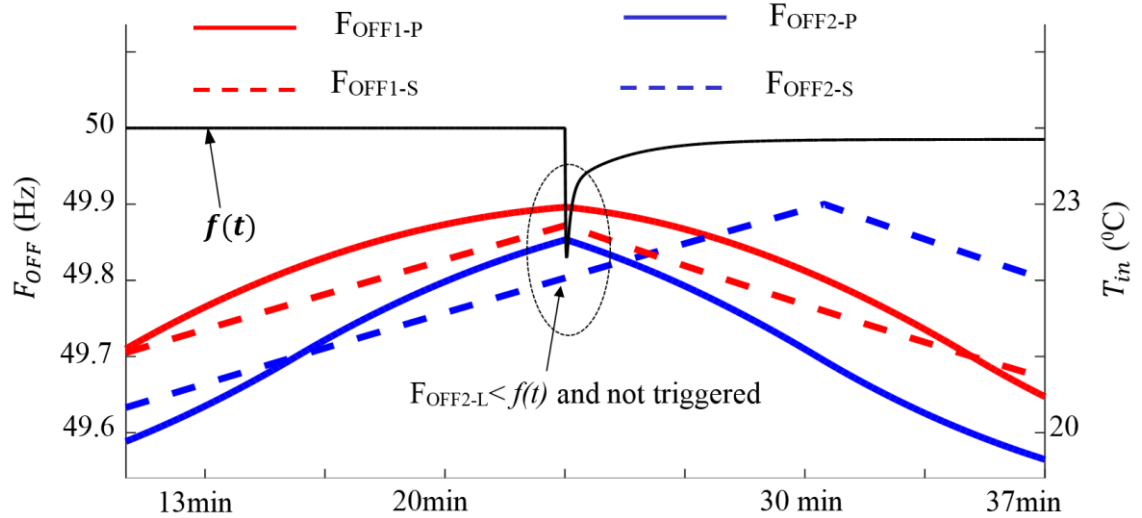
Fig. 5.8 Comparison of trigger frequency (F_{OFF}) of two heat pumps using the characteristics of Curve AB and Slope AB that are shown in Fig. 5.5

113
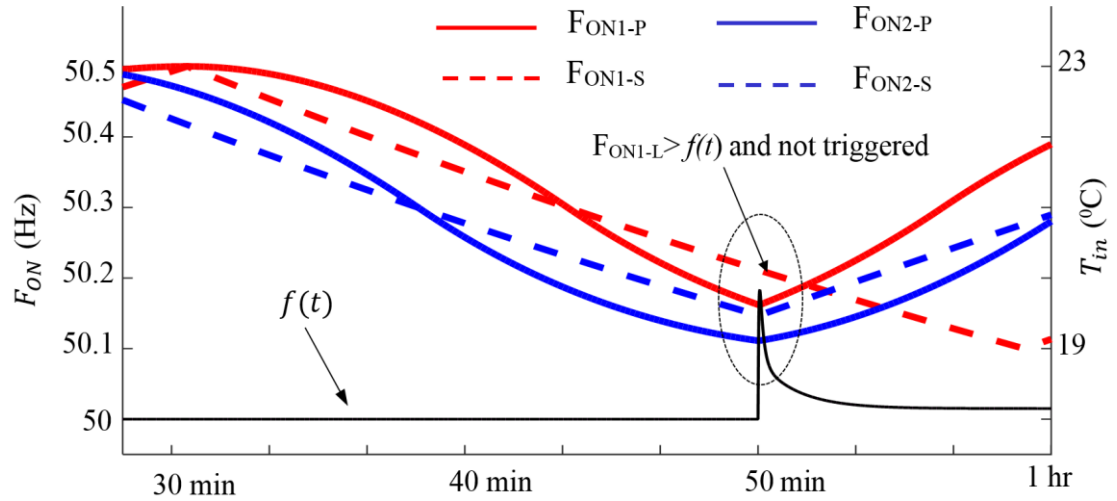
Fig. 5.9 Comparison of trigger frequency (F_{ON}) of two heat pumps using the characteristics of Curve AB and Slope AB that are shown in Fig. 5.6

5.4 Availability of heat pumps for frequency response

Availability of load is defined as the fraction of load that is available to provide low and high frequency response without undermining their inherent function. In real life, only certain number of heat pumps is in ON-state and is available to be switched OFF and only certain number of heat pumps is in OFF-state and is available to be switched ON in response to system frequency.

In this research, the daily average number of heat pumps in the ON state which are available to be switched OFF in response to a low-frequency response is denoted ONHP. The ONHP was estimated in Element Energy report for the 2030 medium uptake scenario in GB [67]. In this study, the ONHP data was used as an input to the model to specify the amount of heat pumps that can provide low-frequency response at each time of the day. The average number of heat pumps that are connected to the grid and are in either the ON and OFF states are denoted NHP. The typical ON and OFF cycles of heat pumps were assumed equal. Therefore, the NHP were assumed as twice as the ONHP. The geographical NHPs were calculated based on the number of householders in each area [133, 134]. The daily NHPs of GB were scaled down to represent the NHPs at each of the eleven distribution network operators in the GB

power system. This is described in Fig. 5.10. The availability of heat pumps at different time of the day is explained in more detail in Chapter 6.
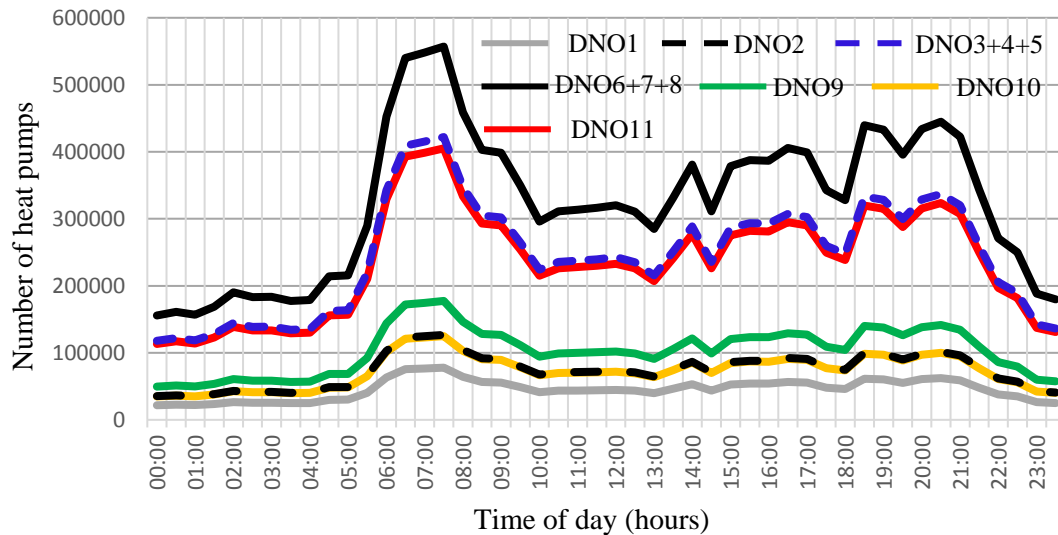
Fig. 5.10 Diurnal variation in average number of heat pumps (NHP), 2030 winter medium scenario

5.5 Case studies based on test systems

5.5.1 Case study on the Scotland interconnected power system

This case study was carried out by connecting a representative model of the aggregated heat pumps to the proposed model of Scotland zones in Fig. 3.3. Aggregated heat pump models were assumed to be allocated in the north and south Scotland zones. The number of heat pumps in Scotland zones was taken from Fig. 5.10 during the day's peak demand (17:00-17:30). The average number of heat pumps in the north Scotland zone was around 55,795 and in south Scotland zone was around 89,504.

The system inertia was considered for the 2029/2030 scenario as depicted in Tables 3.1 and 3.2. The system base load was assumed 4,627 MW in the north Scotland zone and 3,489MW in the south Scotland zone. A loss of 300 MW (0.086 pu) at time 50 sec in the south zone was applied. The ADB controller was used to

control the flow of power through the tie lines and to drive the frequency deviation back to zero after the frequency event. The simulation results are shown in (5.11-5.13).

Fig. 5.11 shows the grid frequency of the north zone (left axis), and the power consumption drawn by the heat pumps at the north zone (right axis). Following the frequency incident, the DFC has reduced the frequency drop to 49.84 Hz from 49.48 Hz within only 2 sec. The DFC has also reduced the overshoot during the frequency recovery. The power consumption of heat pumps was reduced by 32 MW after the frequency event.

Fig. 5.12 shows the grid frequency of the south zone (left axis), and the power consumption of the heat pumps at the south zone (right axis). It can be seen that the frequency has severely dropped due to the large frequency disturbance that occurred in this zone. The DFC has reduced the frequency to 49.5 Hz from 49.12 Hz within 0.8 sec. The power consumption of heat pumps was reduced by 136 MW after the frequency event.

Fig. 5.13 shows the tie line power transfer from the north to the south zone (left axis), and the power consumption which was drawn by the heat pumps (right axis). The reduction of the heat pump demand has not only reduced the frequency deviation, but also reduced the generation power transfer from the north to the south by 50%. This will help to reduce the cost of the generation power transfer service.
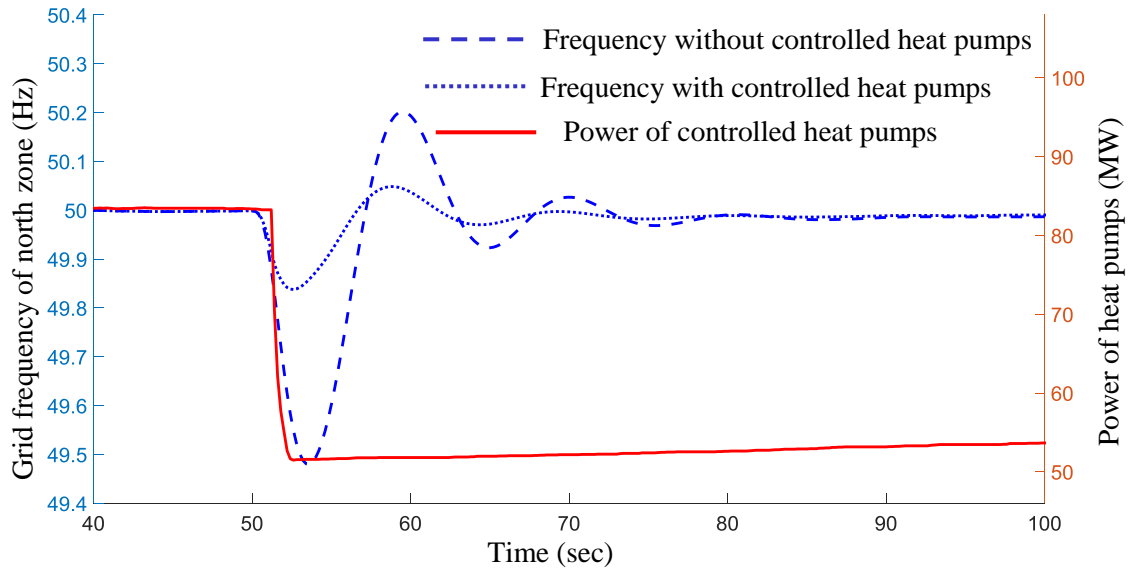
Fig. 5.11 Grid frequency of north Scotland zone (the zone of disturbance)
$$H_{eq} = 1.764$$
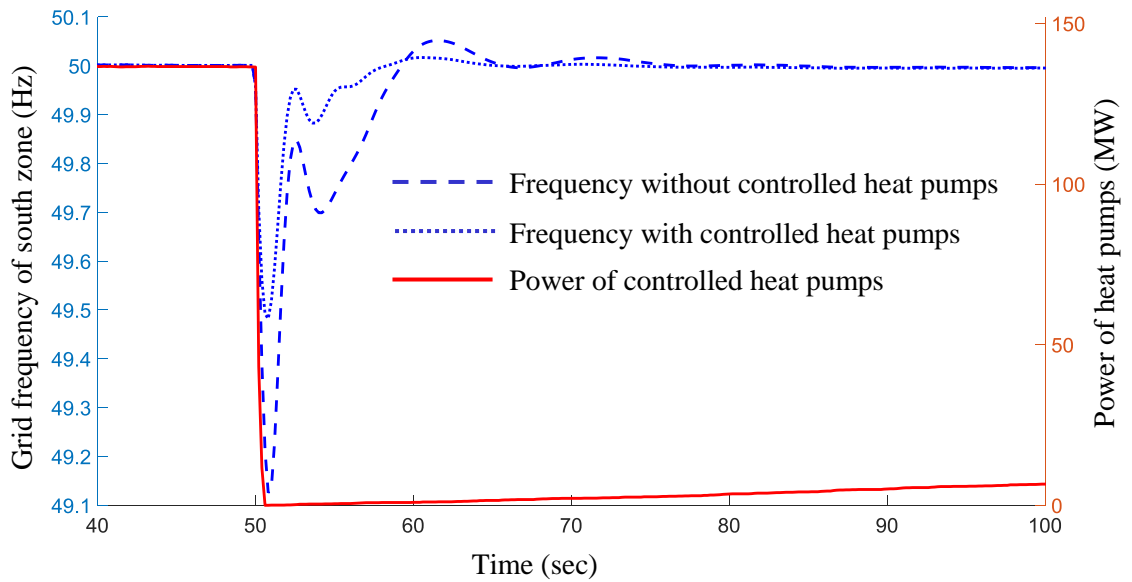
Fig. 5.12 Grid frequency of south Scotland zone, $H_{eq} = 1.274$
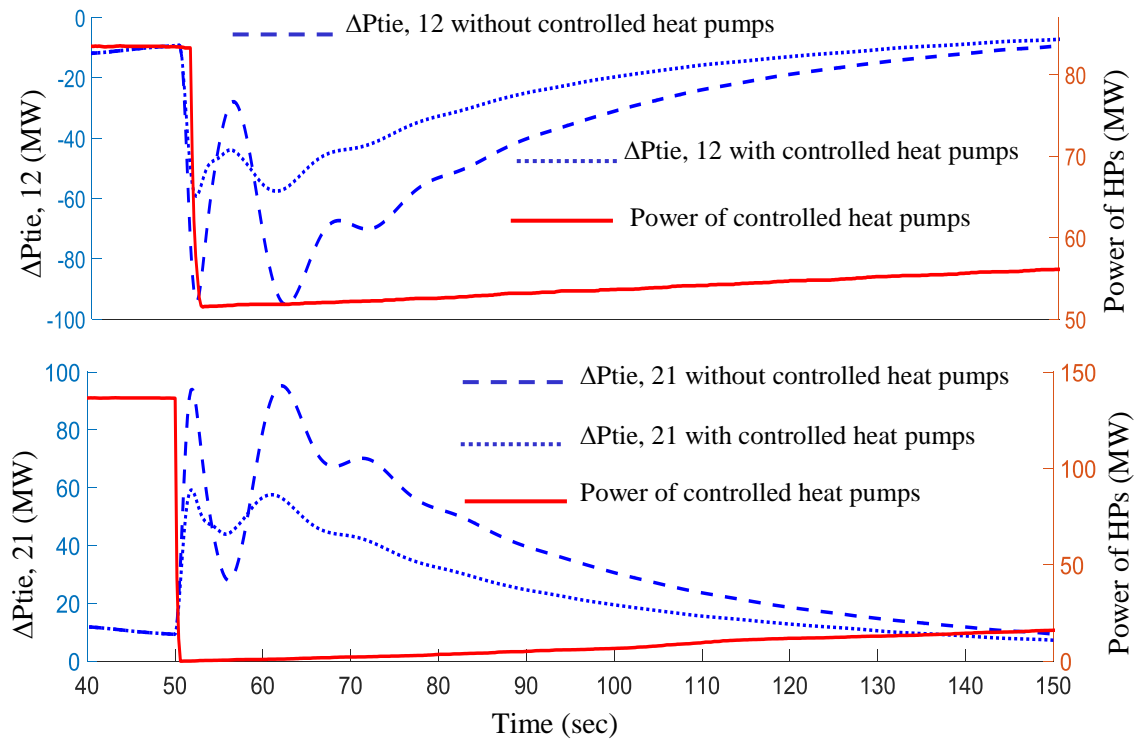
Fig. 5.13 Change of tie-line power transfer

5.5.2　Case study on the GB transmission/generation reduced power system

The heat pump models were integrated into a reduced GB transmission power system model of National Grid. This model is a 36-bus equivalent network representing the National Electricity Transmission System of Great Britain, which was modelled in DIgSILENT by National Grid, as shown in Fig. 5.14. It is an electrodynamic model dispatched according to the National Grid Gone Green 2030 Future Energy Scenario. Each geographic zone in the model represents generation, demand and HVDC interconnectors. Generators within each zone are categorised according to fuel types and are represented by synchronous and static generators. The new nuclear stations are concentrated in the south of the GB power network, and the wind farms in Scotland and offshore.

Aggregated heat pump models were assumed to be allocated in the eleven DNO networks of the GB power system. The zones shown in Table 5.2 are a close geographical reflection to the GB DNOs [135].

The NHPs in each zone were taken from Fig. 5.10 at times 11:00-12:00 (the time of frequency event that happened in 2008 [136]) and 17:00-17:30 (representing the winter evening peak time).
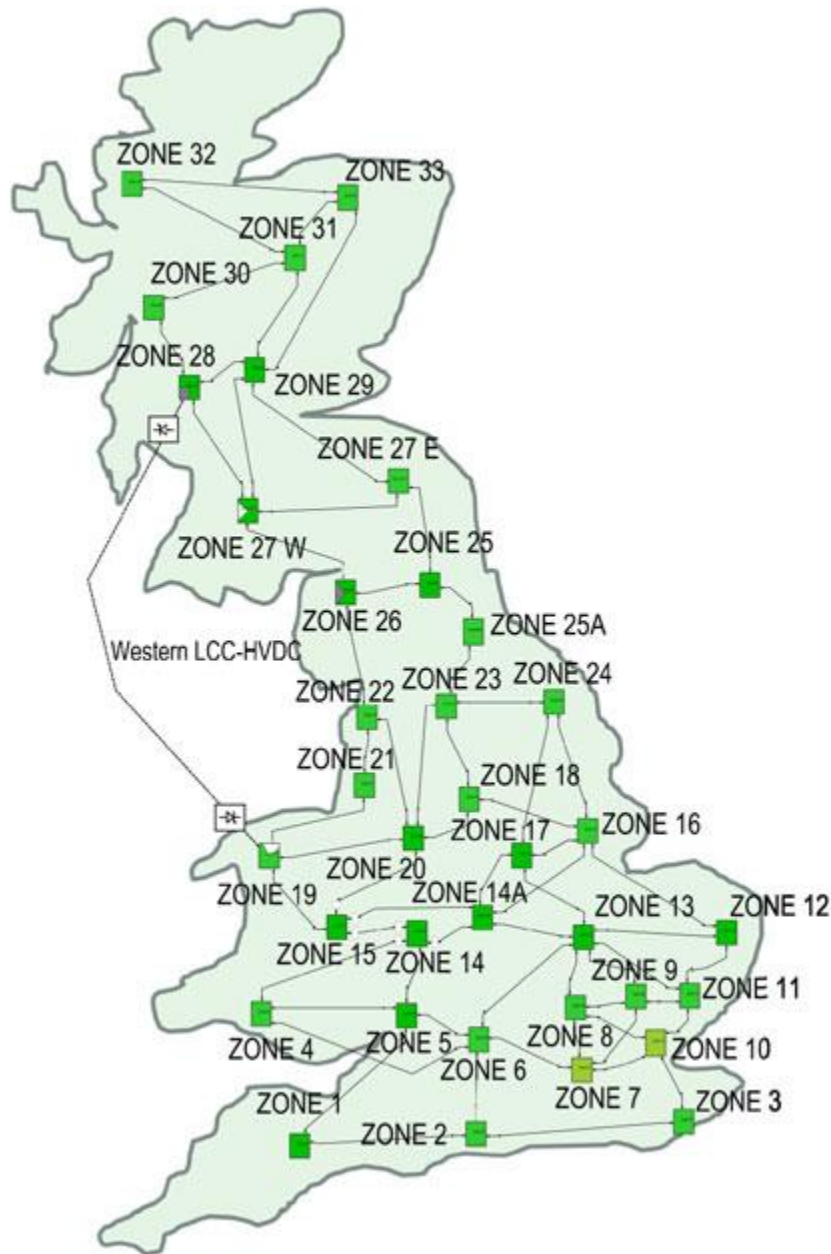
Fig. 5.14 Reduced GB 36-bus/substation transmission model

Table 5.2 Number of heat pumps in each zone

Zone number	Locations-based DNOs	NHPs at 11:30-12:00	NHPs at 17:00-17:30
Z-32	North Scotland (DNO-1)	44,226	55,795
Z-27W	Central and Southern Scotland (DNO-2)	70,946	89,504
Z-18	North East England (DNO-3)	115,041	145,134
Z-26	North West England (DNO-4)	115,041	145,134
Z-14A	Yorkshire (DNO-5)	115,041	145,134
Z-19	East England (DNO-6)	119,832	151,177
Z-15	London (DNO-7)	119,832	151,177
Z-10	South East England (DNO-8)	119,832	151,177
Z-2	Southern England (DNO-9)	100,776	127,137
Z-9	Merseyside, Cheshire, North Walesand North Shropshire (DNO-10)	71,983	90,812
Z-13	E. Midlands, W. Midlands, S. Wales and S. West England (DNO-11)	316,331	399,077
Total		1,308,881	1,651,258

5.5.2.1 Case study 1

This case study considered a frequency event with a profile similar to that which occurred in 2008 [136]. That event was caused when two generators (345MW and 1,237MW) tripped spontaneously within a short time (11:34 am-11:36 am).

To obtain such a frequency profile on the GB system model, the magnitudes of the loss of generation was changed such that the first loss (690MW) was applied at

time 2sec in zone 29. The loss of second generator (1,139MW) was applied after two minutes in zone 12.

The system demand at that time was around 40GW. The inertia constant of the synchronous generators in the model was set to 5sec. The NHPs were taken from Fig. 5.10 as described in Table 5.2 at time 11:30-12:00.

Fig. 5.15 shows the impact of controlled heat pumps on system frequency at different zones. After the first event, the DFC has reduced the frequency drop 0.1Hz from (49.9Hz from 49.8Hz). Following the second incident, the DFC has reduced the frequency drop 0.94Hz (from 48.8Hz to 49.74Hz) and maintained the system frequency within the operating limit. The zoomed shape in Fig. 5.15 shows that the controlled heat pumps distributed over GB zones maintained the frequency deviation in each zone in a nearly similar manner.

Fig. 5.16 shows the changes in the power consumption drawn by heat pumps at different zones. The heat pumps at different locations provided frequency response in proportion to the frequency deviation. In addition, the locations of heat pumps showed little impact on the frequency response they provided.

Fig. 5.17 shows the change of power output delivered by three aggregated synchronous generators (Nuclear and Gas) (see the right axis) and shows the total power of heat pumps (see the left axis). When the first incident occurred, the power consumption of heat pumps was decreased by 300MW and after the second incident, it was decreased by a further 600MW. The power output from synchronous generators was also reduced.
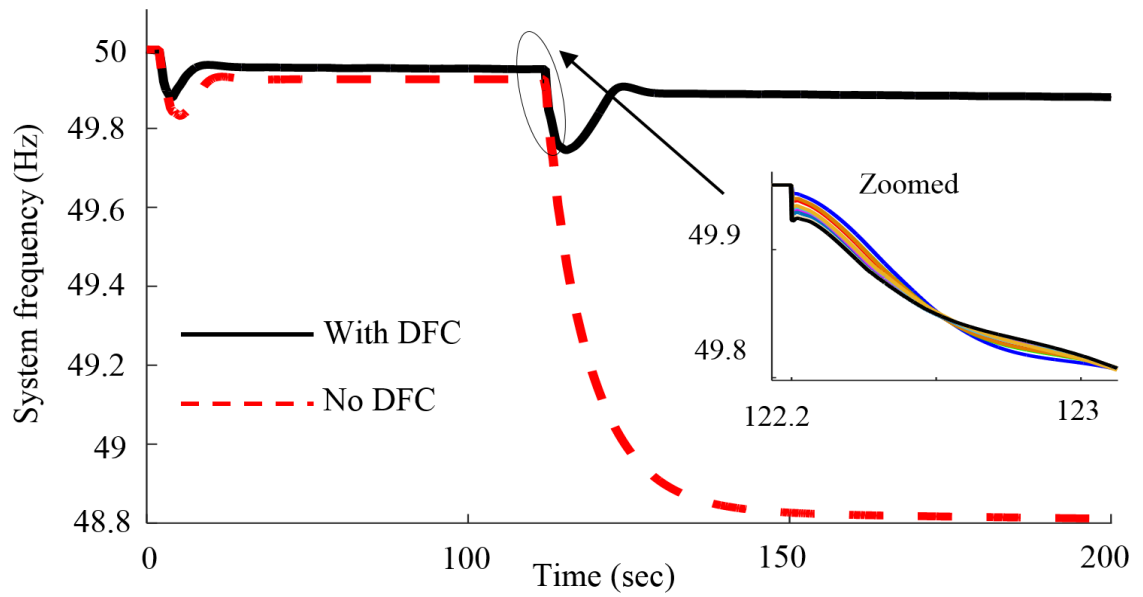
Fig. 5.15 Variation of frequency at different zones
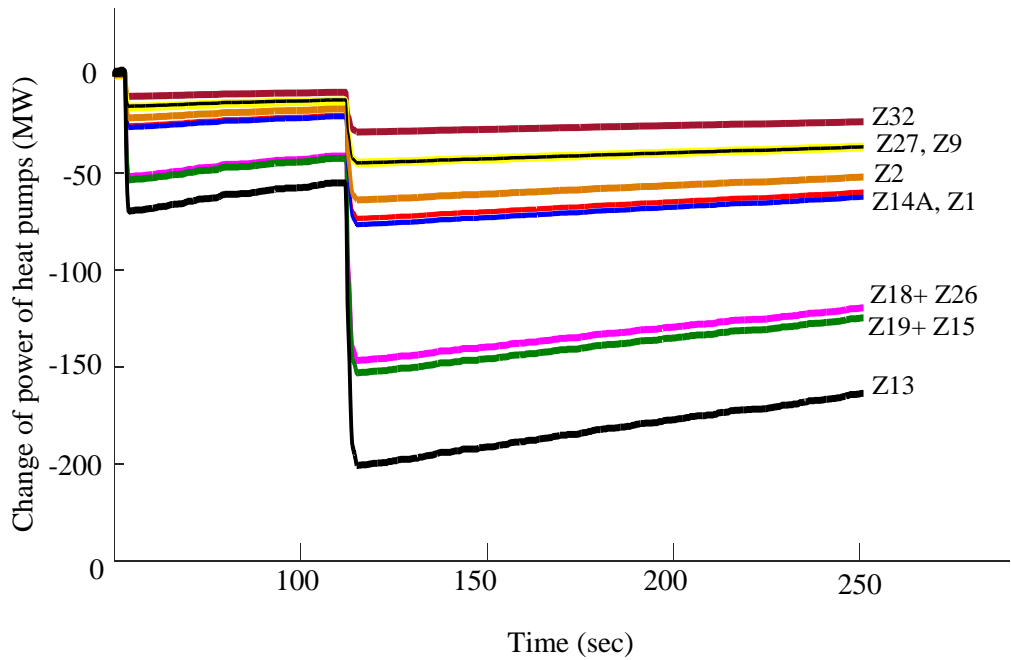
Fig. 5.16 Power reduction of heat pumps at different zones in the reduced GB transmission system model
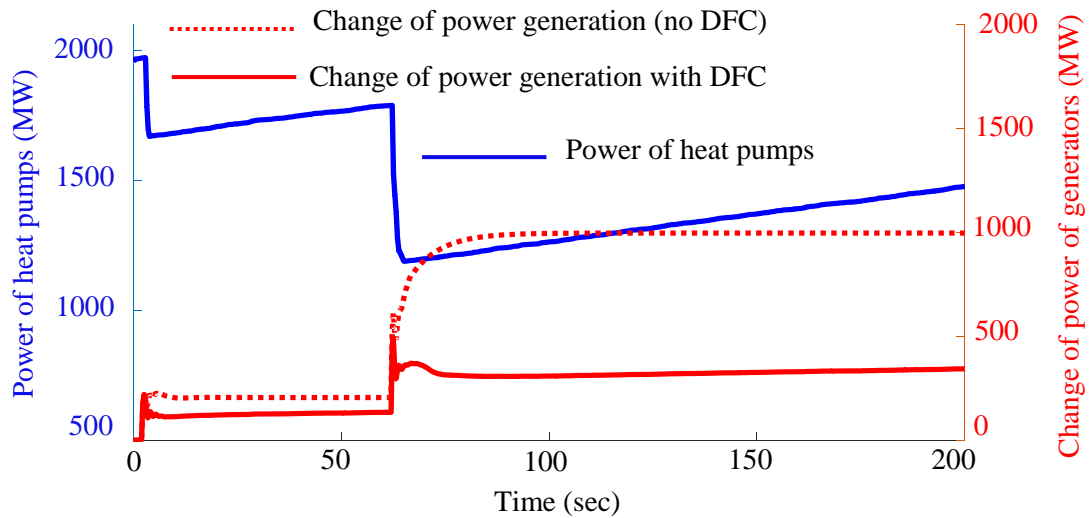
Fig. 5.17 Change of power output of three aggregated generators at different zones and the total power of heat pumps

5.5.2.2 Case study 2

The second case study was carried out for low system inertia with much generation assumed to come from converter connected wind turbines [137]. To represent this, the inertia constant of all synchronous generators was changed to 3sec from 5sec. The system demand of the model was 39GW. The NHPs that are available to provide low-frequency response were taken from Fig. 5.10 at the evening time. This is described in Table 5.2, at time 17:00-17:30.

A 1724MW synchronous generator located in the centre of the GB network was tripped at time 5sec. This generator was chosen to be a close reflection to the infrequent infeed loss, i.e. 1800MW in the GB power system.

Fig. 5.18 shows that the controlled heat pumps have reduced the frequency drop 0.78Hz (from 49Hz to 49.78Hz) and maintained the system frequency within the standard limit.

Fig. 5.19 shows the change of power output from eleven aggregated large synchronous generators (>500 MW) (see the right axis) and the power consumption of heat pumps (see the left axis). The power consumption of heat pumps was reduced

immediately after the frequency drop exceeded the dead-band limit (49.9 Hz). Also, the dependency on the power output from the large generators was reduced.

Fig. 5.20 shows the total change of demand for heat pumps during the half an hour following the event. As can be seen, the DFC effectively reduced 10,00MW from heat pump demand. The heat pump demand recovered within the 30min following the event. This allowed the system frequency to be restored using stand-by generation (responding after 30min) instead of using the power from costly spinning reserve responding in real time. Furthermore, the DFC has caused a little payback after the frequency recovery because the heat pumps have been reconnected gradually, causing a gradual increase of the power consumption.
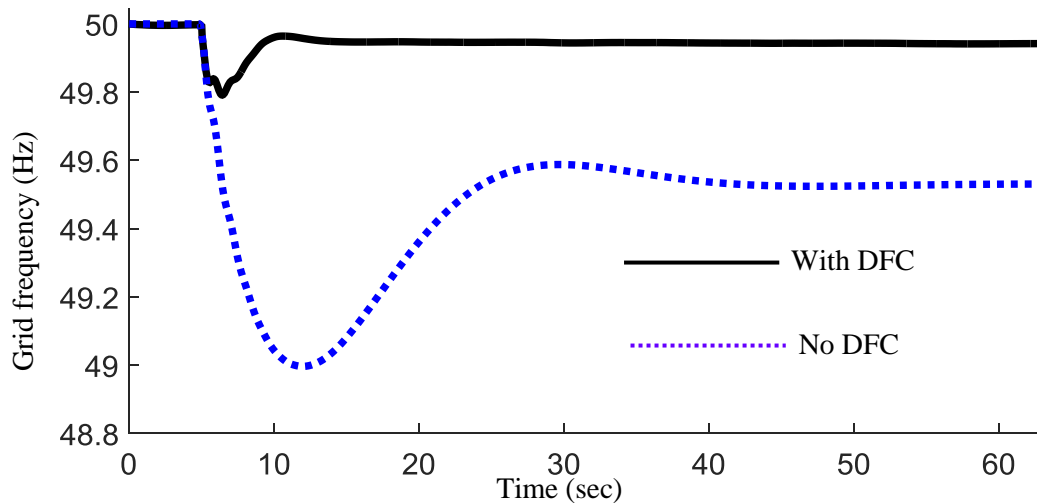
Fig. 5.18 Variation of frequency (with and without DFC)
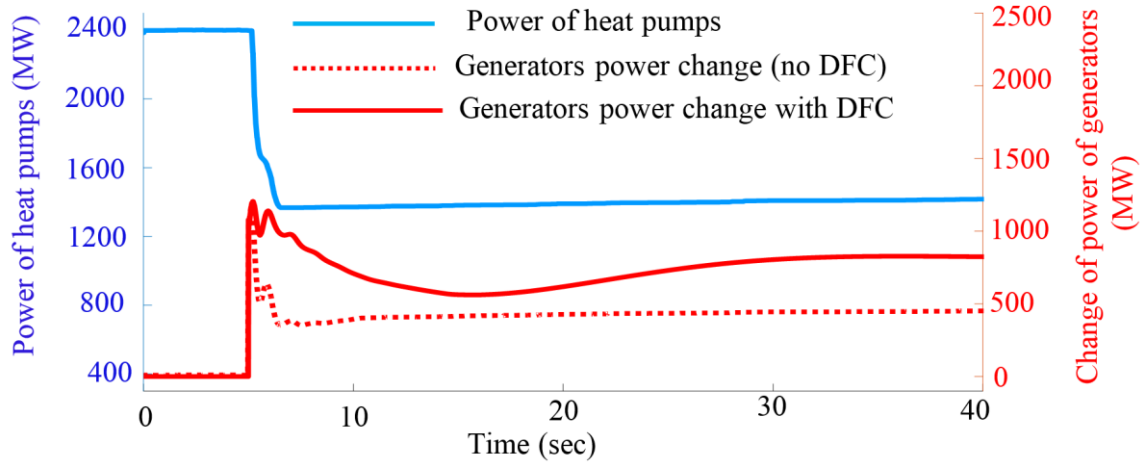
Fig. 5.19 Change of aggregated power output of large generators (<500MW) at different zones and the total power of heat pumps
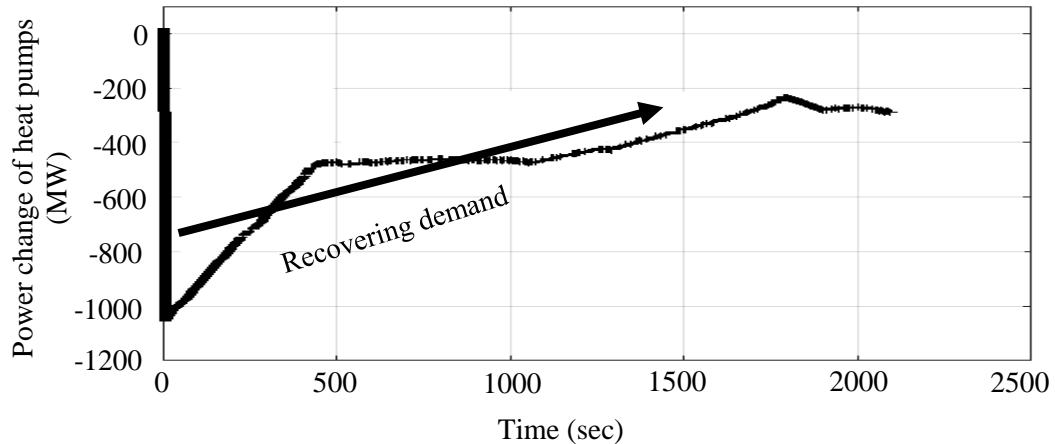
Fig. 5.20 Total demand of heat pumps during 30min following the event

5.5.2.3 Case study 3

A case study was carried out to compare the impact of a population of heat pumps using DFC, with parabolic and slope control techniques. The frequency deviation and RoCoF that would result from large imbalance contingencies ranging from 1.8GW to 4GW were investigated, i.e. the size and speed of the power change were very different. National Grid aims to control the threshold level of RoCoF at an early stage following the incident, i.e.(≤500msec) [137].

The system inertia was set to 3sec and system demand to 39GW. The NHPs were considered as in Table 5.2, at time 17:00-17:30.

Fig. 5.21 shows that a population of heat pumps using the parabolic control technique has reduced the frequency drop more than the slope technique.

Fig. 5.22 shows that the DFC using parabolic technique halted the system RoCoF faster than the slope technique during the first 500msec following the incident.

Fig. 5.23 shows the maximum RoCoF between 400msec to 500msec, following frequency events ranges from 1.8GW to 4GW. Fig. 5.23 shows that the RoCoF was reduced in each event. This is because the parabolic method had assigned to each heat pump an F_{OFF} closer to F_{N1} comparing with the linear method. Hence, the DFC caused more heat pumps to respond within the first 500msec following the frequency event and the frequency deviation was halted earlier.
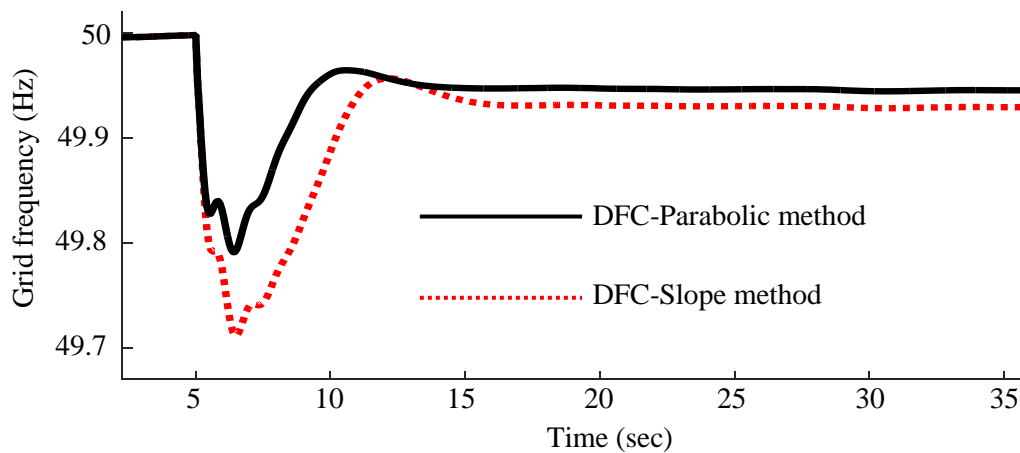
Fig. 5.21 Variation of grid frequency
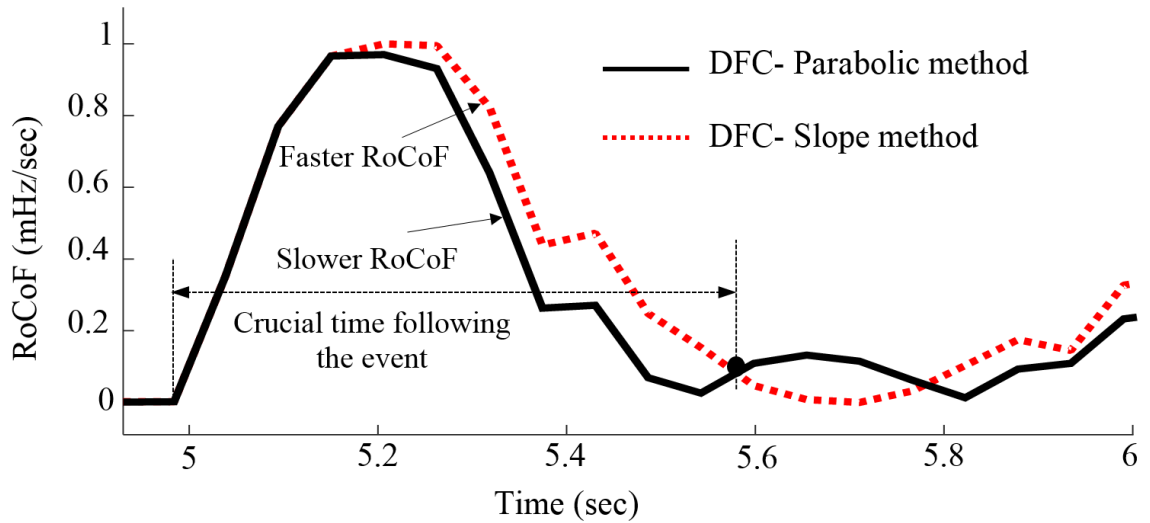
Fig. 5.22 Rate of Change of grid frequency (RoCoF) (loss of 1.724GW)
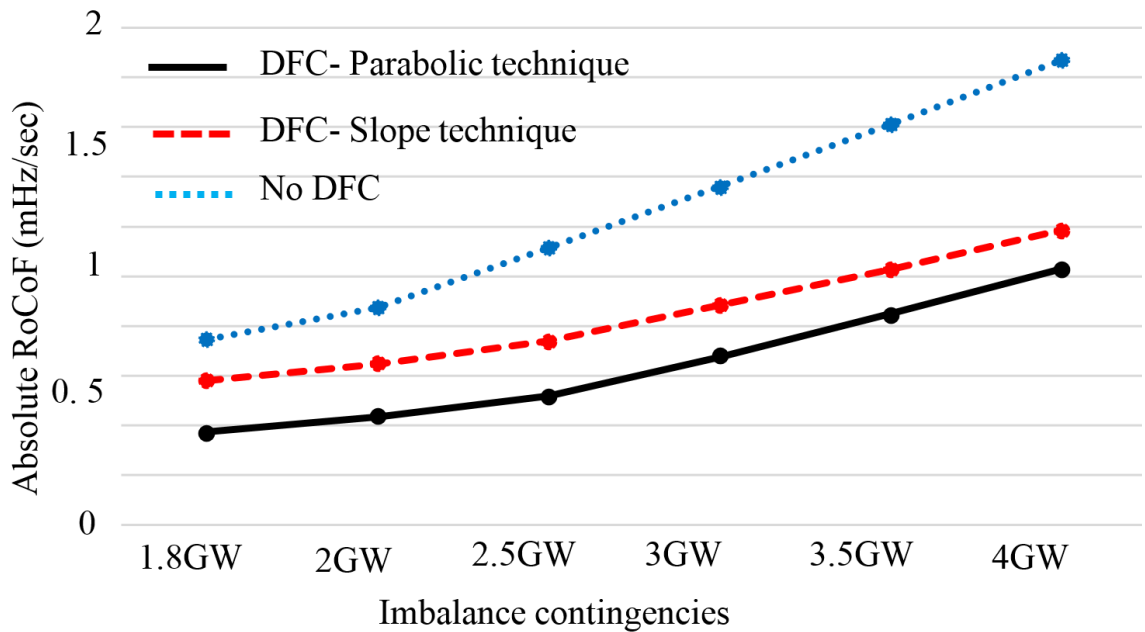
Fig. 5.23 Maximum values of RoCoF between time 400ms and 500ms, following events range from 1.8GW to 4GW. Heq=3sec

5.6   Conclusion

A dynamic frequency controller was developed to allow the heat pumps to alter their power consumption in response to system frequency. The trigger frequencies were improved by using a parabolic shape. The frequency control does not interfere with the temperature control of the buildings.

The model of a population of heat pumps was then incorporated into a Scotland interconnected model and to the reduced Great Britain transmission/generation system model. Case study showed that DFC has reduced the frequency deviation at each of the Scotland zones and reduced the dependency on the generation power transfer service through the tie lines. Case studies also showed that the power consumption of dynamically controlled heat pumps distributed over GB zones was reduced immediately following a frequency drop. Following a loss of generation, the deviation of grid frequency was reduced with the immediate load change of heat pumps. The power drawn from frequency-sensitive generators was also reduced.

A population of controlled heat pumps can provide an opportunity to restore the system frequency by using standby generation (responding after 30 minutes), instead of costly spinning reserve.

Chapter 6

Demand Side Response Aggregation for Balancing Services

The power consumption of domestic units is usually small, and hence the aggregation of large numbers of small units should be adopted to provide sufficient capacity for frequency response. In this chapter, dynamic frequency control was developed to evaluate the capacity from the aggregation of domestic heat pumps and fridges for frequency response. The potential of aggregated load to provide frequency response was estimated at the time of winter and summer days. A relationship between the number of domestic heat pumps and the number of fridges to provide Firm Frequency Response (FFR) service was also investigated.

Case study on the simplified Great Britain power system model was developed. Based on this case study, three scenarios of load combination were simulated according to the availability of load and considering cost saving. Results showed that the controlled aggregated load achieved a similar response in each combination scenario.

The model was then validated with the master GB transmission/generation power system model which is at present used by National Grid. The impact of aggregated heat pumps and fridges was examined geographically over the 11 DNOs of the GB network.

6.1 Introduction

The previous chapter showed that a population of controlled domestic heat pumps is a promising method to provide frequency response to the GB power system. The power consumption of each heat pump unit is small, and the heat pumps' demand in the summer is low. Thus, the aggregation of a large number of small domestic units

must be considered. Also, for the provision of a frequency response services such as FFR service, each system aggregator must adopt a certain amount of load aggregation to deliver 10MW frequency response to the grid as a threshold [63].

6.2   Comparison of heat pumps and fridges

The diagram of a fridge is shown in Fig. 4.8. The fridge consists of Cooler and Freezer compartments. The Cooler compartment is usually large and is used to store the food at cold temperature. The freezer compartment is generally smaller and is used to make ice and store food below a freezing point. When the fridge's compressor is switched ON, the refrigerant material flows through the pipes. The refrigerant goes through the evaporator, and the warm temperature is transferred to the ambient causing the temperature inside the fridge to drop. The thermodynamic model of the Cooler and Freezer is presented in Chapter 4.

The diagram of a heat pump is shown in Fig. 4.1. The heat pump has a reverse operation to the fridge. It transfers heat from a source of heat to the buildings' indoor. The heat gain is absorbed from the environment through the heat pump's evaporator. The refrigerant inside the evaporator is compressed through a compressor which causes its temperature to rise. The hot temperature is then transferred to the building through a heat exchanger. The thermodynamic model of a domestic building equipped with a heat pump is presented in Chapter 4.

1. The ON/OFF cycles and temperature behaviour of a fridge and heat pump are shown in Fig. 6.1. The heat pump has a longer ON, and shorter OFF cycles than the fridge. The typical duration of a heat pump' cycle in a typical building having a range of temperature between (19^0C to 23^0C) is 30min (ON-cycle) and $\geq$30min (OFF-cycle). The cycle time of a typical cooler having a range of temperature between (7.5^0C to 8.5^0C) is 15min (ON-cycle) and 45min (OFF-cycle) [138]. This means that fridges can provide a longer low-frequency response because they have longer OFF-cycle, while heat pumps can provide a longer high-frequency response because they have longer ON- cycle.

2. The temperature difference between the low and high-temperature set-points (T_{min}, T_{max}) of a typical domestic building is ≥4 ^{0}C which is higher than that of the fridge (typically 1-2 ^{0}C). This means that the variation of internal temperature (T_{in}) of a building has a wider range than the change of Cooler temperature (T_{Co}) of a fridge.

There are expected to be 3.8 million heat pumps in GB's dwellings by 2030 [139]. Also, there will be approximately 48 million fridges in Great Britain by 2030 [140]. Each heat pump has a typical power consumption of 3kW, and each fridge has a typical power consumption of 0.1kW. Heat pumps have low demand in the summer, while refrigerators are in service in all seasons and are able to participate in the frequency regulation all the year round.

The power consumption of a fridge and heat pump can be shifted in response to an external signal with little disruption to its temperature storage performance.

3.
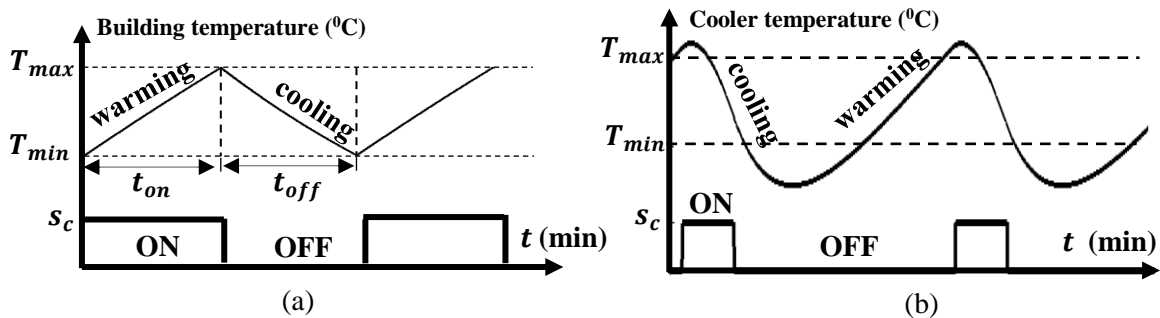
Fig. 6.1 Conventional control (a) heat pump; (b) fridge

6.3 Availability of load

6.3.1 Availability of heat pumps at different time of day

The availability of load is defined as the fraction of load that is available to provide a low and high-frequency response without undermining the internal load function. In real life, only part of the load has ON-state and is available to switch OFF, and only part of the load has OFF-state and is available to switch ON in response to the

131

system frequency. Therefore, system operator needs to be notified about the amount of load that is available to respond to the grid frequency at each time of a day.

In this research, the Availability of Low Response (*ALR*) is defined as the percentage of load that is available to be switched OFF to provide a low-frequency response service. The Availability of High Response (*AHR*) is the percentage of load that is available to be switched ON to provide a high-frequency response service. For heat pumps, data of average ALR_{hp} and AHR_{hp} are gathered and estimated considering the Element Energy's medium uptake scenario for the year 2030 [139]. The ALR_{hp} and AHR_{hp} are half hourly data over a day and are averaged for the winter months in the Great Britain (GB), as presented in Fig. 6.2. It is shown that the response is highest at 06:30 and lowest between 23:00 and 04:00.

The response from heat pumps is seasonal, i.e. they use less power in summer than in the winter due to the lower heating demand. The seasonal effect on the energy consumption of heat pumps over the year is obtained from [139], as shown in Fig. 6.3. The seasonal availability of low-frequency response in winter and summer months are denoted SAL_{winter} and SAL_{summer}. For a high-frequency response, the seasonal availability is denoted SAH_{winter} and SAH_{summer}.
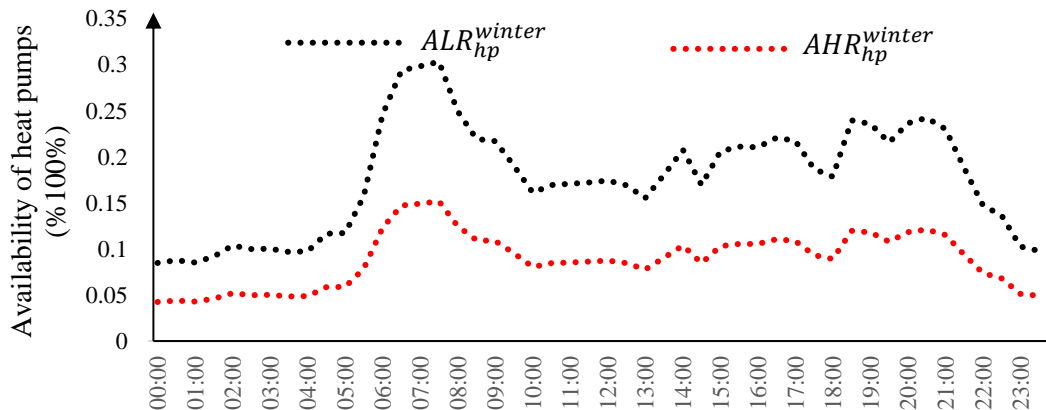
Fig. 6.2 Availability of heat pumps over a Winter day
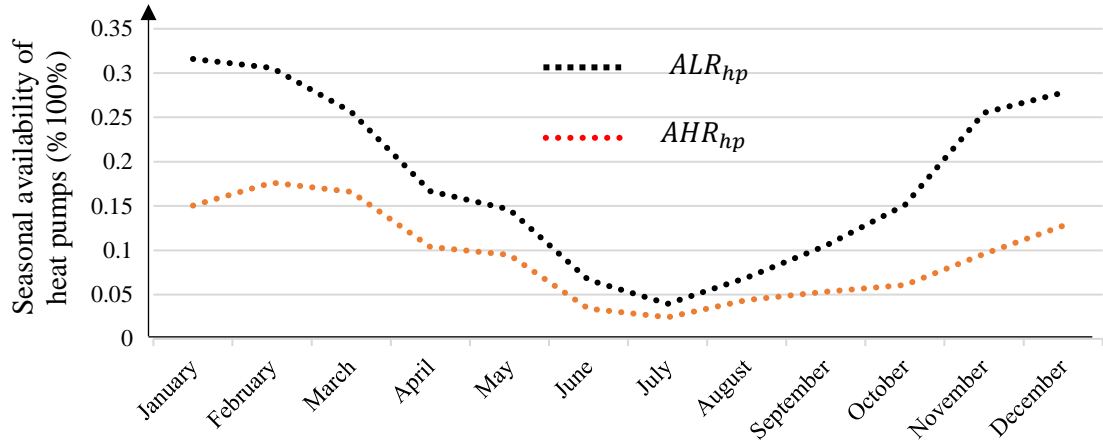
Fig. 6.3 Seasonal Availability (SA) of heat pumps obtained

Based on the ALR_{hp}^{winter}, AHR_{hp}^{winter} (over a winter day) and the seasonal availability, the ALR_{hp}^{summer} and AHR_{hp}^{summer} (over a summer day) are calculated using Equations (6.1) and (6.2) [125]. Fig. 6.4 shows the ALR_{hp}^{summer} and AHR_{hp}^{summer} that are averaged between April to September.

$$ALR_{hp}^{summer} = ALR_{hp}^{winter} x \; \frac{SA_{summer}}{SA_{winter}} \tag{6.1}$$

$$AHR_{hp}^{summer} = AHR_{hp}^{winter} x \; \frac{SA_{winter}}{SA_{summer}} \tag{6.2}$$
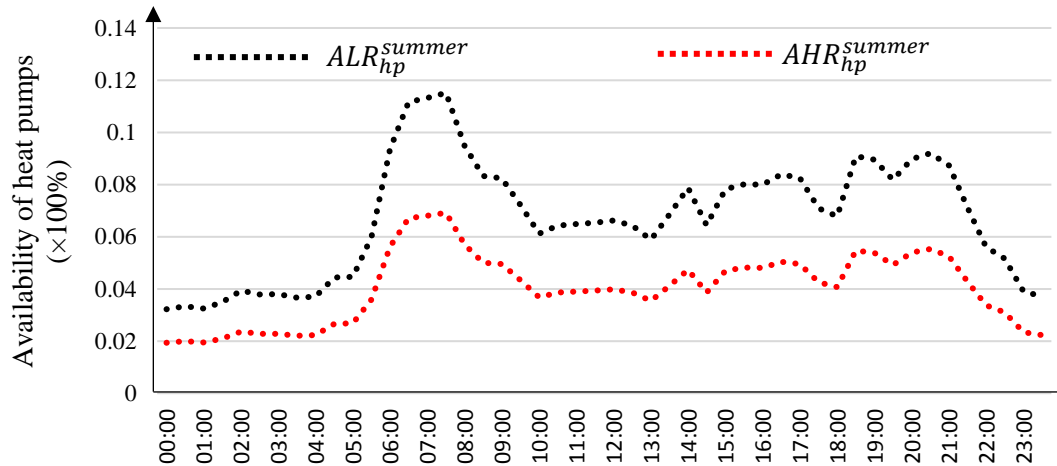
Fig. 6.4 Availability of heat pumps over a Summer day

6.3.2 Availability of fridges at different time of day

For fridges, field test to measure the ALR_{fr} and AHR_{fr} were undertaken for winter months in 2011/2012 [138]. The investigations were carried out on 1,000 fridges in GB homes including diverse types of Coolers/Freezers covering almost 80% of the fridges' market. The average ALR_{fr} and AHR_{fr} in the summer and winter at each hour of a day are shown in Fig. 6.5 and Fig. 6.6. The availability of fridges is nearly constant over the day because fridges are usually engaged to the consumers' use.
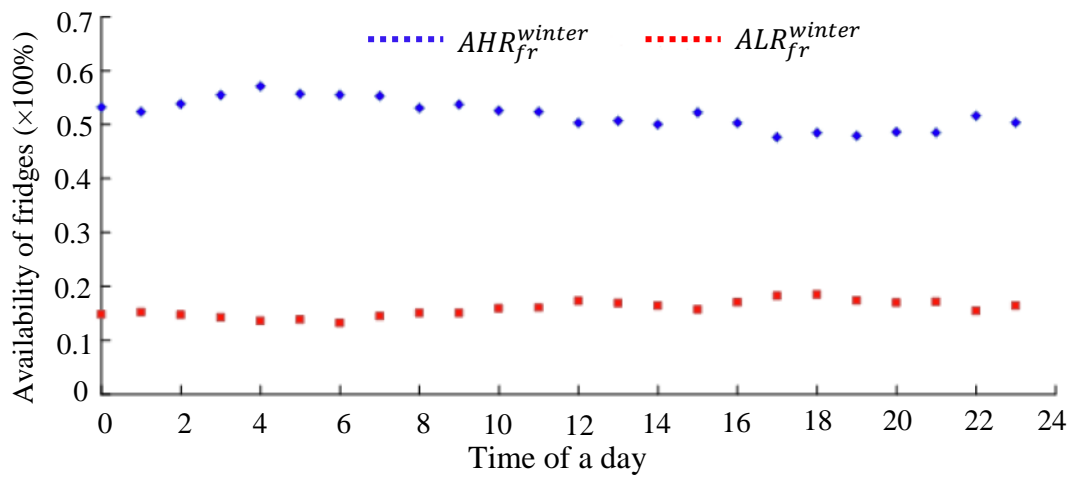
Fig. 6.5 Availability of fridges on a Winter day [138]
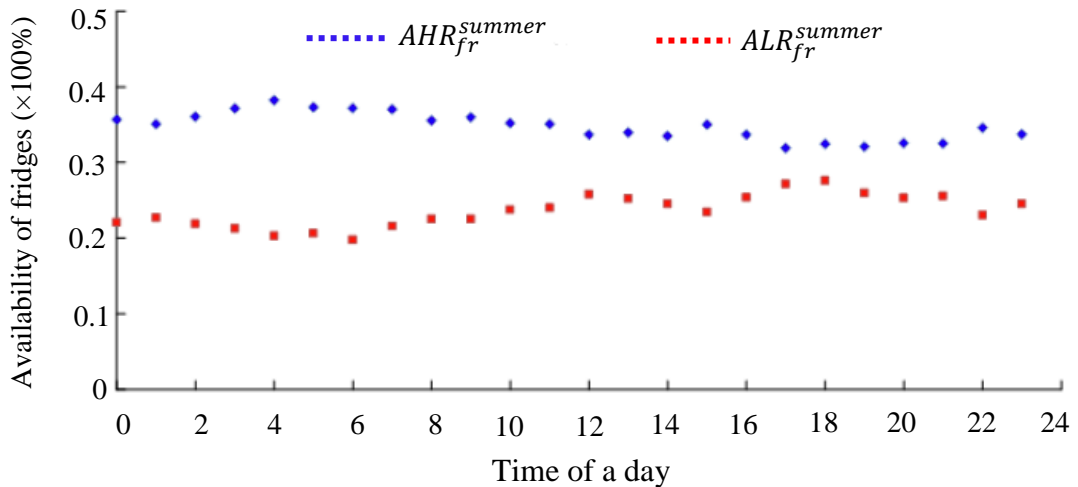
Fig. 6.6 Availability of fridges over a Summer day [138]

6.3.3 Potential response from all fridges and heat pumps

According to the 2030 medium uptake scenario presented in [139], there are expected to be 3.8 million heat pumps in GB's dwellings by 2030. Also, there will be approximately 48 million fridges in GB by 2030 according to [140]. Each heat pump has a typical power consumption of 3kW, and each fridge has a typical power consumption of 0.1kW. Based on the availability of each load presented in Section 6.3.1 and Section 6.3.2, the total availability response from all the heat pumps and fridges over the whole day is calculated by using Equations (6.3) and (6.4).

$$ALR_{total}(t) = \frac{(NALR_{hp} \times NFR) + (NALR_{fr} \times NHP)}{NHP \times NFR} \times 100\% \tag{6.3}$$

$$AHR_{total}(t) = \frac{(NAHR_{hp} \times NFR) + (NAHR_{fr} \times NHP)}{NHP \times NFR} \times 100\% \tag{6.4}$$

where $NALR_{hp}$ and $NAHR_{hp}$ are the numbers of heat pumps that have ON and OFF states respectively. Similarly, $NALR_{fr}$ and $NAHR_{fr}$ are the numbers of fridges that have ON and OFF states respectively. *NHP* is the total number of heat pumps and *NFR* is the total number of fridges.

Fig. 6.7 shows the entire availability of aggregated load from both heat pumps and fridges to provide frequency response to Great Britain's power system. As shown in Fig. 6.7, the potential of the aggregated load for the provision of frequency response is considerable, especially in the winter. At Great Britain's peak demand time (17:00-20:00), the heat pumps and fridges are available to provide a minimum of 3,500MW load decrease in winter and drop to 2,450MW in summer. At the lowest Great Britain demand between (00:00-06:00), the aggregated load is able to provide a minimum of 3,640MW load increase in winter and 2,320MW in summer. It can be observed that the availability of frequency response is always lower in the summer due to lower heat pumps demand.
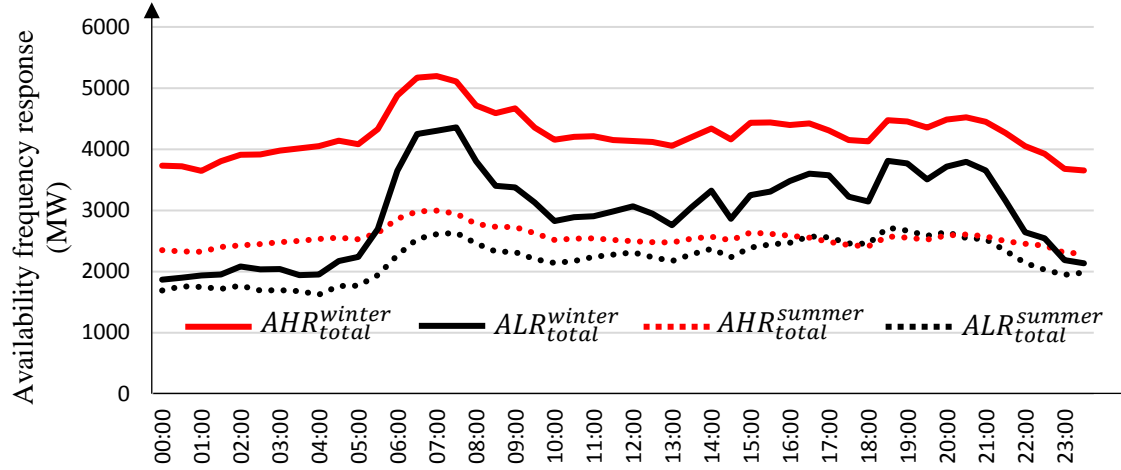
Fig. 6.7 Available frequency response from all heat pumps and fridges over a day

6.4   Load aggregation to provide Firm Frequency Response

Firm Frequency Response (FFR) is one of the most valuable balancing services in Great Britain's power system. Participation in FFR service requires a provision of 10MW as a threshold. National Grid gives the opportunity for small demand side providers to secure a bridging contract in which they can build their volume by aggregating assets [63]. Aggregators or suppliers must be capable of providing a minimum of 10MW to the grid within 30 seconds of a frequency event, such as a power station tripping out.

In this research, the aggregation of certain numbers from both heat pumps and fridges to provide a minimum low frequency response of 10MW to the grid is calculated by using Equation (6.5). The time of the day is divided into five periods according to the availability of load as shown in Fig. 6.8. The intersection point between the red and black slopes represents the aggregation of 8,000 heat pumps and 30,5396 fridges to provide 10 MW of low frequency response over the time 14:00-21:00 (the time that involves the peak demand). The values of ALR_{hp} and ALR_{fr} are the averaged value of the five periods given and are listed in Table 6.1.

$$ALR_{hp} \times NHP \times P_{hp} + ALR_{fr} \times NFR \times P_{fr} \geq 10MW \qquad (6.5)$$

Table 6.1 ALR_{hp} and ALR_{fr} at different time of a aay

Period	time of day	$ALR_{hp}(\times100\%)$	$ALR_{fr}(\times100\%)$
1	10:00-13:30	0.17	0.167
2	14:00-17:00	0.2	0.165
3	17:30-18:00	0.18	0.184
4	18:30-21:00	0.23	0.175
5	22:00-04:00	0.12	0.15
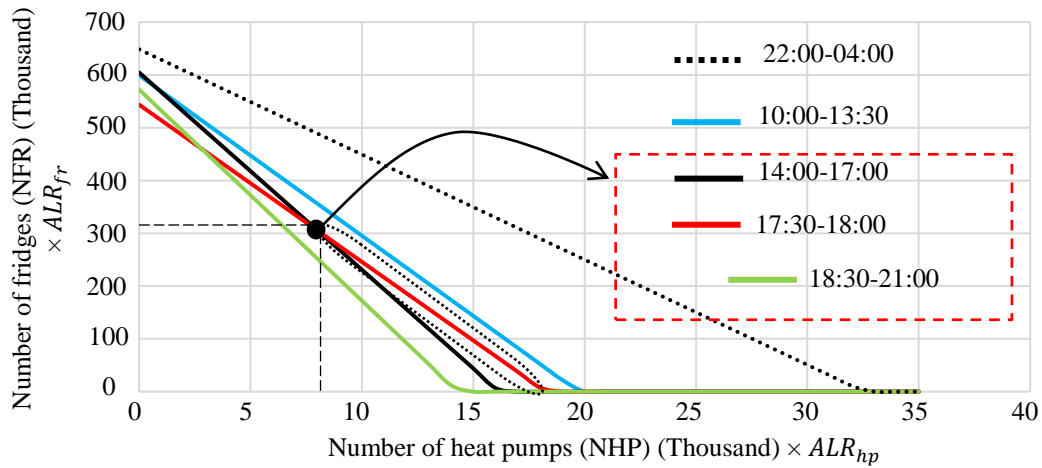
Fig. 6.8 Aggregation of heat pumps and fridges for the provision of 10MW threshold (low frequency response service)

The relationship between the NHPs and NFRs in Equation (6.5) is linear. Hence, the red slope in Fig. 6.8 (shaded area) is used to calculate the combination number of heat pumps and fridges for a large frequency response provision. This slope is scaled up to represent the provision of minimum 100MW. Then, the load scaling factor (δ) is added to represent the power at any combination, as shown in Fig. 6.9. For example, when $\delta = 1$, the resulting combination numbers (NHP and NFR) are used to provide a low frequency response of 100MW. When $\delta = 2$, the resulting combination numbers are used to offer a power of 200MW, etc.

The NHP is used as an input to specify the level of aggregated load using Equation (6.6). The frequency response provided by the heat pumps is higher than the fridges

because the power rate of the heat pump is typically higher. However, the availability of heat pumps is very seasonal and is not always available in large numbers. Therefore, the fridges can compensate the lack of frequency response because fridges are available at every time. In this chapter, three scenarios are considered to provide the same amount of frequency response, where the aggregator can adopt a certain number of heat pumps and fridges according to the availability of the load and based on cost saving.

- **Combination of Low NHP –High NFR**: This scenario is more suitable when heat pumps demand is low. The power rate of a heat pump is typically 30 times the power rate of the fridge. Therefore, an aggregation of a small number of heat pumps requires a vast number of fridges to fill the required frequency response.

- **Combination of Average NHP – Average NFR**: This scenario is more economical than the previous one because it assumes smaller number of units to provide the same amount of frequency response. This scenario can be used when there is a larger number of heat pumps.

- **Combination of High NHP – Low NFR**: This scenario is more appropriate in winter months due to higher heat pumps demand. Hence, the aggregator can adopt a large number of heat pumps and a small number of fridges. This is the most economical scenario as the entire number of responsive units is reduced.

The equation shown in the figure:

$$NFR = -29.1 \times NHP + 5377769.5\delta \qquad \delta: 1,2,.. \qquad (6.6)$$
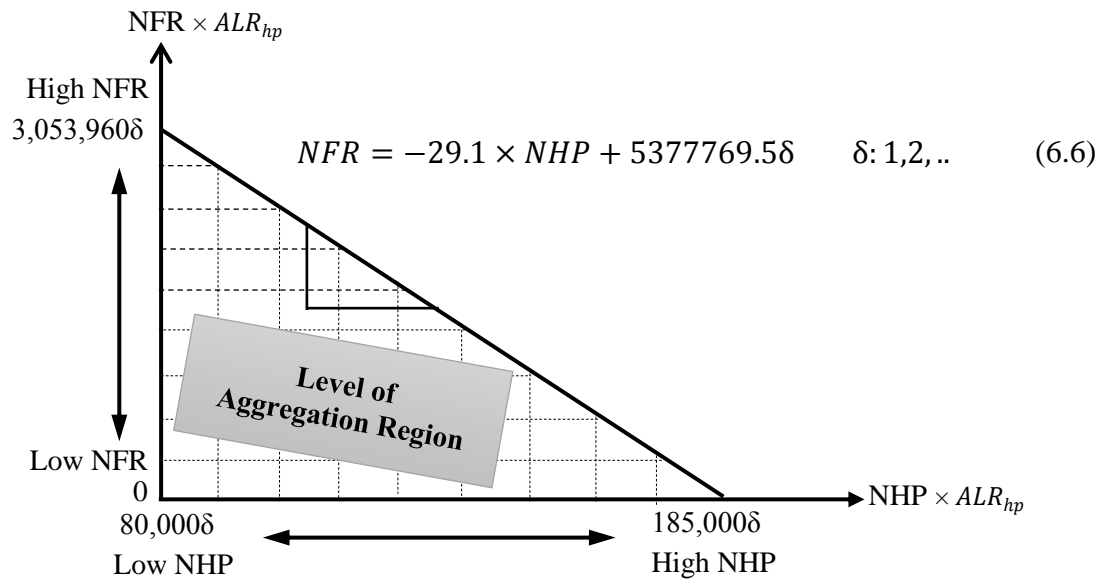
Fig. 6.9 Relationship of the combination of heat pumps and fridges to provide low frequency response service

6.5 Aggregated load control algorithm

This study considers the provision of frequency response based on dynamic FFR service [10, 141]. In this service, the power of several aggregated loads can be controlled to maintain the grid frequency stable (typically 50 Hz) at any time.

A control algorithm is developed to switch OFF or ON each unit in response to a regulation signal. In this research, the grid frequency $f(t)$ is used as the regulation signal. A decentralized dynamic frequency controller (DFC) is designed and applied to each heat pump and the fridge is developed as shown in Fig. 6.10.
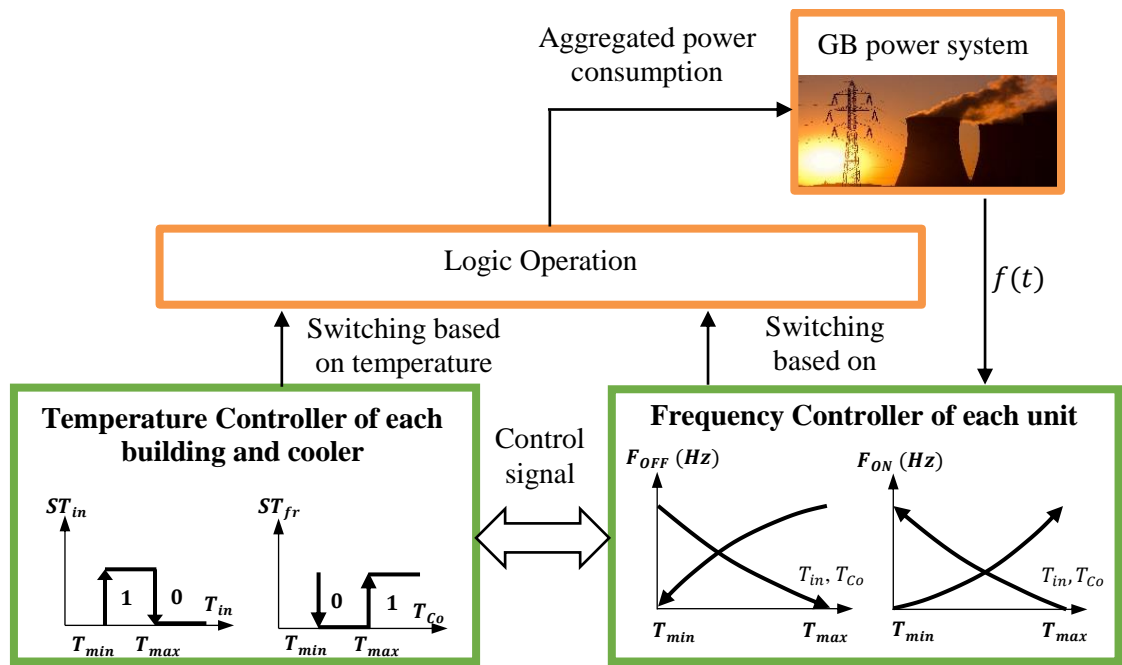
Fig. 6.10 Diagram of dynamic frequency control of each unit
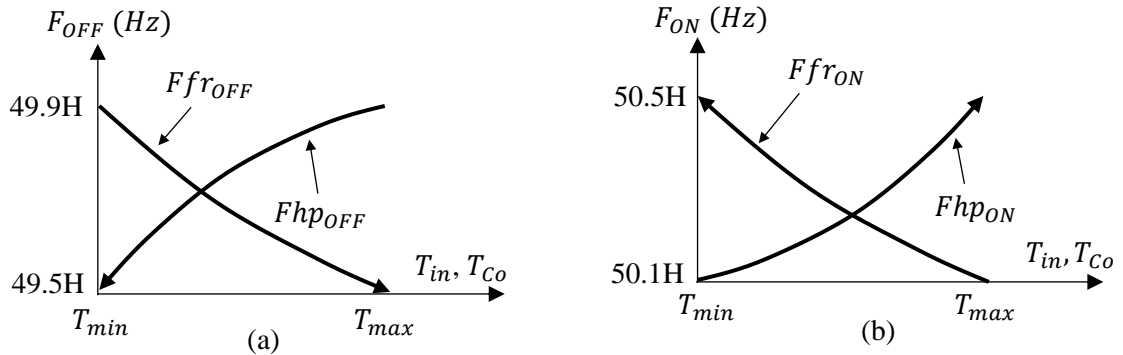
Fig. 6.11 Dynamic trigger frequencies vs the temperature a) Ffr_{OFF} vs T_{Co} and Fhp_{OFF} vs T_{in} b) Ffr_{ON} vs T_{Co} and Fhp_{ON} vs T_{in}

The Temperature Controller measures the temperature of the fridges and buildings, and the Frequency Controller monitors Great Britain's grid frequency continuously. Each unit is assigned with two trigger frequencies F_{OFF} and F_{ON}. The range of F_{OFF} is 49.5–49.9 Hz and the range of F_{ON} is 50.1–50.5 Hz which is consistent with the steady-state limits of grid frequency in the Great Britain power system. The control algorithm compares the grid frequency $f(t)$ with the trigger

frequencies simultaneously and decide to trigger the load. The frequency controller should ensure a smooth switching behaviour and should avoid the high payback that could result from a large number of units recovering at the same time. Therefore, the following techniques are implemented to ensure a smooth and gradual switching events:

- The trigger frequencies of a heat pump Fhp_{OFF} and Fhp_{ON} vary dynamically with the building temperature T_{in} as shown in Fig. 6.11. For a frequency drop, heat pumps are switched OFF in descending order starting from the warmest building. Similarly, for a frequency rise, heat pumps are switched ON in ascending order starting from the coldest building.

- The trigger frequencies of a fridge Ffr_{OFF} and Ffr_{ON} vary dynamically with the cooler temperature T_{Co} as shown in Fig. 6.11. For a frequency drop, fridges are switched OFF in ascending order starting from the coldest cooler. Similarly, for a frequency rise, fridges are switched ON in descending order starting from the warmest cooler.

Fig. 6.12 shows the flowchart of the control system of the aggregated load. The initial temperature T_{in} of a population of buildings and the initial temperature T_{Co} of a population of fridges are diversified by randomising the starting time using a uniform distribution.

The frequency controller should not undermine the internal temperature (T_{in} and T_{Co}). When the temperature exceeds the predefined temperature set-points (typically for a building $T_{min}=19^0$C and $T_{max}=23^0$C and for a cooler $T_{min}=7.5^0$C and $T_{max}=8.5^0$C), the Temperature Controller is prioritized, i.e. Sfr_f follows ST_{CO}, and Shp_f follows ST_{in}. In other words, the final switching signal will only respond to the temperature controller but not to the frequency controller even through the time of a frequency incident. However, when the temperature is within the acceptable limit, the frequency controller is prioritized, i.e. Sfr_f and Shp_f respond to the frequency controller. If $f(t) \leq Ffr_{OFF}$ and/or $f(t) \leq Fhp_{OFF}$, this indicates that

there is a frequency drop signal and hence each unit is switched OFF ($Sfr_f = 0$ and $Shp_f = 0$) to decrease the power demand. If $f(t) \geq Ffr_{ON}$ and/or $f(t) \geq Fhp_{ON}$, this indicates that there is a frequency rise signal and hence the appliance is switched ON ($Sfr_f = 1$ and $Shp_f = 1$) to increase the power demand.
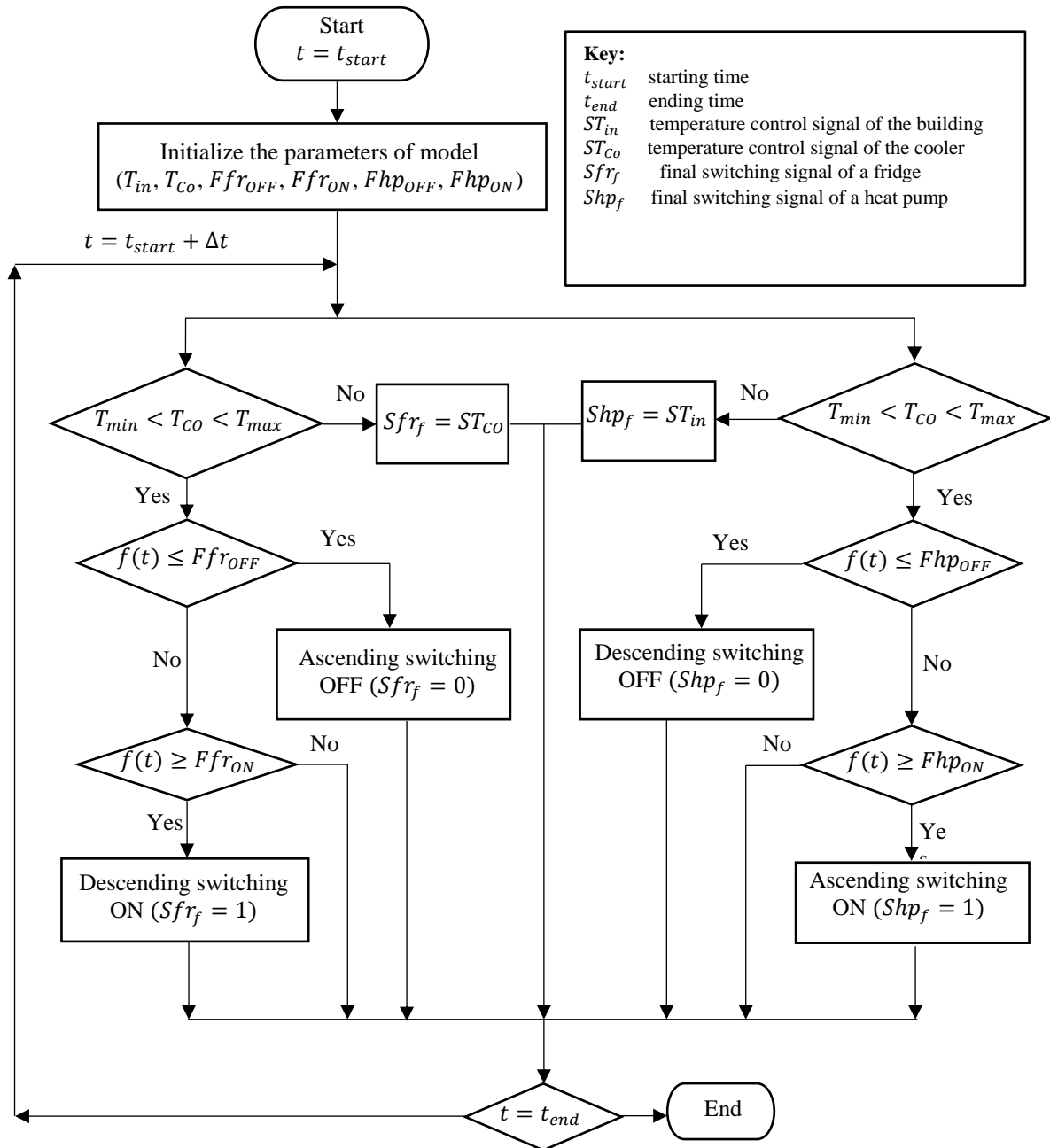
Fig. 6.12 The flowchart of the aggregated load control system

6.6 Simplified Great Britain power system

A simplified model representing the governor, inertia and damping of the Great Britain power system is developed as shown in Fig. 6.13 [19, 142]. The system inertia H_{eq} is 6.5sec which is measured according to the interconnector loss (loss of 1,000 MW) that occurred on September 30, 2012 [92, 143]. The load frequency dependence was lumped into a damping constant D, which was set to 1 p.u. The Great Britain's synchronous generators were represented by governor-turbine transfer functions. For the provision of a primary response, all generators should have a governor droop setting between 3%−5% according to the Great Britain grid code [128]. Some generators are required to provide secondary frequency control. Therefore, the simplified Great Britain power system is represented by two lumped blocks G1 and G2. The block G1 represents 20% of the generators that provide primary frequency response, while the block G2 represents 80% of the generators that provide primary and secondary frequency response as shown in Fig. 6.13. The provision of secondary response was modelled by the supplement integral control loop with gain K_i. The speed governor deadband in blocks G1 and G2 should not be greater than 0.03Hz; however, to increase certainty, it was selected here to be ±0.015Hz [128]. The governor droop is represented by the gain $1/R$ and was set to 20 p.u. The parameters used in Fig. 6.13 are given in Table 6.2, where T_g, T_t, T_{tr}, and T_r are generator-turbine time constants [19].
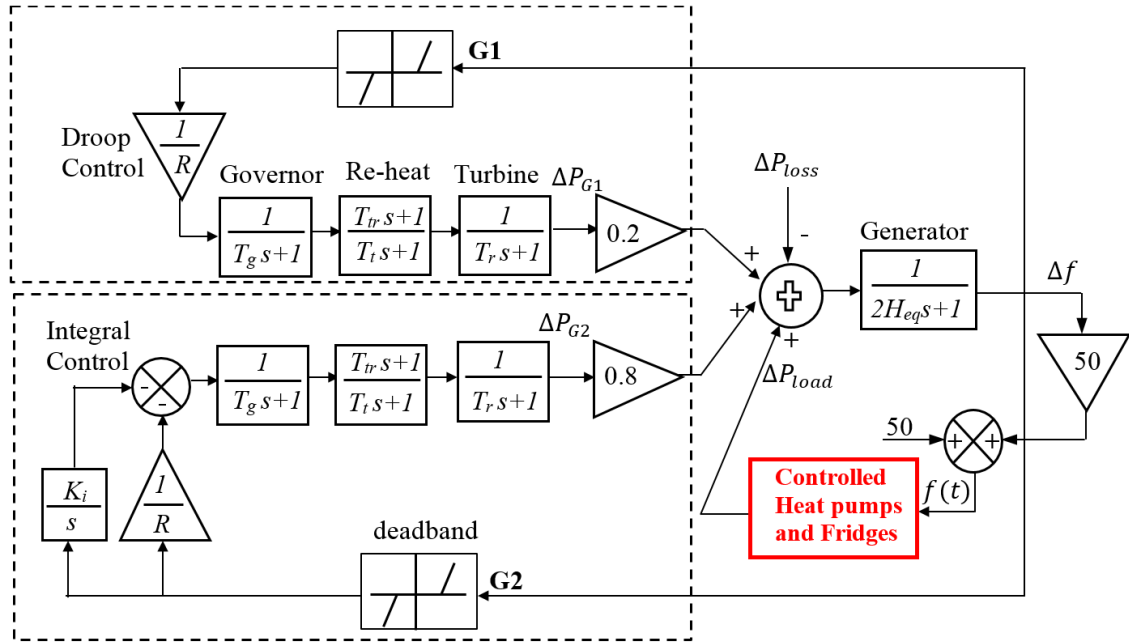
Fig. 6.13 Simplified Great Britain power system model

Table 6.2 Parameters of the simplified Great Britain Power System (based demand=41GW)

$1/R$	T_g	T_{tr}	T_t	T_r	K_i
20	0.2	2	20	0.3	0.05

6.7 Simulation results

6.7.1 Case study based on FFR threshold

A case study was conducted to examine the capability of aggregated load to provide 10MW, representing the minimum amount of low frequency response to participate in FFR. The aggregation of 8,000 heat pumps and 30,5396 fridges was considered. This was estimated over the time interval (14:00-17:00) and (17:30-18:00) based on the intersection point in Fig. 6.8. Fig. 6.14 shows the frequency profile that was injected into the system (see the left axis). The frequency drop at time 470 sec was considered to test the capability of the aggregated controllable loads to reduce their power consumption offering a FFR service. Fig. 6.14 shows

the behaviour of the power consumption drawn by the controlled load during the frequency event (see the right axis). The heat pumps and fridges were switched OFF immediately providing a reduction of 10MW from their power consumption proportional to the frequency drop. Thus, aggregation of the load is able to participate in FFR service. However, provision of 10MW is relatively small to the GB power system, and aggregation of a larger number of units should be adopted.
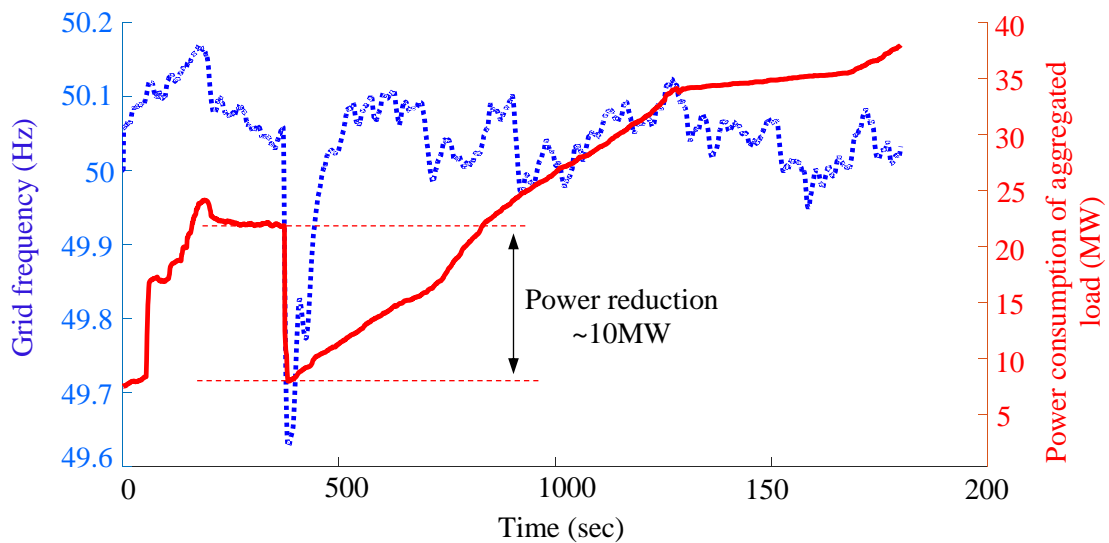
Fig. 6.14 Power reduction from aggregated heat pumps and fridges to provide 10MW in response to a grid frequency

6.7.2 Case study (based on three scenarios) on the simplified Great Britain power system

6.7.2.1 Cost saving by using the aggregated load control

4. The use of the aggregated load control will result in a considerable cost saving. The financial value of the aggregated load control to provide frequency response is calculated using three scenarios. The scenarios are based on different combination of heat pumps and fridges (see Fig. 6.9) for the provision of low frequency response service (maximum 1,000 MW). These scenarios are shown in Table 6.3 and described below:

Scenario 1 (Sn₁) Low NHP - High NFR: this scenario assumed a low availability of heat pumps, and thus 191,250 responsive heat pumps were considered. By using Equation (6.6), and for the provision of 1000MW as a maximum low frequency response, the number of responsive fridges was calculated to be 4,206,046. The frequency response in this scenario was very dependent on the fridges.

Scenario 2 (Sn₂) Average NHP - Average NFR: in this scenario, 238,500 responsive heat pumps and 2,800,516 responsive fridges were connected to grid to provide power reduction of maximum 1000MW from the aggregated load. The number of fridges is reduced by 33% from Sn_1, while the number of heat pumps was increased by 20%.

Scenario 3 (Sn₃) High NHP - Low NFR: This is the most economical scenario as the number of responsive units is reduced to 1,679,717 (about 38.3% from Sn_1) but provide the same frequency response size (i.e. 1,000 MW). In this scenario, 285,785 responsive heat pumps and 1,393,932 responsive fridges were considered to provide power reduction of a maximum 1000MW from the aggregated load. The dependency on the fridges for the frequency response was reduced by 67% from Sn_1. The number of connected heat pumps was increased by 33% from Sn_1.

According to the monthly report of National Grid for the year 2014 [144], the total frequency response of 1,236.4GWh was expected to cost National Grid £5.2 million per month. Therefore, the cost of the overall frequency response of 1MWh per month is £4.2. In this case study, the load aggregators were assumed to provide frequency response of 1,000MW over the time 14:00-21:00 (240 hours in a month). Thus, the value of the aggregated load control is calculated as follows:

$$\text{Value } (\pounds) = \text{Total}_{\text{freq resp.}} (\pounds/\text{MWh}) \times \text{Aggr}_{\text{load resp.}} (\text{MW}) \times t_{\text{availability}}(h) \quad (6.7)$$

According to Equation (6.7), the benefit for the load aggregator to provide frequency response service is £1.01M/month (~£12.12M/year). However, the total value

contribution from each appliance depends on the total number of controlled appliances in each scenario. Each DFC unit is assumed to cost £3 [68]. In Sn_1, the total number of 1.06 million heat pumps and 22.85 million fridges are connected to the grid, and therefore the value contribution from each unit is approximately £7.13, assuming a lifetime of 20 years for each appliance (including the cost of the frequency controller). In Sn_2, there are 1.33 million heat pumps and 15.22 million fridges, the value contribution from each unit is increased to £11.65. In Sn_3, there are 1.59 million heat pumps and 7.6 million fridges, the value contribution from each unit is increased to £23.5.

In conclusion, the third scenario (Sn_3) is more economic for the provision of 1,000 MW of frequency response. The aggregation of larger number of heat pumps and lower number of fridges will provide cost saving to the system operator. However, the technical feasibility of each scenario is important to address.

Table 6.3 Combination scenarios of heat pumps and fridges to provide 1,000 MW

Scenarios	Total NHP	Total NFR	Available NHP for frequency response	Available NFR for frequency response
Sn_1	1,062,500	22,858,945	191,250	4,206,046
Sn_2	1,325,000	15,220,195	238,500	2,800,516
Sn_3	1,587,697	7,575,715	285,785	1,393,932

6.7.2.2 Technical feasibility of the controlled aggregated load on the simplified Great Britain power system

This case study was carried out for the provision of 1,000 MW frequency response to the grid. The heat pump and fridge models were connected to the simplified Great Britain power system as shown in Fig. 6.13.

A loss of two individual generators was applied to the system based on [8]. The loss of the first generator has caused a loss of 345MW at time 11:34 (in the real event) equivalent with time 200 sec in this modelling study. Around two minutes later, the loss of the second generator caused additional loss of 1,237MW. The system demand was 41GW at the time of the frequency incidents.

The simulation was carried out by connecting a number of heat pumps and fridges, listed in Table 6.3, to the simplified GB power system. It was assumed that each heat pump has a typical power consumption of 3kW and each fridge 0.1kW.

Two sets of results during the frequency incident were simulated, with and without the controllable loads. Fig. 6.15 shows the power consumption behaviour of the heat pumps and fridges individually in the three defined scenarios before and after the frequency incidents. It can be seen that the load power has decreased immediately after the two frequency incidents.

Fig. 6.16 shows the power reduction drawn by the aggregated load (see the left axis) and the change of power output of generators (see the right axis) using the three defined scenarios. It can be seen that the entire power reduction from the aggregated load, is almost equal in Sn_1 and Sn_2 (about 660MW) with slightly different value in Sn_3 (about 600MW). The slight difference in Sn_3 is due to less diversity in the load as a total. The use of controlled loads has significantly reduced the power output from synchronous generators (around 50%).

The impact of reducing the power consumption of the aggregated load on the grid frequency is shown in Fig. 6.17. The frequency deviation was reduced to almost the same value when the three scenarios were considered. The first frequency drop was reduced from 49.8Hz to 49.9Hz. Following the second incident, the frequency drop was reduced from 49.22Hz to around 49.58Hz.
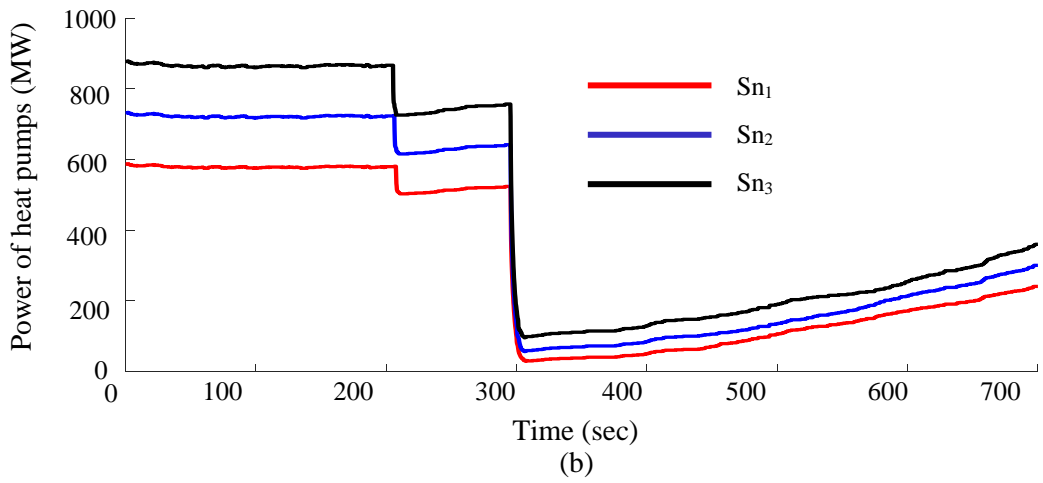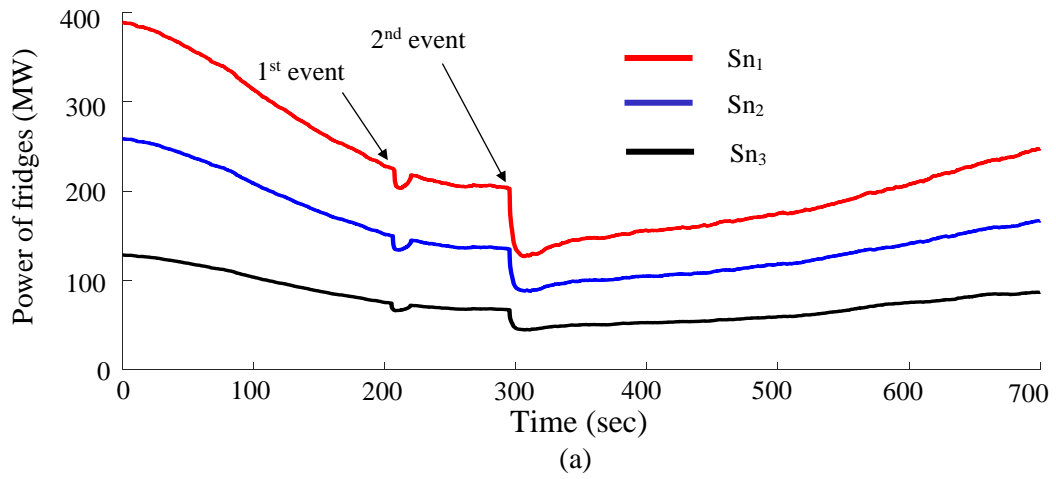
Fig. 6.15 Load power reduction a) fridges b) heat pumps
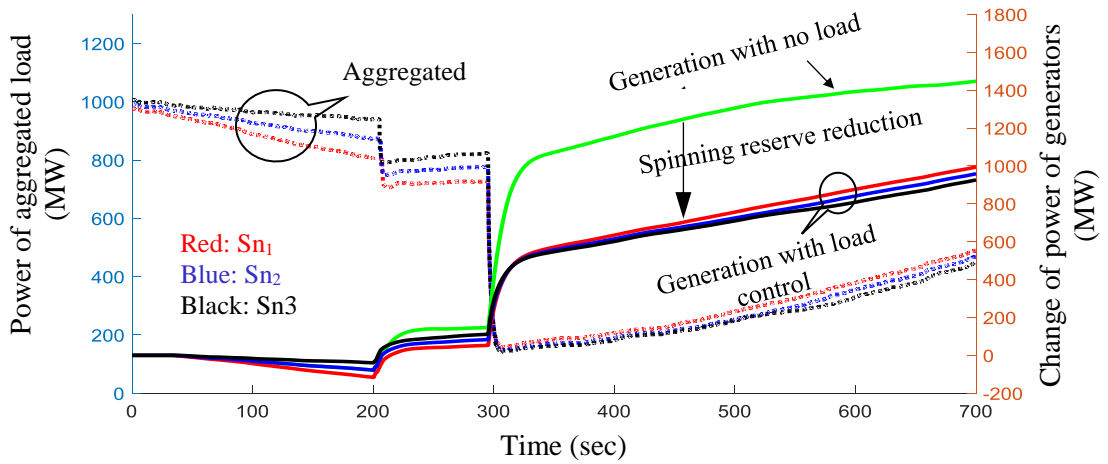
Fig. 6.16 Power reduction of aggregated load and change of power output of the synchronous generators
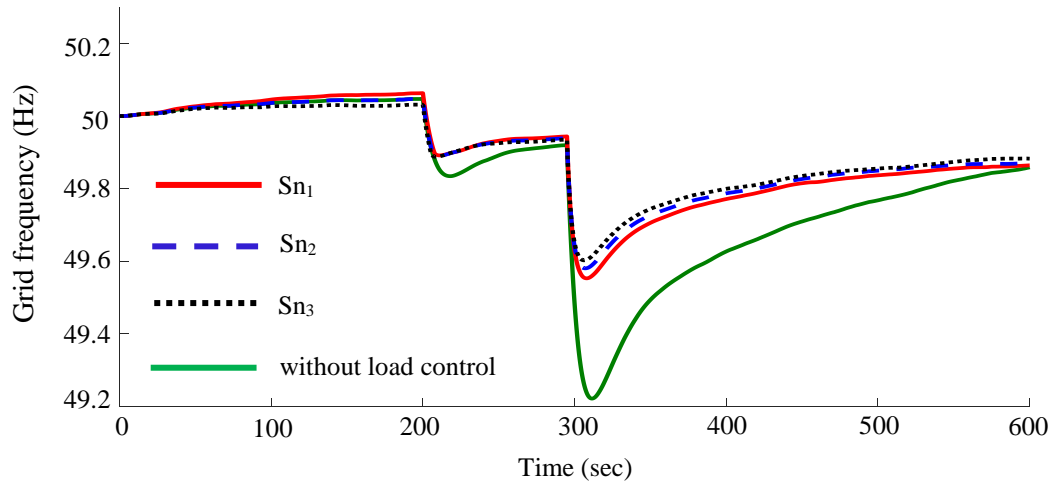
Fig. 6.17 Variation of grid frequency at each load combination scenario

6.7.3 Case study on the GB master transmission and generation system model

This case study was carried out to investigate the geographic response provided by the controlled load. Therefore, the master electrodynamic GB system model was used. The master model was modelled in DIgSILENT by National Grid and is used at present by the GB transmission system operator, National Grid plc. The schematic diagram of the detailed GB transmission system model is shown in [145]. The master model contains detailed buses which represent the present GB transmission and distribution networks. Eleven models (representing the Distribution Networks Operator (DNO)) are connected to the GB transmission system model.

Dynamic Link Library (DLL) between *DIgSILENT power factory* and *Matlab/Simulink* was created to interface around 10 million controlled loads to the master model. An aggregated heat pump and fridge models were connected to a low voltage networks (33-kV bus-bar) in each of the 11 DNO models. Each appliance was equipped with a DFC unit. Table 6.4 illustrates the DNO numbers and relevant stations in which the load models were connected in. The availability of load was obtained based on Fig. 6.7 at time 11:00-11:30 (representing the winter evening peak time). The number of heat pumps and fridges in each DNO was estimated based on the number of electricity customers in different areas, as listed in Table 6.4. The

system condition was set to reflect the winter peak load scenario in 2016. The system demand was around 41 GW. A loss of a generation of a total of 1.8 GW was applied to the master GB power system model at 2sec, which represents the maximum infrequent infeed loss in the GB power system.

Simulation results are shown in (Fig. 6.18-Fig. 6.21). Fig. 6.18 shows the frequency measurements at each DNO area that was connected to heat pump and fridge models. At the first few sub-seconds following the frequency event, the frequency deviation at each DNO was not precisely similar to each other across the whole network. For example, the rate of frequency change at DNO-08 was the fastest and in DNO-03 was the slowest. The DNO-08 is closer to the region of the frequency event than the others, while the DNO-03 is farther to the area of an event than the others. This indicates that the frequency change propagated faster in the areas that are closer to the region of the frequency occurrence.

Fig. 6.19 shows the response drawn by the aggregated load at each DNO. The response of aggregated load showed that there was a little geographical impact on the provision of frequency response. The controlled load in all different areas provided an immediate response in proportional to changes in grid frequency, which imitated the response of the spinning reserve of generators.

Fig. 6.20 shows the power output delivered by four aggregated synchronous generators (see the left axis) and the total power of aggregated load (see the right axis). Following the loss of generation, the power consumption of aggregated load was decreased by almost 1,000MW. The power output from synchronous generators was also reduced.

Fig. 6.21 compares the grid frequency with and without the controlled load after the loss of generation (see the left axis). The controlled aggregated load has reduced the frequency drop from 49.51Hz to 49.87Hz and maintained the system frequency stabilised. Fig. 6.21 also shows the individual response drawn by heat pumps and fridges. The power consumption of heat pumps was reduced by 351MW and fridges by 638MW after the frequency incident. The fridges were hugely diversified, and therefore the frequency response provided by the fridges is high.

Fig. 6.22 shows the values of the absolute RoCoF at the first crucial sub-seconds following the incident (0.4 msec, 0.6msec, 0.8msec, 1sec). The aggregated load control has halted the RoCoF significantly, where the average RoCoF was reduced by 85%.

Table 6.4 Number of aggregated load connected to each DNO

DNO	Description	Station	Busbar	Aggregated load
DNO1	North Scotland	Arbroath	33 KV	1,425,000
DNO2	Central and Southern Scotland	Long Park	33KV	2,290,000
DNO3	North East England	Attercliffe	33KV	2,260,000
DNO4	North West England	Belfield	33 KV	6,160,000
DNO5	Yorkshire (North East)	Barrack Road	33 KV	2,755,000
DNO6	East England	Abberton	33 KV	2,290,000
DNO7	London	Bengeworth Road	33 KV	5,975,000
DNO8	South East England SEPN	Addington	33 KV	3,400,000
DNO9	Southern England SSE Southern	Aldershot	33 KV	3,250,000
DNO10	Merseyside, Cheshire, North Wales North Shropshire	Aberystwth	33 KV	2,320,000
DNO11	East Midlands, West Midlands, SouthWales&South West England	Avonmouth Alfreton 33KV Ketley Barry	33 KV 33 KV 33 KV 33 KV	10,245,000
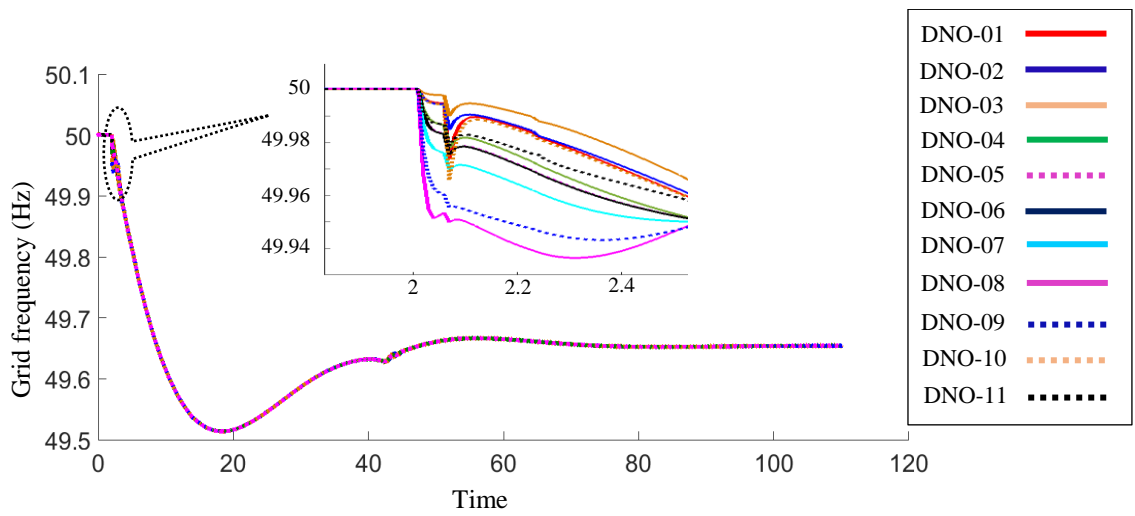
Fig. 6.18 Variation of grid frequency at each DNO
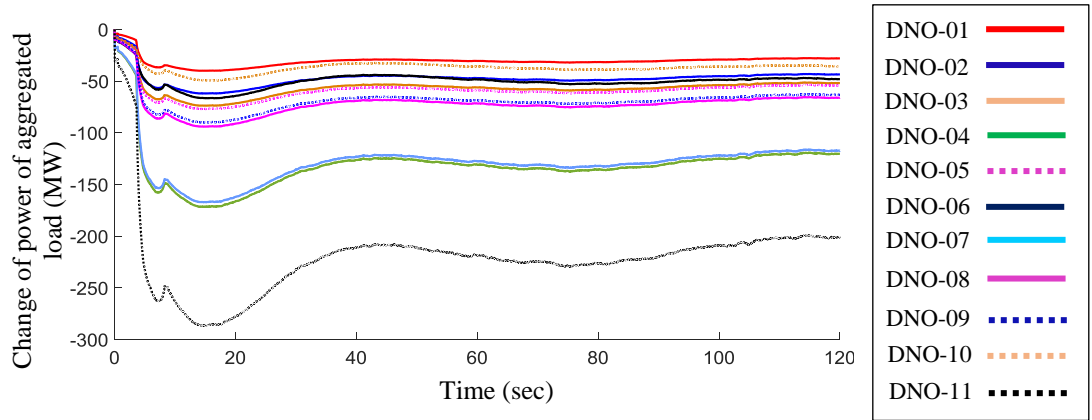
Fig. 6.19 Power reduction of aggregated heat pumps and fridges at each DNO
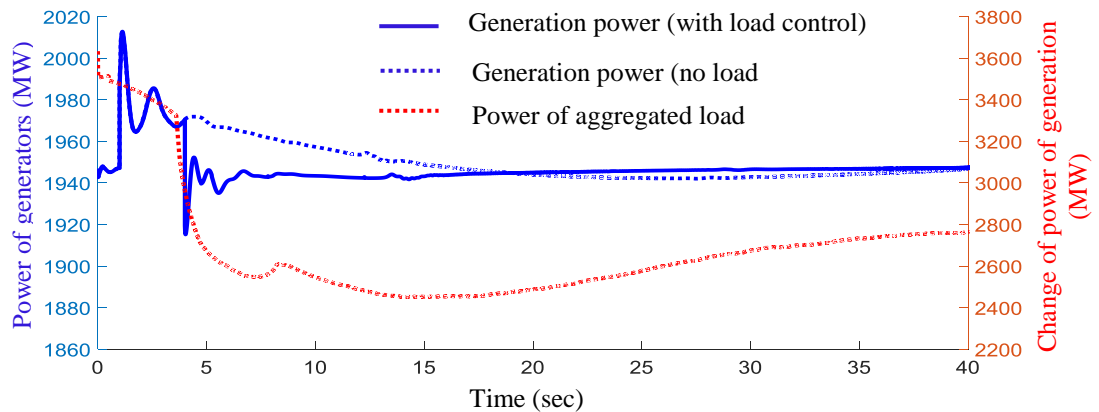
Fig. 6.20 Power of synchronous generators and power of aggregated heat pumps and fridges

153
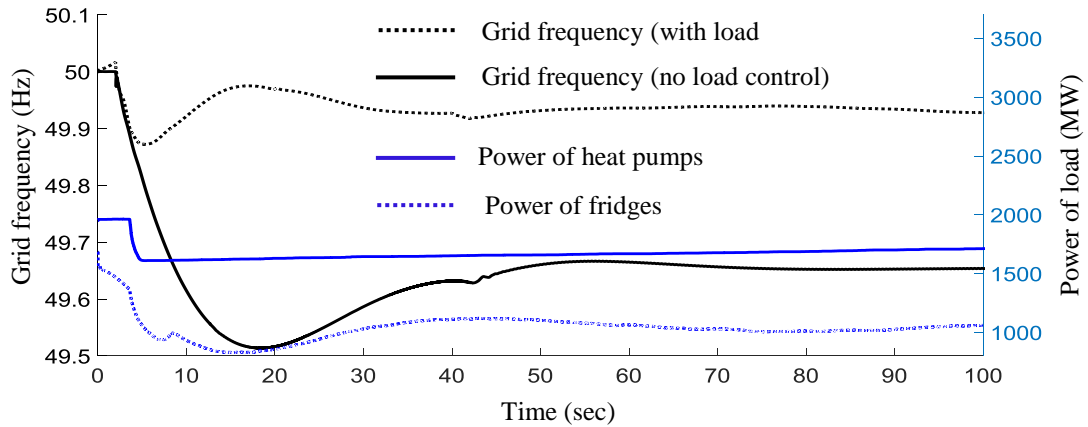
Fig. 6.21 Grid frequency vs load behaviour
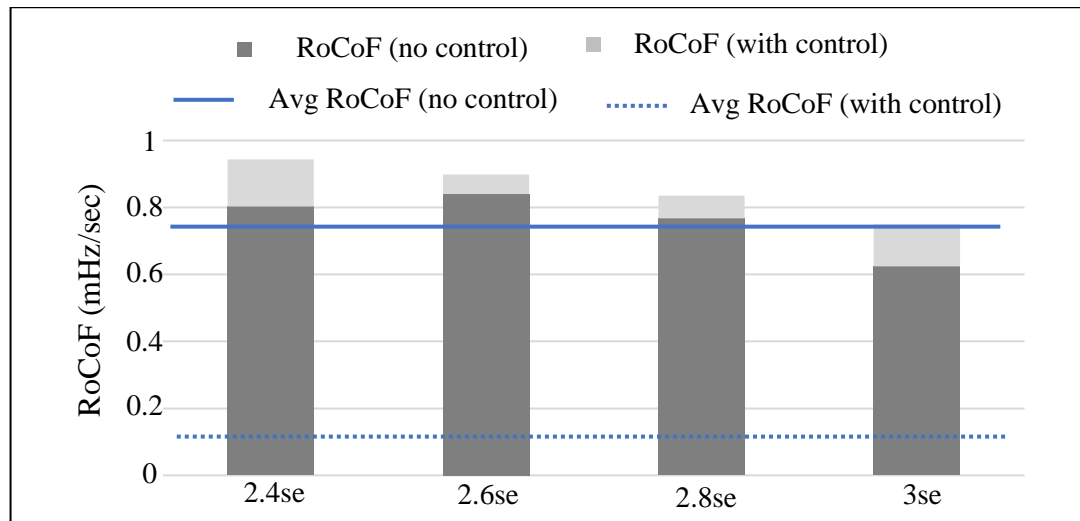
Fig. 6.22 Absolute RoCoF at the first sub-seconds following the frequency event

6.8 Conclusion

This chapter investigated the potential of demand side response from the aggregation of heat pumps and fridges for the frequency control.

A decentralised dynamic frequency control algorithm was developed for the provision of the frequency response service. The control algorithm was coordinated to provide an aggregated response from a population of heat pumps and fridges without undermining the temperature of the buildings and fridges. A relationship

between the number of heat pumps and the number of fridges to provide sufficient FFR service was developed.

The aggregated model was then integrated into a simplified GB power system model. Three scenarios were presented to differentiate the combination of the load according to the load availability and considering cost saving. Results showed that the controlled aggregated load achieved a similar response in each combination scenario. A reduction of 50% in governor action of spinning reserve generators was also achieved.

The model was then validated with the master GB transmission/generation power system model which is at present used by National Grid. The impact of the aggregated load was investigated geographically over the 11 DNOs of the GB network. The measurement of the grid frequency at the DNO nearer to the source of disturbance showed higher deviation than the others. The responsive load in all different areas provided immediate response, mimicking the behaviour of the frequency- sensitive generators. Simulation results also showed the absolute RoCoF at the first crucial sub-seconds following the frequency incident (0.4msec, 0.6msec, 0.8msec, 1sec) was halted. The aggregated load control has reduced the average RoCoF by 85%.

Chapter 7

Conclusions and recommendation for future work

7.1 Conclusions

This research proposed the active control of heat pumps and fridges to address the problem of the fast rate of change of grid frequency. National Grid, in its System Operability Framework 2016 report [6], has clearly stated that reducing system inertia and the resulting increase of the rate of change of frequency may be a real challenge facing Great Britain's future power system. The proposed solutions in this thesis are:

    (i)   The development of an Adaptive Deadbeat (ADB) controller to control both the power interchange in an interconnected power system and the power output of generators in response to the frequency change.

    (ii)   The development of a Dynamic Frequency Controller (DFC) that was applied to domestic heat pumps and fridges enabling them to provide dynamic frequency response, similar to the behaviour of the spinning reserve response of frequency sensitive generators. The aggregated load control algorithm was validated on the National Grid's reduced and master electrodynamic system models.

7.1.1 Adaptive deadbeat controller in an interconnected power system

A simplified interconnected model of the north and south zones of Scotland was developed to represent a region with low system inertia (due to the growth of renewable generation in Scotland). This model was designed to meet the future energy requirements scenario stated by National Grid whereby regional control can be provided in both the north and south of Scotland.

An adaptive deadbeat (ADB) controller was developed to investigate its capability in providing a frequency response to an interconnected power system. This controller was developed to maintain the power flow between the interlinked areas at scheduled values, and to change the power output of generators when there is a frequency deviation. The ADB controller was then incorporated into the simplified interconnected model of the north and south zones of Scotland. The controller's parameters were optimized using particle swarm optimization (PSO) to ensure a robust operation and to maintain the normal operation of the power system. The parameters of the ADB controller were tuned based on the worst (lowest) system inertia; i.e., the 2029/2030 scenario in the Scotland zones, to ensure a robust operation against the expected variations in system inertia. A sudden loss in a generation was injected into the south zone. Then, the response of ADB controller was evaluated by comparing its behaviour with the standard PI and Fuzzy-PI controllers. It was shown that the ADB controller was able to significantly reduce the deviation of grid frequency by dispatching the power from the north zone to the south zone (the low inertia zone). The ADB controller also showed high robustness against a wide range of operating conditions (i.e. when the magnitude and rate of the power change are very different).

7.1.2 Thermodynamic models of heat pumps and fridges

Heat transfer model of a domestic building was developed. The model of a building equipped with a heat pump was used to establish the frequency control algorithm described in Chapter 5. The mathematical model included the modelling of thermostat temperature control that maintains the temperature inside the building within pre-defined temperature setpoints. The heat flow of the building was validated by comparing the simulation results with results of similar equipment from the literature. The population of domestic buildings was generated by giving ranges to the buildings' thermal parameters, based on real measurement found in the

literature. The population of heat pumps was implemented by randomising the starting time of the heat pumps' cycle. For the frequency control study, aggregated heat pump models were identified to represent 3.8 million heat pumps, connected to the 2030 GB power system. Simulation results showed that the power consumption of a population of heat pumps had a similar behaviour when 5,000 or more heat pump models were considered. Thus, the aggregated model with 5,000 heat pumps, multiplied by scaling multiple units, was chosen as the most reasonable model to represent the entire population of heat pumps.

The heat transfer model of a fridge was developed. The population of domestic fridges was generated by giving ranges to the thermal parameters of the fridges based on the parameters found in the literature. The simulation run was initiated by randomising the fridge internal temperature within lower and upper set-points. Additionally, a model describing 10,000 fridges multiplied by 6,000 multiple units, was selected as an appropriate model to describe the total number of fridges connected to the future 2030 GB power system.

7.1.3 The frequency control scheme of domestic heat pumps

A decentralised Dynamic Frequency Response (DFC) algorithm was developed, enabling the heat pumps to change their power consumption in response to system frequency. The DFC algorithm also involved the design of an internal temperature controller of the buildings to maintain the primary function of the heat pumps. The control algorithm ensured a dynamic relationship between the temperature of building and trigger frequencies. When the frequency dropped, heat pumps are switched OFF in descending order starting from the warmest building. For a frequency rise, heat pumps are switched ON in ascending order starting from the coldest building.

The choice of trigger frequencies was improved by using a parabolic shape to the trigger frequencies (F_{OFF} and F_{ON}). The parabolic shape expanded the region of the

switching action which caused more heat pumps to respond to the frequency event earlier. As the grid frequency recovered, the heat pumps were reconnected smoothly. Thus, the substantial load payback that could result from a simultaneous reconnection of substantial load after the frequency event was avoided.

Case studies were undertaken by connecting a representative model of the aggregated heat pumps to the Great Britain electrodynamic reduced system model.

(i) The first case study considered the 2008 frequency event, where two generators (345MW and 1,237MW) tripped individually within a short time (11:34 am-11:36 am). The DFC models of around 1.3 million heat pumps were distributed over Great Britain zones. When the first incident occurred, the DFC has reduced the power consumption of heat pumps by 300MW, and after the second event, it was decreased by a further 600MW to reduce the frequency deviation and rate of change of frequency.

(ii) The second case study considered the loss of 1800MW from the generation power, representing the infrequent infeed loss in the Great Britain power system. The DFC of 1.65 million heat pumps effectively reduced 1000MW from demand power. The DFC that used the parabolic shape for the trigger frequencies halted the grid's rate of change of frequency faster than the slope technique during the first 500msec following the incident.

However, the availability of heat pumps is seasonal. Thus, the aggregation of different types of domestic units for the provision of frequency response must be considered.

7.1.4 Demand side response from the aggregation of heat pumps and fridges

The models of domestic heat pumps and fridges were aggregated to participate in the Firm Frequency Response (FFR) service. According to National Grid, FFR service requires a provision of 10 MW frequency response as a threshold.

The availability of heat pumps in the ON and OFF states which are available to be switched OFF/ ON in response to the frequency change was estimated by Element Energy for its 2030 medium uptake scenario in Great Britain. The availability of fridges was measured through field tests carried out by Open Energi at the time of day. Based on the availability of load and its power consumption rate, a relationship between domestic heat pumps and fridges was developed to calculate the aggregation of both loads for the provision of FFR service.

The aggregated model of heat pumps and fridges was then integrated into a simplified Great Britain power system model. Three scenarios were presented to differentiate the combination of the heat pumps and fridges according to the load availability and considering cost saving. The scenarios were undertaken for the provision of 1,000 MW of low-frequency response.

(i)   The first scenario (Sn_1) was carried out when considering low heat pumps availability, where around 1.06 million responsive heat pumps and about 22.86 million fridges were connected to the grid.

(ii)   The second scenario (Sn_2) was carried out when considering more heat pumps availability, where 1.33 million responsive heat pumps and 15.22 million fridges were connected to the grid.

(iii)   In the third scenario (Sn_3), high heat pumps availability was considered, where 1.58 million responsive heat pumps and 7.57 million fridges were integrated into the grid.

The model was then validated through the integration of the whole model with the master dynamic Great Britain power system model which was developed by National Grid. A Dynamic Link Library (DLL) between DIgSILENT PowerFactory and Matlab/Simulink was created. The interface platform enables 10 million heat pump and fridge models developed in Matlab/Simulink to be connected to the master GB power system model for frequency response study.

The impact of the aggregated load was investigated geographically using the master Great Britain power system model. Simulation results showed that the measurement of the grid frequency at the DNO close to the source of disturbance had higher frequency deviation than the other DNOs. The responsive load in all different areas provided immediate response to the frequency change. It has been shown that the dynamic control of aggregated load has the potential to offer considerable frequency response and a significant reduction in governor action of frequency-sensitive generators. Simulation results also showed the absolute rate of change of frequency at the first crucial sub-seconds following the frequency incident (0.4msec, 0.6msec, 0.8msec, 1sec) was halted. The aggregated load control of heat pumps and fridges has reduced the average RoCoF by 85%.

7.1.5 Financial value of the aggregated load control

The financial value of the aggregated load control to provide frequency response, using three scenarios were briefly estimated. It was shown that the benefit for the load aggregator to provide frequency response service of 1,000 MW is around £1.01M/month (~£12.12M/year). The value contribution from each unit was calculated to be around £23.5/year. The calculation ignored the value that could be earned from the reduction of greenhouse emissions due to reduced part-loading.

7.2 Contributions of the work

- **Develop a novel controller for interconnected power system:**

An Adaptive DeadBeat (ADB) controller was developed to investigate its capability to improve the behaviour of the frequency in an interconnected power system model of the north and south zones of Scotland. This interconnected model was developed to conform to the future energy requirements stated by National Grid whereby regional control can be provided in both the north and south of Scotland. In comparison with PI and Fuzzy-PI methods, simulation results showed that ADB method provided a robust frequency response against a wide range of disturbance conditions.

- **Demonstrate the thermodynamic models of heat pumps and fridges:**

A thermodynamic model of a domestic building equipped with a heat pump was developed in *Matlab/ Simulink*. The physical parameters used in the model were calibrated based on temperature measurement from a typical domestic building reported in the literature. A mathematical model representing the thermodynamic behaviour of a domestic fridge was developed using *Matlab/Simulink*. For validation, temperature curves of the cooler and freezer compartments were compared to results reported in the literature.

- **Build new method for the provision of dynamic frequency control:**

A decentralised Dynamic Frequency Control (DFC) algorithm was developed, enabling the heat pumps to alter their power consumption in response to system frequency. The temperature controller was included in the model to control the temperature of a building. The DFC algorithm ensured a low payback that would result from reconnection of substantial load simultaneously. A logic control algorithm prioritised the temperature control action over the frequency controller. For simulation results, the developed model was incorporated into the interconnected model of north and south zones of Scotland to provide regional

frequency response and to smooth the power interchange between the tie-lines. Around 55,795 heat pumps were connected to the north zone, and 89,504 heat pumps were connected to the south zone. The frequency deviation was reduced from 49.5 Hz to 49.12 Hz. The generation power transfer from the north to the south was also reduced by 50%. Furthermore, collaboration with National Grid led to results' validation at geographical level using the GB dynamic reduced power system model. The collaborated work is explained in ''Collaborative Work'' sub-section.

- **Demonstrate the demand- side response aggregation role for the participation in Firm Frequency Response (FFR) service using National Grid's master model of GB power system.**

The availability of heat pumps and fridges during winter and summer days was presented. Based on the availability of load and considering cost saving, the combination of heat pumps and fridges to provide sufficient FFR service was implemented. A dynamic frequency control algorithm coordinated the aggregated response from a population of heat pumps and fridges without undermining the temperature of the buildings and fridges. For simulation results, the whole model was integrated to the GB's master model through a collaboration with National Grid.

- **Collaborative Work:**

Collaborative works with National Grid, the system operator and owner of the majority of GB transmission system, and Element Energy, an energy consultancy in Great Britain, have added significant contribution to this thesis. For example, the link with Element Energy resulted in sharing the data of the availability of heat pumps over the time of day. This data was used as an input to the DFC model to specify the amount of heat pumps that can provide frequency response at each time of the day.

The work with National Grid gave the opportunity to use two types of models:

i. The GB electrodynamic reduced model which is developed for the 2030 Gone Green scenario.

ii. National Grid's master electrodynamic model which represents the 2016 GB power system.

The both models were developed by National Grid in *DIgSILENT Power Factory.* For connecting the aggregated models to the GB power system models, a Dynamic Link Library (DLL) interface between *DIgSILENT PowerFactory* and *Matlab/Simulink* was implemented. The interface platform enables the heat pump and fridge models, developed in *Matlab/Simulink,* to be connected to the GB power system model for simulation studies.

The capability of heat pumps to provide frequency control was achieved by connecting an aggregated model of 1,651,258 heat pumps to the GB zones. Simulation results showed that 1,308,881 heat pumps (with 3kw power rate of each unit) offered 1,000MW of load reduction following a frequency drop to 49Hz.

The aggregation of around 40 million heat pump and fridge models were connected to medium voltage networks (33-kV bus-bar) in each of the 11 distribution network models within the dynamic master model from National Grid. Simulation results showed that the controlled load in all different areas provides immediate response in proportional to grid frequency. The mean RoCoF was reduced by 85%. A reduction of around 30% in governor action of spinning reserve generators was achieved.

The results from a collaborated work with Element Energy and National Grid were published in a prestigious journal such as IEEE Transaction on Power system and disseminated in the Ebbs and Flow of Energy Systems (EFES) project and awarded best conference paper award.

7.3 Publications

The contribution of chapter-3 was published in:

1. **Mazin T. Muhssin**, Liana M. Cipcigan, Zeyad A. Obaid, Wissam F. AL-Ansari, A novel adaptive deadbeat- based control for load frequency control of low inertia system in interconnected zones north and south of Scotland, *In International Journal of Electrical Power & Energy Systems*, Volume 89, 2017, Pages 52-61.

The contribution of chapter-4 and chapter-5 was published in:

2. **M. T. Muhssin**, L. Cipcigan, N. Jenkins, S. Slater, M. Cheng and Z. Obaid, "Dynamic Frequency Response from Controlled Domestic Heat Pumps," published in *IEEE Transactions on Power Systems*, vol. PP, no. 99, pp. 1-11.

3. **M. T. Muhssin**, L. M. Cipcigan, N. Jenkins, C. Meng, and Z. A. Obaid, "Modelling of a population of Heat Pumps as a Source of load in the Great Britain power system," in *2016 International Conference on Smart Systems and Technologies (SST)*, 2016, pp. 109-113.

4. **M. T. Muhssin**, L. M. Cipcigan, N. Jenkins, M. Cheng, and Z. A. Obaid, "Potential of a Population of Domestic Heat Pumps to Provide Balancing Service," *Journal Tehnički vjesnik/Technical Gazette,* vol. 25, pp. 709-717, 2018.

The contribution part of chapter-6 was published in:

5. **M. T. Muhssin**, L. M. Cipcigan, N. Jenkins, C. Meng, and Z. A. Obaid, "Load Aggregation over a Time of Day to Provide Frequency Response in the Great Britain Power System," Accepted in *9th International Conference on Applied Energy (ICAE)*, 2017.

6. **M. T. Muhssin**, L. M. Cipcigan, S. S. Sami and Z. A. Obaid, "Potential of Aggregated Load Control for the Stabilization of the Grid Frequency," *Applied Energy,* vol. 220, pp. 643-656.

7.4 Recommendation for future work

Possible paths for future work are:

- The open loop transfer functions presented in Chapter 3 are changing in time because they depend on the units committed at every point in time. For example, they will vary due to the variable power output of the intermittent generators. As for the rapid increase of renewable energy sources, this phenomenon will become more pronounced. Future work can investigate re-programming the ADB controller in time (at least whenever the open loop transfer functions in each area change significantly).

- In this research, the building model was represented by a lumped thermal parameter model. The DFC presented in Chapter 5 could be implemented on a more complex building model. The heat flow inside the building is expected to be more accurate if a detailed building model (consists of many rooms) is considered.

- Future work could consider applying the frequency control for other types of loads that have longer ON and OFF cycles so that the frequency response service can be sustained longer. Electric vehicles, water heaters, variable speed heat pumps are good examples.

- Fixed speed heat pump was presented in this thesis, i.e. the temperature control used a fix heat flow that relies on thermostats to switch OFF/ON the heat pumps. However, some of the modern heat pumps are inverter driven and variable speed. The heat flow of such heat pumps can be modulated, instead of using ON/OFF control. So far, inverter-driven heat pumps are not widely used domestically, but they might increase as manufacturers look for more ways to save the energy use. The future work at this point should involve the modelling of the additional electrical part to modulate the heat flow of heat pumps directly. In addition, the dynamic frequency control algorithm developed in Chapter 5 should be further adjusted, to control the operation of inverter-driven heat pumps in response to the grid frequency.

- In this thesis, the dynamic load control works in response to an external signal, such as grid frequency signal. Future work could also investigate whether the same load is able to provide more than one service to the grid, such as frequency and voltage control services, with no conflict.

This thesis focuses on dynamic demand to provide frequency response service, from the technical and operational point of view of the overall grid. Research could be carried out to study the economic viability of the DFC and its benefit to the demand aggregator. The benefits of replacing the spinning reserve capacity of conventional generators and the saving cost that will result from reducing carbon emissions need to be addressed in detail.

References

[1]   National Grid. "Future Energy Scenario," July, 2016 [Online]. Available: http://fes.nationalgrid.com/media/1292/2016-fes.pdf

[2]   National Grid. "Future Energy Scenario," July, 2017 [Online]. Available: http://fes.nationalgrid.com/media/1253/final-fes-2017-updated-interactive-pdf-44-amended.pdf

[3]   Element Energy. "Frequency Sensitive Electric Vehicle and Heat Pump Power Consumption", July. 2015

[4]   Smart Energy GB. *Smart meters explained*. Available: https://www.smartenergygb.org/en/about-smart-meters/what-is-a-smart-meter. [Accessed: 15-Jan-2018]

[5]   Ofgem. "National electricity transmission system security and quality of supply standard (NETS SQSS): Review of infeed losses," September, 2017 [Online]. Available: https://www.ofgem.gov.uk/ofgem-publications/52793/gsr007-decision-letter-final.pdf

[6]   National Grid. "Enhanced Frequency Control Capability (EFCC)," Oct. 2014 [Online]. Available: https://www.ofgem.gov.uk/ofgem-publications/87210/ispefccnget.pdf

[7]   National Grid. Electricity Ten Year Statement. Nov. 2016, [Online]. Available: https://www.nationalgrid.com/sites/default/files/documents/8589937801-ETYS%202016.pdf

[8]   National Grid. *"Frequency response, National Grid", 2015*. Available: http://www2.nationalgrid.com/uk/services/balancing-services/frequency-response/. [Accessed: 01-Oct-2016]

[9]   National Grid. *Mandatory frequency response (MFR)*. Available: https://www.nationalgrid.com/uk/electricity/balancing-services/frequency-response-services/mandatory-response-services?overvie. [Accessed: 01-Jan-2018]

[10]   National Grid. (2016). *Firm Frequency Response (FFR)*. Available: http://www2.nationalgrid.com/UK/Services/Balancing-services/Frequency-response/Firm-Frequency-Response/. [Accessed: 01-Jan-2016]

[11]   National Grid. Demand Side Flexibility Annual Report 2017. Feb 2018, [Online]. Available: http://powerresponsive.com/wp-content/uploads/2018/02/Power-Responsive-Annual-Report-2017.pdf

[12]   D. Natusch. Intelligent Networks & Infrastructure Opportunities. 2013, [Online]. Available: http://www.seclimited.co.uk/wp-content/uploads/2013/03/Inteligent-Networks-and-Infrastructure-Opportunities.pdf.

[13]   H. Bevrani, *Robust power system frequency control*. New York: Springer, 2014.

[14]   H. Bevrani and T. Hiyama, *Intelligent Automatic Generation Control*. New York: DRC Press, Taylor and Francis Group, 2011.

[15]   F. Teng, M. Aunedi, D. Pudjianto, and G. Strbac, "Benefits of Demand-Side Response in Providing Frequency Response Service in the Future GB Power System," *Frontiers in Energy Research,* vol. 3, 2015.

[16]   B. M. Weedy and B. J. Cory, *Electric Power Systems*. New York: John Wiley & Sons Ltd, 1998.

[17]   J. Glover, M. Sarma, and T. Overbye, *Power System Analysis and Design*. Australia: Thomson, 2008.

[18]   P. M. Anderson and A. A. Fouad, *Power System Control and Stability*. New York: Institute of Electrical and Electronics 1994.

[19]   P. Kundur, N. Balu, and M. Lauby, *"Power system stability and control"*. New York: McGraw-Hill, 1994.

[20]   A. Wood, B. Wollenberg, and G. Wollenberg, *Power Generation, Operation, and Control*. New Jersy: Wiley, 2014.

[21]   National Grid plc. (2015). *The Grid Code Issue 5 Revision 14*. Available: http://www2.nationalgrid.com/uk/industry-information/electricity-codes/grid-code/the-grid-code/.

[22]   National Grid. Guidance Notes- Synchronous Generating Units. Sep 2012, [Online].   Available: https://www.nationalgrid.com/sites/default/files/documents/5627-Guidance%20Notes%20–%20Synchronous%20Generating%20Units.pdf

[23]   National Grid. System Operability Framework 2014. Sep 2014 [Online]. Available: http://fes.nationalgrid.com/media/1298/2014-fes.pdf.

[24]   J. B. Ekanayake and N. Jenkins, "''Frequency Response from Wind Turbines"," *Wind Engineering,* vol. 32, no. 6, pp. 573-586, 2008.

[25]   P. M. Ashton, C. S. Saunders, G. A. Taylor, A. M. Carter, and M. E. Bradley, "Inertia Estimation of the GB Power System Using Synchrophasor Measurements," *IEEE Transactions on Power Systems,* vol. 30, pp. 701-709, 2015.

[26]   A. Johnson. Grid Code Frequency Response Working Group System Inertia. [Online].   Available: https://www.nationalgrid.com/sites/default/files/documents/16890-Meeting%208%20-%20Inertia%20presentation.pdf

[27]   National Grid. *"Enhanced Frequency Control Capability (EFCC)," Oct. 2014   [Online]*.   Available: https://www.ofgem.gov.uk/ofgem-publications/87210/ispefccnget.pdf

[28]   D. Spillett and R. Jenkins. Frequency Changes during Large Disturbances and their Impact on the Total System. Aug 2013, [Online]. Available: https://www.nationalgrid.com/sites/default/files/documents/16943-Industry%20Consultation.pdf

[29]   Electrical   installation   &   energy   efficiency   Electrical   engineering Community.   (2013).   *Automatic   Generation   Control*   Available: http://engineering.electrical-equipment.org/power-quality/automatic-generation-control-agc.html. [Accessed: 10-Jan-2017]

[30]   C. Concordia and L. K. Kirchmayer, "Tie-Line Power and Frequency Control of Electric Power Systems [includes discussion]," *Transactions of the American Institute of Electrical Engineers. Part III: Power Apparatus and Systems,* vol. 72, p. 1, 1953.

[31]   N. Cohn, "Some Aspects of Tie-Line Bias Control on Interconnected Power Systems [includes discussion]," *Transactions of the American Institute of Electrical Engineers. Part III: Power Apparatus and Systems,* vol. 75, p. 1, 1956.

[32]   L. K. Kirchmayar, *Economic control of interconnected systems*. New York: Wiley, 1959.

[33]   R. B. Patel, C. Li, X. Yu, and B. McGrath, "Optimal Automatic Generation Control of an Interconnected Power System under Network Constraints," *IEEE Transactions on Industrial Electronics,* vol. PP, pp. 1-1, 2018.

[34]   P. Bhatt, S. P. Ghoshal, and R. Roy, "Load frequency stabilization by coordinated control of Thyristor Controlled Phase Shifters and superconducting magnetic energy storage for three types of interconnected two-area power systems," *International Journal of Electrical Power & Energy Systems,* vol. 32, pp. 1111-1124, 2010.

[35]   U. K. Rout, R. K. Sahu, and S. Panda, "Design and analysis of differential evolution algorithm based automatic generation control for interconnected power system," *Ain Shams Engineering Journal,* vol. 4, pp. 409-421, 2013.

[36]   S. Panda and N. K. Yegireddy, "Automatic generation control of multi-area power system using multi-objective non-dominated sorting genetic algorithm-II," *International Journal of Electrical Power & Energy Systems,* vol. 53, pp. 54-63, 2013.

[37]   L. C. Saikia, J. Nanda, and S. Mishra, "Performance comparison of several classical controllers in AGC for multi-area interconnected thermal system," *International Journal of Electrical Power & Energy Systems,* vol. 33, pp. 394-401, 2011.

[38]   S. A. Taher, M. Hajiakbari Fini, and S. Falahati Aliabadi, "Fractional order PID controller design for LFC in electric power systems using imperialist competitive algorithm," *Ain Shams Engineering Journal,* vol. 5, pp. 121-135, 2014.

[39]   P. Dhanalakshmi and K. Mahadevan, "Assessment of Optimal PID Tuning Controllers for Load Frequency Control," *Wseas Transactions on Power Systems.,* vol. 10, pp. 116-122, 2015.

[40]   Y. Hain, R. Kulessky, and G. Nudelman, "Identification-based power unit model for load-frequency control purposes," *IEEE Transactions on Power Systems,* vol. 15, pp. 1313-1321, 2000.

[41]   R. K. Sahu, T. S. Gorripotu, and S. Panda, "Automatic generation control of multi-area power systems with diverse energy sources using Teaching Learning Based Optimization algorithm," *Engineering Science and Technology, an International Journal,* vol. 19, pp. 113-134, 2016.

[42]   J. Talaq and F. Al-Basri, "Adaptive fuzzy gain scheduling for load frequency control," *IEEE Transactions on Power Systems,* vol. 14, pp. 145-150, 1999.

[43]   C. S. Rao, S. S. Nagaraju, and P. S. Raju, "Automatic generation control of TCPS based hydrothermal system under open market scenario: A fuzzy logic approach," *International Journal of Electrical Power & Energy Systems,* vol. 31, pp. 315-322, 2009.

[44]   J. Nanda and A. Mangla, "Automatic generation control of an interconnected hydro-thermal system using conventional integral and fuzzy logic controller," in *2004 IEEE International Conference on Electric Utility Deregulation, Restructuring and Power Technologies. Proceedings*, 2004, pp. 372-377 Vol.1.

[45]   H. A. Yousef, K. A.-. Kharusi, M. H. Albadi, and N. Hosseinzadeh, "Load Frequency Control of a Multi-Area Power System: An Adaptive Fuzzy Logic Approach," *IEEE Transactions on Power Systems,* vol. 29, pp. 1822-1830, 2014.

[46]   E. Yeşil, M. Güzelkaya, and İ. Eksin, "Self tuning fuzzy PID type load and frequency controller," *Energy Conversion and Management,* vol. 45, pp. 377-390, 2004.

[47]   H. Ebrahimian, H. Manafi, V. Babazadeh, and M. Salavati, "Multi-stage Fuzzy PID Load Frequency Control by Modified Shuffled Frog Leaping," *GMP Review,* vol. 18, pp. 255-260, 2015.

[48]   N. J. Vinoth Kumar and M. M. Thameem Ansari, "A new design of dual mode Type-II fuzzy logic load frequency controller for interconnected power systems with parallel AC–DC tie-lines and capacitor energy storage unit," *International Journal of Electrical Power & Energy Systems,* vol. 82, pp. 579-598, 2016.

[49]   Y. Arya and N. Kumar, "Fuzzy Gain Scheduling Controllers for Automatic Generation Control of Two-area Interconnected Electrical Power Systems," *Electric Power Components and Systems,* vol. 44, pp. 737-751, 2016.

[50]   H. Bevrani, F. Habibi, P. Babahajyani, M. Watanabe, and Y. Mitani, "Intelligent Frequency Control in an AC Microgrid: Online PSO-Based Fuzzy Tuning Approach," *IEEE Transactions on Smart Grid,* vol. 3, pp. 1935-1944, 2012.

[51]   N. Chuang, "Robust H∞ load frequency control in interconnected power systems," *IET Control Theory & Applications,* vol. 10, pp. 67-75, 2016.

[52]   R. Dey, S. Ghosh, G. Ray, and A. Rakshit, "H∞ load frequency control of interconnected power systems with communication delays," *International Journal of Electrical Power & Energy Systems,* vol. 42, pp. 672-684, 2012.

[53]   S. Saha, S. Das, S. Das, and A. Gupta, "A conformal mapping based fractional order approach for sub-optimal tuning of PID controllers with guaranteed dominant pole placement," *Communications in Nonlinear Science and Numerical Simulation,* vol. 17, pp. 3628-3642, 2012.

[54]   F. d. C. da Silva Júnior and A. D. de Araújo, "A Variable Structure Adaptive Pole Placement Control Applied to the Speed Control of a Three Phase Induction Motor," *IFAC Proceedings Volumes,* vol. 40, pp. 1052-1057, 2007.

[55]   M. A. Furini, A. L. S. Pereira, and P. B. Araujo, "Pole placement by coordinated tuning of Power System Stabilizers and FACTS-POD

stabilizers," *International Journal of Electrical Power & Energy Systems,* vol. 33, pp. 615-622, 2011.

[56] Y. Tang, Y. Bai, C. Huang, and B. Du, "Linear active disturbance rejection-based load frequency control concerning high penetration of wind energy," *Energy Conversion and Management,* vol. 95, pp. 259-271, 2015.

[57] H. Badihi, Y. Zhang, and H. Hong, "Design of a Pole Placement Active Power Control System for Supporting Grid Frequency Regulation and Fault Tolerance in Wind Farms," *IFAC Proceedings Volumes,* vol. 47, pp. 4328-4333, 2014.

[58] I. Ahmed. Implementation of PID and deadbeat controllers with the TMS320 Family.   1997,   [Online].   Available: http://www.ti.com/lit/an/spra083/spra083.pdf

[59] A. M. Bouzid, J. M. Guerrero, A. Cheriti, M. Bouhamida, P. Sicard, and M. Benghanem, "A survey on control of electric power distributed generation systems for microgrid applications," *Renewable and Sustainable Energy Reviews,* vol. 44, pp. 751-766, 2015.

[60] T. Rybicki and P. Ostalczyk, "Variable- Fractional Order Dead-Beat Control of An Electromagnetic Servo-Part I," *IFAC Proceedings Volumes,* vol. 39, pp. 95-100, 2006.

[61] Element Energy. Demand side response in the non-domestic sector. July 2012, [Online]. Available: http://www.element-energy.co.uk/wordpress/wp-content/uploads/2012/07/Demand-Side-Response-in-the-non-domestic-sector.pdf

[62] Electricity Demand-Side Response. *"The Parliamentray Office of Science and   Technology   London,"Jan.   2014*.   Available: http://researchbriefings.parliament.uk/ResearchBriefing/Summary/POST-PN-452#fullreport

[63] Energy UK. Ancillary services report 2017. April 2017, [Online]. Available: https://www.energy-uk.org.uk/publication.html?task=file.download&id=6138

[64] Sustainable Energy Regulation. Demand-side management. [Online]. Available: http://africa-toolkit.reeep.org/modules/Module14.pdf

[65] J. Hong, "The Development, Implementation, and Application of Demand Side Management and control (DSM+c) Algorithm for Integrating Microgeneration System within Built Environment," Ph.D. thesis, Department of Mechanical Engineering, University of Strathclyde, 2009.

[66] G. Strbac, "Demand side management: Benefits and challenges," *Energy Policy,* vol. 36, pp. 4419-4426, 2008.

[67] Element Energy, "Frequency Sensitive Electric Vehicle and Heat Pump Power Consumption," Element Energy. July 2015.

[68] J. A. Short, D. G. Infield, and L. L. Freris, "Stabilization of Grid Frequency Through Dynamic Demand Control," *IEEE Transactions on Power Systems,* vol. 22, pp. 1284-1293, 2007.

[69] M. Aunedi, P. A. Kountouriotis, J. E. O. Calderon, D. Angeli, and G. Strbac, "Economic and Environmental Benefits of Dynamic Demand in Providing

Frequency Regulation," *IEEE Transactions on Smart Grid,* vol. 4, pp. 2036-2048, 2013.

[70]   P. Bradley, M. Leach, and J. Torriti. A review of current and future costs and benefits of demand response for electricity. Nov. 2011, [Online]. Available: https://www.surrey.ac.uk/ces/files/pdf/1011_WP_Bradley_et_al_DemandResponse_3.pdf

[71]   L. Jia and L. Tong, "Dynamic Pricing and Distributed Energy Management for Demand Response," *IEEE Transactions on Smart Grid,* vol. 7, pp. 1128-1136, 2016.

[72]   N. O′Connell, P. Pinson, H. Madsen, and M. O′Malley, "Benefits and challenges of electrical demand response: A critical review," *Renewable and Sustainable Energy Reviews,* vol. 39, pp. 686-699, 2014.

[73]   UK Power Networks. Industrial and Commercial Demand Response for outage management and as an alternative to network reinforcement. Sep. 2014, [Online]. Available: http://innovation.ukpowernetworks.co.uk/innovation/en/Projects/tier-2-projects/Low-Carbon-London-(LCL)/Project-Documents/LCL%20Learning%20Report%20-%20A4%20-%20Industrial%20and%20Commercial%20Demand%20Side%20Response%20for%20outage%20management%20and%20as%20an%20alternative%20to%20network%20reinforcement.pdf

[74]   DECC, "Table 3.03: Average domestic gas and electricity consumption, UK, 2008 to 2015 " Energy Consumption in the UK (ECUK)2016.

[75]   DECC, "Table 1.10: Final Energy Consumption by Fuel, by sector, in primary energy equivalents: 1970 to 2015," Energy Consumption in the UK (ECUK), 2016.

[76]   DECC, "Table 3.08: Total electricity consumption by household domestic appliances: 1970 to 2015," Energy Consumption in the UK (ECUK), 2016.

[77]   Frontier Economics. Future potential for DSR in GB. Oct. 2015, [Online]. Available: https://www.gov.uk/government/uploads/system/uploads/attachment_data/file/467024/rpt-frontier-DECC_DSR_phase_2_report-rev3-PDF-021015.pdf

[78]   B. Drysdale, J. Wu, and N. Jenkins, "Flexible demand in the GB domestic electricity sector in 2030," *Applied Energy,* vol. 139, pp. 281-290, 2015.

[79]   Open Energi. *Demand Response Market Overview, Glossary of Demand Response Services*. Available: http://www.openenergi.com/wp-content/uploads/2015/10/Demand-Response-Glossary-V7-.pdf. [Accessed: 01-Oct-2016]

[80]   S. P. Borg, N. J. Kelly, A. Markopoulos, P. A. Strachan, C.Porteous, and T.Sharpe, "Communal residential laundry washing and drying - can it provide demand-side electrical load flexibility?," presented at the 2nd International conference in microgeneration and related technologies, Glasgow, 2011.

[81]   Z. Akhtar, B. Chaudhuri, and S. Y. R. Hui, "Primary Frequency Control Contribution From Smart Loads Using Reactive Compensation," *IEEE Transactions on Smart Grid,* vol. 6, pp. 2356-2365, 2015.

[82] M. R. V. Moghadam, R. T. B. Ma, and R. Zhang, "Distributed Frequency Control in Smart Grids via Randomized Demand Response," *IEEE Transactions on Smart Grid,* vol. 5, pp. 2798-2809, 2014.

[83] L. Chun-Feng, L. Chun-Chang, and W. Chi-Jui, "Effect of battery energy storage system on load frequency control considering governor deadband and generation rate constraint," *IEEE Transactions on Energy Conversion,* vol. 10, pp. 555-561, 1995.

[84] M. Avendano-Mora and E. H. Camm, "Financial assessment of battery energy storage systems for frequency regulation service," in *2015 IEEE Power & Energy Society General Meeting*, 2015, pp. 1-5.

[85] P. M. R. Almeida, J. A. P. Lopes, F. J. Soares, and L. Seca, "Electric vehicles participating in frequency control: Operating islanded systems with large penetration of renewable power sources," in *2011 IEEE Trondheim PowerTech*, 2011, pp. 1-6.

[86] S. Izadkhast, P. Garcia-Gonzalez, P. Frías, and P. Bauer, "Design of Plug-In Electric Vehicle's Frequency-Droop Controller for Primary Frequency Control and Performance Assessment," *IEEE Transactions on Power Systems,* vol. 32, pp. 4241-4254, 2017.

[87] P. M. R. Almeida, F. J. Soares, and J. A. P. Lopes, "Electric vehicles contribution for frequency control with inertial emulation," *Electric Power Systems Research,* vol. 127, pp. 141-150, 2015.

[88] J. Meng, Y. Mu, H. Jia, J. Wu, X. Yu, and B. Qu, "Dynamic frequency response from electric vehicles considering travelling behavior in the Great Britain power system," *Applied Energy,* vol. 162, pp. 966-979, 2016.

[89] Y. Mu, J. Wu, J. Ekanayake, N. Jenkins, and H. Jia, "Primary Frequency Response From Electric Vehicles in the Great Britain Power System," *IEEE Transactions on Smart Grid,* vol. 4, pp. 1142-1150, 2013.

[90] V. Trovato, F. Teng, and G. Strbac, "Role and Benefits of Flexible Thermostatically Controlled Loads in Future Low-Carbon Systems," *IEEE Transactions on Smart Grid,* vol. PP, pp. 1-1, 2017.

[91] Z. A. Obaid, L. M. Cipcigan, M. T. Muhssin, and S. S. Sami, "Development of a water heater population control for the demand-side frequency control," in *2017 IEEE PES Innovative Smart Grid Technologies Conference Europe (ISGT-Europe)*, 2017, pp. 1-6.

[92] M. Cheng, J. Wu, S. J. Galsworthy, C. E. Ugalde-Loo, N. Gargov, W. W. Hung*, et al.*, "Power System Frequency Response From the Control of Bitumen Tanks," *IEEE Transactions on Power Systems,* vol. 31, pp. 1769-1778, 2016.

[93] M. Al Essa, "Demand Response Design of Domestic Heat Pumps," *Designs,* vol. 2, p. 1, 2018.

[94] S. A. Pourmousavi and M. H. Nehrir, "Real-Time Central Demand Response for Primary Frequency Regulation in Microgrids," *IEEE Transactions on Smart Grid,* vol. 3, pp. 1988-1996, 2012.

[95] J. Kondoh, "A direct load management scheme to control appliances and EVs while considering end users comfort," presented at the Proc. Of Grid-Interop 2009, Deven, CO, USA, Nov. 2009.

[96] J. Kondoh, N. Lu, and D. J. Hammerstrom, "An Evaluation of the Water Heater Load Potential for Providing Regulation Service," *IEEE Transactions on Power Systems,* vol. 26, pp. 1309-1316, 2011.

[97] N. Lu, "An Evaluation of the HVAC Load Potential for Providing Load Balancing Service," *IEEE Transactions on Smart Grid,* vol. 3, pp. 1263-1270, 2012.

[98] S. Koch, M. Zima, and G. Andersson, "Active coordination of thermal household appliances for load management purpose," presented at the IFAC Symposium on Power Plants and Power Systems Control, Finland, July 2009.

[99] B. Biegel, L. H. Hansen, P. Andersen, and J. Stoustrup, "Primary Control by ON/OFF Demand-Side Devices," *IEEE Transactions on Smart Grid,* vol. 4, pp. 2061-2071, 2013.

[100] D. Wang, S. Ge, H. Jia, C. Wang, Y. Zhou, N. Lu*, et al.*, "A Demand Response and Battery Storage Coordination Algorithm for Providing Microgrid Tie-Line Smoothing Services," *IEEE Transactions on Sustainable Energy,* vol. 5, pp. 476-486, 2014.

[101] L. Zhou, Y. Li, B. Wang, Z. Wang, and X. Hu, "Provision of Supplementary Load Frequency Control via Aggregation of Air Conditioning Loads," *Energies,* vol. 8, p. 12417, 2015.

[102] A. Molina-Garcia, F. Bouffard, and D. S. Kirschen, "Decentralized Demand-Side Contribution to Primary Frequency Control," *IEEE Transactions on Power Systems,* vol. 26, pp. 411-419, 2011.

[103] Z. Xu, J. Ostergaard, M. Togeby, and C. Marcus-Moller, "Design and Modelling of Thermostatically Controlled Loads as Frequency Controlled Reserve," in *2007 IEEE Power Engineering Society General Meeting*, 2007, pp. 1-6.

[104] V. Trovato, I. M. Sanz, B. Chaudhuri, and G. Strbac, "Advanced Control of Thermostatic Loads for Rapid Frequency Response in Great Britain," *IEEE Transactions on Power Systems,* vol. 32, pp. 2106-2117, 2017.

[105] Z. Xu, J. Ostergaard, and M. Togeby, "Demand as Frequency Controlled Reserve," *IEEE Transactions on Power Systems,* vol. 26, pp. 1062-1071, 2011.

[106] M. Cheng, S. S. Sami, and J. Wu, "Benefits of using virtual energy storage system for power system frequency response," *Applied Energy,* vol. 194, pp. 376-385, 2017.

[107] M. Cheng, J. Wu, S. J. Galsworthy, N. Gargov, W. H. Hung, and Y. Zhou, "Performance of industrial melting pots in the provision of dynamic frequency response in the Great Britain power system," *Applied Energy,* vol. 201, pp. 245-256, 2017.

[108] M. Wang-Hansen, R. Josefsson, and H. Mehmedovic, "Frequency Controlling Wind Power Modeling of Control Strategies," *IEEE Transactions on Sustainable Energy,* vol. 4, pp. 954-959, 2013.

[109] National Grid. Future Energy Scenarios. July. 2015, [Online]. Available: http://fes.nationalgrid.com/media/1295/2015-fes.pdf

[110] National Grid. Electricity Ten Year Statement 2016. Nov. 2016, [Online]. Available: https://www.nationalgrid.com/sites/default/files/documents/8589937801-ETYS%202016.pdf

[111] I. Ahmed. Implementation of PID and Deadbeat Controllers with the TMS320 Family. 1997, [Online]. Available: http://www.ti.com/lit/an/spra083/spra083.pdf

[112] National Grid, "The Grid Code Issue 5 Revision 18," National Grid2016.

[113] I. Iancu, "A Mamdani Type Fuzzy Logic Controller, Fuzzy Logic - Controls, Concepts, Theories and Applications," ed: Elmer P. Dadios, 2012.

[114] R. Dorf and R. Bishop, *Modern Control Systems*. New Jersey: Pearson Education, 2008.

[115] R. K. Mudi and N. R. Pal, "A robust self-tuning scheme for PI- and PD-type fuzzy controllers," *IEEE Transactions on Fuzzy Systems,* vol. 7, pp. 2-16, 1999.

[116] Y. d. Valle, G. K. Venayagamoorthy, S. Mohagheghi, J. C. Hernandez, and R. G. Harley, "Particle Swarm Optimization: Basic Concepts, Variants and Applications in Power Systems," *IEEE Transactions on Evolutionary Computation,* vol. 12, pp. 171-195, 2008.

[117] H. Garg, "Reliability, Availability and Maintainability Analysis of Industrial Systems Using PSO and Fuzzy Methodology," *MAPAN,* vol. 29, pp. 115-129, 2014.

[118] National Grid. "System Operability Framework 2015," Nov. 2015 [Online]. Available: https://www.nationalgrid.com/sites/default/files/documents/44046-SOF%202015%20Full%20Document.pdf

[119] Greenfields. *Air Source heat pump overview*. Available: http://greenfieldspenrith.com/renewable-energy-cumbria/air-source-commercial-heat-pump-installers/. [Accessed: 15-July-2017]

[120] Z. Taylor, K. Gowri, and S. Katipamula. GridLAB-D Technical Support Document: Residential End-Use Module Version 1.0, July. 2008 [Online]. Available: http://www.pnl.gov/main/publications/external/technical_reports/PNNL-17694.pdf

[121] Y. A. Cengel, *Heat Transfer: A Practical Approach.* New York: McGraw Hill Higher Education, 2003.

[122] N. Lu, J. Zhang, P. Du, and Y. V. Makarov, "Controller for thermostatically controlled loads.," United States. Patent, 2013.

[123] J. Hong, N. J. Kelly, I. Richardson, and M. Thomson, "Assessing heat pumps as flexible load," *Proceedings of the Institution of Mechanical Engineers, Part A: Journal of Power and Energy,* vol. 227, pp. 30-42, 2012.

[124] V. Dimitriou, "Lumped Parameter thermal modelling for UK domestic buildings based on measured operational data," Ph.D. thesis, Loughborough University, 2016.

[125] M. Cheng, "Dynamic Demand for Frequency Response Services in the Great Britain Power System," Ph.D. thesis, Institute of Energy, Cardiff Universiy, Cardiff, UK, 2014.

[126] National Grid. "Future Energy Scenarios, Table: PD25: Electricity: Cold appliances" July. 2016 [Online]. Available: http://fes.nationalgrid.com/fes-document/

[127] A. Information. *Appliance 441 Information: Frequently Asked Question*. Available: http://www.appliance411.com/faq/defrostproblem.shtml. [Accessed: 10-July-2017]

[128] National Grid plc. "The Grid Code Issue 5 Revision 18," Aug. 2016 [Online]. Available: http://www2.nationalgrid.com/uk/industry-information/electricity-codes/grid-code/the-grid-code/

[129] The Parliamentary Office of Science and Technology. (2014, Electricity Demand-Side Response. January, 2014. [Online]. Available: http://researchbriefings.parliament.uk/ResearchBriefing/Summary/POST-PN-452

[130] National Grid plc. *"Frequency Control by Demand Management,"*. Available: http://www2.nationalgrid.com/uk/services/balancing-services/frequency-response/frequency-control-by-demand-management/. [Accessed:01-May-2016]

[131] National Grid. *Firm Frequency Response (FFR)* Available: https://www.nationalgrid.com/sites/default/files/documents/Firm%20Frequency%20Response%20%28FFR%29%20Interactive%20Guidance%20v1%200_0.pdf. [Accessed:10-Jan-2018]

[132] R. Green. "The Effects of Cycling on Heat Pump Performance," Department of Energy and Climate Change (DECC), Nov. 2012 [Online]. Available: https://www.gov.uk/government/uploads/system/uploads/attachment_data/file/65695/7389-effects-cycling-heat-pump-performance.pdf

[133] DCLG, "Table 401: Household projections," Department for Communities and Local Government. 2016.

[134] NRS, "Table1: Household estimates for Scotland by council area. ," National Records of Scotland. 2016.

[135] National Grid. *Distribution Network Operator (DNO) Companies*. Available: http://www2.nationalgrid.com/UK/Our-company/Electricity/Distribution-Network-Operator-Companies/. [Accessed:09-March-2017]

[136] National Grid. Report of the National Grid Investigation into the Frequency Deviation and Automatic Demand Disconnection that occurred on the 27th May 2008," Feb. 2009 [Online]. Available: http://www.nationalgrid.com/NR/rdonlyres/E19B4740-C056-4795-A567-91725ECF799B/32165/PublicFrequencyDeviationReport.pdf

[137] National Grid, "Frequency changes during large disturbances and their Impact on the Total System," National Grid. Aug. 2013.

[138] M. Chang, "Dynamic Demand for Frequency Response Services in the Great Britain Power System," Ph.D. thesis, Institute of Energy, Cardiff Universiy, Cardiff, UK, 2014.

[139] Element Energy. "Frequency Sensitive Electric Vehicle and Heat Pump Power Consumption", July. 2015 [Online].

[140] Department for Business and Energy and Industrial Strategy. Energy Consumption in the UK. Nov 2016, [Online]. Available: https://www.gov.uk/government/uploads/system/uploads/attachment_data/file/573269/ECUK_November_2016.pdf

[141] Open Energi. *Demand Response Market Overview, Glossary of Demand Response Services.* . Available: http://www.openenergi.com/wp-content/uploads/2015/10/Demand-Response-Glossary-V7-.pdf. [Accessed: 01-Oct-2016]

[142] J. B. Ekanayake and N. Jenkins, "Frequency Response from Wind Turbines," *Wind Engineering,* vol. 32, no. 6, pp. 573-586, 2008.

[143] National Grid. Frequency Changes during Large Disturbances and their Impact on the Total System. Aug. 2013 [Online] Available: https://www.nationalgrid.com/sites/default/files/documents/16943-Industry%20Consultation.pdf

[144] National Grid, "Firm Frequency Response Market Information, monthly report," National Grid. Feb. 2014.

[145] National Grid plc. "Electricity Ten Year Statement 2014-Figure A1.3: GB Existing Transmission System, Nov. 2014," [Online]. Available: https://www.nationalgrid.com/sites/default/files/documents/37787-ETYS%202014%20Appendix%20A1.3%20to%20A1.6%20-%20GB%20Existing%20Transmission%20System%20-%20Schematic.pdf

Appendix A

This appendix demonstrates the data of the generation capacity distributed over Scotland boundary and zones.

Table 8.1 Upper north SHE transmission boundary (B0)

Station	Owner / Developer	Fuel Type	2015	2020	2030
Shin	SSE Ltd	Hydro	18	18	18
Cantick Head	SSE Renewables	Marine	0	95	160
Costa Head, Westray South and Brough Head	SSE Ltd	Marine	0	30	300
Duncansby	Scottish Power Ltd	Marine	0	95	95
Marwick Head	Scottish Power Ltd	Marine	0	49	49
Meygen	MeyGen Ltd	Marine	0	154	237
Bad a Cheo Wind Farm	RWE Npower Ltd	Onshore Wind	0	30	30
Baillie and Bardnaheigh	Baillie Wind Farm Ltd	Onshore Wind	52	52	52
Beinn Tharsuinn	Scottish Power Ltd	Onshore Wind	29	29	29
Boulfruich	Boulfruich Wind Farm Ltd	Onshore Wind	14	14	14
Burn of Whilk	Scottish Power Ltd	Onshore Wind	22	22	22
Camster	E.On	Onshore Wind	50	50	50
Causeymire	Causeymire Wind Farm Limited	Onshore Wind	48	48	48
Coire Na Cloiche	RockbySea Ltd	Onshore Wind	0	30	30
Dalnessie	SSE Ltd	Onshore Wind	0	81	81
Glencassley	Scottish Power Ltd	Onshore Wind	0	65	65
Glenmorie	Wind Energy Ltd	Onshore Wind	0	114	114
Gordonbush	SSE Ltd	Onshore Wind	70	70	70
Gordonbush Wind Farm Extension	SSE Ltd	Onshore Wind	0	38	38
Halsary	Scottish Power Ltd	Onshore Wind	28.5	28.5	28.5
Kilbruar		Onshore Wind	67	67	67
Lairg - Achany	SSE Ltd	Onshore Wind	38	40.5	40.5
Limekilns	Infinergy Ltd	Onshore Wind	0	90	90
Novar	RWE Npower Ltd	Onshore Wind	18	18	18
Novar 2	Novar 2 Wind Farm Ltd	Onshore Wind	32	32	32
Rosehall	E.ON UK plc	Onshore Wind	25	25	25
Sallachy	WKN Ltd	Onshore Wind	0	66	66
Spittal Hill	Spittal Hill Wind Farm Ltd	Onshore Wind	0	21	21
Strathy North & South	SSE Ltd	Onshore Wind	76	226	226
Strathy Wood	E.ON UK plc	Onshore Wind	0	84	84
Stroupster	Stroupster Wind Farm Ltd	Onshore Wind	32	32	32
Wathegar 2	Scottish Power Ltd	Onshore Wind	0	22	22

Table 8.2 North west SHE transmission boundary (B1)

Station	Owner	Fuel Type	2015	2020	2030
Stoneywood Mills	Stoneywood	Gas	12	12	12
Aigas	SSE Ltd	Hydro	20	20	20
Ceannacroc	SSE Ltd	Hydro	20	20	20
Culligran	SSE Ltd	Hydro	19	19	19
Deanie	SSE Ltd	Hydro	38	38	38
Fasnakyle	SSE Ltd	Hydro	77	77	77
Glendoe	SSE Ltd	Hydro	100	100	100
Glenmoriston	SSE Ltd	Hydro	6	6	6
Glenmoriston	SSE Ltd	Hydro	36	36	36
Grudie Bridge	SSE Ltd	Hydro	22	22	22
Invergarry	SSE Ltd	Hydro	20	20	20
Kilmorack	SSE Ltd	Hydro	20	20	20
Kinlochleven	Alcan Aluminium	Hydro	20	20	20
Livishie	SSE Ltd	Hydro	15	15	15
Luichart	SSE Ltd	Hydro	34	34	34
Mossford	SSE Ltd	Hydro	19	19	19
Orrin	SSE Ltd	Hydro	18	18	18
Quoich	SSE Ltd	Hydro	18	18	18
Torr Achilty		Hydro	15	15	15
Lag Na Greine	Lewis Wind Power	Marine	0	20	40
Allt Duine	RWE Npower Ltd	Onshore Wind	0	87	87
Aultmore	Vattenfall Ltd	Onshore Wind	0	30	30
Beinneun Wind Farm	Blue Energy	Onshore Wind	0	109	109
Ben Aketil	Ben Aketil Wind	Onshore Wind	28	28	28
Berry Burn	Statkraft	Onshore Wind	67	67	67
Bhlaraidh Wind Farm	SSE Ltd	Onshore Wind	0	0	108
Boyndie	Boyndie Wind	Onshore Wind	21	21	21
Cairn Uish	Rothes Wind Ltd	Onshore Wind	51	51	51
Cairn Uish 2	Rothes Wind Ltd	Onshore Wind	41	41	41
Corriegarth	North British Windpower Ltd	Onshore Wind	70	70	70
Corriemollie	E.ON UK plc	Onshore Wind	0	48	48
Druim Lethann		Onshore Wind	0	39	39
Dummuies	Dummuies Wind	Onshore Wind	12	12	12
Dunmaglass	SSE Ltd	Onshore Wind	94	94	94
Edinbane	Vattenfall Ltd	Onshore Wind	41	41	41
Edintore Wind Farm	Scottish Hydro Distribution plc	Onshore Wind	0	21	21
Eishken	International Power	Onshore Wind	0	133	133
Fairburn Wind		Onshore Wind	40	40	40
Farr	Farr Wind Farm	Onshore Wind	92	92	92
Glen Kyllachy	RWE Npower	Onshore Wind	0	48.5	48.5
Glen Ullinish	Kilmac Energy	Onshore Wind	0	0	42
Glens of Foudland	Glens of Foudland Wind Farm Ltd	Onshore Wind	26	26	26
Hill of Towie	Hill of Towie Ltd	Onshore Wind	48	48	48

179

Lochluichart	LZN Ltd	Onshore Wind	69	69	69
Millennium	Falck Renewables	Onshore Wind	65	65	65
Millennium South	Falck Renewables Wind Ltd	Onshore Wind	0	25	50
Muaithebheal	Uisenis Power Ltd	Onshore Wind	0	150	150
Paul's Hill	Pauls Hill Wind Ltd	Onshore Wind	70	70	70
Pentland Road	Pentland Road Windfarm Ltd	Onshore Wind	13.8	18	18
Stornoway Wind Stage 1	Lewis Wind Power Ltd	Onshore Wind	0	39	39
Stornoway Wind Stage 2	Lewis Wind Power Ltd	Onshore Wind	0	0	91
Stronelairg	SSE Ltd	Onshore Wind	0	241.2	241.2
Tom Nan Clach	Infinergy Ltd	Onshore Wind	0	75	75
Tomatin	Eurus Energy UK Ltd	Onshore Wind	30	30	30
Viking	Viking Energy Ltd	Onshore Wind	0	412	412
Coire Glas	SSE Ltd	Pumped_Storage	0	0	612
Foyers	SSE Ltd	Pumped_Storage	300	300	300

Table 8.3 North to south SHE transmission boundary (B2)

Station	Owner / Developer	Fuel Type	2015	2020	2030
Peterhead	SSE Ltd	Gas	400	400	400
Norwegian Link 2	NorthConnect KS	Interconnector	0	0	1400
Beatrice	SSE Ltd	Offshore Wind	0	700	1000
Moray Firth	Repsol & EDP Renewables	Offshore Wind	0	780	1500
Clashindarroch	Vattenfall Ltd	Onshore Wind	37	37	37
Dorenell	Infinergy Ltd	Onshore Wind	0	220	220
Kildrummy	Kildrummy Wind Farm Ltd	Onshore Wind	18	18	18
Mid Hill	Fred Olsen Renewables	Onshore Wind	75	75	75
Tullo	Eneco Wind UK Ltd	Onshore Wind	17	17	17
Tullo 2	Eneco Wind UK Ltd	Onshore Wind	25	25	25

Table 8.4 Argyll and Kintyre boundary (B3b)

Station	Owner / Developer	Fuel Type	2015	2020	2030
Clachan	SSE Ltd	Hydro	40	40	40
Inverawe	SSE Ltd	Hydro	25	25	25
Nant	SSE Ltd	Hydro	15	15	15
Sloy	SSE Ltd	Hydro	152	152	152
Sound of Islay	Scottish Power Ltd	Marine	10	10	10
A Chruach	Novera Energy plc	Onshore Wind	43	50	50
An Suidhe	An Suidhe Wind Farm Ltd	Onshore Wind	21	21	21
Ardchonnel	RWE NPower Renewables Ltd	Onshore Wind	0	0	41
Ardkinglas	Iberdrola Renewable Energies	Onshore Wind	19	19	19
Beinn an Tuirc	Scottish Power Ltd	Onshore Wind	30	30	30
Beinn an Tuirc 2	Scottish Power Ltd	Onshore Wind	44	44	44
Carraig Gheal	Green Power	Onshore Wind	46	46	46
Cour	SSE Ltd	Onshore Wind	23	23	23
Deucheran Hill	E.ON UK plc	Onshore Wind	15	15	15
Tangy	SSE Ltd	Onshore Wind	19	19	19
Tangy III	SSE Renewables Ltd	Onshore Wind	0	39	39

Table 8.5 SHE transmission to SP transmission boundary (B4)

Station	Owner / Developer	Fuel Type	2015	2020	2030
Cashlie	SSE Ltd	Hydro	11	11	11
Clunie	SSE Ltd	Hydro	60	60	60
Errochty	SSE Ltd	Hydro	75	75	75
Finlarig	SSE Ltd	Hydro	16	16	16
Lochay	SSE Ltd	Hydro	48	48	48
Pitlochry	SSE Ltd	Hydro	16	16	16
Rannoch	SSE Ltd	Hydro	45	45	45
St Fillans	SSE Ltd	Hydro	17	17	17
Tummel	SSE Ltd	Hydro	34	34	34
Firth of Forth SHETL	Seagreen Wind Energy Limited	Offshore Wind	0	1075	1075
Braes of Doune	Airtricity Developments (Scotland) Ltd	Onshore Wind	74	74	74
Crossburns	West Coast Energy	Onshore Wind	0	99	99
Drumderg	SSE Ltd	Onshore Wind	32	32	32
Griffin - Stage One	SSE Ltd	Onshore Wind	78	78	78
Griffin - Stage One	SSE Ltd	Onshore Wind	78	78	78
Griffin - Stage Two	SSE Ltd	Onshore Wind	0	48	48

Table 8.6 North to south SP transmission boundary (B5)

Station	Owner / Developer	Fuel Type	2015	2020	2030
Cruach Mhor	Scottish Power Ltd	Onshore Wind	29	29	29
Markinch Biomass CHP Plant	RWE Npower Ltd	Biomass	55	55	55
Longannet	Scottish Power Ltd	Coal	2284	2284	2284
Exxon Mossmoran	Exxon Mobil	Gas	16	16	16
Islay Marine Energy Park	DP Marine	Marine	0	0	180
Blackcraig	SSE Ltd	Onshore Wind	0	58	58
Calderwater	Community Windpower Ltd	Onshore Wind	33	33	33
Earlsburn	Falck Renewables	Onshore Wind	35	35	35
Harelaw	Gamesa Energy UK	Onshore Wind	80	80	80
Kype Muir	Banks Renewables	Onshore Wind	0	100	100
Moorhouse Farmers	Falck Renewables	Onshore Wind	48	48	48
Tormywheel	PM Renewables Ltd	Onshore Wind	32	32	32
West Browncastle Wind Farm	Falck Renewables	Onshore Wind	36	36	36
Cruachan	Scottish Power Ltd	Pumped_Storage	440	440	440

Table 8.7 SP transmission to NGET boundary (B6)

Station	Owner / Developer	Fuel Type	2015	2020	2030
Steven's Croft	E.ON UK plc	Biomass	45	45	45
BP Grangemouth	Grangemouth CHP	Gas	120	120	120
Caledonian Paper	UPM-KYMMENE	Gas	20	20	20
Tongland		Hydro	33	33	33
Hunterston	EDF	Nuclear	947	947	947
Torness	EDF	Nuclear	1216	1216	1216
Firth of Forth	Seagreen Wind Energy	Offshore	0	0	2615
Inch Cape	Repsol & EDP	Offshore	0	1050	1050
Neart na Gaoithe	Mainstream	Offshore	0	450	450
Afton	E.ON UK plc	Onshore	68	68	68
Aikengall	Community Wind Power	Onshore	48	48	48
Aikengall 2	Community Wind Power	Onshore	0	108	108
Andershaw		Onshore	35	35	35
Arecleoch	Scottish Power Ltd	Onshore	120	120	120
Assel Valley	Scottish Power Ltd	Onshore	33	33	33
Bankend Rig	SP Distribution Ltd	Onshore	14	14	14
Benbrack & Quantans Hill	E.ON UK plc	Onshore	0	72	72
Black Law	Scottish Power Ltd	Onshore	121	121	121
Blacklaw Extension	Scottish Power Ltd	Onshore	69	69	69
Bowbeat	E.ON UK plc	Onshore	33	33	33

Brockloch Rig	Fred Olsen Renewables	Onshore	75	75	75
Clyde North & South	Clyde Wind Farm	Onshore	512.6	512.6	512.6
Crystal Rig	Crystal Rig Windfarm	Onshore	62	62	62
Crystal Rig 2	Crystal Rig II Ltd	Onshore	0	62	62
Crystal Rig 2	Crystal Rig II Ltd	Onshore	138	138	138
Cumberhead		Onshore	0	99	99
Dalswinton	Dalswinton Wind Farm	Onshore	30	30	30
Dersalloch	Scottish Power Ltd	Onshore	69	69	69
Dunlaw Extension	Scottish Power Ltd	Onshore	30	30	30
Earlshaugh	Wind Energy Ltd	Onshore	0	55	55
Ewe Hill	Scottish Power Ltd	Onshore	12	66	66
Fallago	Fallago Rig Wind Farm	Onshore	144	144	144
Galawhistle	Infinis	Onshore	0	55	55
Glen App Windfarm	Scottish Power Ltd	Onshore	0	51	51
Glenmount	RWE Npower	Onshore	0	73	73
Hadyard Hill	SSE Ltd	Onshore	117	117	117
Harestanes	Scottish Power Ltd	Onshore	163	163	163
Hunterston Test Centre	SSE	Onshore	25	25	25
Kennoxhead	PNE Wind UK	Onshore	0	60	60
Kilgallioch	Scottish Power Ltd	Onshore	274	274	274
Loch Hill	Loch Hill Windfarm	Onshore	0	27	27
Loch Urr	E.ON UK plc	Onshore	0	84	84
Longpark	Longpark Windfarm Ltd	Onshore	38	38	38
Margree	NBW Wind Energy Ltd	Onshore	0	42	42
Mark Hill	Scottish Power Ltd	Onshore	56	56	56
Middle Muir		Onshore	0	64.6	64.6
Minsca	Minsca Wind Farm	Onshore	38	38	38
Newfield	Wind Energy Ltd	Onshore	0	53	53
Pencloe	NBW Wind Energy Ltd	Onshore	0	63	93
South Kyle	Vattenfall	Onshore	0	165	165
Toddleburn	SSE Ltd	Onshore	28	28	28
Whitelee	Scottish Power Ltd	Onshore	322	322	322
Whitelee Extension	Scottish Power Ltd	Onshore	206	206	206
Whiteside Hill	SSE Ltd	Onshore	0	27	27
Windy Standard III	Fred Olson	Onshore	0	44	44

Appendix B

This appendix considers the combination of heat pumps and fridges to provide FFR service during the summer season.

Fig. 9.1 shows the combination of heat pumps and fridges to provide 500MW of low-frequency response service over the summer season. The time of the day is divided into five periods according to the availability of load in the summer. The values of ALR_{hp} and ALR_{fr} are the averaged value of the five periods given and are listed in Table 9.1.

For simulation results, the aggregation of 87 thousand heat pumps and 2.5 million fridges was considered. This was estimated over the time interval 17:30-18:00 based on the estimation shown in Fig. 9.1. The heat pump and fridge models were connected to the simplified Great Britain power system that was presented in chapter 6. The loss of 1800MW from the generation power, representing the infrequent infeed loss in the Great Britain power system was applied to the simplified GB power system at time 100sec. Fig. 9.2 shows the grid frequency after the loss of generation with and without the use of aggregated load control. Fig. 9.3 shows the behaviour of the power consumption driven by the controlled heat pumps and fridges, and the power change of the synchronous generators. It can be seen from Fig. 9.3 that the heat pumps were less effective appliances to support the grid frequency during the summer in the GB. Hence, all the available heat pumps were switched OFF to provide only 250MW of low frequency response. Consequently, huge number of fridges (about 2.5 million) were switched to compensate the required of frequency response. For lager frequency response provision, an extreme number of fridges are required which is not feasible. It can be concluded that different types of load which are available in the summer should be adopted to stabilize the GB grid frequency over the summer season.
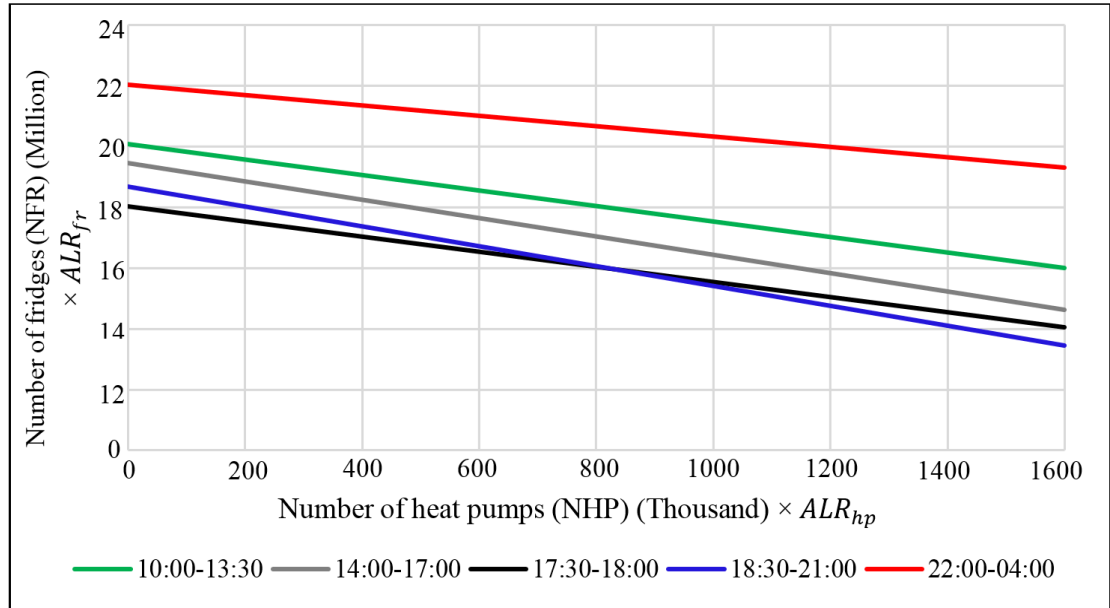
Fig. 9.1 Aggregation of heat pumps and fridges for the provision of 500MW (low frequency response service) during the summer season

Table 9.1 ALR_{hp} and ALR_{fr} at different time of a summer day

Period	time of day	ALR_{hp}(×100%)	ALR_{fr} (×100%)
1	10:00-13:30	0.0212	0.25
2	14:00-17:00	0.0258	0.257
3	17:30-18:00	0.0228	0.2775
4	18:30-21:00	0.029	0.267
5	22:00-04:00	0.0128	0.227

185
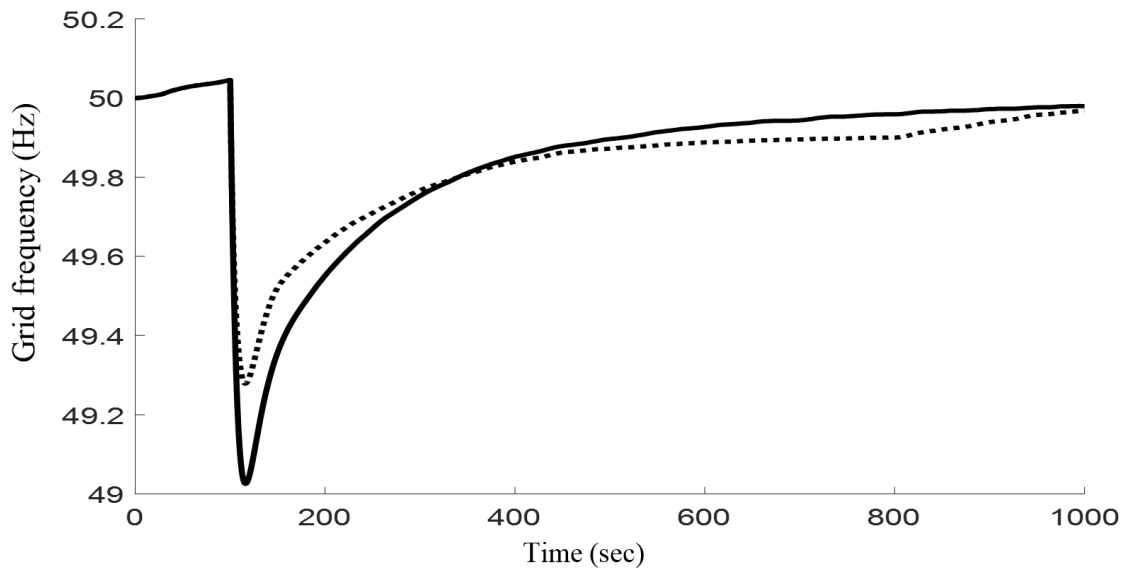
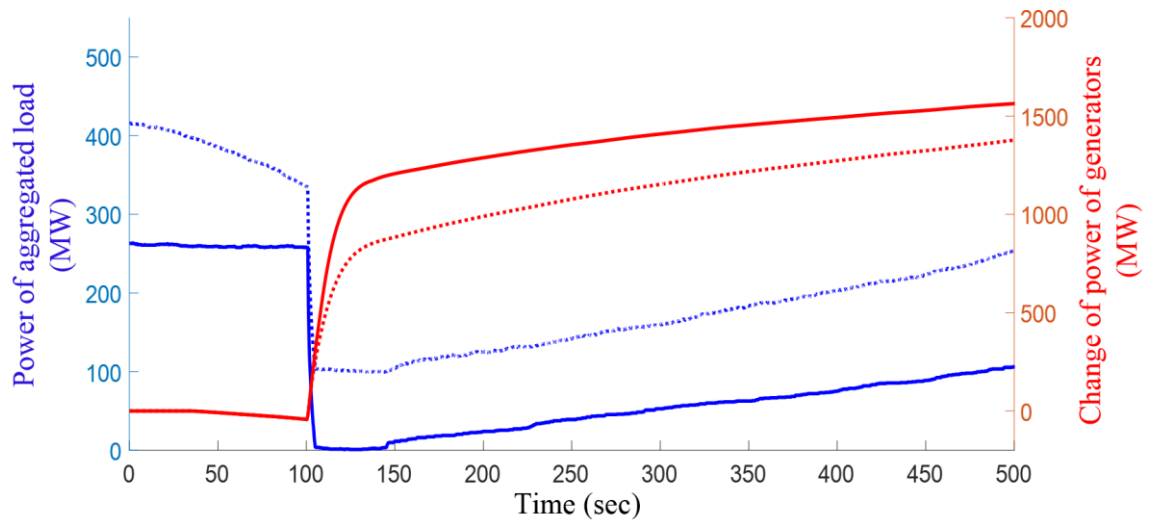**Fig. 9.2 Variation of grid frequency at each load combination scenario**

Fig. 9.3 Power reduction of aggregated load and change of power output of the synchronous generators

Appendix C

The dynamic frequency control algorithms of the aggregation of heat pumps and fridges are applied to provide continuous frequency response in proportion to frequency changes. Dynamic response is automatically delivered for all variations in frequency outside of the dead-band (50Hz ±0.015Hz) [1]. The aggregated load has a maximum of 500 MW when the grid frequency drops to 49.5 Hz (i.e. to represent the capacity of the aggregated load in the summer). Simulation was implemented by injecting a profile recording the GB power system frequency into the dynamically controlled load as shown in Fig. 10.1. As can be seen, the power output of aggregated load dynamically changes following the frequency variation.
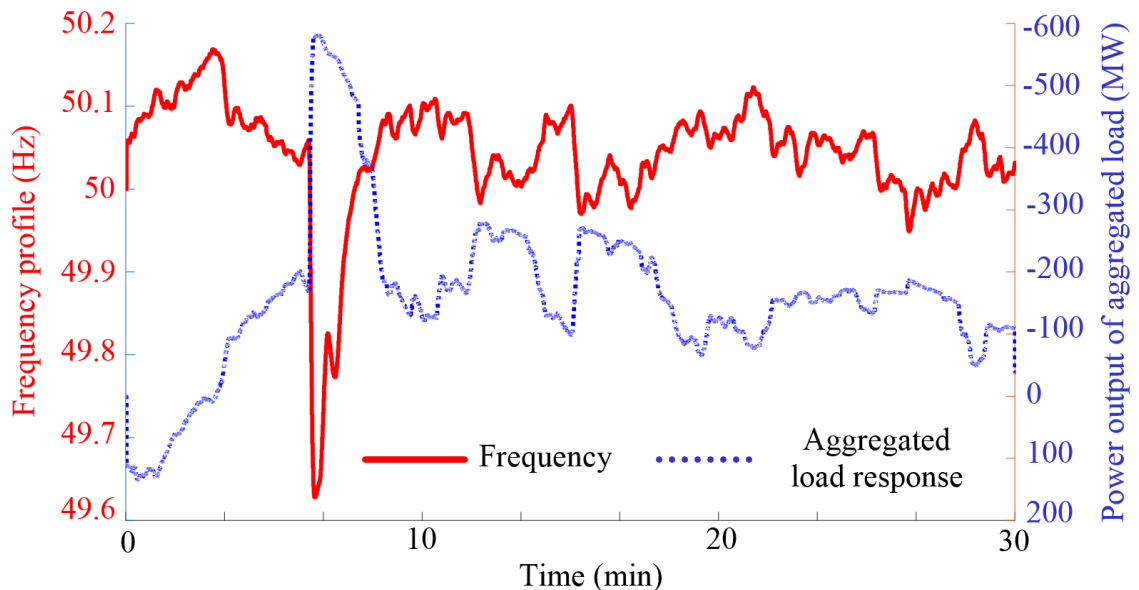

Fig. 10.1 Continuous behaviour of the aggregated load in response to frequency variations

Appendix D

During low frequency response incident, the heat pumps are switched OFF gradually starting from the warmest buildings. The more the frequency drop increases, the more heat pumps are switched OFF in descending order. This can be shown in Fig. 11.1. It was assumed that a frequency drop occurred at time 200 sec and restored to the normal operation after a short time. From Fig. 11.1, we can see that certain number of heat pumps were switched OFF starting from the hottest buildings (note that the rest of heat pumps were not triggered because their trigger frequencies stayed lower than the grid frequency). Similarly, during high frequency response incident, the heat pumps will be switched ON gradually starting from the coldest buildings. The more the frequency rise increases, the more heat pumps are switched ON in ascending order. This can be shown in Fig. 11.2.
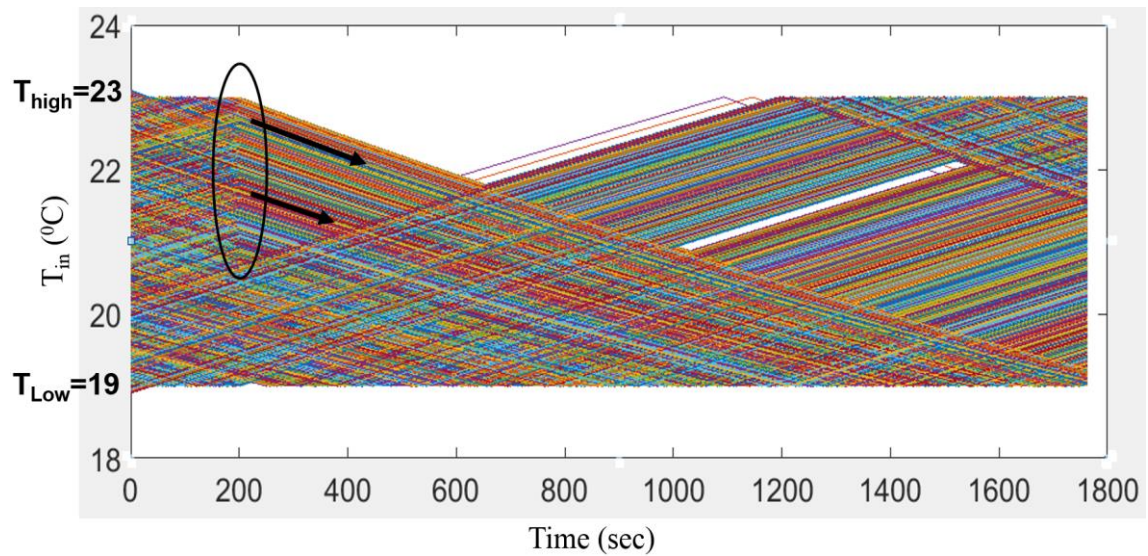

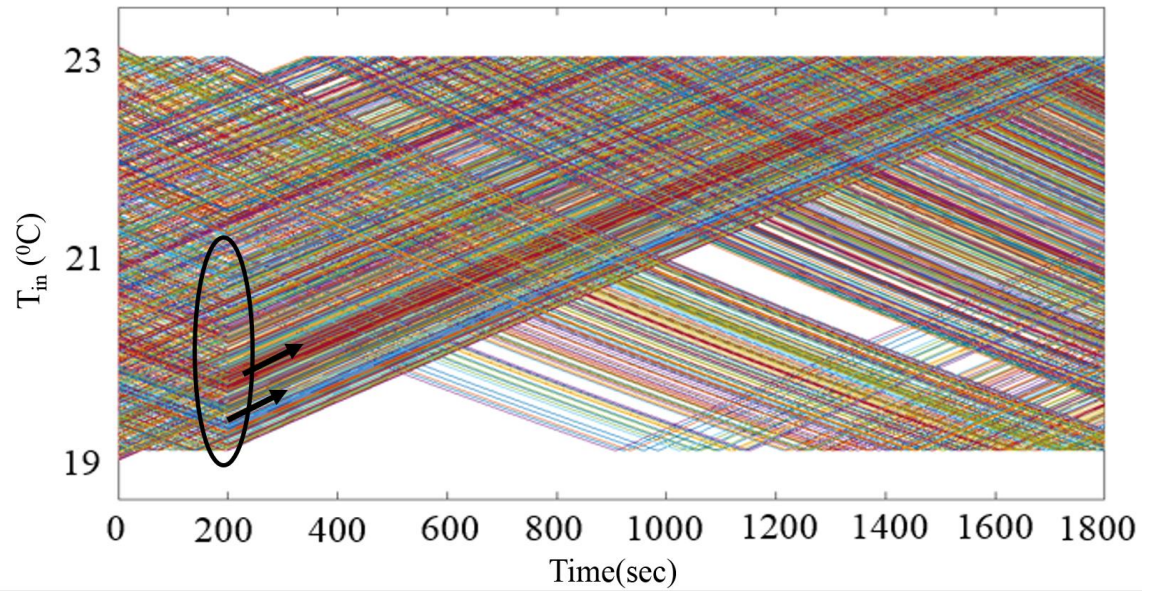**Fig. 11.1 Temperature profile of a population of building during a frequency drop incident**

Fig. 11.2 Temperature profile of a population of building during a frequency rise incident

Appendix E

This appendix considers the effect of constant mismatch between the power of supply and demand (i.e. constant frequency deviation) on the temperature behaviour of buildings. Fig. 12.1(a) shows the injected grid frequency which was dropped lower than 49.50Hz and then restored to approximately 49.78Hz. When the frequency dropped to lower than 49.50Hz, all the heat pumps were switched OFF because their trigger frequencies became higher than the grid frequency (Consult Section 5.2 for more details about the relationship between trigger frequencies and grid frequency). Fig. 12.1(b) shows the temperature behaviour of one building. As explained in Section 5.2, the total numbers of switching events were limited to three every 30min. We can see that limiting the switching events maintained the temperature variable within the range 19^0C to 20.5^0C and hence the comfort of the people inside the building have not been undermined. Fig. 12.1(c) reflects a more realistic shape of a population of buildings having their temperature variable with respect to the frequency deviation but their acceptable levels of temperature have not been undermined.
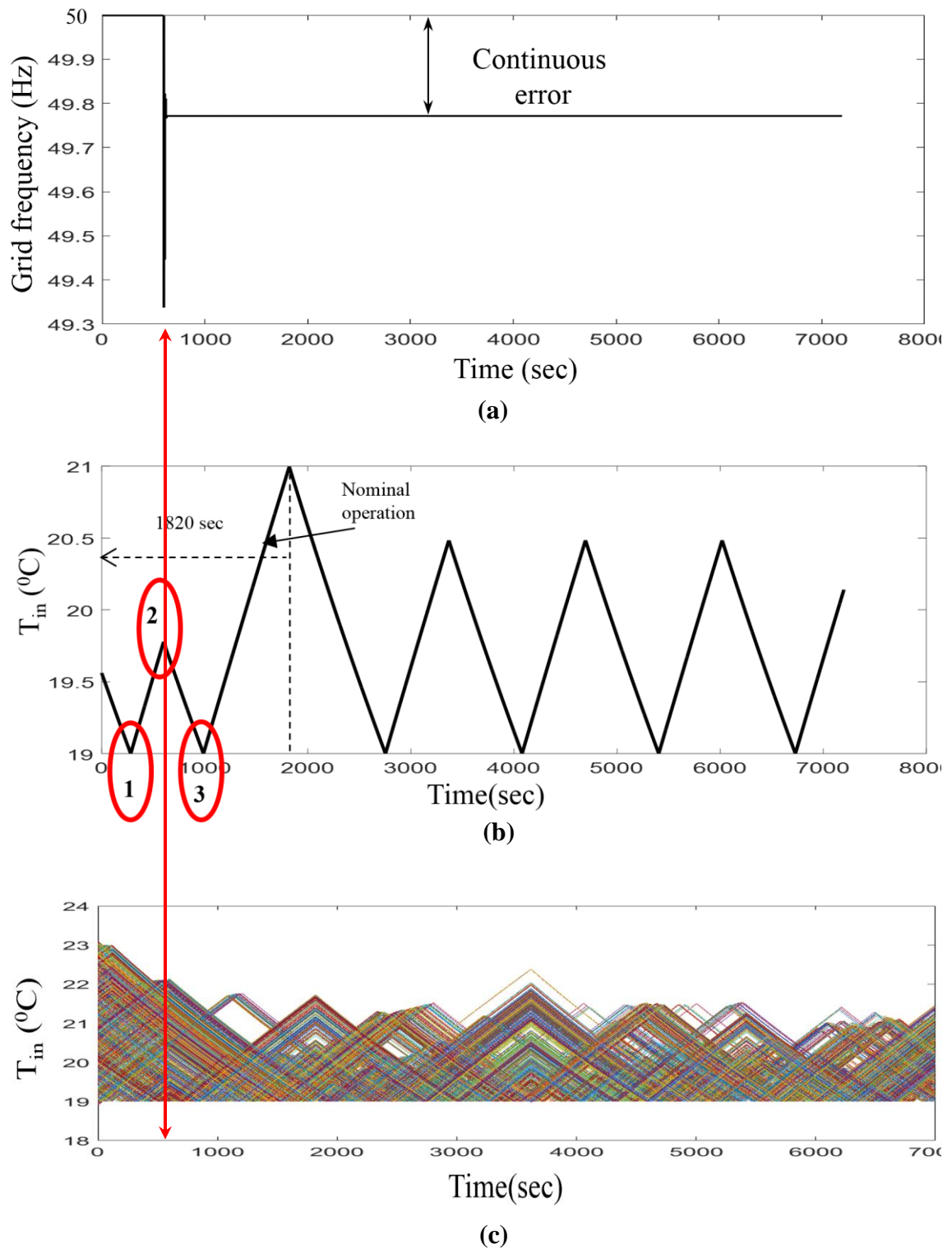
Fig. 12.1 The effect of frequency drop on the temperature of buildings, (a) injected frequency drop, (b) temperature of one building, (c) temperature of a population of buildings.